frontiers | Research Topics

Advances in tick-borne diseases

Edited by
Omid Teymournejad and Deepak Kumar

Coordinated by
Aditya Kumar Sharma

Published in
Frontiers in Cellular and Infection Microbiology

ISSN 1664-8714
ISBN 978-2-8325-6508-7
DOI 10.3389/978-2-8325-6508-7

Generative AI statement
Any alternative text (Alt text) provided alongside figures in the articles in this ebook has been generated by Frontiers with the support of artificial intelligence and reasonable efforts have been made to ensure accuracy, including review by the authors wherever possible. If you identify any issues, please contact us.

About Frontiers

Frontiers is more than just an open access publisher of scholarly articles: it is a pioneering approach to the world of academia, radically improving the way scholarly research is managed. The grand vision of Frontiers is a world where all people have an equal opportunity to seek, share and generate knowledge. Frontiers provides immediate and permanent online open access to all its publications, but this alone is not enough to realize our grand goals.

Frontiers journal series

The Frontiers journal series is a multi-tier and interdisciplinary set of open-access, online journals, promising a paradigm shift from the current review, selection and dissemination processes in academic publishing. All Frontiers journals are driven by researchers for researchers; therefore, they constitute a service to the scholarly community. At the same time, the *Frontiers journal series* operates on a revolutionary invention, the tiered publishing system, initially addressing specific communities of scholars, and gradually climbing up to broader public understanding, thus serving the interests of the lay society, too.

Dedication to quality

Each Frontiers article is a landmark of the highest quality, thanks to genuinely collaborative interactions between authors and review editors, who include some of the world's best academicians. Research must be certified by peers before entering a stream of knowledge that may eventually reach the public - and shape society; therefore, Frontiers only applies the most rigorous and unbiased reviews. Frontiers revolutionizes research publishing by freely delivering the most outstanding research, evaluated with no bias from both the academic and social point of view. By applying the most advanced information technologies, Frontiers is catapulting scholarly publishing into a new generation.

What are Frontiers Research Topics?

Frontiers Research Topics are very popular trademarks of the *Frontiers journals series*: they are collections of at least ten articles, all centered on a particular subject. With their unique mix of varied contributions from Original Research to Review Articles, Frontiers Research Topics unify the most influential researchers, the latest key findings and historical advances in a hot research area.

Find out more on how to host your own Frontiers Research Topic or contribute to one as an author by contacting the Frontiers editorial office: frontiersin.org/about/contact

Advances in tick-borne diseases

Topic editors
Omid Teymournejad — University of Illinois Chicago, United States
Deepak Kumar — University of Southern Mississippi, United States

Topic coordinator
Aditya Kumar Sharma — University of Illinois Chicago, United States

Citation
Teymournejad, O., Kumar, D., Sharma, A. K., eds. (2025). *Advances in tick-borne diseases*. Lausanne: Frontiers Media SA. doi: 10.3389/978-2-8325-6508-7

Table of contents

frontiers | Frontiers in Cellular and Infection Microbiology

TYPE Editorial
PUBLISHED 13 June 2025
DOI 10.3389/fcimb.2025.1630872

OPEN ACCESS

EDITED AND REVIEWED BY
Jon Skare,
Texas A&M Health Science Center,
United States

*CORRESPONDENCE
Omid Teymournejad
ot3@uic.edu
Aditya Kumar Sharma
aditya.sharmaphd@gmail.com

RECEIVED 18 May 2025
ACCEPTED 30 May 2025
PUBLISHED 13 June 2025

CITATION
Teymournejad O, Sharma AK and Kumar D (2025) Editorial: Advances in tick-borne diseases. *Front. Cell. Infect. Microbiol.* 15:1630872. doi: 10.3389/fcimb.2025.1630872

Editorial: Advances in tick-borne diseases

Omid Teymournejad[1,2]*, Aditya Kumar Sharma[1,3]* and Deepak Kumar[4]

[1]Department of Pathology, College of Medicine, University of Illinois at Chicago, Chicago, IL, United States, [2]Office of Disease Control, Division of Laboratories, Illinois Department of Public Health, Chicago, IL, United States, [3]Department of Life Sciences, School of Biosciences and Technology, Galgotias University, Greater Noida, Uttar Pradesh, India, [4]Center for Molecular and Cellular Biosciences, School of Biological, Environmental, and Earth Sciences, University of Southern Mississippi, Hattiesburg, MS, United States

KEYWORDS

tick-borne diseases, severe fever with thrombocytopenia syndrome (SFTS), multi-epitope vaccine, metalloprotease BcEnhancin, tick *Ixodes ricinus*, *Bartonella henselae*

Editorial on the Research Topic
Advances in tick-borne diseases

Tick-borne diseases have a long history, which begin with Victor Babes description of Texas cattle fever in 1888 caused by the protozoan parasite *Babesia bigemina* and transmitted by the tick *Rhipicephalus annulatus* (Vannier et al., 2015). In 1893, Theobald Smith and Frederick Kilborne provided the first experimental proof of tick-mediated transmission by demonstrating that *Rhipicephalus annulatus* ticks transmitted a protozoan parasite *Babesia bigemina* to cattle, establishing our foundational understanding about vector-borne disease (Vannier et al., 2015). In 1906, Rocky Mountain spotted fever, caused by *Rickettsia rickettsii* and transmitted by the Rocky Mountain wood tick (*Dermacentor andersoni*), was identified as the first recognized tick-borne rickettsial disease, marking a significant milestone in the advancement of vector biology research (Walker, 1985; Liu, 2015).

In 1975, a cluster of arthritis cases in Lyme, Connecticut linked to the tick *Ixodes scapularis* (previously *Ixodes dammini*) led to the identification of Lyme disease caused by the spirochete *Borrelia burgdorferi*. Lyme disease presents with symptoms ranging from fever and rash to severe joint and neurological complications if untreated, and it remains the most prevalent tick-borne disease in the United States, with approximately 500000 cases annually and an economic burden exceeding $1 billion (Williamson and Calabro, 1984; Anderson and Magnarelli, 1994). Recent decades have seen the emergence of new tick-borne diseases, including Anaplasmosis, Ehrlichiosis, Tick-borne Relapsing Fever, Powassan virus, and Crimean-Congo Hemorrhagic Fever (Ismail et al., 2022; Sharma et al., 2023). These diseases pose significant challenges due to gaps in understanding their biology, diagnostics and treatment. This editorial highlight research published in the Research Topic "*Advances in tick-borne diseases*." (Figure 1).

The Research Topic begins with a multicenter retrospective cohort study by Fang et al., which aimed to identify risk factors associated with fatal outcomes and evaluate the efficacy of glucocorticoid therapy in patients with Severe Fever with Thrombocytopenia Syndrome (SFTS), a viral tick-borne disease. Using regression analyses and nomograms, Fang et al. identified old age, consciousness disturbance, low monocyte count, prolonged activated partial thromboplastin time and high viral load as predictors of fatal outcome of SFTS. The research paper concluded that high-dose glucocorticoid (GC) therapy should be used

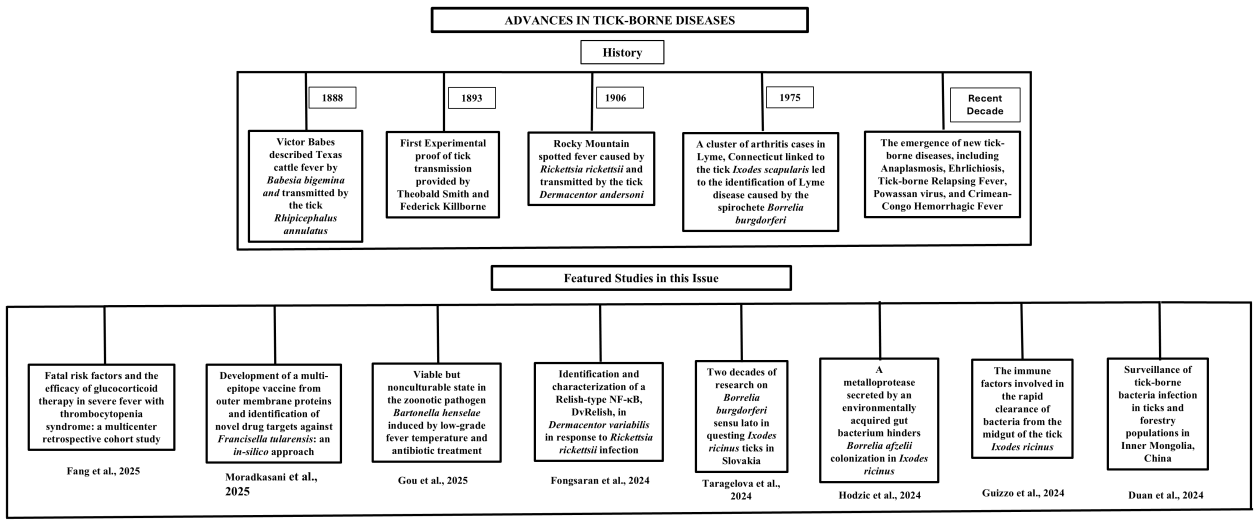

FIGURE 1
Flowchart illustrating a brief history of tick-borne diseases and content of the editorial.

cautiously as relatively high doses and early GC therapy increase mortality in SFTS patients, while low-dose GC treatment in patients with severe symptoms and low aspartate aminotransferase levels improved survival. This predictive model aids in risk stratification and guides tailored GC therapy for SFTS patients.

In another work, Moradkasani et al. employed *in silico* strategies to develop a multi-epitope vaccine (MEV) against *Francisella tularensis*, a highly infectious tick-borne bacterium. Using subcellular localization tools and reverse vaccinology pipelines, Moradkasani et al. screened 1921 proteins and identified 12 vaccine candidates. In this study, authors proposed MEV designed for seven immunodominant epitopes from four outer membrane proteins (including two hypothetical proteins, an OmpA family protein, and PD40), which each having properties including increased antigenicity, solubility, thermostability and half-life. Additionally, the study proposed 10 novel drug targets involved in translation, methylation and porphyrin biosynthesis, providing broad treatment options against various *F. tularensis* strains and addressing limitations in current tularemia treatments.

Similarly, Fongsaran et al. characterized *DvRelish*, a Relish-type NF-κB transcription factor in the tick *Dermacentor variabilis*, and its role in immune defense against *Rickettsia* infection. The authors found an increased *DvRelish* expression in tick hemocytes during *Rickettsia* infection compared to control. Also, RNA interference-mediated knockdown of *DvRelish* led to an increased rickettsial loads at 48 hours post-infestation, underscoring the role of *DvRelish* in the tick immune response. These findings highlight *DvRelish* as a central regulator of tick immunity and suggest that NF-κB signaling significantly influences vector competence for *Rickettsia* spp.

Further, Gou et al. demonstrated that *Bartonella henselae*, a zoonotic tick-borne bacterium, evades host cell responses due to its ability to enter into a viable but nonculturable (VBNC) state under stress conditions, such as fever (38.8°C for 19 days) or antibiotic exposure (4 days). Studies demonstrated that, despite losing culturability, VBNC cells remained viable and retained intact cellular structures, as evidenced by transmission electron microscopy. Notably, the proteomic data demonstrated that the proteins associated with host cell invasion and stress resistance are upregulated and proteins related to cell signaling and cellular processes were downregulated. Studies also showed that *Bartonella henselae* can survive hostile conditions by entering a VBNC state and this state contributes to drug resistance, host invasion, diagnostic and treatment challenges.

Next, Taragelova et al. summarized a 20-year surveillance study (1999–2019) of *Ixodes ricinus* ticks across 16 locations in Slovakia, testing 17,249 questing ticks for *Borrelia burgdorferi* sensu lato (s.l.). The key findings of the study include an overall prevalence of 18.8%, with 15.1% of nymphs and 24.3% of adults testing positive. Nine species within the *B. burgdorferi* s.l. complex were identified, including *Borrelia afzelii*, *B. garinii/B. bavariensis*, *B. valaisiana, B. lusitaniae*, *B. burgdorferi* sensu stricto, *B. spielmanii, B. bissettii*, *B. kurtenbachii*. Out of these *Borrelia afzelii* (37.1%), *B.garinii/B. bavariensis* (24.7%), and *B. valaisiana* (15.4%) were the most frequent and found at all the study sites whereas *B. lusitaniae*, *B. burgdorferi* sensu stricto, *B. bavariensis* and *B. spielmanii* were found in four samples and *B. bissettii* and *B. kurtenbachii* were also recorded in single cases. Additionally, the infection rate of *Borrelia burgdorferi* s.l. varied across habitats, with the highest prevalence observed in natural environments and the lowest in urban settings. These findings underscore the importance of long-term surveillance to evaluate the influence of climatic and socioeconomic factors on the distribution of tick-borne diseases.

Towards understanding the significance of gut microbiota in determining tick vector competence and defining the vector competence, Hodzic et al. revealed that *Bacillus cereus* LTG-1, an environmentally acquired gut bacterium in *Ixodes ricinus*, impairs *Borrelia afzelii* colonization through a secreted metalloprotease referred as *BcEnhancin*. Oral administration of *B. cereus* LTG-1 or purified *BcEnhancin* degraded the glycan-rich peritrophic matrix in the tick gut, which reduce *B. afzelii* load. Additionally, qRT-PCR

data revealed that *myd88* and *peritrophin 1* genes were upregulated after 48 h of administration of recombinant BcEnhancin. Both genes are linked to immune system and peritrophic matrix in the tick gut respectively. These findings highlight the tick gut microbiome's role in shaping vector competence and offer new insights into the interactions among *Borrelia*, ticks, and their resident microbes.

In a similar direction, Guizzo et al. investigated the immune response of *Ixodes ricinus* ticks following exposure to either the Gram-positive bacterium *Micrococcus luteus* or the Gram-negative *Pantoea* sp. Although the tick midgut harbors a limited and inconsistent microbiota about which our understanding remains incomplete, the ticks were able to rapidly clear artificial infections with both *M. luteus* and *Pantoea* sp. Transcriptomic and proteomic analyses revealed several constitutively expressed antimicrobial peptides including defensins, amidase effectors, lysozymes, and gamma interferon-inducible lysosomal thiol reductases (GILTs). Antimicrobial activity assays confirmed that defensins 1 and 8 are highly effective against Gram-positive bacteria such as *Micrococcus luteus*. These findings suggest that a pre-existing and multi-component antimicrobial system in the tick midgut plays a central role in rapidly eliminating invading microbes.

Lastly, the editorial concludes with the study by Duan et al., who investigated tick-borne bacteria and their associated infections in Arxan, Inner Mongolia, China, by analyzing 282 *Ixodes persulcatus*, 13 *Dermacentor silvarum* ticks, and 245 human blood samples. Using 16S rDNA sequencing and species-specific PCR, the authors detected *Candidatus Rickettsia tarasevichiae* (89%) and *Borrelia garinii* (17%) as the most prevalent pathogens in *I. persulcatus*, with 13% coinfection. In human samples, *B. garinii* (4.9%), *Rickettsia slovaca* (0.82%), and *Coxiella burnetii* (0.41%) were detected, with seroprevalence for spotted fever group rickettsiae (SFGR) and *B. burgdorferi* at 5.71% and 13.47%, respectively. The study confirmed *B. garinii* transmission from ticks to humans and reported the first detection of *B. miyamotoi* (7%) in ticks and *R. slovaca* (0.82%) in humans in Arxan, highlighting the need for ongoing surveillance.

Overall, we believe that collection of research articles featured in this Research Topic advance our understanding of tick-borne diseases by elucidating pathogen biology, vector competence, and host immune responses. From predictive models for SFTS treatment to innovative vaccine strategies for *Francisella tularensis* and insights into tick microbiome interactions, these findings pave the way for improved diagnostics, therapeutics, and prevention strategies. As tick-borne diseases continue to emerge and expand due to environmental and climatic changes, sustained research and surveillance are critical to mitigate their global public health impact.

Author contributions

OT: Project administration, Data curation, Writing – original draft, Conceptualization, Supervision, Methodology, Investigation, Writing – review & editing, Validation, Formal Analysis. AS: Data curation, Validation, Project administration, Formal Analysis, Methodology, Investigation, Conceptualization, Writing – review & editing, Supervision, Writing – original draft. DK: Supervision, Validation, Conceptualization, Methodology, Investigation, Visualization, Writing – review & editing, Formal Analysis, Project administration.

Funding

The author(s) declare that no financial support was received for the research and/or publication of this article.

Conflict of interest

The authors declare that the research was conducted in the absence of any commercial or financial relationships that could be construed as a potential conflict of interest.

Generative AI statement

The author(s) declare that no Generative AI was used in the creation of this manuscript.

Publisher's note

References

Anderson, J. F., and Magnarelli, L. A. (1994). Lyme disease: a tick-associated disease originally described in Europe, but named after a town in Connecticut. *Am. Entomologist* 40, 217–228. doi: 10.1093/ae/40.4.217

Ismail, N., Sharma, A., Soong, L., and Walker, D. H. (2022). Review: protective immunity and immunopathology of ehrlichiosis. *Zoonoses* 2. doi: 10.15212/ZOONOSES-2022-0009

Liu, D. (2015). "Rickettsia," in *Molecular Medical Microbiology* (Amsterdam, Netherlands: Elsevier), 2043–2056.

Sharma, A. K., Dhasmana, N., and Arora, G. (2023). Bridging the gap: exploring the connection between animal and human health. *Zoonotic Dis.* 3, 176–178. doi: 10.3390/zoonoticdis3020014

Vannier, E. G., Diuk-Wasser, M. A., Ben Mamoun, C., and Krause, P. J. (2015). Babesiosis. *Infect. Dis. Clin. North Am.* 29, 357–370. doi: 10.1016/j.idc.2015.02.008

Walker, D. H. (1985). Rickettsiae.

Williamson, P. K., and Calabro, J. J. (1984). "Lyme disease—a review of the literature," in *Seminars in arthritis and rheumatism* (Amsterdam, Netherlands: Elsevier), 229–234.

frontiers | Frontiers in Public Health

TYPE Original Research
PUBLISHED 29 February 2024
DOI 10.3389/fpubh.2024.1302133

OPEN ACCESS

EDITED BY
Omid Teymournejad,
University of Illinois Chicago, United States

REVIEWED BY
Xin-Ru Wang,
Upstate Medical University, United States
Marina Eremeeva,
Georgia Southern University, United States

*CORRESPONDENCE
Qin Hao
haoqin@icdc.cn
Aiying Dong
dongaiying68@126.com

†These authors have contributed equally to this work and share first authorship

RECEIVED 04 October 2023
ACCEPTED 09 February 2024
PUBLISHED 29 February 2024

CITATION
Duan L, Zhang L, Hou X, Bao Z, Zeng Y, He L, Liu Z, Zhou H, Hao Q and Dong A (2024) Surveillance of tick-borne bacteria infection in ticks and forestry populations in Inner Mongolia, China.
Front. Public Health 12:1302133.
doi: 10.3389/fpubh.2024.1302133

Surveillance of tick-borne bacteria infection in ticks and forestry populations in Inner Mongolia, China

Like Duan[1†], Lin Zhang[1], Xuexia Hou[1], Zihao Bao[1], Yu Zeng[1], Lijuan He[1], Zeliang Liu[2], Haijian Zhou[1], Qin Hao[1*†] and Aiying Dong[2*]

[1]National Institute for Communicable Disease Control and Prevention, Chinese Center for Disease Control and Prevention, National Key Laboratory of Intelligent Tracking and Forecasting for Infectious Diseases, Beijing, China, [2]Affiliated Hospital of North China University of Science and Technology, Tangshan, China

Ticks are one of the most important vectors that can transmit pathogens to animals and human beings. This study investigated the dominant tick-borne bacteria carried by ticks and tick-borne infections in forestry populations in Arxan, Inner Mongolia, China. Ticks were collected by flagging from May 2020 to May 2021, and blood samples were collected from individuals at high risk of acquiring tick-borne diseases from March 2022 to August 2023. The pooled DNA samples of ticks were analyzed to reveal the presence of tick-borne bacteria using high-throughput sequencing of the 16S rDNA V3–V4 region, and species-specific polymerase chain reaction (PCR) related to sequencing was performed to confirm the presence of pathogenic bacteria in individual ticks and human blood samples. All sera samples were examined for anti-SFGR using ELISA and anti-*B. burgdorferi* using IFA and WB. A total of 295 ticks (282 *Ixodes persulcatus* and 13 *Dermacentor silvarum*) and 245 human blood samples were collected. *Rickettsia*, *Anaplasma*, *Borrelia miyamotoi*, and *Coxiella endosymbiont* were identified in *I. persulcatus* by high-throughput sequencing, while *Candidatus R. tarasevichiae* (89.00%, 89/100), *B. garinii* (17.00%, 17/100), *B. afzelii* (7.00%, 7/100), and *B. miyamotoi* (7.00%, 7/100) were detected in *I. persulcatus*, as well the dual co-infection with *Candidatus R. tarasevichiae* and *B. garinii* were detected in 13.00% (13/100) of *I. persulcatus*. Of the 245 individuals, *B. garinii* (4.90%, 12/245), *R. slovaca* (0.82%, 2/245), and *C. burnetii* (0.41%, 1/245) were detected by PCR, and the sequences of the target genes of *B. garinii* detected in humans were identical to those detected in *I. persulcatus*. The seroprevalence of anti-SFGR and anti-*B. burgdorferi* was 5.71% and 13.47%, respectively. This study demonstrated that *Candidatus R. tarasevichiae* and *B. garinii* were the dominant tick-borne bacteria in *I. persulcatus* from Arxan, and that dual co-infection with *Candidatus R. tarasevichiae* and *B. garinii* was frequent. This is the first time that *B. miyamotoi* has been identified in ticks from Arxan and *R. solvaca* has been detected in humans from Inner Mongolia. More importantly, this study demonstrated the transmission of *B. garinii* from ticks to humans in Arxan, suggesting that long-term monitoring of tick-borne pathogens in ticks and humans is important for the prevention and control of tick-borne diseases.

KEYWORDS

tick-borne bacteria, *Ixodes persulcatus*, co-infection, spotted fever group Rickettsia, Inner Mongolia

Introduction

Ticks are obligate hematophagous ectoparasites of terrestrial vertebrates that can transmit various pathogens to humans and are considered to be the second most notable vectors worldwide after mosquitoes (1). By the end of 2018, 103 tick-borne pathogens were detected in China, of which 65 were newly identified in the past two decades (2). Notable bacteria such as *Rickettsia*, *Borrelia*, *Coxiella*, *Anaplasma*, and *Ehrlichia* (2–4), have been detected in a wide range of tick species that can cause spread of relevant zoonotic diseases. Annually expanding geographic ranges and increasing populations of ticks, partly driven by climate change, demographic growth, and increased overseas travel and trade, have become serious threats to public health (5, 6). However, systematic and comprehensive investigations of tick-borne pathogens have not been conducted in tick habitats in China because of the limitations of investigation regions and research technology.

Inner Mongolia Autonomous Region, located in northern China, is well-known for its various landscapes and is one of the natural foci of various tick-borne diseases in China (7–10). Arxan, on the border between China and Mongolia in the northeastern Inner Mongolia, features abundant wildlife resources and a developed livestock industry that provides a suitable environment for ticks to survive and reproduce. Trade activities at border crossings and tourism have partly increased the risk of tick-borne diseases. For instance, the average annual incidence of tick-borne encephalitis (TBE) in Arxan from 2006 to 2013 was 188.48/1000000, indicating that Arxan has the highest incidence of TBE in China (11). However, tick-borne bacteria in Arxan have not been studied in recent years. Therefore, investigating the status of bacterial infections in ticks and humans plays an important role in the prevention and control of tick-borne diseases in Arxan.

In this study, we performed high-throughput sequencing of the 16S rDNA V3–V4 region to detect tick-borne bacteria carried by ticks, and species-specific polymerase chain reaction (PCR) was performed to confirm the presence of pathogenic bacteria in ticks and participants at a high risk of tick-borne diseases in Arxan. Furthermore, antibodies against dominant tick-borne bacteria were detected using Enzyme-Linked Immunosorbent Assay (ELISA), Indirect Immunofluorescence Assay (IFA), and Western Blotting (WB) assays, providing complete and comprehensive monitoring of tick-borne bacteria and a theoretical basis for the prevention and control of tick-borne diseases.

Materials and methods

Collection and identification of ticks

Free-living ticks were collected from ground vegetation by dragging white cloth in May 2020 and 2021 in Arxan, Inner Mongolia, China (Figure 1). All collected ticks were placed in breathable and moistened bottles and transported to the laboratory as soon as possible at room temperature (20–25°C). Tick species were identified based on morphological characterization and verified using sequences of mitochondrial 16S rDNA genes, as previously described (12). After identification, the ticks were stored at −80°C until use.

Collection of human blood samples

Patients with tick-borne diseases mostly work in the field, including as forestry workers (13–15). These workers had a high possibility of tick exposure and therefore, were defined as groups at high risk of acquiring tick-borne diseases. We simultaneously collected anticoagulated (EDTA blood) and non-anticoagulant blood samples from 245 participants (232 males and 13 females) working in the field from March 2022 to August 2023. The workplaces of these participants were Tianchi forest farm (8.57%, 21/245), Sandur forest farm (15.92%, 39/245), Lixin forest farm (16.33%, 40/245), Irsh forest farm (28.16%, 69/245), Xing'an Service Area (8.98%, 22/245), Jinjianggou Service Area (11.84%, 29/245) and Transportation Company (10.20%, 25/245), respectively. The median age of all participants was 53.00 years (range 23–60 years). All the participants provided written informed consent to participate in this study. Sera were isolated from non-anticoagulant blood samples and stored at −20°C for serological tests. Anticoagulated blood samples were used for DNA extraction.

DNA extraction

All ticks were washed with 75% ethanol and rinsed thrice with sterile water to remove environmental contaminants. Except for the 182 *I. persulcatus* samples used for the isolation and culture of *B. burgdorferi*, the remaining 100 *I. persulcatus* and 13 *D. silvarum* samples were used for DNA extraction. Individual tick samples were homogenized in 180 µL buffer ATL, then genomic DNA was extracted using the DNeasy Blood & Tissue Kit (QIAGEN, Germany) according to the manufacturer's instructions. Similarly, the genomic DNA of human blood samples was extracted from anticoagulated blood using the DNeasy Blood & Tissue Kit (QIAGEN, Germany). Each time DNA extraction was performed, an extraction control (water) was added. All DNA samples from both ticks and human blood were stored at −80°C until use.

High-throughput sequencing

Individual DNA samples of ticks were mixed in an equal volume (10 µL) to prepare pooled DNA samples (3 or 4 DNA samples for a pool). One hundred *I. persulcatus* DNA samples were mixed to prepare 32 pools (N1–N24 and N29–N36), and 13 *D. silvarum* DNA samples were mixed for 4 pools (N25–N28). All pooled DNA samples were sent to Biomarker Technologies Co., Ltd. (Beijing, China) for high-throughput sequencing of the 16S rDNA V3–V4 region on an Illumina NovaSeq 6,000 platform (Illumina, San Diego, CA, United States) with a sequencing depth of 80,000. The bioinformatics analysis of raw data was performed with the aid of the BMK Cloud (Biomarker Technologies Co., Ltd., Beijing, China). Raw data were filtered according to the quality of a single nucleotide using Trimmomatic (version 0.33) (16). Primer sequences were identified and removed using Cutadapt (version 1.9.1) (17). Clean reads obtained from the previous steps were assembled using USEARCH (version 10) (18) and followed by chimera removal using UCHIME (version 8.1) (19). Effective reads were generated and used for subsequent analyses. Sequences with similarity ≥97% were clustered into the same operational taxonomic unit (OTU) by USEARCH (version 10). Taxonomic annotation of the OTUs was performed based on the Naive Bayes classifier in QIIME2 (20) using the

10.3389/fpubh.2024.1302133

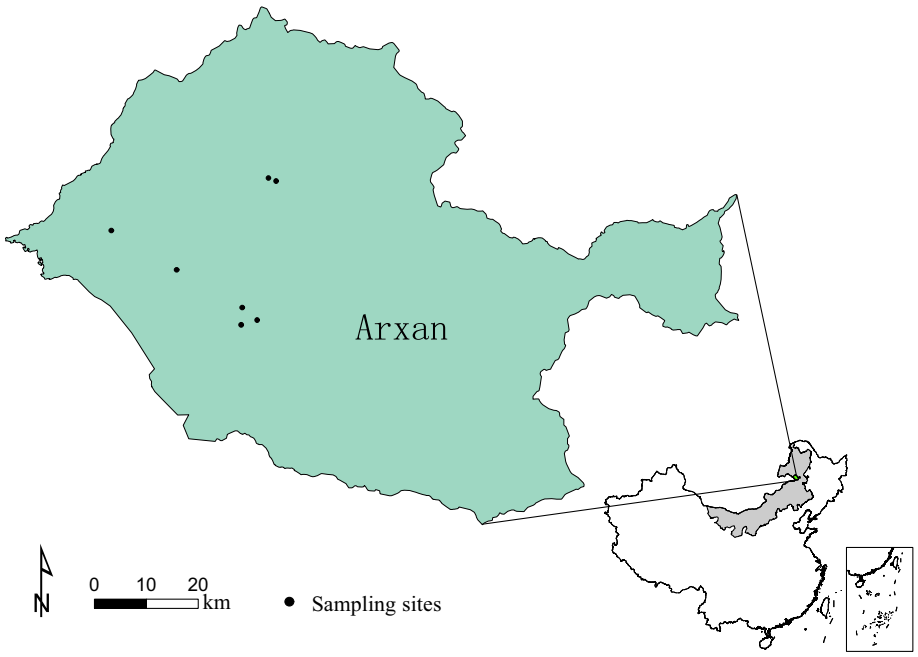

FIGURE 1
Map of the tick sampling sites in Arxan, Inner Mongolia, China.

SILVA database (release 132) (19), following which a relative abundance table and histogram for each sample at the level of the phylum, class, order, family, genus, and species were calculated and displayed. Alpha diversity, including Chao1, ACE, Shannon, and Simpson indices, were calculated and displayed using QIIME2 and R software.

Polymerase chain reaction

According to the results of high-throughput sequencing and tick-borne bacteria prevalently detected in Inner Mongolia, the presence of *Borrelia burgdorferi*, *B. miyamotoi*, *Anaplasma phagocytophilum*, spotted fever group rickettsia, *Ehrlichia chaffeensis*, and *Coxiella burnetii* were tested in ticks and human blood samples using nested PCR or traditional PCR. The PCR primer sequences are listed in Table 1. PCR was performed using a PCR system (SensoQuest, Germany). The PCR system was totally 25 μL, including 12.5 μL Premix Taq™ (TaKaRa), 1 μL upper primer (10 μm), 1 μL lower primer (10 μm), 5 μL each individual DNA sample and 5.5 μL ddH_2O. Positive (recombinant plasmid containing the target gene), negative (water), and extraction controls were used for PCR amplification in each PCR experiment. For nested PCR, 1 μL of the primary PCR production was used as the template for the second round. All amplified products were electrophoresed on a 1.5% agarose gel and the positive products were purified and sequenced. The acquired nucleotide sequences were submitted to National Center for Biotechnology Information Genbank and compared with available sequences deposited using the Basic Local Assignment Search Tool.[1] Additionally, human blood samples that were positive for SFGR based on nested PCR were tested using qPCR targeting *gltA* gene. qPCR was performed using a Probe qPCR mix (Premix Ex Taq™,TaKaRa) on a LightCycler 480 System (Roche Diagnostics, United States).

Phylogenetic analysis

Reference sequences of target genes downloaded from GenBank were aligned with the positive amplicon sequences using the ClustalW method with default parameters in MEGA11.0. One of the same nucleotide sequences detected in a tick or blood sample was selected as the representative sequence. Phylogenetic analysis was performed using the neighbor-joining algorithm, and bootstrap values were set for 1,000 replicates.

Serological tests

Based on the results of the high-throughput sequencing and PCR assays, SFGR and *B. burgdorferi* were the dominant tick-borne bacteria in Arxan. All serum samples were tested anti-SFGR by ELISA and anti-*B. burgdorferi* using IFA and WB. ELISA kits acquired from Enzyme Immune Industrial Co., Ltd. (Jiangsu, China) were used to detect anti-SFGR IgG and IgM according to the manufacturer's instructions. The cutoff value was the mean optical density (OD) of the negative control wells plus 0.15. Samples with OD values less than the cut-off value were considered negative. Samples with OD values greater than or equal to the cut-off value were considered positive.

IFA and WB were performed as previously described (29). First, all the serum samples were tested for anti-*B. burgdorferi* by IFA. A titer of ≥1/128 for IgG or 1:64 for IgM was considered positive. For IgG, samples that were positive at a titer of 1/64 but presented a weak

1 https://blast.ncbi.nlm.nih.gov/Blast.cgi

10.3389/fpubh.2024.1302133

TABLE 1 Target genes and primer sequences used for PCR.

Bacteria	Target gene	Primer name	Sequence (5′–3′)	Size (bp)	References
B.burgdorferi	5S-23S rRNA IGS	F1 R1 F2 R2	CGACCTTCTTCGCCTTAAAGC TAAGCTGACTAATACTAATTACCC TCCTAGGCATTCACCATA GAGTTCGCGGGAGA	255	(21)
B.miyamotoi	glpQ	F1 R1 F2 R2	CACCATTGATCATAGCTCACAG CTGTTGGTGCTTCATTCCAGTC GCTAGTGGGTATCTTCCAGAAC CTTGTTGTTTATGCCAGAAGGGT	424	(22)
SFGR	ompA	Rr190.70 Rr190.701 Rr190.70 Rr190.602	ATGGCGAATATTTCTCCAAAA GTTCCGTTAATGGCAGCATCT ATGGCGAATATTTCTCCAAAA AGTGCAGCATTGGCTCCCCCT	533	(23)
SFGR	gltA	Cs2d CsendR Rpcs877 Rpcs1258	ATGACCAATGAAAATAATAAT CTTATACTCTCTATGTACA GGGGACCTGCTCACGGCGG ATTGCAAAAAGTACAGTGAACA	341	(8)
SFGR	gltA	F R P	GTGAATGAAAGATTACACTATTTAT GTATCTTAGCAATCATTCTAATAGC 6-FAM-CTATTATGCTTGCGGCTGTCGGTTC-TAMRA	166	(24)
AP	16S rRNA	AP-F AP-R	GTCGAACGGATTATTCTTTATAGCTTG TATAGGTACCGTCATTATCTTCCCTAC	389	(25)
EC	16S rRNA	ECC ECB H3 H1	AGAACGAACGCTGGCGGCAAGCC CGTATTACCGCGGCTGCTGGCA TATAGGTACCGTCATTATCTTCCCTAT CAATTGCTTATAACCTTTTGGTTATAAAT	389	(26, 27)
CB	IS1111	F1 R1 F2 R2	TACTGGGTGTTGATATTGC CCGTTTCATCCGCGGTG GTAAAGTGATCTACACGA TTAACAGCGCTTGAACGT	297	(28)

SFGR, spotted fever group rickettsia; AP, *Anaplasma phagocytophilum*; EC, *Ehrlichia chaffeensis*; CB, *Coxiella burnetii*.

fluorescence signal at a titer of 1/128 were considered equivocal. For IgM, samples that were positive at a titer of 1/32 but presented a weak fluorescence signal at a titer of 1/64 were considered equivocal. Subsequently, all sera with positive and equivocal (IgG or IgM) results were further analyzed by WB (both IgG and IgM). The positive criteria were at least one band of P83/100, P66, P58, P39, P30, OspC, OspA, and P17 in the IgG test and at least one band of P83/100, P58, P41, OspA, P30, OspC, and P17 in the IgM test (30).

Statistical analysis

Statistical analysis was performed using Pearson's χ^2 test and $p < 0.05$ was considered significant.

Results

Identification of ticks

A total of 295 adult hard ticks were identified as *Ixodes persulcatus* ($n = 282$) and *Dermacentor silvarum* ($n = 13$) based on morphological characteristics and mitochondrial 16S rDNA sequences. The nucleotide sequence data of mitochondrial 16S rDNA in this study will appear in GenBank under the following accession numbers: OR841358–OR841362 for *I. persulcatus*, OR841363–OR841367 for *D. silvarum*.

The overview of high-throughput sequencing

A total of 2,413,890 effective reads (range 69,960–76,736 reads, average 75434.06 reads) of high quality (Q20 > 98.94%, shown in Additional file 1: Supplementary Table S1) were obtained from 32 pooled *I. persulcatus* samples. Subsequently, the effective reads were clustered into 1,445 Operational Taxonomic Units (OTU), which belonged to 32 phyla, 79 classes, 191 orders, 348 families, and 594 genera. Moreover, 303,375 effective reads were acquired from four pooled DNA samples of *D. silvarum* (range 75,414–76,021 reads, average 75843.75 reads), all of which were of high quality (Q20 > 98.93%, shown in Additional file 1: Supplementary Table S1), and 1,430 OTUs were generated, belonging to 31 phyla, 78 classes, 190 orders, 346 families, and 588 genera.

Alpha diversity reflects species richness and diversity of individual samples. The Ace and Chao1 indices, which were calculated to measure species richness, were more than 1068.34 and 1098.66, respectively, in each pool (Additional file 2: Supplementary Table S2). Shannon and Simpson indices were used to measure species diversity, which were affected by species abundance and community evenness in the sample community. With the same species abundance, the greater the uniformity of each species in the community, the larger the Shannon and Simpson indices values, indicating higher species diversity in the sample. Shannon diversity rarefaction (Figure 2) reflects the microbial diversity of each sample at different sequencing amounts, and was used to determine whether the sequencing depth was sufficient. All pools were highly diverse, with Simpson indices more than 0.85 except for N23. The species accumulation curve reflects the relationship between the sample size and the number of annotated species, and can be used to determine whether the sample size was sufficient. The species accumulation curve of *I. persulcatus* at the genus level is shown in Figure 3. The number of *D. silvarum* pooled DNA samples was insufficient for the analysis of the species cumulative curve.

Species annotation and taxonomic analysis

Taxonomic assignment revealed that the relative abundances of the genera were highly variable in the microbiome of *I. persulcatus* (Figure 4). At least 594 genera were presented in *I. persulcatus*, including *Rickettsia*, *Acinetobacter*, *Methylotenera*, *Methylomonas*, *Psychrobacter*. *Rickettsia* was the most common genus, with a relative abundance >22.61% in the seven pools (Additional file 3: Supplementary Table S3). *Borrelia*, with a relative abundance of 0.15–0.35%, was detected in three pools and further identified as *B. miyamotoi*. Likewise, *Coxiella* (0.01–0.02%) was identified in five pools and further confirmed to be *Coxiella endosymbiont*. *Anaplasma* (0.01%) was present in two pools, but species-level annotation was lacking (Additional file 4, Supplementary Table S4).

Similarly, *Rickettsia* was the most abundant genus in *D. silvarum* (Additional file 3: Supplementary Table S3). *Coxiella* was identified in each *D. silvarum* pool and confirmed to be *Coxiella endosymbiont* at the species level (Additional file 4: Supplementary Table S4), whereas *Borrelia* was not detected in *D. silvarum*.

Prevalence of tick-borne bacteria in ticks and humans

Candidatus R. tarasevichiae (89.00%, 89/100), *B. garinii* (17.00%, 17/100), *B. afzelii* (7.00%, 7/100), and *B. miyamotoi* (7.00%, 7/100) were detected in *I. persulcatus*, while *R. raoultii* (69.23%, 9/13) was detected in *D. silvarum* (Table 2). More importantly, *B. garinii* (4.90%, 12/245), *R. slovaca* (0.82%, 2/245), and *C. burnetii* (0.41%, 1/245) were detected in the human blood samples. Neither *Ehrlichia* DNA nor *Anaplasma* DNA was detected in ticks or human blood samples. The qPCR results showed a cycle threshold value of 38.86 for one of those 2 individuals that were detected positive for *R. slovaca* using nested PCR targeting *ompA* gene.

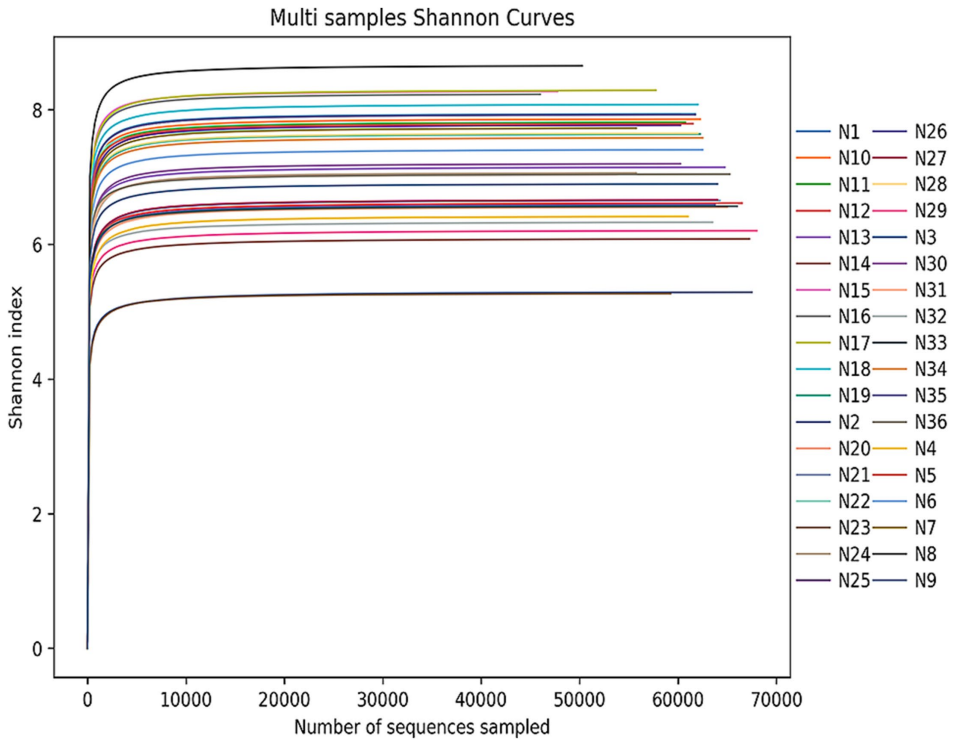

FIGURE 2
Shannon index rarefaction curve of 36 pools of *I. persulcatus* and *D. silvarum*. When the curve tends to be flat, it means that the sequencing data are sufficient for analysis, and the Shannon index will not increase with increasing sequencing data.

10.3389/fpubh.2024.1302133

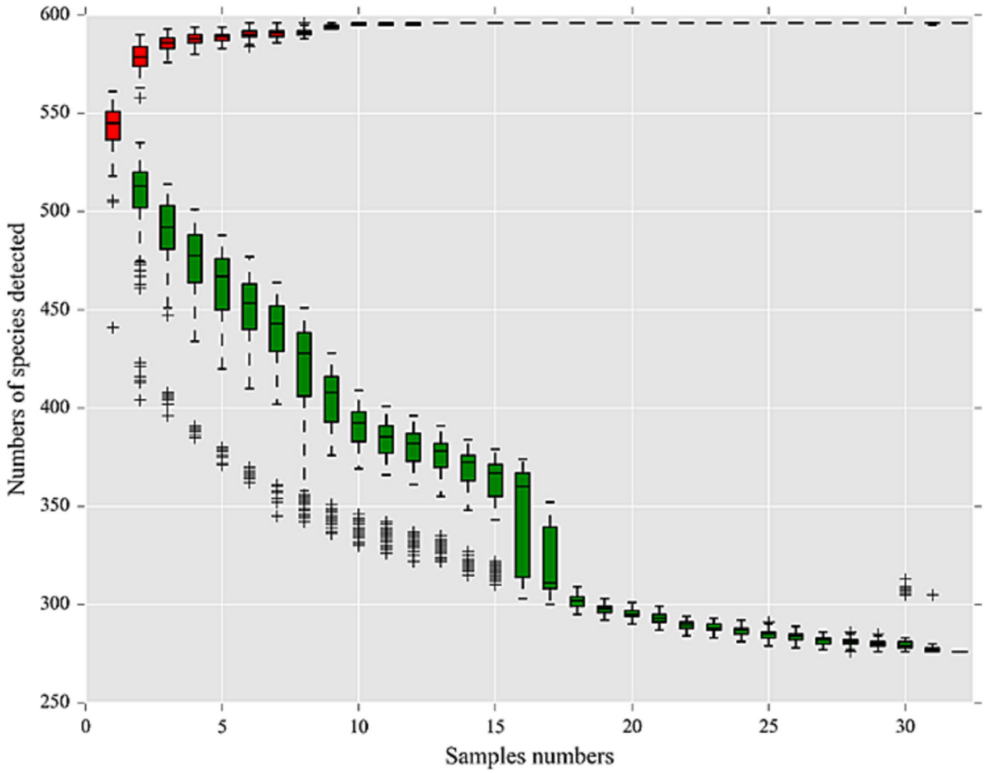

FIGURE 3
Species accumulation curve at genus level of 32 pools of *I. persulcatus*. Red boxes represent the accumulation curve of detected species numbers, and green boxes form the common curve of detected species numbers. When the curve tends to be flat, it means that the sample size is sufficient for the analysis.

Phylogenetic analysis

Phylogenetic tree based on *ompA* gene sequences of SFGR was shown in Figure 5. Of the 72 *I. persulcatus* positive for *Candidatus R. tarasevichiae*, all PCR amplicon sequences were identical (NMG-R1) and placed in a clade with *Candidatus R. tarasevichiae* from China (MN450410.2, MK576116.1). Two amplicon sequences (NMG-R102 and NMG-R105) detected in *D. silvarum* were closely related to strain Khabarovsk (AH015610.2, type strain of *R. raoultii*), and *R. raoultii* from China (KY474577.1 and MF511260.1). In particular, *R. slovaca* was detected in two individuals; both sequences were identical (H-R16) and clustered with strain 13-B (U43808.1, type strain of *R. slovaca*), and *R. slovaca* from China (MF002534.1), Russia (MT511330.1). In the phylogenetic tree based on *gltA* gene (Figure 6), 89 sequences amplified from *I. persulcatus* were identical (NMG-G1) and placed in a clade with *Candidatus R. tarasevichiae* from China (MN450396.2, JX996054.1). Two amplicon sequences (NMG-G102 and NMG-G105) detected in *D. silvarum* belonged to the same branch as *R. raoultii* from China (MF511250.1).

Seventeen *I. persulcatus* were positive for *B. garinii*. After removing duplicate sequences, the remaining 12 sequences were used to build the phylogenetic tree of *B. burgdorferi*. The 11 sequences were found to be closely related to strain 20047 (CP028861.1, type strain of *B. garinii*), *B. garinii* from China (JX888456.1, DQ156524.1, and HQ434240.1), and Russia (AM748051.1), another sequence (NMG-B49) was clustered with *B. garinii* (KY273110.1) from France. Similarly, 12 human blood samples were identified as positive for *B. garinii*, and all sequences were identical to each other (H-B1) and matched 100% with the sequences (NMG-B61) from *I. persulcatus* and *B. garinii* strain PD91 (HQ434240.1). We detected *B. afzelii* in seven *I. persulcatus* samples; two sequences (NMG-B12 and NMG-B50) fell into the same branch as strain VS461 (L30135.1, type strain of *B. afzelii*), *B. afzelii* from China (HQ434325.1) and Germany (MW489229.1) after the elimination of equal sequences (Figure 7).

Among the seven *I. persulcatus* samples positive for *B. miyamotoi*, all sequences were identical (NMG-M6) and closely related to strain HT31 (AB900798.1, type strain of *B. miyamotoi*), *B. miyamotoi* from China (KU749386.1), Japan (CP004217.2), and Russia (MK955928.1, KJ950108.1), which belong to the Siberian type (Figure 8).

In addition, the sequence (H-C74) detected in a blood sample fell into the same branch as strain Namibia belonging to genomic group IV (CP007555.1), *C. burnetii* from China (KR697576.1) (Figure 9).

Co-infection of pathogenic bacteria in ticks

In the present study, 27 *I. persulcatus* samples (27.00%, 27/100) were found to be co-infected with more than one bacterium (Table 3). Dual co-infection with *B. garinii* and *Candidatus R. tarasevichiae* (13.00%, 13/100) was most frequent in *I. persulcatus*. There was no co-infection in the participants according to PCR results.

10.3389/fpubh.2024.1302133

FIGURE 4
Relative abundances of top 10 microorganisms at the genus level in pooled *I. persulcatus* DNA samples.

TABLE 2 Prevalence of tick-borne bacteria in ticks and humans.

Bacteria	Target gene	*I. persulcatus* (n = 100)	*D. silvarum* (n = 13)	Humans (*n* = 245)
Candidatus R. tarasevichiae	ompA	72 (72.00%)	–	–
	gltA	89 (89.00%)	–	–
	Total	89 (89.00%)	–	–
R. raoultii	ompA	–	9 (69.23%)	–
	gltA	–	8 (61.54%)	–
	Total	–	9 (69.23%)	–
R. slovaca	ompA	–	–	2 (0.82%)
	gltA	–	–	–
	Total	–	–	2 (0.82%)
B. garinii	5S-23S rRNA IGS	17 (17.00%)	–	12 (4.90%)
B. afzelii	5S-23S rRNA IGS	7 (7.00%)	–	–
B. miyamotoi	glpQ	7 (7.00%)	–	–
burnetii	IS1111	–	–	1 (0.41%)

Seroprevalence of SFGR and *Borrelia burgdorferi*

Among the 245 serum samples, 14 were positive for anti-SFGR by ELISA, of which four were only positive for IgG and 10 were positive for IgM and IgG (Table 4). Both IgG and IgM antibodies against SFGR were negative in those 2 individuals who were detected positive for *R. slovaca* using PCR. Forty serum samples were seropositive for *B. burgdorferi* using IFA, and positive samples were further detected by WB; 33 of them were positive for anti-*B. burgdorferi* IgG (Table 4). The representative image of positive western blotting reactions was displayed in

10.3389/fpubh.2024.1302133

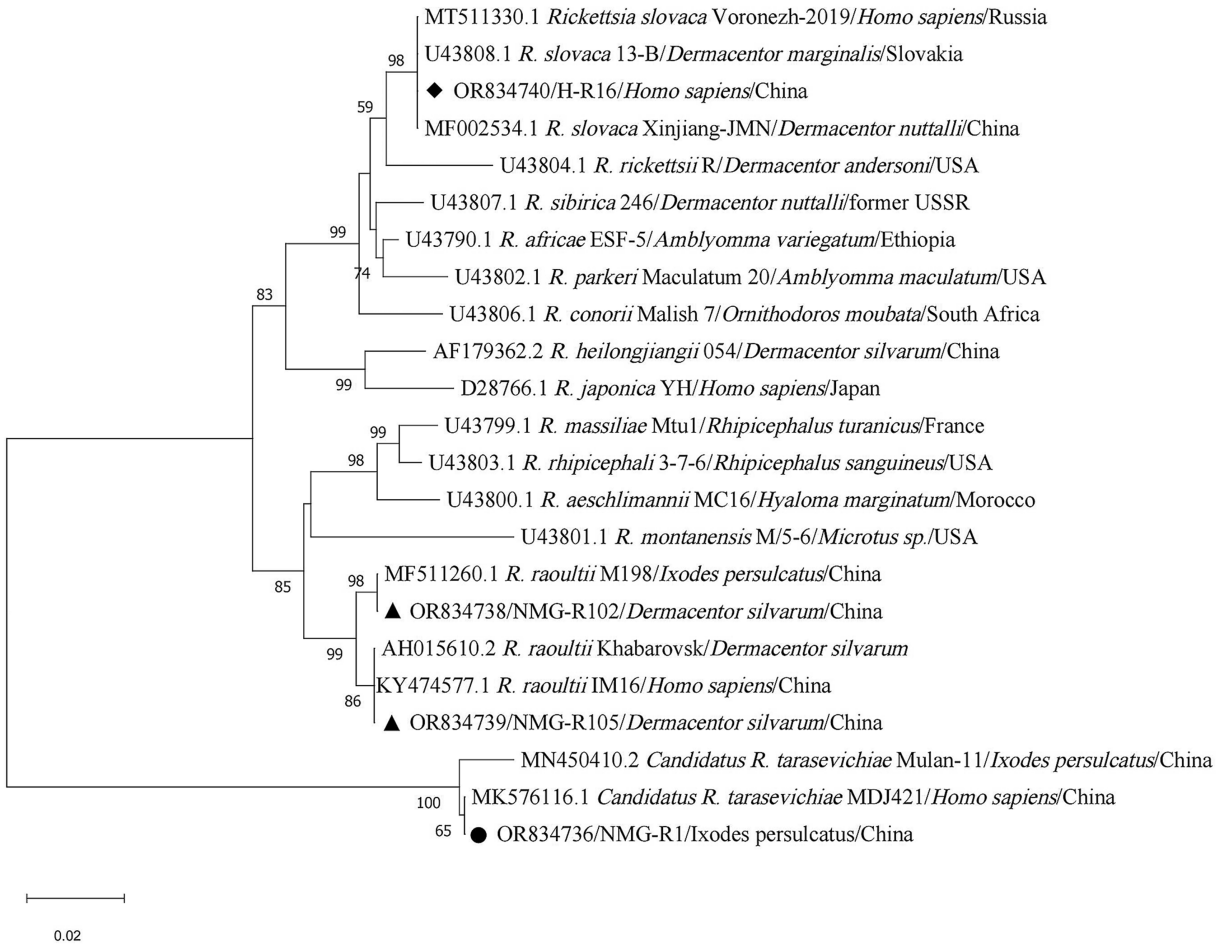

FIGURE 5
Phylogenetic analysis for *ompA* gene of SFGR. The sequences clustered as *Candidatus R. tarasevichiae* were marked as "●," *R. raoultii* were marked as "▲," *R. slovaca* were marked as "◆."

Additional file 5 (Supplementary Figure S1). Two serum samples were positive for both anti-*B. burgdorferi* IgG and anti-SFGR IgG.

No significant difference in the seroprevalence of antibodies against SFGR and *B. burgdorferi* according to sex, age, or workplace was observed (Table 5).

Discussion

Ticks are recognized as one of the most important vectors of a wide variety of diseases in humans and animals. In recent years, an increasing number of tick-borne infections have stimulated the investigation of ticks and tick-borne pathogens (31, 32). In this study, we applied 16S rDNA V3–V4 region high-throughput sequencing combined with species-specific PCR to detect tick-borne bacteria in free-living ticks and humans at high risk of tick-borne diseases in Arxan, Inner Mongolia, China. Subsequently, the seroprevalence of antibodies against SFGR and *B. burgdorferi* was determined to understand the infection rate of major tick-borne bacteria in the participants.

In this survey, the collected free-living ticks were mainly *I. persulcatus* with a small number of *D. silvarum*. Arxan City is located in northeastern China, which is mainly covered by coniferous and broad-leaved forests and is characterized by strong seasonality in temperature, providing a favorable habitat for *I. persulcatus*. The natural habitats of *D. silvarum* were characterized by middle to high elevations, shrub grasslands, and low precipitation during the driest month (2). In addition, we collected ticks in May 2020 and May 2021. The peak for *I. persulcatus* adults occurred in late May (33), while *D. silvarum* peaked in mid-April (34). Due to the limitation of the sampling season, sampling sites, and the number of ticks collected, only a small number of *D. silvarum* were collected.

High-throughput sequencing of 16S rDNA has been widely used to study microbial communities in ticks. For example, Runlsi et al. identified 189 genera in *Haemaphysalis longicornis* through high-throughput sequencing at the Illumina HiSeq platform, including *Anaplasma, Rickettsia*, and *Ehrlichia* (35). Jun et al. used high-throughput sequencing to study the microbial diversity of *D. nuttalli* and revealed the presence and relative abundance of the bacterial genera *Rickettsia*, *Anaplasma* and *Coxiella* (8). In the present study, at least 32 phyla, 79 classes, 191 orders, 348 families,

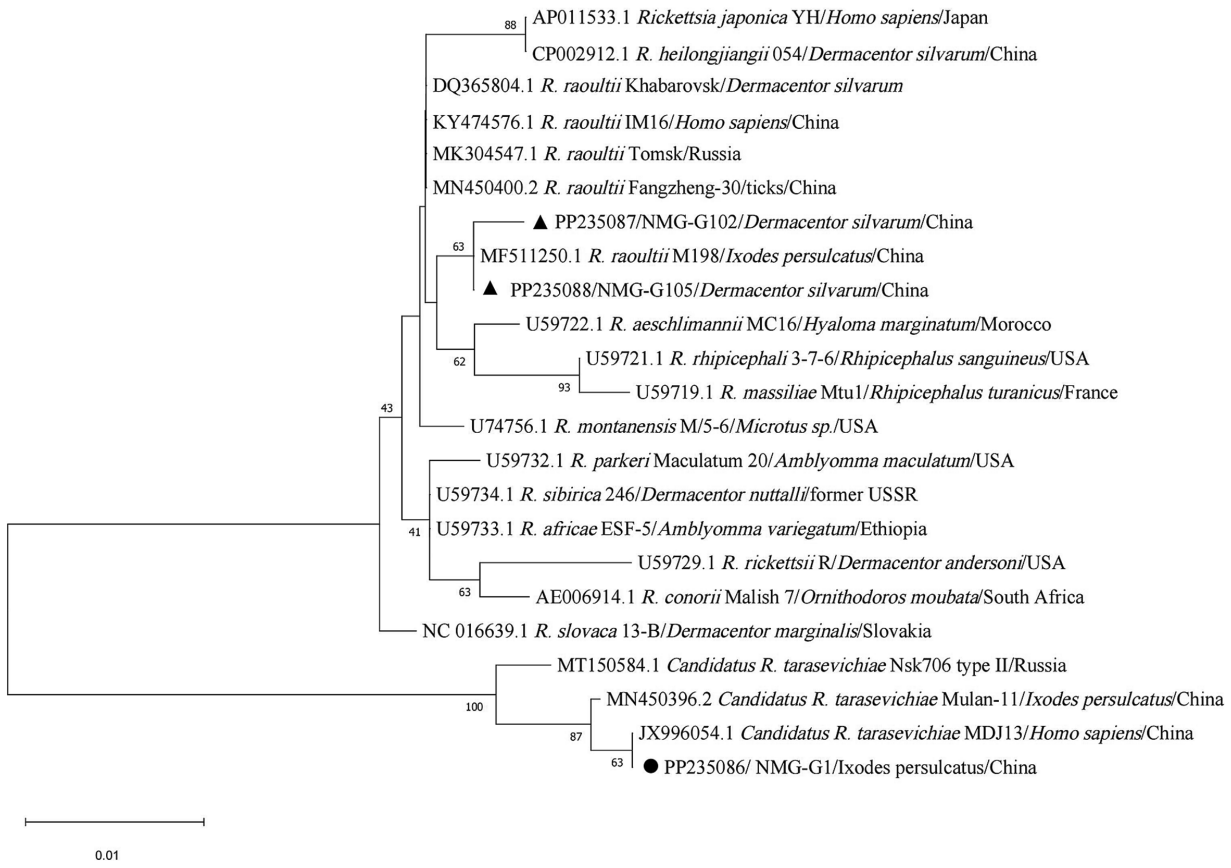

FIGURE 6
Phylogenetic analysis for *gltA* gene of SFGR. The sequences clustered as *Candidatus R. tarasevichiae* were marked as "●," *R. raoultii* were marked as "▲."

and 594 genera were detected in pooled DNA samples of *I. persulcatus*, and the Ace and Chao1 indices were more than 1068.34 and 1098.66, respectively, in each pool indicating that all pools were of highly species richness. Simpson indices were more than 0.85 except for N23 indicating that almost all pools were highly diverse. Of 594 genera, *Rickettsia*, *Anaplasma*, *Coxiella*, and *Borrelia*, were detected in pooled DNA samples of *I. persulcatus* through high-throughput sequencing of the 16S rDNA V3–V4 region, *Rickettsia* was recognized as the most common genus. *Candidatus R. tarasevichiae* and three *Borrelia* species (*B. garinii*, *B. afzelii* and *B. miyamotoi*) were identified in *I. persulcatus* by nested PCR, whereas only *R. raoultii* was detected in *D. silvarum*.

Candidatus R. tarasevichiae was first detected in *I. persulcatus* collected from the southern Urals and Siberia in 2003 (36) and was then found in *Haemaphysalis japonica* and *D. silvarum* from the Russian Far East (37, 38). Human cases of *Candidatus R. tarasevichiae* infection were first identified using laboratory molecular testing in eastern China in 2012 (39). In the present study, *Candidatus R. tarasevichiae* was detected in 89.00% of *I. persulcatus*, which was considered the dominant genotype of SFGR carried by *I. persulcatus* in Arxan.

Rickettsia solvaca was first isolated from *D. marginatus* ticks in Slovakia in 1968, and subsequent investigations reported that *R. solvaca* is widely distributed in *Dermacentor* ticks (40). Tian et al. firstly detected *R. slovaca* in *D. silvarum* collected from Xinjiang Autonomous Region, China in 2012 (41). In the present study, *R. slovaca* was detected in two participants using nested PCR targeting *ompA* gene. This is the first study to report the presence of *R. slovaca* has been found in humans in Inner Mongolia, China.

Rickettsia raoultii was first detected in *Dermacentor* ticks collected in Russia in 1999 (42) and then isolated from *Dermacentor* ticks in France, and named in 2008 (43). Similar to *R. slovaca*, *R. raoultii* was more common among *Dermacentor* ticks. Other hard ticks infected with *R. raoultii* have been reported by several groups in recent years, including the *Haemaphysalis*, *Hyalomma*, and *Ixodes* ticks (44–46). In this study, *R. raoultii* was detected in nine *D. silvarum* using nested PCR.

Candidatus R. tarasevichiae, *R. slovaca*, and *R. raoultii* were all pathogenic genotypes of spotted fever group Rickettsia. The SFG patients present with rashes, eschar, fever, fatigue, anorexia, nausea, and local lymph node enlargement. A few patients had neurological manifestations such as coma, neck stiffness, and Kernig's sign (47). Combined with the presence of anti-SFGR antibodies among participants, public health workers in the area need to be aware of the risk of SFGR infection; regularly conduct education campaigns on tick bite prevention; and monitor populations, ticks, and animal hosts.

10.3389/fpubh.2024.1302133

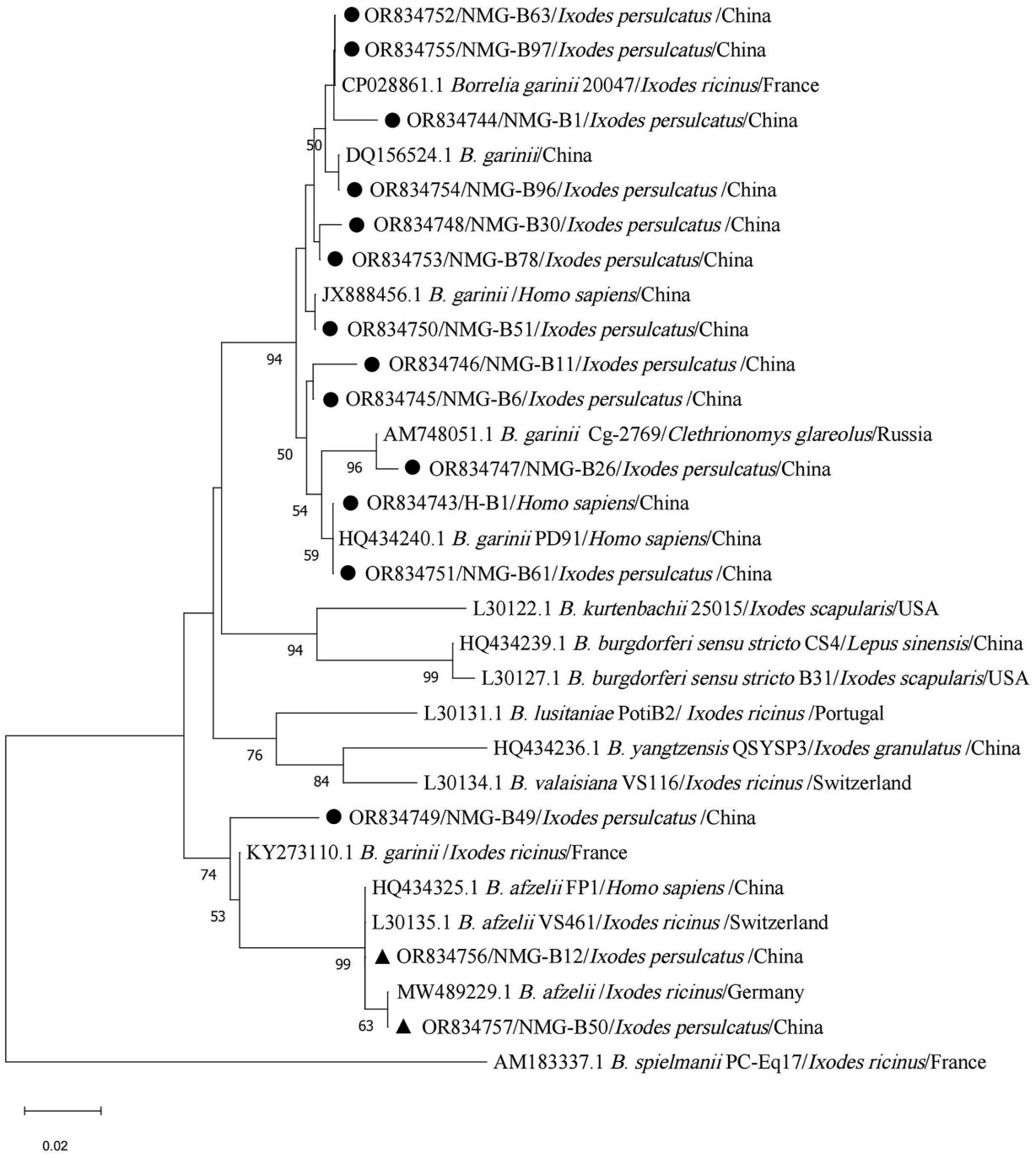

FIGURE 7
Phylogenetic analysis for 5S-23S rRNA intergenic spacer region of *B. burgdorferi sensu lato*. The sequences clustered as *B. garinii* were marked as "●," *B. afzelii* were marked as "▲."

Borrelia burgdorferi, first isolated from *I. persulcatus* in 1982 (48), was the causative pathogen of Lyme disease. In our previous study, two *B. garinii* strains were isolated from ticks in Arxan, suggesting that this area was the natural focus of Lyme disease (49). Through nested PCR targeting 5S-23S rRNA IGS, *B. garinii* was the dominant genotype of *B. burgdorferi* carried by *I. persulcatus* collected from Arxan, followed by *B. afzelii*, and the two genotypes were dominant causative genotypes of *B. burgdorferi* in China. We also detected *B. garinii* in 12 participants, and these 12 sequences were identical to the sequence (NMG-B61) detected in *I. persulcatus*, indicating the transmission of *B. garinii* from ticks to humans in Arxan. The positivity rate of anti-*B. burgdorferi* in participants was 13.47% based on the IFA results and confirmed by Western Blot assay, which was similar to the positive rate of forestry

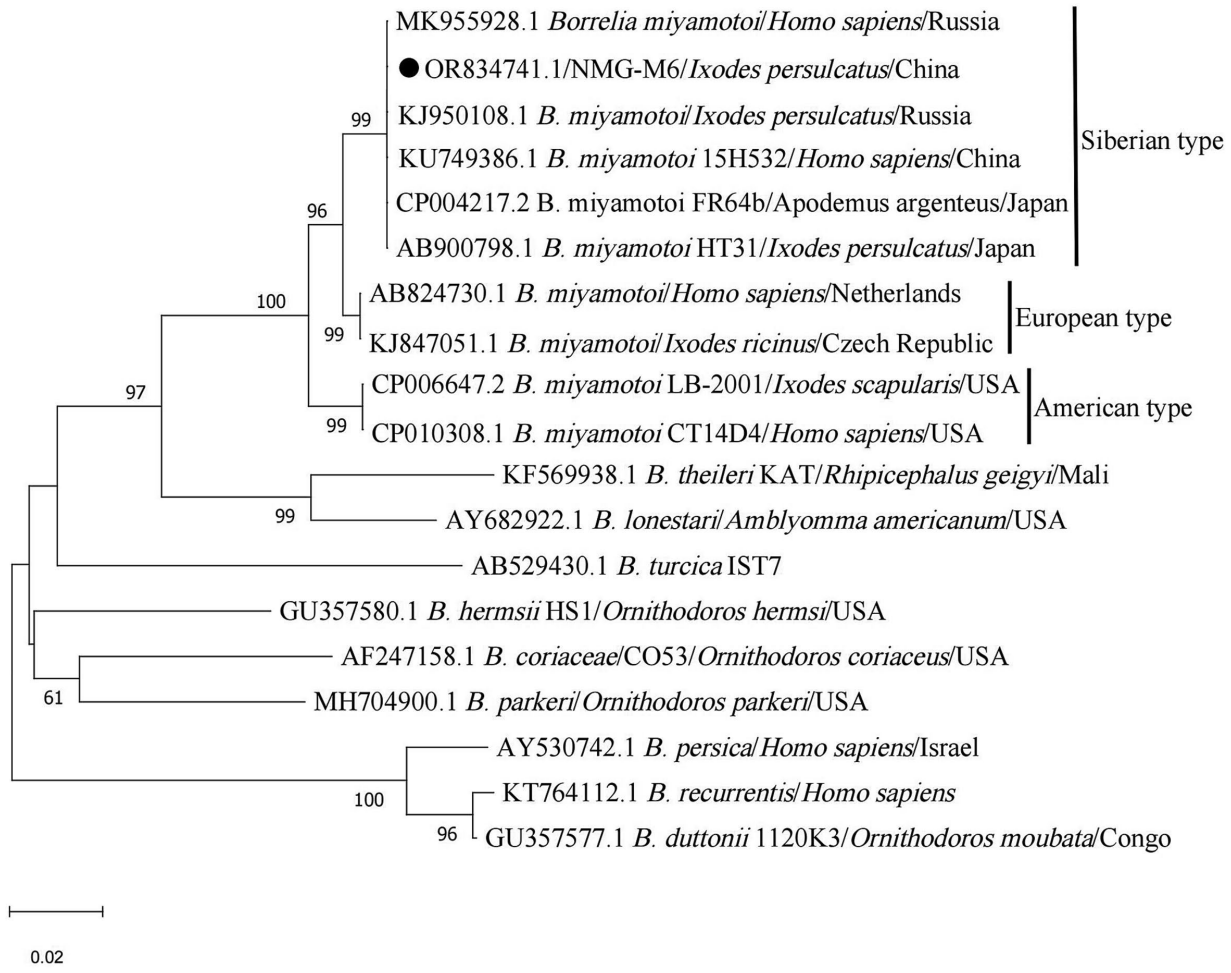

FIGURE 8
Phylogenetic analysis for *glpQ* gene of *B. miyamotoi*. The sequence clustered as *B. miyamotoi* was marked as "●."

populations in Inner Mongolia (15). Human Lyme disease generally occurs in stages, from the early localized stage of erythema migrans, fatigue, chills, and fever, to a late disseminated stage of intermittent bouts of arthritis with severe joint pain and swelling and neurological symptoms (29). Thus, Lyme disease should be considered by clinicians with the forestry workers who had correlated symptoms with Lyme disease in Arxan.

B. miyamotoi, initially identified and isolated in Japan in 1994 (50), is the causative agent of *B. miyamotoi* disease with generalized flu-like symptoms. Human cases of *B. miyamotoi* infection have been reported in European countries (51, 52), the United States (53, 54), Australia (55), and Japan (56). A survey of *B. miyamotoi* in Inner Mongolia suggested that 2.6% of *I. persulcatus* carried *B. miyamotoi* and 1.7% of patients bitten by ticks were infected with *B. miyamotoi* (57). In this study, *B. miyamotoi* which belongs to the Siberian type, was detected in 7% of *I. persulcatus*. This is the first report of this bacterium that has been detected in ticks from Arxan, indicating that local forestry populations are at risk of *B. miyamotoi* infection.

Coxiella burnetii, the causative agent of Q fever, is transmitted to humans via inhalation of infected aerosols or tick bites (58). In our study, *C. burnetii* was detected in one participant, indicating that extensive and in-depth monitoring of *C. burnetii* in ticks and animal hosts should be conducted to identify the risk of infection in the local population.

Ticks can acquire multiple pathogenic species during blood feeding on their vertebrate hosts, and humans may be infected by more than one pathogen carried by ticks. In this study, *Candidatus R. tarasevichiae* and *B. garinii* were the dominant pathogens detected in *I. persulcatus*, which, to some extent, explains why the rate of co-infection with *B. burgdorferi* and SFGR was the highest in *I. persulcatus*. Two participants tested positive for antibodies against both *B. burgdorferi* and SFGR, indicating that cases of coinfection with *B. burgdorferi* and SFGR were present in Arxan, Inner Mongolia. In recent years, concurrent infections with multiple tick-borne agents have been reported, including co-infection with *B. burgdorferi s.l* and *A. phagocytophilum* (59), *Babesia microti* and *B. burgdorferi s.l* (60), SFGR and severe fever with thrombocytopenia syndrome virus (61), etc. Pathogens may behave synergistically, indifferently, or antagonistically within common human hosts, thus prolonging the duration of symptoms and modulating disease severity (31). Additionally, the presence of concurrent infections may be neglected

10.3389/fpubh.2024.1302133

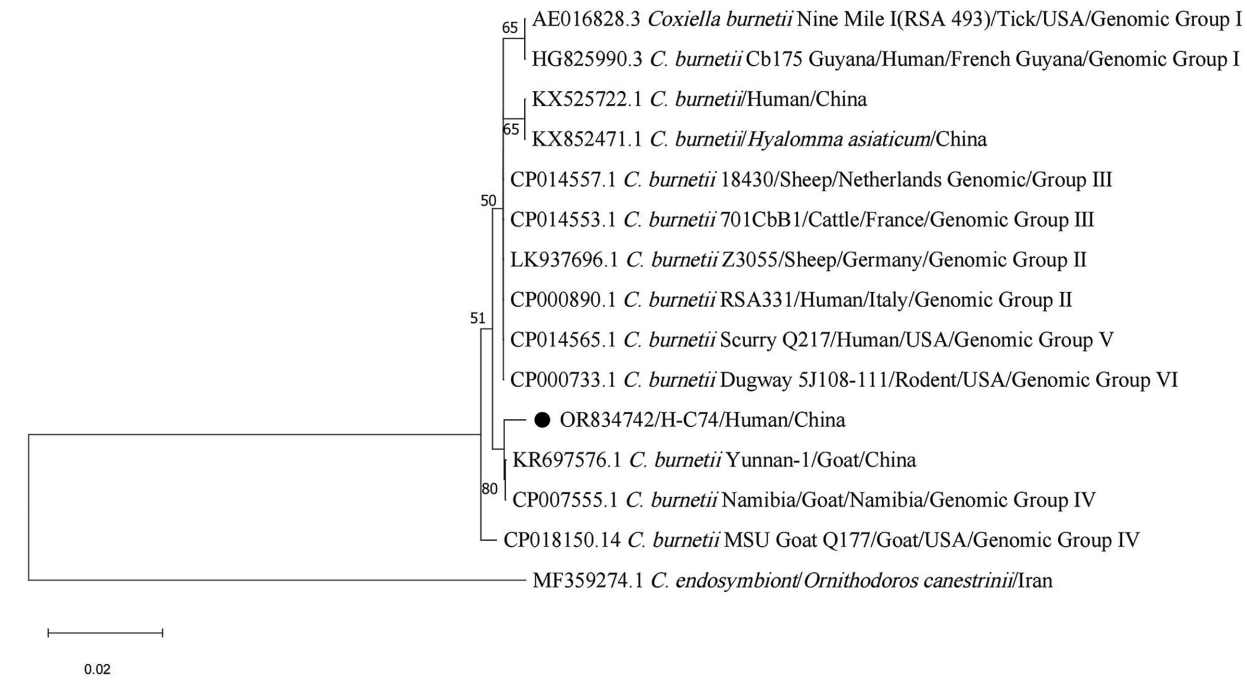

FIGURE 9
Phylogenetic analysis for *IS1111* gene of *C. burnetii*. The sequence clustered as *C. burnetii* was marked as "●."

TABLE 3 Prevalence of co-infection with tick-borne bacteria in *I. persulcatus*.

Bacteria	Number of ticks positive for co-infection (%)
Double	
B.garinii, Candidatus R. tarasevichiae	13 (13.00%)
B.afzelii, Candidatus R. tarasevichiae	7 (7.00%)
B.miyamotoi, Candidatus R. tarasevichiae	3 (3.00%)
Triple	
B.garinii, B.miyamotoi, Candidatus R. tarasevichiae	4 (4.00%)
Total	27 (27.00%)

TABLE 4 Seroprevalence of antibodies against *B. burgdorferi* and SFGR.

Antibody	Samples	*B. burgdorferi*		SFGR
		IFA	WB	ELISA
IgM	245	1 (0.41%)	–	–
IgG	245	38 (15.51%)	33 (13.47%)	4 (1.63%)
IgM and IgG	245	1 (0.41%)	–	10 (4.08%)
Total	245	40 (16.33%)	33 (13.47%)	14 (5.71%)

when multiple pathogens are encountered, which results in missed diagnoses and poses an additional challenge for a definitive diagnosis. Therefore, when treating patients with suspected tick-borne diseases, clinicians in this area should consider the possibility of coinfection. Long-term monitoring of tick-borne pathogens in ticks and humans should be investigated in the future.

TABLE 5 Differences in seroprevalence of antibodies against *B. burgdorferi* and SFGR according to sex, age, and workplace.

	No. tested	*B.burgdorferi*			SFGR		
		WB-Positive	Positive rate (%)	*p*	ELISA-Positive	Positive rate (%)	*p*
Sex							
Male	232	31	13.36	1.000	12	5.17	0.353
female	13	2	15.38		2	15.38	
Age							
21~	13	1	7.69	0.337*	–	–	0.202*
31~	27	3	11.11		4	14.81	
41~	51	11	21.57		2	3.92	
51~60	154	18	11.69		8	5.19	
Workplace							
Tianchi Forestry	21	3	14.29	0.628*	1	4.76	0.316*
Sandur Forestry	39	4	10.26		2	5.13	
Lixin Forestry	40	9	22.50		3	7.50	
Irsh Forestry	69	7	10.14		4	5.80	
Transportation Company	25	3	12.00		2	8.00	
Xing'an Service Area	22	4	18.18		4	18.18	
Jinjianggou Service Area	29	3	10.34		–	–	

*Fisher's exact text.

Data availability statement

The datasets presented in this study can be found in online repositories. The names of the repository/repositories and accession number(s) can be found at: [https://www.ncbi.nlm.nih.gov/ AND OR841358–OR841362 for *I. persulcatus*, OR841363–OR841367 for *D. silvarum*].

Ethics statement

The studies involving humans were approved by the ethics committee of National Institute for Communicable Disease Control and Prevention, Chinese Center for Disease Control and Prevention, Beijing, China. The studies were conducted in accordance with the local legislation and institutional requirements. The participants provided their written informed consent to participate in this study. The manuscript presents research on animals that do not require ethical approval for their study.

Author contributions

LD: Data curation, Formal analysis, Validation, Visualization, Writing – original draft. LZ: Investigation, Formal analysis. XH: Investigation, Methodology. ZB: Methodology. YZ: Investigation. LH: Methodology. ZL: Methodology. HZ: Supervision, Writing – review & editing. QH: Project administration, Supervision, Investigation, Formal analysis, Writing – original draft, Writing – review & editing. AD: Supervision, Writing – review & editing.

Funding

The author(s) declare financial support was received for the research, authorship, and/or publication of this article. This study was supported by the National Science and Technology Major Project of China (2017ZX10303404006003), an autonomous project for the National Institute for Communicable Disease Control and Prevention, Chinese Center for Disease Control and Prevention (32055), and operation of public health emergency response mechanism-prevention and control of infectious diseases (2100410029).

Acknowledgments

We thank the National Key Laboratory of Intelligent Tracking and Forecasting for Infectious Diseases, the National Institute for Communicable Disease Control and Prevention, and the Chinese Center for Disease Control and Prevention for their technical support. We would like to thank Editage (www.editage.cn) for English language editing.

Conflict of interest

The authors declare that the research was conducted in the absence of any commercial or financial relationships that could be construed as a potential conflict of interest.

Publisher's note

All claims expressed in this article are solely those of the authors and do not necessarily represent those of their affiliated organizations, or those of the publisher, the editors and the reviewers. Any product that may be evaluated in this article, or claim that may be made by its manufacturer, is not guaranteed or endorsed by the publisher.

Supplementary material

The Supplementary material for this article can be found online at: https://www.frontiersin.org/articles/10.3389/fpubh.2024.1302133/full#supplementary-material

References

1. Dantas-Torres F, Chomel BB, Otranto D. Ticks and tick-borne diseases: a one health perspective. *Trends Parasitol*. (2012) 28:437–46. doi: 10.1016/j.pt.2012.07.003

2. Zhao GP, Wang YX, Fan ZW, Ji Y, Liu M-J, Zhang W-H, et al. Mapping ticks and tick-borne pathogens in China. *Nat Commun*. (2021b) 12:1075. doi: 10.1038/s41467-021-21375-1

3. Al-Hosary A, Răileanu C, Tauchmann O, Fischer S, Nijhof AM, Silaghi C. Tick species identification and molecular detection of tick-borne pathogens in blood and ticks collected from cattle in Egypt. *Ticks Tick-Borne Diseases*. (2021) 12:101676. doi: 10.1016/j.ttbdis.2021.101676

4. Capligina V, Seleznova M, Akopjana S, Freimane L, Lazovska M, Krumins R, et al. Large-scale countrywide screening for tick-borne pathogens in field-collected ticks in Latvia during 2017–2019. *Parasit Vectors*. (2020) 13:351. doi: 10.1186/s13071-020-04219-7

5. Gilbert L. The impacts of climate change on ticks and tick-borne disease risk. *Annu Rev Entomol*. (2021) 66:373–88. doi: 10.1146/annurev-ento-052720-094533

6. Madison-Antenucci S, Kramer LD, Gebhardt LL, Kauffman E. Emerging tick-borne diseases. *Clin Microbiol Rev*. (2020) 33:e18. doi: 10.1128/CMR.00083-18

7. Gaowa W, Wulantuya , Sato K, Liu D, Cui Y, Yin X, et al. Surveillance of Borrelia miyamotoi-carrying ticks and genomic analysis of isolates in Inner Mongolia. *China Paras Vectors*. (2021) 14:368. doi: 10.1186/s13071-021-04809-z

8. Jiao J, Lu Z, Yu Y, Ou Y, Fu M, Zhao Y, et al. Identification of tick-borne pathogens by metagenomic next-generation sequencing in Dermacentor nuttalli and Ixodes persulcatus in Inner Mongolia. *China Parasit Vectors*. (2021) 14:287. doi: 10.1186/s13071-021-04740-3

9. Kong Y, Zhang G, Jiang L, Wang P, Zhang S, Zheng X, et al. Metatranscriptomics reveals the diversity of the tick Virome in Northwest China. *Microbiol Spect*. (2022) 10:e0111522. doi: 10.1128/spectrum.01115-22

10. Liu D, Wulantuya FH, Fan H, Li F, Li F, Gao T, et al. Co-infection of tick-borne bacterial pathogens in ticks in Inner Mongolia. *PLoS Negl Trop Dis*. (2023) 17:e0011121. doi: 10.1371/journal.pntd.0011121

11. Sun R. *Study on Spatiotenporal distribution of tick-borne encephalitis in China*. [dissertation/master's thesis]. Hefei (AH): Anhui Medical University (2016).

12. Black WC, Piesman J. Phylogeny of hard-and soft-tick taxa (Acari: Ixodida) based on mitochondrial 16S rDNA sequences. *Proc Natl Acad Sci USA*. (1994) 91:10034–8. doi: 10.1073/pnas.91.21.10034

13. De Keukeleire M, Robert A, Luyasu V, Kabamba B, Vanwambeke SO. Seroprevalence of Borrelia burgdorferi in Belgian forestry workers and associated risk factors. *Parasit Vectors*. (2018) 11:277. doi: 10.1186/s13071-018-2860-2

14. Stark JH, Li X, Zhang JC, Burn L, Valluri SR, Liang J, et al. Systematic review and Meta-analysis of Lyme disease data and Seropositivity for Borrelia burgdorferi, China, 2005–2020. *Emerg Infect Dis*. (2022) 28:2389–97. doi: 10.3201/eid2812.212612

15. Zhang Z, Wan K, Zhang J, Zhu G, Dou G, Li M, et al. Study on Epidemiology and Etiology of Lyme Disease in China. *Chin J Epidemiol*. (1997) 18:8–11.

16. Bolger AM, Lohse M, Usadel B. Trimmomatic: a flexible trimmer for Illumina sequence data. *Bioinformatics*. (2014) 30:2114–20. doi: 10.1093/bioinformatics/btu170

17. Callahan BJ, McMurdie PJ, Rosen MJ, Han AW, Johnson AJA, Holmes SP. DADA2: high-resolution sample inference from Illumina amplicon data. *Nat Methods*. (2016) 13:581–3. doi: 10.1038/nmeth.3869

18. Edgar RC. UPARSE: highly accurate OTU sequences from microbial amplicon reads. *Nat Methods*. (2013) 10:996–8. doi: 10.1038/nmeth.2604

19. Quast C, Pruesse E, Yilmaz P, Gerken J, Schweer T, Yarza P, et al. The SILVA ribosomal RNA gene database project: improved data processing and web-based tools. *Nucleic Acids Res*. (2013) 41:D590–6. doi: 10.1093/nar/gks1219

20. Bolyen E, Rideout JR, Dillon MR, Bokulich NA, Abnet CC, Al-Ghalith GA, et al. Reproducible, interactive, scalable and extensible microbiome data science using QIIME 2. *Nat Biotech*. (2019) 37:852. doi: 10.1038/s41587-019-0209-9.

21. Zhang L, Miao G, Hou X, Li B, Hao Q. Evaluation of nested PCR and real-time PCR in host surveillance of Lyme disease. *Chin J Vector Biol & Control*. (2018) 29:425–7. doi: 10.11853/j.issn.1003.8280.2018.05.001

22. Schwan TG, Schrumpf ME, Hinnebusch BJ, Anderson DE, Konkel ME. GlpQ: an antigen for serological discrimination between relapsing fever and Lyme borreliosis. *J Clin Microbiol*. (1996) 34:2483–92. doi: 10.1128/jcm.34.10.2483-2492.1996

23. Roux V, Fournier PE, Raoult D. Differentiation of spotted fever group rickettsiae by sequencing and analysis of restriction fragment length polymorphism of PCR-amplified DNA of the gene encoding the protein rOmpA. *J Clin Microbiol*. (1996) 34:2058–65. doi: 10.1128/jcm.34.9.2058-2065.1996

24. Socolovschi C, Mediannikov O, Sokhna C, Tall A, Diatta G, Bassene H, et al. Rickettsia felis-associated uneruptive fever. *Senegal Emerg Infect Diseases*. (2010) 16:1140–2. doi: 10.3201/eid1607.100070

25. Overzier E, Pfister K, Thiel C, Herb I, Mahling M, Silaghi C. Anaplasma phagocytophilum in questing Ixodes ricinus ticks: comparison of prevalences and partial 16S rRNA gene variants in urban, pasture, and natural habitats. *Appl Environ Microbiol*. (2013) 79:1730–4. doi: 10.1128/AEM.03300-12

26. Anderson BE, Sumner JW, Dawson JE, Tzianabos T, Greene CR, Olson JG, et al. Detection of the etiologic agent of human ehrlichiosis by polymerase chain reaction. *J Clin Microbiol*. (1992) 30:775–80. doi: 10.1128/jcm.30.4.775-780.1992

27. Dawson JE, Stallknecht DE, Howerth EW, Warner C, Biggie K, Davidson WR, et al. Susceptibility of white-tailed deer (Odocoileus virginianus) to infection with Ehrlichia chaffeensis, the etiologic agent of human ehrlichiosis. *J Clin Microbiol*. (1994) 32:2725–8. doi: 10.1128/jcm.32.11.2725-2728.1994

28. Fenollar F, Fournier PE, Raoult D. Molecular detection of Coxiella burnetii in the sera of patients with Q fever endocarditis or vascular infection. *J Clin Microbiol*. (2004) 42:4919–24. doi: 10.1128/JCM.42.11.4919-4924.2004

29. Zhang L, Zhu X, Hou X, Li H, Yang X, Chen T, et al. Prevalence and prediction of Lyme disease in Hainan province. *PLoS Negl Trop Dis*. (2021) 15:e0009158. doi: 10.1371/journal.pntd.0009158

30. Jiang Y, Wan K, Geng Z, Hou X. Standard criteria of Western blot for the diagnosis of Lyme disease caused by Borrelia garinii in China. *Chin J Microbiol Immunol*. (2005) 7:594–8. doi: 10.3760/j:issn:0254-5101.2005.07.020

31. Cutler SJ, Vayssier-Taussat M, Estrada-Peña A, Potkonjak A, Mihalca AD, Zeller H. Tick-borne diseases and co-infection: current considerations. *Ticks Tick-Borne Diseases*. (2021) 12:101607. doi: 10.1016/j.ttbdis.2020.101607

32. Rodino KG, Theel ES, Pritt BS. Tick-borne diseases in the United States. *Clin Chem*. (2020) 66:537–48. doi: 10.1093/clinchem/hvaa040

33. Xu S. *Studies on population ecology of Ixodes persulcatus and its infection with the tick-borne pathogens*. [dissertation/master's thesis]. Shijiazhuang (HB): Hebei Normal University (2015).

34. Yu Z. *Studies of population ecology of Dermacentor silvarum and antimicrobial Molecales of egg wax in Amblyomma hebraeum* [dissertation/master's thesis]. Shijiazhuang (HB): Heibei Normal University (2011).

35. Cao R, Ren Q, Luo J, Tian Z, Liu W, Zhao B, et al. Analysis of microorganism diversity in from Shaanxi, China, based on metagenomic sequencing. *Front Genet*. (2021) 12:723773. doi: 10.3389/fgene.2021.723773

36. Shpynov S, Fournier P-E, Rudakov N, Raoult D. Candidatus Rickettsia tarasevichiae in Ixodes persulcatus ticks collected in Russia. *Ann N Y Acad Sci*. (2003) 990:162–72. doi: 10.1111/j.1749-6632.2003.tb07358.x

37. Igolkina Y, Rar V, Vysochina N, Ivanov L, Tikunov A, Pukhovskaya N, et al. Genetic variability of Rickettsia spp. in Dermacentor and Haemaphysalis ticks from the Russian Far East. *Ticks Tick-Borne Diseases*. (2018) 9:1594–603. doi: 10.1016/j.ttbdis.2018.07.015

38. Mediannikov O, Sidelnikov Y, Ivanov L, Fournier PE, Tarasevich I, Raoult D. Far eastern tick-borne rickettsiosis: identification of two new cases and tick vector. *Ann N Y Acad Sci*. (2006) 1078:80–8. doi: 10.1196/annals.1374.010

39. Jia N, Zheng YC, Jiang JF, Ma L, Cao WC. Human infection with Candidatus Rickettsia tarasevichiae. *N Engl J Med*. (2013) 369:1178–80. doi: 10.1056/NEJMc1303004

40. Parola P, Paddock CD, Raoult D. Tick-borne rickettsioses around the world: emerging diseases challenging old concepts. *Clin Microbiol Rev*. (2005) 18:719–56. doi: 10.1128/CMR.18.4.719-756.2005

41. Tian ZC, Liu GY, Shen H, Xie J-R, Luo J, Tian M-Y. First report on the occurrence of Rickettsia slovaca and Rickettsia raoultii in Dermacentor silvarum in China. *Parasit Vectors*. (2012) 5:19. doi: 10.1186/1756-3305-5-19

42. Rydkina E, Roux V, Rudakov N, Gafarova M, Tarasevich I, Raoult D. New Rickettsiae in ticks collected in territories of the former Soviet Union. *Emerg Infect Dis*. (1999) 5:811–4. doi: 10.3201/eid0506.990612

43. Mediannikov O, Matsumoto K, Samoylenko I, Drancourt M, Roux V, Rydkina E, et al. Rickettsia raoultii sp. nov., a spotted fever group rickettsia associated with Dermacentor ticks in Europe and Russia. *Int J Syst Evol Microbiol*. (2008) 58:1635–9. doi: 10.1099/ijs.0.64952-0

44. Guo W-P, Wang Y-H, Lu Q, Xu G, Luo Y, Ni X, et al. Molecular detection of spotted fever group rickettsiae in hard ticks, northern China. *Transbound Emerg Dis*. (2019) 66:1587–96. doi: 10.1111/tbed.13184

45. Lu M, Ji Y, Zhao H, Wang W, Tian J, Duan C, et al. Circulation of multiple Rickettsiales bacteria in ticks from Sichuan province. *Southwest China Microbial Pathogenesis*. (2023) 183:106313. doi: 10.1016/j.micpath.2023.106313

46. Teng Z, Shi Y, Zhao N, Zhang X, Jin X, He J, et al. Molecular detection of tick-borne bacterial and protozoan pathogens in Haemaphysalis longicornis (Acari: Ixodidae) Ticks from free-ranging domestic sheep in Hebei Province, China. *Pathogens*. (2023) 12:763. doi: 10.3390/pathogens12060763

47. Fang L-Q, Liu K, Li X-L, Liang S, Yang Y, Yao H-W, et al. Emerging tick-borne infections in mainland China: an increasing public health threat. *Lancet Infect Dis*. (2015) 15:1467–79. doi: 10.1016/S1473-3099(15)00177-2

48. Burgdorfer W, Barbour AG, Hayes SF, Benach JL, Grunwaldt E, Davis JP. Lyme disease-a tick-borne spirochetosis? *Science*. (1982) 216:1317–9. doi: 10.1126/science.7043737

49. Duan LK, Hou XX, Zhang L, Bao ZH, Liu ZL, Shi QY, et al. Detection and genotyping of Borrelia burgdorferi from free-living ticks in Arxan area, Inner Mongolia. *China Chin J Vector Biol Control*. (2022) 33:642–7. doi: 10.11853/j.issn.1003.8280.2022.05.006

50. Fukunaga M, Takahashi Y, Tsuruta Y, Matsushita O, Ralph D, McClelland M, et al. Genetic and phenotypic analysis of Borrelia miyamotoi sp. nov., isolated from the ixodid tick Ixodes persulcatus, the vector for Lyme disease in Japan. *Int J Syst Bacteriol*. (1995) 45:804–10. doi: 10.1099/00207713-45-4-804

51. Hovius JWR, Wever B, Sohne M, Brouwer MC, Coumou J, Wagemakers A, et al. A case of meningoencephalitis by the relapsing fever spirochaete Borrelia miyamotoi in Europe. *Lancet*. (2013) 382:658. doi: 10.1016/S0140-6736(13)61644-X

52. Hrnková J, Golovchenko M, Musa AS, Needham T, Italiya J, Ceacero F, et al. Borrelia spirochetes in European exotic farm animals. *Front Vet Sci*. (2022) 9:996015. doi: 10.3389/fvets.2022.996015

53. Krause PJ, Narasimhan S, Wormser GP, Rollend L, Fikrig E, Lepore T, et al. Human Borrelia miyamotoi infection in the United States. *N Engl J Med*. (2013) 368:291–3. doi: 10.1056/NEJMc1215469

54. Xu G, Luo C-Y, Ribbe F, Pearson P, Ledizet M, Rich SM. Borrelia miyamotoi in human-biting ticks, United States, 2013–2019. *Emerg Infect Dis*. (2021) 27:3193–5. doi: 10.3201/eid2712.204646

55. Tobudic S, Burgmann H, Stanek G, Winkler S, Schötta A-M, Obermüller M, et al. Human Borrelia miyamotoi infection, Austria. *Emerg Infect Dis*. (2020) 26:2201–4. doi: 10.3201/eid2609.191501

56. Kumagai Y, Sato K, Taylor KR, Zamoto-Niikura A, Imaoka K, Morikawa S, et al. A relapsing fever group Borrelia sp. is widely distributed among wild deer in Japan. *Ticks Tick-Borne Diseases*. (2018) 9:465–70. doi: 10.1016/j.ttbdis.2017.12.016

57. Gao Y, Lv X-L, Han S-Z, Wang W, Liu Q, Song M. First detection of Borrelia miyamotoi infections in ticks and humans from the northeast of Inner Mongolia. *China Acta Tropica*. (2021) 217:105857. doi: 10.1016/j.actatropica.2021.105857

58. Melenotte C, Million M, Raoult D. New insights in Coxiella burnetii infection: diagnosis and therapeutic update. *Expert Rev Anti-Infect Ther*. (2020) 18:75–86. doi: 10.1080/14787210.2020.1699055

59. Moniuszko-Malinowska A, Dunaj J, Andersson MO, Chmielewski T, Czupryna P, Groth M, et al. Anaplasmosis in Poland – analysis of 120 patients. *Ticks Tick-Borne Diseases*. (2021) 12:101763. doi: 10.1016/j.ttbdis.2021.101763

60. Diuk-Wasser MA, Vannier E, Krause PJ. Coinfection by Ixodes tick-borne pathogens: ecological, epidemiological, and clinical consequences. *Trends Parasitol*. (2016) 32:30–2. doi: 10.1016/j.pt.2015.09.008

61. Zhao B, Hou H, Gao R, Tian B, Deng B. Mononucleosis-like illnesses due to co-infection with severe fever with thrombocytopenia syndrome virus and spotted fever group rickettsia:a case report. *BMC Infect Dis*. (2021a) 21:829. doi: 10.1186/s12879-021-06434-8

62. Zhang Z, Wan K, Zhang J, Zhu G, Dou G, Li M, et al. Study on epidemiology and etiology of Lyme disease in China. *Chin J Epidemiol*. (1997) 18:8–11.

frontiers | Frontiers in Cellular and Infection Microbiology

TYPE Original Research
PUBLISHED 13 August 2024
DOI 10.3389/fcimb.2024.1450353

OPEN ACCESS

EDITED BY
Deepak Kumar,
University of Southern Mississippi,
United States

REVIEWED BY
Ala E. Tabor,
The University of Queensland, Australia
Benjamin Cull,
University of Minnesota Twin Cities,
United States

*CORRESPONDENCE
Petr Kopáček
kopajz@paru.cas.cz

RECEIVED 17 June 2024
ACCEPTED 25 July 2024
PUBLISHED 13 August 2024

CITATION
Guizzo MG, Frantová H, Lu S, Kozelková T, Čížhalová K, Dyčka F, Hrbatová A, Tonk-Rügen M, Perner J, Ribeiro JM, Fogaça AC, Zurek L and Kopáček P (2024) The immune factors involved in the rapid clearance of bacteria from the midgut of the tick *Ixodes ricinus*. *Front. Cell. Infect. Microbiol.* 14:1450353. doi: 10.3389/fcimb.2024.1450353

The immune factors involved in the rapid clearance of bacteria from the midgut of the tick *Ixodes ricinus*

Melina Garcia Guizzo[1,2], Helena Frantová[1], Stephen Lu[2], Tereza Kozelková[1,3], Kristýna Čížhalová[4], Filip Dyčka[3], Alena Hrbatová[5], Miray Tonk-Rügen[6], Jan Perner[1], José M. Ribeiro[2], Andrea C. Fogaça[7], Ludek Zurek[4] and Petr Kopáček[1*]

[1]Institute of Parasitology, Biology Centre of the Czech Academy of Sciences, České Budějovice, Czechia, [2]Vector Biology Section, Laboratory of Malaria and Vector Research, National Institute of Allergy and Infectious Diseases (NIAID), Bethesda, MD, United States, [3]Faculty of Science, University of South Bohemia, Ceske Budejovice, Czechia, [4]Department of Microbiology, Nutrition and Dietetics/CINeZ, Czech University of Life Sciences, Prague, Czechia, [5]Central European Institute of Technology (CEITEC), University of Veterinary Sciences, Brno, Czechia, [6]Institute for Insect Biotechnology, Justus Liebig University of Giessen, Giessen, Germany, [7]Department of Parasitology, Institute of Biomedical Sciences, University of São Paulo, São Paulo, Brazil

Ticks are obligate hematophagous arthropods that transmit a wide range of pathogens to humans as well as wild and domestic animals. They also harbor a non-pathogenic microbiota, although our previous study has shown that the diverse bacterial microbiome in the midgut of *Ixodes ricinus* is quantitatively poor and lacks a core. In artificial infections by capillary feeding of ticks with two model bacteria (Gram-positive *Micrococcus luteus* and Gram-negative *Pantoea* sp.), rapid clearance of these microbes from the midgut was observed, indicating the presence of active immune mechanisms in this organ. In the current study, RNA-seq analysis was performed on the midgut of *I. ricinus* females inoculated with either *M. luteus* or *Pantoea* sp. or with sterile water as a control. While no immune-related transcripts were upregulated by microbial inoculation compared to that of the sterile control, capillary feeding itself triggered dramatic transcriptional changes in the tick midgut. Manual curation of the transcriptome from the midgut of unfed *I. ricinus* females, complemented by the proteomic analysis, revealed the presence of several constitutively expressed putative antimicrobial peptides (AMPs) that are independent of microbial stimulation and are referred to here as 'guard' AMPs. These included two types of midgut-specific defensins, two different domesticated amidase effector 2 (Dae2), microplusin/ricinusin-related molecules, two lysozymes, and two gamma interferon-inducible lysosomal thiol reductases (GILTs). The *in vitro* antimicrobial activity assays of two synthetic mature defensins, defensin 1 and defensin 8, confirmed their specificity against Gram-positive bacteria showing exceptional potency to inhibit the growth of *M. luteus* at nanomolar

concentrations. The antimicrobial activity of midgut defensins is likely part of a multicomponent system responsible for the rapid clearance of bacteria in the tick midgut. Further studies are needed to evaluate the role of other identified 'guard' AMPs in controlling microorganisms entering the tick midgut.

KEYWORDS

tick, Ixodes, midgut microbiome, immune system, antimicrobial peptide, defensin, *Micrococcus luteus*

Highlights

- The capillary feeding triggers dramatic transcriptomic changes in the midgut of unfed *Ixodes ricinus* females.
- Bacterial inoculation by capillary feeding does not induce upregulation of immune-related factors in the *I. ricinus* midgut.
- The immune-related factors are constitutively present in the midgut of unfed ticks and referred to as 'guard' AMPs,
- Midgut-specific defensins exert a strong antimicrobial activity against Gram-positive bacteria.

Introduction

The commensal gut microbiota may contribute to many aspects of a host biology including food digestion, nutrient production, defense against pathogens, and detoxification of harmful substances (Azambuja et al., 2005; Mcfall-Ngai et al., 2013). Arthropods are the largest phylum of all living organisms and exhibit a wide range of physiological dependence on the gut microbiome. In blood-feeding arthropods, the gut microbiome is usually abundant and stable and plays a critical role in vector physiology and vector competence (Azambuja et al., 2005; Caragata and Short, 2022; Pavanelo et al., 2023; Wang et al., 2023). For example, the gut microbiota of *Aedes aegypti* is required for normal fecundity and vector competence (Harrison et al., 2023) and *Rhodnius prolixus* has been shown to rely on gut microbes to reach adulthood (Gilliland et al., 2023). In contrast, ticks appear to be an exception. A poor and unstable bacterial microbiome in the midgut has been described for the genera *Ixodes*, *Amblyomma*, and *Rhipicephalus*, indicating that this trait is shared by all tick species (Ross et al., 2018; Guizzo et al., 2020; Pavanelo et al., 2020; Maldonado-Ruiz et al., 2021).

With the aim of manipulating the microbial abundance of the tick midgut, we previously artificially fed *Ixodes ricinus* females with Gram-positive (*Micrococcus luteus*) and Gram-negative bacteria (*Pantoea* sp.) isolated from the unfed female midgut. The organ could not be colonized as the bacteria were eliminated very quickly (Guizzo et al., 2022). This led us to hypothesize that bacterial clearance triggered in the midgut of unfed females is critical for maintaining the low microbial levels during blood feeding.

To decipher the factors responsible for controlling bacterial proliferation in the midgut of *I. ricinus* females, in the current study, schematically outlined in the Figure 1, we determined the differential expression of transcripts in response to inoculation with *M. luteus* or *Pantoea* sp. While the expression of immune transcripts was apparently not upregulated upon bacterial feeding, transcripts such as defensins, domesticated amidase effector 2 (dae2), and microplusin (ricinusin) were found to be highly expressed in the midgut of unfed females. We propose that these antimicrobial peptides (AMPs) act as guards of the tick midgut and contribute to control of invading microorganisms.

Materials and methods

Biological materials

Adult *I. ricinus* females were collected with a flag in a forest near České Budějovice, Czech Republic. Adult females were kept in humid chambers at 24°C, a relative humidity of ~95% and a day/night period of 15/9 hrs. and blood-fed on guinea pigs (*Cavia porcellus*). A pathogen-free laboratory colony of *I. ricinus* ticks was established from the laid eggs and underwent the entire developmental cycle (larvae, nymphs, adults) in the tick breeding facility of the Institute of Parasitology, Biology Centre CAS. All experimental animals were handled in accordance with the Animal Protection Law of the Czech Republic No. 246/1992 Sb., ethics approval No. 25/2020.

Capillary inoculation of ticks with bacteria

Unfed adult *I. ricinus* females from the pathogen-free laboratory colony described above were experimentally orally inoculated using the glass capillary with either *Pantoea* sp. (10^7 CFU/ml) or *M. luteus* (10^7 CFU/ml) previously isolated from the unfed midgut of *I. ricinus* females (Guizzo et al., 2022). As a control, the ticks were fed autoclaved tap water (uninoculated ticks). All ticks were fed for 1 hour at 28°C in a humid chamber. The volume

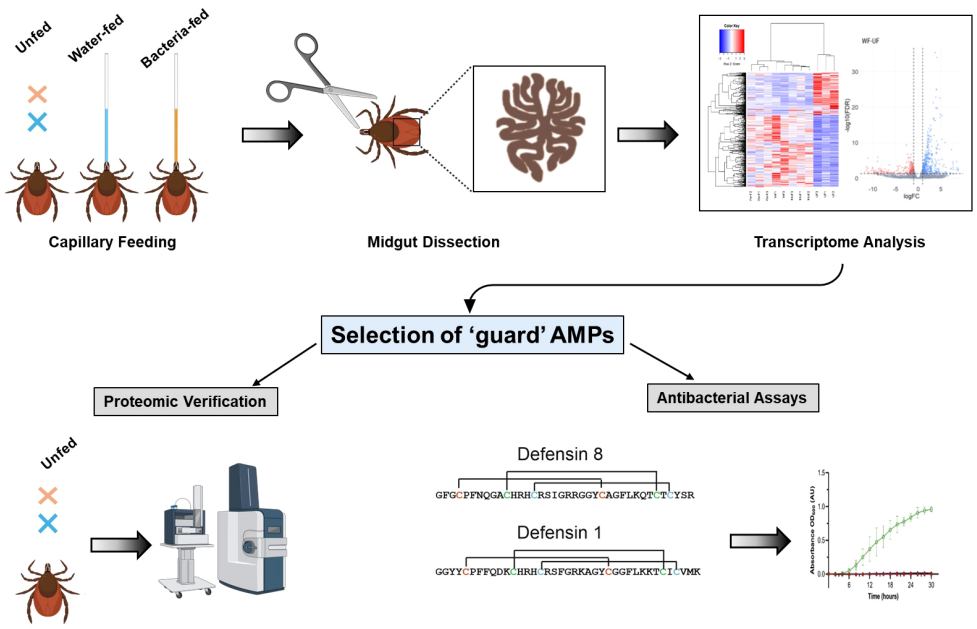

FIGURE 1
Workflow of the experiments conducted in this study. The midgut of ticks inoculated with bacteria or uninfected (feeding sterile water) and unfed ticks were dissected and submitted for RNA-seq analysis. Identification of transcripts encoding potential antimicrobial 'guard' peptides constitutively expressed in unfed ticks was verified by the proteomic analysis. The antimicrobial activity of two midgut-specific synthetic mature defensins was tested *in vitro* against selected Gram-positive and Gram-negative bacteria.

ingested by each tick was determined using a ruler and converted into the number of bacterial cells ingested per tick. A control group of unfed females was also included. Prior to dissection, ticks were washed with 0.05% sodium hypochlorite for 1 min, followed by 1 min in 70% ethanol and 3 consecutive washes in sterile water for 10 seconds each to prevent microbial contamination from the tick surface (Binetruy et al., 2019). Ticks were dissected and the total RNA was isolated from pools of 8 midguts per replicate using the NucleoSpin® RNA kit (Macherey-Nagel, USA) and eluted in 40 µl of RNAse-free water. The isolated RNA was quantified using a NanoDrop®ND-1000 spectrophotometer (Thermo Scientific, USA), and three independent biological replicates from each group were submitted for Illumina sequencing. Quality control of submitted RNA samples, construction of non-stranded cDNA libraries and Illumina reading of 150 bp paired ends were performed by Novagene Co., Ltd. as previously described in detail for the red poultry-mite RNAseq analysis (Ribeiro et al., 2023).

Transcriptome analysis

The quality of the raw Illumina reads obtained from the midgut of unfed, uninoculated, and inoculated *I. ricinus* females were inspected using the FastQC tool (https://www.bioinformatics.babraham.ac.uk/projects/fastqc). Illumina adaptors and low-quality sequences, specifically those with a Phred quality score (Q) below 20, were removed using the TrimGalore software (https://github.com/FelixKrueger/TrimGalore). Subsequently, the clean reads from all libraries were merged and subjected to *de novo* assembly using Trinity (2.9.0) (Grabherr et al., 2011) and ABySS (2.3.1) (Simpson et al., 2009). Sequences obtained from both assemblers were merged and the sequences that were at least 95% identical were consolidated using the CD-HIT software (Fu et al., 2012). Putative coding sequences (CDSs) were extracted based on the presence of a putative signal peptide or similarity to previously deposited sequences. All potential open reading frames (ORFs) of at least 175 nucleotides were extracted and blasted against several databases, including a subset of the non-redundant protein database from NCBI(NR), UNIPROTKB, refseq-vertebrate and a tick-specific database (TSF) (Ribeiro and Mans, 2020). CDSs were extracted if they had a coverage of 70% or more for a matching protein. In parallel, all ORFs starting with a methionine and at least 40 amino acids long were submitted to the signalP (3.0) software (Bendtsen et al., 2004). Sequences containing a putative signal peptide were assigned to ORFs, and the methionine codon closest to the 5' terminal was selected as the start codon of the transcript. The relative quantification of each CDS was estimated using the transcript per million (TPM) parameter by mapping the trimmed Illumina reads to the final list of CDSs using RSEM software (Li and Dewey, 2011). To assess the quality of our *de novo* assembly and the CDS extraction pipeline, we used the benchmark of the universal single-copy ortholog (BUSCO) with the Arachnida database (Seppey et al., 2019). For functional annotation and differential expression analysis, we extracted CDSs with an average TPM of at least 5 in one of the biological conditions (unfed, uninfected or infected). The CDSs were blasted against multiple databases (subset of the NR database, UNIPROTKB, Enzyme Committee (EC), MEROPS, CDD, KOG, PFAM, SMART, and TSF) and assigned

to specific functional classes, including their coverage and identity scores, using an *in-house* program that scans a vocabulary (~400 words) and the order of occurrence in the proteins matched from the BLAST results. The annotated CDSs were exported to a Windows-compatible, hyperlinked Excel file, available for download (see Data Availability below, Supplementary File 1).

Proteomic analysis of midguts from unfed *I. ricinus* females

Midguts of unfed *I. ricinus* females were dissected on a drop of ice-cold phosphate-buffered saline (PBS) and transferred to a microtube and stored at −80°C until further use. Proteomic analysis was performed in triplicates, using 10 midguts per sample. Samples were homogenized in 200 µL of 50 mM Na-phosphate buffer, pH 7.5, supplemented with 7 M urea, 2 M thiourea, 2% CHAPS and Halt™ protease inhibitors (Thermo Fisher Scientific) and then 10 µg of proteins were digested in solution with trypsin (Pierce Trypsin Protease, MS Grade, Thermo Fisher Scientific) as described previously (Kozelkova et al., 2023). After desalting using the Stage tips solid phase C18 disc (Empore), peptides were subjected to NanoLS ESI/MS/MS analysis performed on an UltiMate™ 3000 RSLCnano system (Thermo Fisher Scientific) coupled online to the timsTOF Pro mass spectrometer (Bruker Daltonics) (Kozelkova et al., 2023). The data were analyzed using the MaxQuant software (version 1.6.14) with the integrated search engine Andromeda (Cox and Mann, 2008). The databases of *I. ricinus* and the guinea pig (08. 06. 2021 and 28.07.2021, respectively) available in the Uniprot and the contaminant database included in the MaxQuant software were used for protein identification. Data analysis parameters and label-free quantification (LFQ) algorithms were applied as described by (Kozelkova et al., 2023). LFQ intensity values were log2 transformed in Perseus software (version 1.6.14.0 (Tyanova et al., 2016)). Contaminants, host proteins, and proteins identified in only one of the three replicates were excluded from further analysis.

Defensin sequences and synthetic peptides

Defensin 1 [corresponding to the prepro-defensin 1 according to the recently published annotation of the *I. ricinus* genome (Cerqueira De Araujo et al., 2024)] was previously identified as encoded by the transcript Ir-113775, which is upregulated in the later phase of tick feeding, as revealed by a transcriptomic analysis of *I. ricinus* midgut (Perner et al., 2016). The sequence of the mature defensin 1 is GGYYCPFFQDKCHRHCRSFGRKAGYCG GFLKKTCICVMK (Mw 4.491 Da). The three predicted disulfide bridges connect the cysteine residues C5-C26, C12-C34 and C16-C36. The defensin encoded by the transcript seqSigP-776440 in the midgut transcriptome of unfed *I. ricinus* females (current study) corresponds to prepro-defensin 8 (Cerqueira De Araujo et al., 2024). The sequence of the mature defensin 8 is GFGCPFNQ GACHRHCRSIGRRGGYCAGFLKQTCTCYSR (Mw 4.194 Da) with a disulfide bridge pattern linking C4-C24, C11-C32 and C15-C34. Mature defensins 1 and 8 with targeted cross-linking of cysteine residues were synthesized, purified and analyzed by HPLC and mass spectrometry by Pepmic Co., Ltd (Suzhou, China) with a declared purity >90% and delivered as a lyophilized powder.

Antibacterial assays

Staphylococcus aureus (CCM 4223), *Staphylococcus epidermidis* (CCM 7221), *Pseudomonas aeruginosa* (CCM 3955), and *Escherichia coli* (D31) were obtained from the Czech Collection of Microorganisms, Faculty of Science, Masaryk University in Brno, Czech Republic. *Micrococcus luteus* and *Microbacterium maritypicum* were isolated from the midgut of *I. ricinus* (Guizzo et al., 2022) on Tryptic Soy Agar (TSA) (Sigma Aldrich, USA) and stored at -80°C in the cryo-medium. The bacterial strains were cultured on TSA at 37°C overnight, diluted in Mueller Hinton (MH) broth (Sigma Aldrich, USA) to OD_{600} = 0.1 AU, and then diluted 100× to reach the cell density 1–2 × 10^6 CFU/mL.

One-millimolar stock solutions of the synthetic mature defensins 1 and 8 were prepared in sterile distilled water. Assays were performed as previously described (Tonk et al., 2015). Briefly, 10 µL of the peptide stock solutions were serially diluted 2-fold in MH medium to which bacteria suspensions adjusted to an initial OD_{600} = 0.005 or OD_{600} = 0.05 for *M. luteus* were added. The concentrations of synthetic defensins tested ranged from 250 µM to 8 nM. Bacterial growth was monitored at 30°C by reading the OD_{600} every 20 min for 48 h (orbital shaking) on the Eon™ Microplate Spectrophotometer (BioTek Instruments, VT, USA). As a positive control, bacteria were cultured without defensins. The measured OD_{600} of the negative control (MH medium alone) was subtracted from the absorbance values as a background. All measurements were performed in independent triplicates.

Effect of the reduction of the disulfide bridges of defensins on the growth inhibition of *M. luteus*

Ten microliters of 1 mM solutions of the synthetic mature defensin 1 or 8 were mixed with 10 µL of 20 mM dithiothreitol (DTT) and heated to 75°C. After 5 min, the solutions were spun down, diluted 5-fold in MH medium (to a final concentration of 100 µM for peptides and 2 mM for DTT) and used as stock solutions for the antibacterial assay. Untreated peptides, DTT-treated peptides or DTT only were serially diluted 2-fold in MH medium to which a suspension of *M. luteus* (OD_{600} = 0.05) was added. The peptide concentrations tested ranged from 25 µM to ~ 0.8 nM and from 500 µM to 15 nM for DTT alone. Bacteria were incubated at 30°C and the growth was measured discontinuously from 24 h to 64 h using a Tecan M200 Infinite Pro Microplate Reader (Tecan, Austria).

Statistical analysis

Differential expression analysis of a putative CDS was performed using the edgeR package (Robinson et al., 2010) for R. The expression of a CDS was considered statistically different if a log2(fold change) was greater than 1 or less than -1 and the false discovery rate (FDR) was less than 0.05. The volcano plot was generated using the *ggplot2* package for R.

Data availability

The transcriptome data were deposited to the National Center of Biotechnology and Information (NCBI) under the BioProject PRJNA685402, with the BioSamples SAMN17086831 - SAMN17086834. The raw Illumina reads were submitted to the Sequence Reads Archives (SRA) under accessions SRR13257934 – SRR13257945. The putative CDS were submitted to the Transcriptome Shotgun Assembly (TSA) under the accession GIYG00000000. The Supplementary File 1 can be downloaded from the following link: https://proj-bip-prod-publicread.s3.amazonaws.com/transcriptome/Iricinus/InfectedMg/Supplementary_file_1.zip. The mass spectrometry proteomics data from tick hemolymph were deposited to the ProteomeXchange Consortium via the PRIDE partner repository PXD053128.

Results

Overview of the transcriptome data of the midgut of *I. ricinus*

Illumina sequencing of 12 libraries from the midgut of unfed, uninoculated (water fed), and inoculated *I. ricinus* yielded a total of 461,359,915 high-quality reads. These reads were assembled *de novo*, resulting in 679,580 putative transcripts. Alignment of the trimmed Illumina reads to these transcripts yielded consistent alignment rates across all libraries, averaging 29.2% ± 1.1%, with the exception of one water fed tick (sample WF2), which had a significantly lower mapping rate of 8.86% and was excluded from further analysis. The putative CDSs were extracted with a minimum TPM value of 5 in at least one biological condition, resulting in a final set of 17,185 putative CDS (Supplementary File 1). The quality of *de novo* assembly and CDS prediction by BUSCO showed that our current dataset has a high overall quality with a completeness of 73.1%, which is consistent with previous RNA-seq analyses of the tick midgut (Lu et al., 2023, 2024).

Initial data exploration through dimensional analysis revealed that all biological samples clustered well within their respective biological groups, except for uninoculated (water fed, WF) sample WF2 (Figure 2A). This outlier in combination with the strikingly low mapping rates indicates a significant sequencing bias in this sample. Therefore, we decided to exclude this sample from our study. Furthermore, our dimensional analysis revealed two prominent clusters that distinguished between unfed and fed ticks. Remarkably, despite the exposure to Gram-positive and Gram-negative bacteria, the transcriptional profile of inoculated ticks strongly resembled that of the uninoculated (WF) ticks.

Hierarchical clustering of the 17,185 putative transcripts illustrated the congruence among our biological replicates and the transcriptional coherence within our artificially fed samples (Figure 2B). In particular, a biphasic pattern emerged between fed and unfed ticks, with transcripts that were abundant in unfed ticks being downregulated in fed samples and *vice versa*. This pattern emphasizes the onset of feeding as the primary stimulus for transcriptional changes in the tick midgut and confirms the success of capillary feeding as a method to artificially infect ticks.

Furthermore, the differential expression analysis revealed 683 modulated CDSs between uninoculated (WF) and unfed (UF) ticks (Figure 2C). In contrast, we observed a limited number of CDSs differentially expressed between *M. luteus* (Mic) and uninoculated (WF) ticks (17 CDSs) or between *Pantoea* sp. (Pan) and uninoculated (WF) ticks (10 CDSs). Notably, none of the 27 modulated CDSs between bacteria inoculated and uninoculated ticks (WF) were included in the Immunity class (Supplementary File 1). However, we observed several CDSs of antimicrobial peptides in the midgut of unfed ticks (Supplementary File 1). In total, these CDSs accounted for 2.7% of the total (Figure 3).

Potential antimicrobial 'guard' peptides in the midgut of unfed females

The rapid clearance of bacteria from the midgut of *I. ricinus* (Guizzo et al., 2022) combined with the results of differential transcriptome analysis prompted us to search the midgut of unfed females for transcripts encoding proteins and peptides known in the literature to exert antimicrobial (bacteriolytic or bacteriostatic) activity in ticks (Fogaça et al., 2021). These included the small (~ 4 kDa) cationic peptides defensins ((Wu et al., 2022)), Dae-2 (Chou et al., 2015; Hayes et al., 2020), cysteine- and histidine-rich microplusins (ricinusin) (Fogaca et al., 2004; Lai et al., 2004), and c-type lysozymes (Kopacek et al., 1999; Simser et al., 2004; Tanaka et al., 2010). In addition to these well-characterized molecules, we also found the homologue of a glycine-rich acanthoscurrin from the tarantula spider that has been reported to be active against *E. coli* (Gram-negative) and the yeast *Candida albicans* (Lorenzini et al., 2003). Finally, we turned our attention to the putative gamma-interferon-inducible lysosomal thiol reductase (GILT), which is known to exert a function in MHC class II-restricted antigen processing in mammals (West and Cresswell, 2013) and has been shown to be involved in innate immunity in *Drosophila* and the malaria mosquito vector *Anopheles gambiae* (Kongton et al., 2014; Schleicher et al., 2018; Yang et al., 2020). These transcripts were reproducibly and consistently present in the midgut of unfed females (Table 1), with TPM levels unaffected by bacterial or sterile water capillary feeding (Supplementary File 1).

To confirm the presence of the potential 'guard' AMPs in the unfed midgut of females and to shed the light on other proteins that may serve as 'guard' defense molecules against ingested environmental bacteria, a semiquantitative label-free proteomic analysis was performed. A total of 920 proteins were identified in

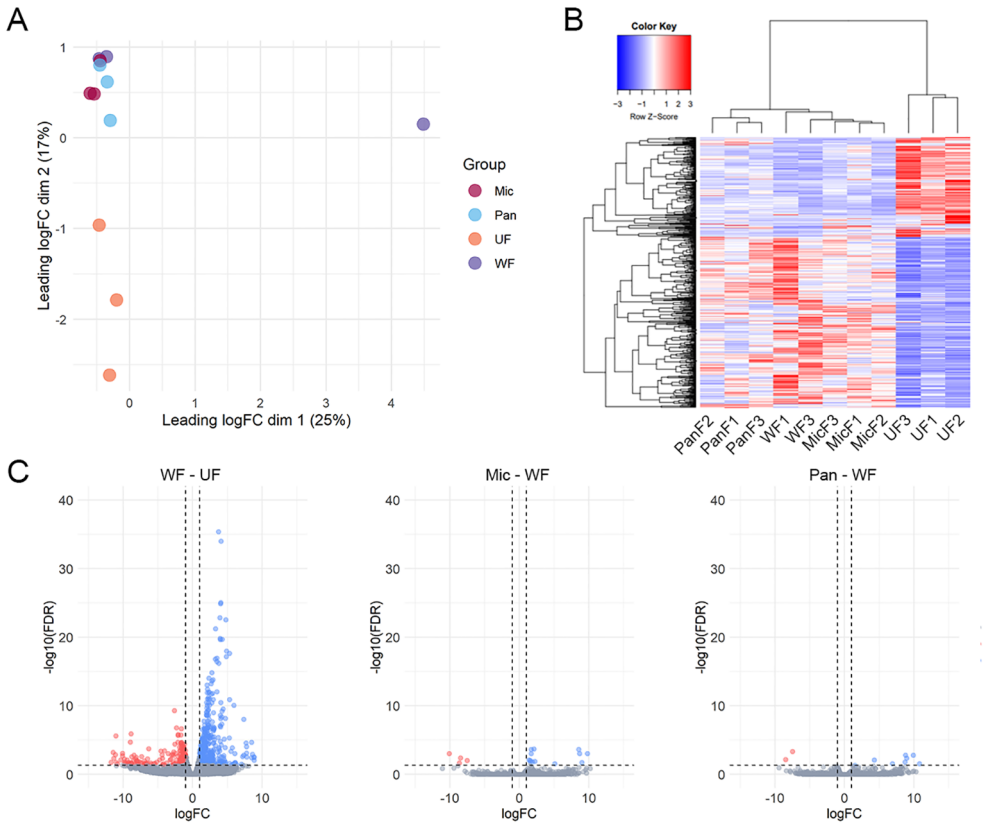

FIGURE 2
Overview of *I. ricinus* midgut RNA-sequencing. **(A)** Multidimensional plot based on the transcripts that presented an average TPM value ≥ 5 in at least one biological condition, unfed (UF), artificially fed with water (WF), *Pantoea* (Pan) or *M. luteus* (Mic). **(B)** Heatmap plot using the normalized TPM values of each transcript. PanF1,2,3 – *Pantoea* sp. – fed (inoculated); WF1,3 – water fed (uninoculated); MicF1,2,3 – *M. luteus* fed (inoculated); UF1,2,3 – unfed. **(C)** Volcano plots highlighting the differentially expression transcripts identified between the pairwise comparisons between uninoculated (water fed, WF) and unfed (UF), *M. luteus*-inoculated ticks (Mic) and WF or *Pantoea*-inoculated ticks and WF. Transcripts were considered differentially expressed when a LogFC (FC – fold change) higher than 1 or lesser than -1 (vertical line) alongside an FDR (False Discovery Rate) < 0.05 (horizontal line) was found. Upregulated transcripts are shown as blue dots, downregulated transcripts as red dots and non-differentially expressed transcripts as gray dots.

three independent biological replicates. After filtering step, a total of 689 proteins (host and ticks) remained, among which the 650 *I. ricinus*–specific proteins were used for further analysis (Supplementary Excel Table S2). From the 10 CDSs of 'guard' AMPs identified in the midgut of unfed females, the presence of 5 was confirmed by proteomic analysis (Table 1). In addition to the RNA-seq dataset, proteomic analysis revealed the presence of another form of defensin, named defensin 1 (Table 1), which has previously been found to be expressed in the midgut of *I. ricinus* during the later stages of feeding (Perner et al., 2016).

Gene expression of potential 'guard' antimicrobial peptides

The transcript seqSigP-776440, which encodes defensin 8 [according to the recent annotation of the *I. ricinus* genome (Cerqueira De Araujo et al., 2024)], was among the most abundantly expressed immune CDSs in the midgut of unfed *I. ricinus* (Supplementary File 1). In addition, its encoded protein (V5IGJ0) was detected in the midgut of all groups of ticks examined (Table 1). Although no transcript encoding defensin 1 [Ir-113775 (GenBank JAP75178) (Perner et al., 2016)] was identified, the abundance of its encoded protein Q7YXK5 was relatively high in the midgut of unfed females (Table 1). The sequences of *I. ricinus* defensins 8 were compared with selected closely related homologs of other hard tick species (Supplementary Figure S1). The signature residue for these types of defensin is the tyrosine next to the C-terminal cysteine residue, whereas the C-terminal motif for defensin 1 is CVMK (Supplementary Figure S1).

Another highly abundant transcript [Irseq_658490 (Table 1)] identified in the midgut of unfed ticks encodes an ortholog of *I. scapularis* Dae-2 (GenBank B7PLT0.2), which has recently been characterized as the effector molecule that protects the tick from infections with commensal bacteria on the host skin, e.g. Gram-positive *Staphylococcus epidermidis* (Hayes et al., 2020). The blastp search revealed the presence of a different, much less expressed form of Dae-2 (named Dae-2 type2) in the transcriptome of *I. ricinus*, encoded by the transcript Irseq_1462568 (Table 1). Orthologs of the dae-2 type2 form were only found in the closely related tick species *I. scapularis* and *I. persulcatus* (Supplementary Figure S2), but not in other hard ticks. While the protein (A0A131Y7K5) encoded by the

10.3389/fcimb.2024.1450353

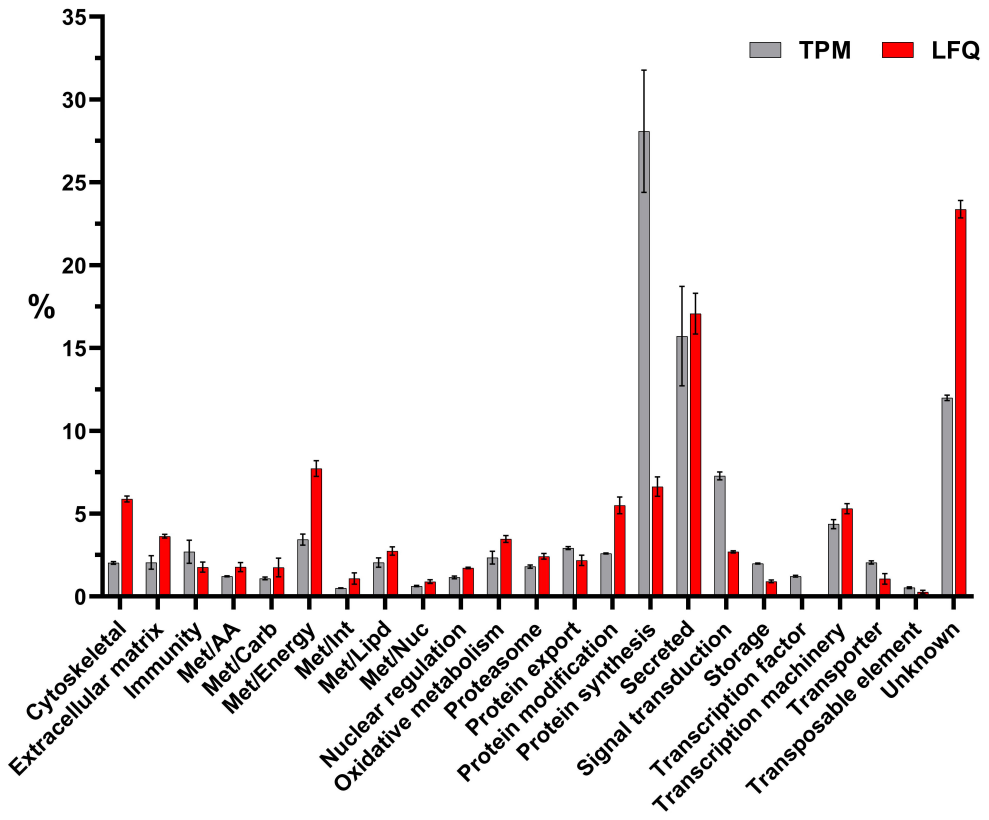

FIGURE 3
Functional classification of transcripts (in gray) or proteins (in red) identified in the midguts of unfed *I. ricinus* females by transcriptomic and proteomic analysis, respectively. Bars represent the average TPM (transcript per million) or LFQ (label-free quantification) percentage values for each class, while error bars represent the standard deviation of the mean.

TABLE 1 Antimicrobial peptides in the unfed female midgut of *Ixodes ricinus* identified by transcriptomic and proteomic analysis.

Transcript/ protein name	Transcript ID	GenBank Access. No.	UF1 TPM	UF2 TPM	UF3 TPM	Protein-Uniprot Access. No.	Group 1 Log2 LFQ	Group2 Log2 LFQ	Group 3 Log2 LFQ
Defensin 8	seqSigP-776440	MBK3725883.1	2332,86	4663,32	195,98	V5IGJ0	17.99	18.95	14.45
Defensin 1	nd	JAP75178.1	-	-	-	Q7YXK5	19.23	19.69	18.04
Dae2-type1	Irseq_658490	MBK3726561.1	4197,98	4682,16	2256,61	A0A131Y7K5	15.27	15.78	14.86
Dae2-type2	Irseq_1462568	MBK3727421.1	148,94	48,27	16,71	nd	-	-	-
Microplusin/ Ricinusin	Irseq_818892	MBK3728589.1	557,27	267,62	517,72	A0A6B0UTF6	18.26	18.23	17.18
Microplusin - type 2	Irseq_1035813	MBK3730421.1	21,51	41,08	77,71	nd	-	-	-
c-type lysozyme 1	seqSigP-924189	MBK3722801.1	476,02	1616,31	393,08	nd	-	-	-
Lysozyme-like	Irseq_1030185	MBK3725204.1	7,71	20,79	1,67	nd	-	-	-
Acanthoscurrin-like	seqSigP-1078729	MBK3720576.1	28,89	13,84	37,66	nd	-	-	-
GILT	Irseq_909409	MBK3726697.1	812,9	658,04	435,1	A0A0K8RMQ6	15.83	15.01	14.03
GILT-like	seqSigP-678986	MBK3724106.1	883,2	1035,0	1088,6	V5HBD3	15.44	15.05	14.92

nd, not detected.

Dae2 type1 transcript (Irseq_658490) was present in homogenates from unfed midgut, the Dae2 type2 protein was not detected, probably due to its low expression.

Several transcripts detected in the midgut of unfed *I. ricinus* were annotated as microplusins, as they encode histidine-rich proteins with a conserved pattern of cysteine residues to the characterized microplusin from the cattle tick *Rhipicephalus microplus* (Fogaca et al., 2004) or hebraein from *Amblyomma hebraeum* (Lai et al., 2004). These molecules are ubiquitously expressed in a variety of tick tissues and can be broadly categorized into two main groups based on their amino acid sequences: (i) type1 ricinusins and (ii) type2 microplusins (Urbanova et al., 2024). The group of ricinusins is represented by the transcript Irseq_818892 and microplusins by the much less expressed transcript Irseq_1035813 (Table 1). Orthologs of both types are found in the genome of *I. scapularis*, but with relatively low similarity to the original *R. microplus* microplusin (GenBank AAO48942.1) (Supplementary Figure S3). In line with their expression (TPM values), only the type1 ricinusin (A0A6B0UTF6) was detected in the unfed midgut by proteome analysis (Table 1).

Another dominantly expressed transcript (seqSigP-924189) in unfed midgut encodes an invertebrate c-type lysozyme (type1). On the other hand, expression of the related c-type lysozyme-like type2 (transcript Irseq_1030185) was marginal (Table 1). While distinct orthologs of the type1 lysozyme were found in a variety of hard tick species, the type2 ortholog was only identified in *I. scapularis* (Supplementary Figure S4). However, none of these lysozyme isoforms were detected at the protein level in the midgut of ticks (Table 1).

The *I. ricinus* transcript seqSigP-1078729 was annotated as acanthoscurrin, according to its identical *I. scapularis* ortholog acanthoscurrin 2-like (GenBank XP_029824929.2). However, despite the C-terminal glycine-rich motifs, the relationship with the characterized AMP from the tarantula spider (Lorenzini et al., 2003) is questionable (Supplementary Figure S5).

Several studies as well as our unpublished data from ticks indicate a possible role of GILT-related molecules in invertebrate immunity (Kongton et al., 2014; Zhou et al., 2017; Schleicher et al., 2018; Yang et al., 2020). The GILT transcript Irseq_909409 was very abundant in the midgut of unfed *I. ricinus* and its encoded protein (A0A0K8RMQ60) was clearly detected in midgut homogenates (Table 1). The orthologs of *I. ricinus* GILT with a well-conserved active site and GILT signature motifs are present in a variety of tick species, although their overall sequence similarity to other characterized invertebrate GILTs (Kongton et al., 2014; Zhou et al., 2017; Schleicher et al., 2018; Liu et al., 2019) is rather low (Supplementary Figure S6). In addition, the transcript seqSigP-678986, which encodes a GILT-related protein (V5HBD3) orthologous to the GILT-like protein 1 of *I. scapularis* (GenBank XP_042145453.1), was also highly abundant in the midgut transcriptome and proteome of unfed ticks (Table 1; Supplementary Figure S6).

Antimicrobial activity of midgut defensins

We selected two midgut defensins to evaluate their potential as 'guard' AMPs. The antimicrobial activity of the synthetic mature defensins 1 and 8 was tested against four Gram-positive bacteria (*M. luteus, Staphylococcus aureus, S. epidermidis, Microbacterium maritypicum*) (Figure 4) and two Gram-negative bacterial strains (*Pseudomonas aeruginosa* and *E. coli*) (not shown). Both defensins inhibited the growth of all Gram-positive bacteria in a low concentration range of 0.008 μM to 1.95 μM; however, did not show any activity against the two Gram-negative bacteria at the highest concentration (250 μM) tested (Table 2).

Since both peptides were highly effective in inhibiting *M. luteus* up to the lowest tested concentration (8 nM), the assay was repeated with lower concentrations. A minimum inhibitory activity (MIC) in the nanomolar range for the mature defensin 1 and the defensin 8, specifically 30 nM and 6 nM, respectively, was determined (Table 2). We also investigated the effect of disulfide bridge reduction on the MIC of defensins after their treatment with DTT. Reduction of the disulfide bridges significantly increased the MIC of the mature defensin 1 by ~100-fold (MIC of 3 μM), but had no effect on the activity of the mature defensin 8, which retained the same MIC of 6 nM (Table 2) in its oxidized form. Importantly, DTT alone had no effect on the growth of *M. luteus* at the highest concentration tested (500 μM).

Discussion

Tick midgut is a primary site for interactions with ingested microbes, including pathogens that ticks transmit (Hajdusek et al., 2013). Despite the fact that microbes in the tick midgut environment appear to have optimal conditions for their proliferation, as the blood is nutrient-rich, extracellular proteases are absent, and the pH is neutral (Sojka et al., 2013), the opposite is true, and the midgut of several tick species has been described as close to sterile (Ross et al., 2018; Guizzo et al., 2020; Pavanelo et al., 2020; Maldonado-Ruiz et al., 2021). In the previous study, we have shown that both, Gram-positive (*M. luteus*) and Gram-negative (*Pantoea* sp.), bacteria are rapidly dramatically reduced in the midgut of unfed *I. ricinus* after experimental inoculation by the capillary feeding (Guizzo et al., 2022). This result suggests that this effective antibacterial response is crucial for maintaining low microbial levels in the tick gut. However, it was not clear whether the immediate response in the tick midgut is triggered rapidly or whether the tick has a constitutive guard immune system ready to eliminate the encountered bacteria. To investigate factors that may be responsible for this apparent refractoriness to bacterial proliferation, we analyzed the transcriptome of the midgut of unfed females challenged with either *M. luteus* or *Pantoea* sp. or sterile water by capillary feeding and compared it to that of midguts of unfed ticks that had not been treated at all. The transcriptome of ticks that ingested sterile water and bacteria-containing water drastically changed compared to that of unfed ticks; however, no clear upregulation of immune-related transcripts was observed. These results suggested that the antimicrobial factors responsible for the rapid bacterial clearance in the tick midgut, referred to as 'guard' AMPs, are expressed constitutively. Therefore, we focused our attention to the expression of transcripts encoding known AMPs (Kopacek et al., 2010; Hajdusek et al., 2013; Fogaça et al.,

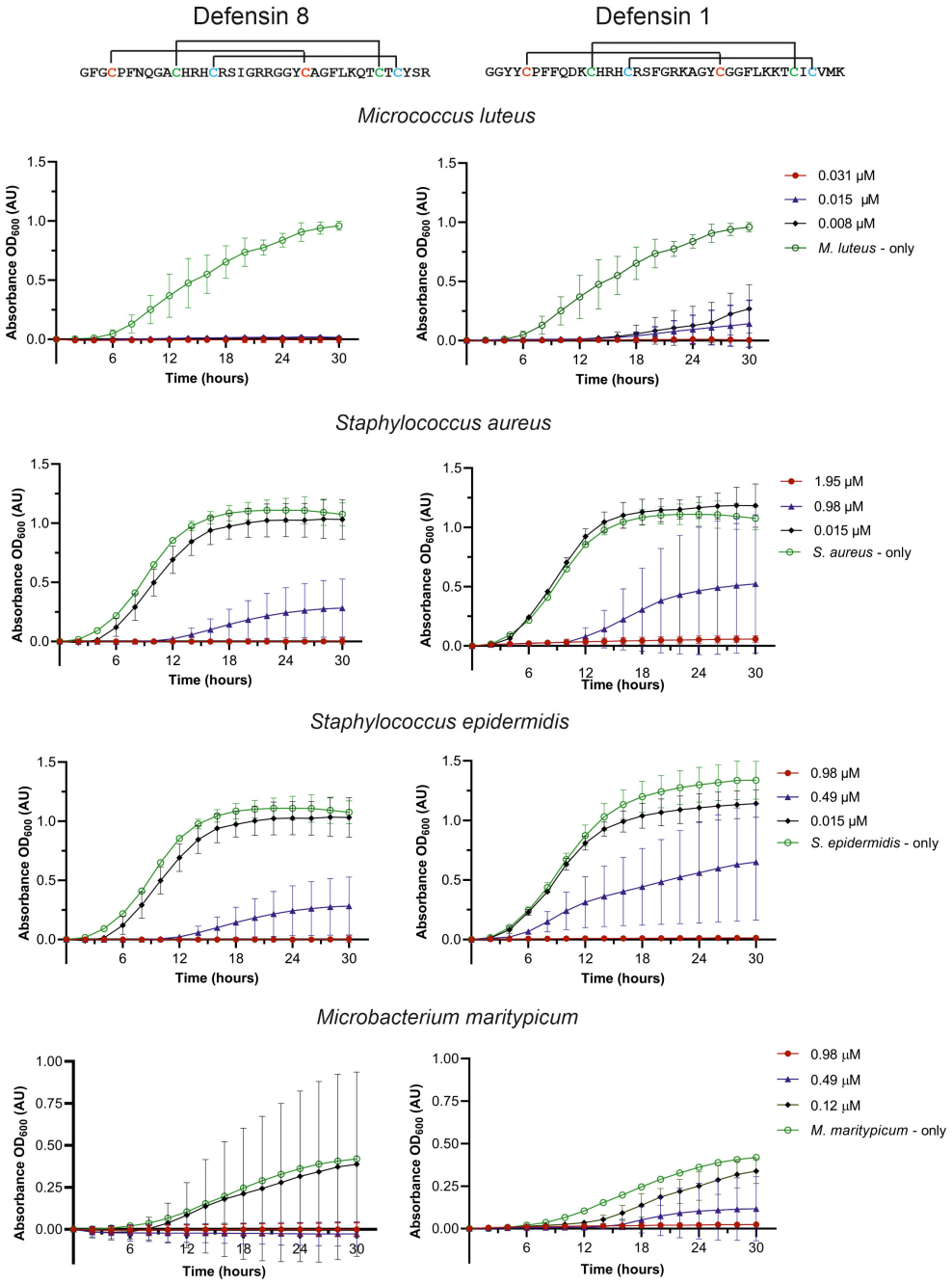

FIGURE 4
Effect of the synthetic mature defensin 1 and 8 on the inhibition of bacterial growth. Control bacterial growth curves (without defensins) are shown in green, at the minimum inhibitory concentration (MIC) needed for 100% inhibition in red, at the highest concentration with no inhibition in black, and at the concentration in the range of about 50% inhibition in blue.

2021). Among the potential 'guard' AMPs, we identified the abundantly expressed defensin 8, which is annotated as the prepro-defensin 8 in the genome of *I. ricinus* (Cerqueira De Araujo et al., 2024). This defensin was not previously found in any tissue-specific transcriptome of *I. ricinus* (including salivary glands, hemocytes, fat body or midgut (Schwarz et al., 2013; Kotsyfakis et al., 2015; Perner et al., 2016, 2018; Urbanova et al., 2024). However, close orthologs of *I. ricinus* defensin 8 have already been described in other hard ticks, such as persulcatusin from the taiga tick *Ixodes persulcatus* (Saito et al., 2009), longicin from *Haemaphysalis longicornis* (Tsuji et al., 2007), and holosins from the Australian paralysis tick *Ixodes holocyclus* (Cabezas-Cruz et al., 2019)(Supplementary Figure S1). Proteomic analyses confirmed the presence of the mature defensin 8 in the midgut adult *I. ricinus* females (this study) as well as in nymphs in the early stages of their feeding (Kozelkova et al., 2023). The recently published longitudinal transcriptomic analysis of the midgut of *I. scapularis*, ranging from unfed to fully engorged and detached females (Lu et al., 2023)

10.3389/fcimb.2024.1450353

TABLE 2 Bacterial growth inhibition assays by synthetic mature defensins and the effect of S-S bridges reduction by treatment with DTT.

Bacterial species	Minimum inhibitory concentration			
	Defensin 1 (mature)	Defensin 8 (mature)	Defensin 1 (mature) DTT – treated	Defensin 8 (mature) DTT – treated
M. luteus	0.031 µM (0.56 µg/mL)	0.008 µM (0.13 µg/mL)	3.0 µM (54 µg/mL)	0.006 µM (0.1 µg/mL)
S. aureus	1.95 µM (35 µg/mL)	1.95 µM (33 µg/mL)		
S. epidermidis	0.98 µM (18 µg/mL)	0.98 µM (16 µg/mL)		
M. maritypicum	0.98 µM (18 µg/mL)	0.49 µM (8 µg/mL)		
E. coli	>250 µM (>4500 µg/mL)	>250 µM (>4500 µg/mL)		
P. aeruginosa	>250 µM (>4500 µg/mL)	>250 µM (>4500 µg/mL)		

revealed the presence of several defensin isoforms (annotated as 4 kDa defensins or defensin-like isoforms), all closely related to *I. ricinus* defensin 8. The XP_040070918.2 isoform is abundantly expressed in unfed *I. scapularis* females with TPM values comparable to those of *I. ricinus* in this study (Table 3). Similar to *I. ricinus*, no transcript encoding an ortholog of defensin 1 was found in the *I. scapularis* midgut transcriptome (Table 3). Defensin 1 with the characteristic C-terminal motif CVMK is encoded by the duplicated genes prepro-defensin 1 and prepro-defensin 3 (Cerqueira De Araujo et al., 2024). The identical defensin molecule, designated def1 (GenBank AAP94724), was previously identified among the molecules induced in *I. ricinus* females by blood feeding (Rudenko et al., 2005). It was later reported to be expressed mainly in the tick midgut and active against Gram-positive bacteria (Chrudimska et al., 2011). In addition to the expression of the defensin 1 in the midgut of engorged *I. ricinus* females (Perner et al., 2016), an identical transcript was also identified in the transcriptome of the salivary glands of *I. ricinus* (Schwarz et al., 2013). Accordingly, the mature defensin-1 peptide was identified by the proteomics analyses in the midgut of nymphs (Kozelkova et al., 2023) and unfed females (this study) as well as in the salivary glands of *I. ricinus* (Bensaoud et al., 2022).

Another putative 'guard' AMP of *I. ricinus* midgut is Dae-2 (Hayes et al., 2020). This antimicrobial effector molecule, first described in *I. scapularis* (Dae2^{Is}), is present in the saliva and in the midgut and has been shown to eliminate Gram-positive bacteria such as *S. epidermidis* at a physiologically relevant concentration of 2 µM. The RNA interference (RNAi) silencing of Dae2^{Is} significantly increased the load of *Staphylococcus* in comparison to that of the control. In addition, the injection of specific anti-Dae2^{Is} antibodies via the anal pore increased the levels of *S. epidermidis* in the midgut and resulted in a significantly lower tick survival rate (Hayes et al., 2020). The *I. ricinus* transcript Irseq_658490, which encodes the ortholog of Dae2^{Is} (Dae2 type1),

TABLE 3 Expression of "guard" genes orthologs in unfed *I.scapularis* midgut (from Lu et al., 2023).

Transcript	*I. scapularis* ortholog ID	UF1 TPM	UF2 TPM	UF3 TPM	Average TPM	Std Dev. TPM	UF *I. ricinus* average TPM[a]
Defensin 8	XP_040070918.2	2184,54	1847,72	2406,26	2146,17	281,24	2397
Defensin 1	nd	-	-	-	-	-	-
Dae2-type1	XP_040077735.1	1405,79	1240,27	1657,25	1434,44	209,96	3712
Dae2-type2	XP_040066081.1	4,26	5,75	1,92	3,98	1,93	71
Microplusin/Ricinusin	XP_040074415.1	25,51	40,29	45,5	37,10	10,37	448
Microplusin - type 2	XP_040074403.1	10,73	4,99	14,57	10,10	4,82	47
c-type lysozyme 1	XP_002399439.3	17,59	3,13	9,3	10,01	7,26	828
Lysozyme-like	XP_029833110.3	22,71	11,53	16,08	16,77	5,62	10
Acanthoscurrin-like	nd		–	–	-	–	27
GILT	XP_029827235.2	672,94	871,92	987,99	844,28	159,33	635
GILT-like	XP_042145453.1	143,07	140,79	195,19	159,68	30,77	1002

nd, not detected, [a]values derived from the Table 1 (this work).

was also abundantly expressed in the midgut of unfed ticks and is also present as a protein in midgut homogenates (Table 1). The transcripts of another form of Dae2 (Dae2 type2), identified in *I. ricinus*, and its ortholog in *I. scapularis* (Supplementary Figure S2) were only marginally expressed in the midgut of unfed ticks of both species (Table 3). Whether Dae2 type2 contributes to antibacterial defense remains to be investigated.

The antibacterial activity of cysteine- and histidine-rich proteins has only been demonstrated for two tick molecules; microplusin isolated from the hemolymph of the cattle tick *R. microplus* (Fogaca et al., 2004) and hebraein isolated from the hemolymph of the fed *A. hebraeum* females (Lai et al., 2004). *In vitro* studies have shown that the histidine residues of the microplusin of *R. microplus* chelate metallic ions such as copper and thus affect the respiration of *M. luteus* (Silva et al., 2009) and the fungus *Cryptococcus neoformans* (Silva et al., 2011). The gene expression of a microplusin transcript was upregulated by an experimental infection of the tick *Amblyomma aureolatum* with the tick-borne pathogen *Rickettsia rickettsii*. Knockdown of microplusin increased the acquisition of rickettsiae by feeding on infected rabbits, suggesting that this AMP plays an important role in bacterial control (Martins et al., 2019). There are two groups of microplusin-related molecules in *I. ricinus*: type 1, referred to as ricinusin, and type 2, which is more closely related to microplusin/hebraein due to the histidine-rich C-terminus (Supplementary Figure S3). The expression of type 1 ricinusin in the midgut of unfed *I. ricinus* was significantly higher than that of type 2 microplusin and, accordingly, only ricinusin was detected in the midgut proteome (Table 1). The TPM-based semi-quantitative expression profile of the corresponding orthologs in *I. scapularis* (Lu et al., 2023) also showed that the presence of type 2 microplusin is marginal compared to type 1 ricinusin (Table 3). Our previous analysis of the transcriptome of the fat body of *I. ricinus*, complemented by the proteome of the hemolymph (Urbanova et al., 2024), showed that ricinusin is one of the most abundant transcripts expressed in the fat body and that the corresponding protein is very abundant in the hemolymph. However, it remains to be experimentally proven whether the ricinusins and/or micropusins of *Ixodes* sp. play a bacteriostatic or fungistatic role in antimicrobial defense, as has been reported for microplusin of *R. microplus* (Fogaca et al., 2004).

C-type lysozyme is one of the very potent molecules active against Gram-positive bacteria, such as *M. luteus*, as we demonstrated two decades ago using lysozyme isolated from the midgut contents of the soft tick *Ornithodoros moubata* (Kopacek et al., 1999; Grunclova et al., 2003). Two immune-responsive c-type lysozymes were cloned and characterized from the EST library of the hemocytes of the hard tick *Dermacentor variabilis* and the embryonic cell line DAE100 of *Dermacentor andersoni* (Simser et al., 2004). Another c-type lysozyme called HlLysozyme was cloned from the hard tick *H. longicornis* and was shown to be expressed in different tick tissues (mainly in hemocytes) and to respond to the challenge with both Gram-positive and Gram-negative bacteria. Recombinant HlLysozyme was able to lyse Gram-positive *Micrococcus lysodeikticus* (*luteus*) in a concentration-dependent manner (Tanaka et al., 2010). The identification of a relatively abundantly expressed transcript encoding c- type lysozyme 1 in the midgut of unfed *I. ricinus* suggests its potential role in defense against Gram-positive bacteria. However, despite its high expression, the encoded enzyme was not detected by proteomic analysis (Table 1). The expression of orthologs of c- type lysozyme 1 and lysozyme-like type 2 in the midgut of *I. scapularis* (Lu et al., 2023) suggests their exclusive presence only in the unfed stage, with TPM values of both enzymes being rather low (Table 3). Therefore, the contribution of lysozymes to the total antimicrobial activity in the unfed midgut of *Ixodes* sp. is questionable.

GILTs belong to the family of thioredoxin-type oxidoreductases, which are responsible for the reduction of disulfide bonds in the acidic pH of lysosomes (Arunachalam et al., 2000; West and Cresswell, 2013). Three forms of GILTs have been identified in the fruit fly *D. melanogaster* (Supplementary Figure S6) and reported to be expressed mainly in the fat body and hemocytes (Kongton et al., 2014). Their knockdown in mutant flies increased infection by the Gram-negative *E. coli*, while overexpression decreased bacterial proliferation (Kongton et al., 2014). Conversely, CRISPR/Cas9 deletion of the gene encoding mosGILT of the mosquito *A. gambiae* resulted in refractoriness to malaria parasites *Plasmodium berghei* and *Plasmodium falciparum* (Yang et al., 2020). In addition, mutants had underdeveloped ovaries, egg development was reduced, and production of 20-hydroxyecdysone (20E) was lower (Yang et al., 2020). Indeed, RNA-seq analysis of mosGILT null mutants showed the modulation of transcripts related to the oogenesis and to the synthesis of 20-hydroxyecdysone (Arora et al., 2024). In addition, an upregulation of transcripts encoding anti-*Plasmodium* effectors, including one Clip domain serine protease (CLIPs), four thioester-containing protein 1 (TEP1), one peptidoglycan recognition proteins (PGRPs), and one defensin was observed in mutant mosquitos. The authors hypothesized that the reduction of the ovary development, which is a consequence of the absence of mosGILT, may intensify the immune response, reducing *Plasmodium burden* (Arora et al., 2024). In mosquito saliva, mosGILT binds to *Plasmodium* sporozoites, reducing the rate of cell crossing and parasite displacement, leading to a reduction in mouse infection (Schleicher et al., 2018). The role of GILTs expressed in the midgut of ticks remains to be investigated. In addition to their proposed role in midgut immunity, the disulfide-reducing activity of tick GILTs may also be involved in the activation of cysteine cathepsins in the acidic environment of the digestive endo-lysosomes (Sojka et al., 2013).

Functional *in vivo* testing of the antimicrobial activities of the identified 'guard' AMPs in the midgut of unfed ticks using RNAi-mediated silencing is difficult to impossible, as the RNAi machinery is significantly reduced in the metabolic resting state (De La Fuente et al., 2007). Therefore, only *in vitro* testing of either isolated and purified AMPs, such as microplusin from *R. microplus* (Fogaca et al., 2004) or lysozyme from *O. moubata* (Kopacek et al., 1999) or the production of recombinant proteins for antimicrobial testing, as demonstrated for Dae^{Is} (Hayes et al., 2020), offer a solution for testing most 'guard' AMPs identified in this work. Defensins thus represent the only feasible exception for *in vitro* testing, as their size of about 40 amino acid residues allows their chemical synthesis. To test the antimicrobial activity of the mature defensin 1 and defensin 8, we used the experimental platform previously used to test other

tick defensins (Tonk et al., 2014, 2015; Cabezas-Cruz et al., 2019). Our results clearly confirmed the antibacterial specificity of the two tested defensins 1 and 8 against Gram-positive bacteria *S. aureus*, *S. epidermidis* and *M. maritypicum* at typically reported micromolar concentrations (Saito et al., 2009; Chrudimska et al., 2011; Tonk et al., 2014, 2015). In contrast, the minimal inhibitory concentrations of defensins 1 and 8 against *M. luteus* were about two orders of magnitude lower and in the nanomolar range. As far as we know, such a low MIC has not been reported for any other invertebrate defensin. The chemically sophisticated synthesis of defensins made it possible to test role of disulfide bridges in the defensin antibacterial activity. Our results showed that the reduction of defensin 1 suppressed its activity against *M. luteus* by about 100-fold, whereas no change in MIC was observed for defensin 8 (Table 2). This difference suggests that disulfide bridges are important for defensin-1 activity, but not for the activity of defensin-8.

The expression of defensin 8 in the midgut of unfed *I. ricinus* and the expression of defensin 1 in the later stages of feeding (Perner et al., 2016), which show similar efficacy in inhibiting the growth of Gram-positive bacteria, lead us to speculate on the complementary roles of an 'early' and a 'late' defensin in the rapid elimination of Gram-positive environmental bacteria ingested during blood feeding. However, the detection of the 'late' defensin in the midgut proteome of unfed females, which may have been preserved from the nymphal stage (Kozelkova et al., 2023), suggest that the real situation is more complex.

Overall, our results indicate that the tick midgut deploys a number of non-induced immune factors as a first line of defense to protect ticks from environmental microorganisms during their long-term fasting period. Deciphering specific roles of the individual components of tick midgut immunity is a task for future studies.

Data availability statement

The datasets presented in this study can be found in online repositories. The names of the repository/repositories and accession number(s) can be found in the article/Supplementary Material.

Ethics statement

All experimental animals were handled in accordance with the Animal Protection Law of the Czech Republic No. 246/1992 Sb., ethics approval No. 25/2020. The study was conducted in accordance with the local legislation and institutional requirements.

Author contributions

MG: Conceptualization, Writing – original draft, Writing – review & editing, Investigation, Methodology. HF: Investigation, Methodology, Writing – review & editing. SL: Investigation, Methodology, Writing – review & editing, Data curation, Software, Writing – original draft. TK: Data curation, Investigation, Methodology, Writing – original draft, Writing – review & editing. KČ: Data curation, Investigation, Methodology, Writing – review & editing. FD: Data curation, Methodology, Writing – review & editing, Software. AH: Methodology, Writing – review & editing, Investigation. MT: Investigation, Methodology, Writing – review & editing. JP: Writing – review & editing, Conceptualization, Formal analysis, Supervision. JR: Supervision, Writing – review & editing, Data curation, Software, Validation. AF: Supervision, Writing – review & editing, Conceptualization, Funding acquisition. LZ: Conceptualization, Funding acquisition, Supervision, Writing – review & editing. PK: Conceptualization, Data curation, Formal analysis, Funding acquisition, Supervision, Writing – original draft, Writing – review & editing.

Funding

The author(s) declare financial support was received for the research, authorship, and/or publication of this article. This work was primarily supported by the joint project of Czech Science Foundation Grant No. 22–12648J to PK and LZ and FAPESP No. 2021/03649–4 to AF. This work utilized the computational resources of the NIH HPC Biowulf cluster (http://hpc.nih.gov). Funding was provided in part by the Intramural Research Program of the NIAID/NIH (Vector-Borne Diseases: Biology of Vector Host Relationship, Z01 AI000810-18).

Conflict of interest

The authors declare that the research was conducted in the absence of any commercial or financial relationships that could be construed as a potential conflict of interest.

Publisher's note

Supplementary material

The Supplementary Material for this article can be found online at: https://www.frontiersin.org/articles/10.3389/fcimb.2024.1450353/full#supplementary-material

References

Arora, G., Tang, X., Cui, Y., Yang, J., Chuang, Y. M., Joshi, J., et al. (2024). mosGILT controls innate immunity and germ cell development in *Anopheles Gambiae*. *BMC Genomics* 25, 42. doi: 10.1186/s12864-023-09887-0

Arunachalam, B., Phan, U. T., Geuze, H. J., and Cresswell, P. (2000). Enzymatic reduction of disulfide bonds in lysosomes: characterization of a gamma-interferon-inducible lysosomal thiol reductase (GILT). *Proc. Natl. Acad. Sci. U.S.A.* 97, 745–750. doi: 10.1073/pnas.97.2.745

Azambuja, P., Garcia, E. S., and Ratcliffe, N. A. (2005). Gut microbiota and parasite transmission by insect vectors. *Trends Parasitol.* 21, 568–572. doi: 10.1016/j.pt.2005.09.011

Bendtsen, J. D., Nielsen, H., Von Heijne, G., and Brunak, S. (2004). Improved prediction of signal peptides: SignalP 3.0. *J. Mol. Biol.* 340, 783–795. doi: 10.1016/j.jmb.2004.05.028

Bensaoud, C., Tenzer, S., Poplawski, A., Medina, J. M., Jmel, M. A., Voet, H., et al. (2022). Quantitative proteomics analysis reveals core and variable tick salivary proteins at the tick-vertebrate host interface. *Mol. Ecol.* 31, 4162–4175. doi: 10.1111/mec.16561

Binetruy, F., Dupraz, M., Buysse, M., and Duron, O. (2019). Surface sterilization methods impact measures of internal microbial diversity in ticks. *Parasit Vectors* 12, 268. doi: 10.1186/s13071-019-3517-5

Cabezas-Cruz, A., Tonk, M., Bleackley, M. R., Valdes, J. J., Barrero, R. A., Hernandez-Jarguin, A., et al. (2019). Antibacterial and antifungal activity of defensins from the Australian paralysis tick, *Ixodes holocyclus*. *Ticks Tick Borne Dis.* 10, 101269. doi: 10.1016/j.ttbdis.2019.101269

Caragata, E. P., and Short, S. M. (2022). Vector microbiota and immunity: modulating arthropod susceptibility to vertebrate pathogens. *Curr. Opin. Insect Sci.* 50, 100875. doi: 10.1016/j.cois.2022.100875

Cerqueira De Araujo, A., Noël, B., Bretaudeau, A., Labadie, K., Boudet, M., Tadrent, N., et al. (2024). Genome sequences of four *Ixodes* species expands understanding of tick evolution. *bioRxiv* 2024, 1–69. doi: 10.1101/2024.02.29.581698

Chou, S., Daugherty, M. D., Peterson, S. B., Biboy, J., Yang, Y., Jutras, B. L., et al. (2015). Transferred interbacterial antagonism genes augment eukaryotic innate immune function. *Nature* 518, 98–101. doi: 10.1038/nature13965

Chrudimska, T., Slaninova, J., Rudenko, N., Ruzek, D., and Grubhoffer, L. (2011). Functional characterization of two defensin isoforms of the hard tick *Ixodes ricinus*. *Parasit Vectors* 4, 63. doi: 10.1186/1756-3305-4-63

Cox, J., and Mann, M. (2008). MaxQuant enables high peptide identification rates, individualized p.p.b.-range mass accuracies and proteome-wide protein quantification. *Nat. Biotechnol.* 26, 1367–1372. doi: 10.1038/nbt.1511

De La Fuente, J., Kocan, K. M., Almazan, C., and Blouin, E. F. (2007). RNA interference for the study and genetic manipulation of ticks. *Trends Parasitol.* 23, 427–433. doi: 10.1016/j.pt.2007.07.002

Fogaca, A. C., Lorenzini, D. M., Kaku, L. M., Esteves, E., Bulet, P., and Daffre, S. (2004). Cysteine-rich antimicrobial peptides of the cattle tick *Boophilus microplus*: isolation, structural characterization and tissue expression profile. *Dev. Comp. Immunol.* 28, 191–200. doi: 10.1016/j.dci.2003.08.001

Fogaça, A. C., Sousa, G., Pavanelo, D. B., Esteves, E., Martins, L. A., Urbanova, V., et al. (2021). Tick immune system: what is known, the interconnections, the gaps, and the challenges. *Front. Immunol.* 12. doi: 10.3389/fimmu.2021.628054

Fu, L., Niu, B., Zhu, Z., Wu, S., and Li, W. (2012). CD-HIT: accelerated for clustering the next-generation sequencing data. *Bioinformatics* 28, 3150–3152. doi: 10.1093/bioinformatics/bts565

Gilliland, C. A., Patel, V., Mccormick, A. C., Mackett, B. M., and Vogel, K. J. (2023). Using axenic and gnotobiotic insects to examine the role of different microbes on the development and reproduction of the kissing bug *Rhodnius prolixus* (Hemiptera: Reduviidae). *Mol. Ecol.* 32, 920–935. doi: 10.1111/mec.16800

Grabherr, M. G., Haas, B. J., Yassour, M., Levin, J. Z., Thompson, D. A., Amit, I., et al. (2011). Full-length transcriptome assembly from RNA-Seq data without a reference genome. *Nat. Biotechnol.* 29, 644–652. doi: 10.1038/nbt.1883

Grunclova, L., Fouquier, H., Hypsa, V., and Kopacek, P. (2003). Lysozyme from the gut of the soft tick *Ornithodoros moubata*: the sequence, phylogeny and post-feeding regulation. *Dev. Comp. Immunol.* 27, 651–660. doi: 10.1016/S0145-305X(03)00052-1

Guizzo, M. G., Dolezelikova, K., Neupane, S., Frantova, H., Hrbatova, A., Pafco, B., et al. (2022). Characterization and manipulation of the bacterial community in the midgut of *Ixodes ricinus*. *Parasit Vectors* 15, 248. doi: 10.1186/s13071-022-05362-z

Guizzo, M. G., Neupane, S., Kucera, M., Perner, J., Frantova, H., Da Silva Vaz, I., et al. (2020). Poor unstable midgut microbiome of hard ticks contrasts with abundant and stable monospecific microbiome in ovaries. *Front. Cell Infect. Microbiol.* 10. doi: 10.3389/fcimb.2020.00211

Hajdusek, O., Sima, R., Ayllon, N., Jalovecka, M., Perner, J., de la Fuente, J., et al. (2013). Interaction of the tick immune system with transmitted pathogens. *Front. Cell Infect. Microbiol.* 3. doi: 10.3389/fcimb.2013.00026

Harrison, R. E., Yang, X., Eum, J. H., Martinson, V. G., Dou, X., Valzania, L., et al. (2023). The mosquito *Aedes aEgypti* requires a gut microbiota for normal fecundity, longevity and vector competence. *Commun. Biol.* 6, 1154. doi: 10.1038/s42003-023-05545-z

Hayes, B. M., Radkov, A. D., Yarza, F., Flores, S., Kim, J., Zhao, Z., et al. (2020). Ticks resist skin commensals with immune factor of bacterial origin. *Cell* 183, 1562–1571.e1512. doi: 10.1016/j.cell.2020.10.042

Kongton, K., Mccall, K., and Phongdara, A. (2014). Identification of gamma-interferon-inducible lysosomal thiol reductase (GILT) homologues in the fruit fly *Drosophila melanogaster*. *Dev. Comp. Immunol.* 44, 389–396. doi: 10.1016/j.dci.2014.01.007

Kopacek, P., Hajdusek, O., Buresova, V., and Daffre, S. (2010). Tick innate immunity. *Adv. Exp. Med. Biol.* 708, 137–162.

Kopacek, P., Vogt, R., Jindrak, L., Weise, C., and Safarik, I. (1999). Purification and characterization of the lysozyme from the gut of the soft tick *Ornithodoros moubata*. *Insect Biochem. Mol. Biol.* 29, 989–997. doi: 10.1016/S0965-1748(99)00075-2

Kotsyfakis, M., Kopacek, P., Franta, Z., Pedra, J. H. F., and Ribeiro, J. M. C. (2015). Deep sequencing analysis of the *ixodes ricinus* haemocytome. *PloS Negl. Trop. Dis.* 9, e0003754. doi: 10.1371/journal.pntd.0003754

Kozelkova, T., Dycka, F., Lu, S., Urbanova, V., Frantova, H., Sojka, D., et al. (2023). Insight into the dynamics of the *ixodes ricinus* nymphal midgut proteome. *Mol. Cell Proteomics* 22, 100663. doi: 10.1016/j.mcpro.2023.100663

Lai, R., Takeuchi, H., Lomas, L. O., Jonczy, J., Rigden, D. J., Rees, H. H., et al. (2004). A new type of antimicrobial protein with multiple histidines from the hard tick, *Amblyomma hebraeum*. *FASEB J.* 18, 1447–1449. doi: 10.1096/fj.03-1154fje

Li, B., and Dewey, C. N. (2011). RSEM: accurate transcript quantification from RNA-Seq data with or without a reference genome. *BMC Bioinf.* 12, 323. doi: 10.1186/1471-2105-12-323

Liu, M., Liu, L., Abbas, M. N., Kausar, S., Zhang, J. W., Ye, Z. Z., et al. (2019). Involvement of gamma interferon inducible lysosomal thiol reductase in the innate immune responses of red swamp crayfish, *Procambarus clarkii*. *Dev. Comp. Immunol.* 99, 103405. doi: 10.1016/j.dci.2019.103405

Lorenzini, D. M., Da Silva, P. I. Jr., Fogaca, A. C., Bulet, P., and Daffre, S. (2003). Acanthoscurrin: a novel glycine-rich antimicrobial peptide constitutively expressed in the hemocytes of the spider *Acanthoscurria gomesiana*. *Dev. Comp. Immunol.* 27, 781–791. doi: 10.1016/S0145-305X(03)00058-2

Lu, S., Martins, L. A., Kotal, J., Ribeiro, J. M. C., and Tirloni, L. (2023). A longitudinal transcriptomic analysis from unfed to post-engorgement midguts of adult female *Ixodes scapularis*. *Sci. Rep.* 13, 11360. doi: 10.1038/s41598-023-38207-5

Lu, S., Waldman, J., Parizi, L. F., Junior, I., and Tirloni, L. (2024). A longitudinal transcriptomic analysis of *Rhipicephalus microplus* midgut upon feeding. *Ticks Tick Borne Dis.* 15, 102304. doi: 10.1016/j.ttbdis.2023.102304

Maldonado-Ruiz, L. P., Neupane, S., Park, Y., and Zurek, L. (2021). The bacterial community of the lone star tick (*Amblyomma americanum*). *Parasit Vectors* 14, 49. doi: 10.1186/s13071-020-04550-z

Martins, L. A., Malossi, C. D., Galletti, M., Ribeiro, J. M., Fujita, A., Esteves, E., et al. (2019). The Transcriptome of the Salivary Glands of Amblyomma aureolatum Reveals the Antimicrobial Peptide Microplusin as an Important Factor for the Tick Protection Against Rickettsia rickettsii Infection. *Front. Physiol.* 10. doi: 10.3389/fphys.2019.00529

Mcfall-Ngai, M., Hadfield, M. G., Bosch, T. C., Carey, H. V., Domazet-Loso, T., Douglas, A. E., et al. (2013). Animals in a bacterial world, a new imperative for the life sciences. *Proc. Natl. Acad. Sci. U.S.A.* 110, 3229–3236. doi: 10.1073/pnas.1218525110

Pavanelo, D. B., Piloto-Sardiñas, E., Maitre, A., Abuin-Denis, L., Kopáček, P., Cabezas-Cruz, A., et al. (2023). Arthropod microbiota: shaping pathogen establishment and enabling control. *Front. Arachn. Sci.* 2. doi: 10.3389/frchs.2023.1297733

Pavanelo, D. B., Schroder, N. C. H., Pin Viso, N. D., Martins, L. A., Malossi, C. D., Galletti, M., et al. (2020). Comparative analysis of the midgut microbiota of two natural tick vectors of *Rickettsia rickettsii*. *Dev. Comp. Immunol.* 106, 103606. doi: 10.1016/j.dci.2019.103606

Perner, J., Kropackova, S., Kopacek, P., and Ribeiro, J. M. C. (2018). Sialome diversity of ticks revealed by RNAseq of single tick salivary glands. *PloS Negl. Trop. Dis.* 12, e0006410. doi: 10.1371/journal.pntd.0006410

Perner, J., Provaznik, J., Schrenkova, J., Urbanova, V., Ribeiro, J. M., and Kopacek, P. (2016). RNA-seq analyses of the midgut from blood- and serum-fed *Ixodes ricinus* ticks. *Sci. Rep.* 6, 36695. doi: 10.1038/srep36695

Ribeiro, J. M., Hartmann, D., Bartosova-Sojkova, P., Debat, H., Moos, M., Simek, P., et al. (2023). Blood-feeding adaptations and virome assessment of the poultry red mite *Dermanyssus gallinae* guided by RNA-seq. *Commun. Biol.* 6, 517. doi: 10.1038/s42003-023-04907-x

Ribeiro, J. M. C., and Mans, B. J. (2020). TickSialoFam (TSFam): A database that helps to classify tick salivary proteins, a review on tick salivary protein function and evolution, with considerations on the tick sialome switching phenomenon. *Front. Cell Infect. Microbiol.* 10. doi: 10.3389/fcimb.2020.00374

Robinson, M. D., Mccarthy, D. J., and Smyth, G. K. (2010). edgeR: a Bioconductor package for differential expression analysis of digital gene expression data. *Bioinformatics* 26, 139–140. doi: 10.1093/bioinformatics/btp616

Ross, B. D., Hayes, B., Radey, M. C., Lee, X., Josek, T., Bjork, J., et al. (2018). Ixodes scapularis does not harbor a stable midgut microbiome. *ISME J.* 12, 2596–2607. doi: 10.1038/s41396-018-0161-6

Rudenko, N., Golovchenko, M., Edwards, M. J., and Grubhoffer, L. (2005). Differential expression of *Ixodes ricinus* tick genes induced by blood feeding or Borrelia burgdorferi infection. *J. Med. Entomol* 42, 36–41. doi: 10.1093/jmedent/42.1.36

Saito, Y., Konnai, S., Yamada, S., Imamura, S., Nishikado, H., Ito, T., et al. (2009). Identification and characterization of antimicrobial peptide, defensin, in the taiga tick, *Ixodes persulcatus*. *Insect Mol. Biol.* 18, 531–539. doi: 10.1111/j.1365-2583.2009.00897.x

Schleicher, T. R., Yang, J., Freudzon, M., Rembisz, A., Craft, S., Hamilton, M., et al. (2018). A mosquito salivary gland protein partially inhibits *Plasmodium* sporozoite cell traversal and transmission. *Nat. Commun.* 9, 2908. doi: 10.1038/s41467-018-05374-3

Schwarz, A., Von Reumont, B. M., Erhart, J., Chagas, A. C., Ribeiro, J. M., and Kotsyfakis, M. (2013). *De novo Ixodes ricinus* salivary gland transcriptome analysis using two next-generation sequencing methodologies. *FASEB J.* 27, 4745–4756. doi: 10.1096/fj.13-232140

Seppey, M., Manni, M., and Zdobnov, E. M. (2019). BUSCO: assessing genome assembly and annotation completeness. *Methods Mol. Biol.* 1962, 227–245. doi: 10.1007/978-1-4939-9173-0_14

Silva, F. D., Rezende, C. A., Rossi, D. C., Esteves, E., Dyszy, F. H., Schreier, S., et al. (2009). Structure and mode of action of microplusin, a copper II-chelating antimicrobial peptide from the cattle tick *Rhipicephalus* (*Boophilus*) *microplus*. *J. Biol. Chem.* 284, 34735–34746. doi: 10.1074/jbc.M109.016410

Silva, F. D., Rossi, D. C., Martinez, L. R., Frases, S., Fonseca, F. L., Campos, C. B., et al. (2011). Effects of microplusin, a copper-chelating antimicrobial peptide, against *Cryptococcus neoformans*. *FEMS Microbiol. Lett.* 324, 64–72. doi: 10.1111/fml.2011.324.issue-1

Simpson, J. T., Wong, K., Jackman, S. D., Schein, J. E., Jones, S. J., and Birol, I. (2009). ABySS: a parallel assembler for short read sequence data. *Genome Res.* 19, 1117–1123. doi: 10.1101/gr.089532.108

Simser, J. A., Macaluso, K. R., Mulenga, A., and Azad, A. F. (2004). Immune-responsive lysozymes from hemocytes of the American dog tick, *Dermacentor variabilis* and an embryonic cell line of the Rocky Mountain wood tick, *D. andersoni*. *Insect Biochem. Mol. Biol.* 34, 1235–1246. doi: 10.1016/j.ibmb.2004.07.003

Sojka, D., Franta, Z., Horn, M., Caffrey, C. R., Mares, M., and Kopacek, P. (2013). New insights into the machinery of blood digestion by ticks. *Trends Parasitol.* 29, 276–285. doi: 10.1016/j.pt.2013.04.002

Tanaka, T., Kawano, S., Nakao, S., Umemiya-Shirafuji, R., Rahman, M. M., Boldbaatar, D., et al. (2010). The identification and characterization of lysozyme from the hard tick *Haemaphysalis longicornis*. *Ticks Tick Borne Dis.* 1, 178–185. doi: 10.1016/j.ttbdis.2010.09.001

Tonk, M., Cabezas-Cruz, A., Valdes, J. J., Rego, R. O., Chrudimska, T., Strnad, M., et al. (2014). Defensins from the tick *Ixodes scapularis* are effective against phytopathogenic fungi and the human bacterial pathogen *Listeria grayi*. *Parasit Vectors* 7, 554. doi: 10.1186/s13071-014-0554-y

Tonk, M., Cabezas-Cruz, A., Valdes, J. J., Rego, R. O., Grubhoffer, L., Estrada-Pena, A., et al. (2015). *Ixodes ricinus* defensins attack distantly-related pathogens. *Dev. Comp. Immunol.* 53, 358–365. doi: 10.1016/j.dci.2015.08.001

Tsuji, N., Battsetseg, B., Boldbaatar, D., Miyoshi, T., Xuan, X., Oliver, J. H. Jr., et al. (2007). Babesial vector tick defensin against *Babesia* sp. parasites. *Infect. Immun.* 75, 3633–3640. doi: 10.1128/IAI.00256-07

Tyanova, S., Temu, T., Sinitcyn, P., Carlson, A., Hein, M. Y., Geiger, T., et al. (2016). The Perseus computational platform for comprehensive analysis of (prote)omics data. *Nat. Methods* 13, 731–740. doi: 10.1038/nmeth.3901

Urbanova, V., Lu, S., Kalinova, E., Martins, L., Kozelkova, T., Dycka, F., et al. (2024). From the fat body to the hemolymph: Profiling tick immune and storage proteins through transcriptomics and proteomics. *Insect Biochem. Mol. Biol.* 165, 104072. doi: 10.1016/j.ibmb.2024.104072

Wang, J., Gao, L., and Aksoy, S. (2023). Microbiota in disease-transmitting vectors. *Nat. Rev. Microbiol.* 21, 604–618. doi: 10.1038/s41579-023-00901-6

West, L. C., and Cresswell, P. (2013). Expanding roles for GILT in immunity. *Curr. Opin. Immunol.* 25, 103–108. doi: 10.1016/j.coi.2012.11.006

Wu, J., Zhou, X., Chen, Q., Chen, Z., Zhang, J., Yang, L., et al. (2022). Defensins as a promising class of tick antimicrobial peptides: a scoping review. *Infect. Dis. Poverty* 11, 71. doi: 10.1186/s40249-022-00996-8

Yang, J., Schleicher, T. R., Dong, Y., Park, H. B., Lan, J., Cresswell, P., et al. (2020). Disruption of mosGILT in *Anopheles Gambiae* impairs ovarian development and *Plasmodium* infection. *J. Exp. Med.* 217, 1–13. doi: 10.1084/jem.20190682

Zhou, M., Abbas, M. N., Kausar, S., Jiang, C. X., and Dai, L. S. (2017). Transcriptome profiling of red swamp crayfish (*Procambarus clarkii*) hepatopancreas in response to lipopolysaccharide (LPS) infection. *Fish Shellfish Immunol.* 71, 423–433. doi: 10.1016/j.fsi.2017.10.030

frontiers | Frontiers in Cellular and Infection Microbiology

TYPE Original Research
PUBLISHED 10 October 2024
DOI 10.3389/fcimb.2024.1476266

OPEN ACCESS

EDITED BY
Deepak Kumar,
University of Southern Mississippi,
United States

REVIEWED BY
Andréa Cristina Fogaça,
University of São Paulo, Brazil
Erich Loza Telleria,
Charles University, Czechia

*CORRESPONDENCE
Adnan Hodžić
adnan.hodzic@univie.ac.at
David Berry
david.berry@univie.ac.at

RECEIVED 05 August 2024
ACCEPTED 17 September 2024
PUBLISHED 10 October 2024

CITATION
Hodžić A, Veinović G, Alić A, Seki D, Kunert M, Nikolov G, Sukara R, Šupić J, Tomanović S and Berry D (2024) A metalloprotease secreted by an environmentally acquired gut bacterium hinders *Borrelia afzelii* colonization in *Ixodes ricinus*.
Front. Cell. Infect. Microbiol. 14:1476266.
doi: 10.3389/fcimb.2024.1476266

A metalloprotease secreted by an environmentally acquired gut bacterium hinders *Borrelia afzelii* colonization in *Ixodes ricinus*

Adnan Hodžić[1]*, Gorana Veinović[2], Amer Alić[3], David Seki[1,4], Martin Kunert[1], Georgi Nikolov[1], Ratko Sukara[2], Jovana Šupić[3], Snežana Tomanović[2] and David Berry[1,4]*

[1]Centre for Microbiology and Environmental Systems Science, Department of Microbiology and Ecosystem Science, Division of Microbial Ecology, University of Vienna, Vienna, Austria, [2]Institute for Medical Research, National Institute of Republic of Serbia, University of Belgrade, Belgrade, Serbia, [3]Department of Clinical Sciences of Veterinary Medicine, Faculty of Veterinary Medicine, University of Sarajevo, Sarajevo, Bosnia and Herzegovina, [4]Joint Microbiome Facility of the Medical University of Vienna and the University of Vienna, Vienna, Austria

Although the importance of the microbiome in the context of tick biology and vector competence has recently come into a broader research focus, the field is still in its infancy and the complex ecological interactions between the tick residential bacteria and pathogens are obscure. Here, we show that an environmentally acquired gut bacterium has the potential to impair *Borrelia afzelii* colonization within the tick vector through a secreted metalloprotease. Oral introduction of either *Bacillus cereus* LTG-1 isolate or its purified enhancin (*Bc*Enhancin) protein significantly reduces *B. afzelii* burden in the guts of *Ixodes ricinus* ticks. This effect is attributed to the ability of *Bc*Enhancin to degrade a glycan-rich peritrophic matrix (PM), which is a gut protective barrier essential for *Borrelia* survival. Our study highlights the importance of the gut microbiome in determining tick vector competence and provides a deeper mechanistic insight into the complex network of interactions between *Borrelia*, the tick, and the tick microbiome.

KEYWORDS

***Borrelia afzelii*, enhancin, gut microbiome, *Ixodes ricinus*, peritrophic matrix**

1 Introduction

Lyme borreliosis (LB) is an emerging and the most prevalent vector-borne infectious disease in the temperate regions of the Northern Hemisphere. It is caused by the spirochetes of the *Borrelia burgdorferi* sensu lato complex, which includes at least 20 different species, six of which are recognized human pathogens (Steinbrink et al., 2022). These extracellular bacteria are engaged in a complex enzootic life cycle that involves

vertebrate reservoir hosts, mainly rodents and birds, and ticks of the genus *Ixodes*. The castor bean tick, *Ixodes ricinus*, is the main vector of LB in Europe, where most human cases are caused by *Borrelia afzelii*, *Borrelia garinii*, and less often by *B. burgdorferi* sensu stricto (hereafter *B. burgdorferi*) (Steere et al., 2016).

Borrelial pathogens have evolved multiple strategies for survival in the tick vector and the vertebrate host. After ingestion from an infected vertebrate, the spirochetes colonize the tick gut and remain attached to the epithelium for several months until the next blood meal. During this phase, *Borrelia* must overcome several barriers to survive a hostile gut environment, including humoral and cellular immune responses, endocytic digestion, and toxic products associated with blood digestion (Estrada-Peña et al., 2018). To confront these challenges, *Borrelia* induces extensive transcriptional changes and modulates the gut environment (Kurokawa et al., 2020). Interactions between the pathogen and the tick gut are thus critical for colonization as well as spirochete transmission to a mammalian host (Kurokawa et al., 2020; Pal et al., 2021). Mounting evidence suggests that residential gut bacteria may also affect the colonization of pathogens within the tick vector, but the molecular mechanisms of these interactions are not fully elucidated (Narasimhan et al., 2014; Gall et al., 2016; Abraham et al., 2017; Narasimhan et al., 2017; Ross et al., 2018; Landesman et al., 2019; Sperling et al., 2020; Narasimhan et al., 2022; Wu-Chuang et al., 2023). This is of particular importance for *Borrelia* species considering that they lack interbacterial effector and immunity genes required for survival in a polymicrobial environment, which makes them highly susceptible to inhibition by cohabiting bacteria (Ross et al., 2018). In line with this observation, a higher abundance and diversity of the microbial communities in wild-caught ticks compared to laboratory-reared ticks have been associated with increased colonization resistance to *B. afzelii* (Jacquet et al., 2017; Guizzo et al., 2020). Moreover, the abundance of *Borrelia* negatively correlates with the increased burden of certain bacterial taxa, such as *Bacillus*, *Pseudomonas*, and Enterobacteriaceae (Ross et al., 2018; Landesman et al., 2019; Grandi et al., 2023; Wu-Chuang et al., 2023).

The tick gut microbiome is important for the formation of an acellular and glycan-rich structure known as a peritrophic matrix (PM) (Narasimhan et al., 2014). The arthropod PM is analogous to the vertebrate mucosal layer, and it serves as a physical barrier that separates the gut lumen from the epithelia and protects the epithelium from invading pathogens and their toxins (Kitsou et al., 2021). In *Ixodes* ticks, the PM is a transient structure that forms in the early stages of blood feeding, usually 9-12 hours after tick attachment, and which remains intact for several days (Zhu et al., 1991; Grigoreva and Amosova, 2004). Dysbiosis induced by environmental changes has been shown to interrupt PM formation by diminishing the expression of peritrophin, a core structural component of the PM, and the compromised integrity of the protective barrier in *Ixodes scapularis* ticks impairs the ability of *B. burgdorferi* to colonize the gut (Narasimhan et al., 2014). An intact PM, therefore, appears to be decisive for *Borrelia* persistence within the tick vector as it serves as a shield that protects the spirochetes from detrimental luminal components during colonization of the gut epithelium (Kariu et al., 2013; Narasimhan et al., 2014; Kurokawa et al., 2020; Kitsou et al., 2021; Yang et al., 2021).

These findings prompted us to investigate whether PM-degrading proteins from tick-associated bacteria can affect *B. afzelii* colonization. Our results show that enhancin, a metalloprotease with mucinase activity that is produced and secreted by a *Bacillus cereus* strain isolated from *I. ricinus* ticks (*Bc*Enhancin), reduces *B. afzelii* levels by impairing the integrity of the PM.

2 Materials and methods

2.1 Ticks

Unfed and pathogen-free *I. ricinus* females were obtained from a tick colony at the Insect Services GmbH, Berlin, Germany. Upon arrival, the ticks were kept in a desiccator at 22°C and ~ 97% relative humidity under a 14:10-hour light-dark photoperiod for at least seven days before feeding experiments. A capillary feeding technique was employed for tick infections, so animal experimentations and ethical permissions were not required.

2.2 Isolation and characterization of tick gut bacteria

Host-seeking *I. ricinus* ticks were collected from three different locations in the city of Vienna by flagging the vegetation (Supplementary Figure S1). Overall, 524 ticks (415 nymphs, 67 females, and 42 males) were collected between April and July 2023 and processed for bacteria isolation. After identification, ticks were surface sterilized with 1% sodium hypochlorite solution for 3 min, 70% ethanol for 1 min, and then rinsed in three successive baths of sterile water (Guizzo et al., 2022). The last rinse water was plated and incubated under the same conditions as gut samples to control the efficacy of the decontamination protocol. The guts were aseptically dissected under a stereomicroscope (Olympus SZ61, Japan) using sterile surgical blades (No. #11, Integra Miltex, Japan) and fine tip forceps and then homogenized either individually or in pools (three adults or five nymphs) in 200 µl sterile phosphate-buffered saline (PBS). The gut homogenates were streaked onto Brain heart infusion (BHI) agar (Oxoid, UK) supplemented with 5 g/l yeast extract (Oxoid, UK) and 5 mg/l hemin (Sigma-Aldrich, MO, USA), and incubated at 22°C and 37°C under aerobic and anaerobic (anaerobic tent, 85% N_2, 10% CO_2, 5% H_2) conditions for 72 h. Two plates per sample were used for each incubation condition. Individual bacterial colonies with distinct morphologies were picked from the plate, dissolved in nuclease-free water, and used as a template for amplification of the 16S rRNA gene by colony PCR (Riva et al., 2023) using the universal eubacterial primers 27f and 1492r (Supplementary Table S1). Amplification was conducted in a T100

Thermal Cycler (Bio-Rad Laboratories, Germany) under the following conditions: initial denaturation 95°C for 4 min followed by 35 cycles of 95°C for 30 s, 51°C for 30 s, 72°C for 1.5 min, and a final elongation at 72°C for 10 min. PCR products were separated by electrophoresis on a 1.5% agarose gel stained with GelRed (Biotium, CA, USA). Purification of the amplicons and Sanger sequencing were conducted by Microsynth AG (Vienna, Austria). The DNA sequences were edited with BioEdit software v.7.2.5 (Hall, 1999) and EzBioCloud's identification service (ezbiocloud.net) was employed for similarity-based searches against quality-controlled databases of 16S rRNA gene sequences (Yoon et al., 2017). The growth condition and the isolation source for each bacterial isolate are summarized in Supplementary Table S2.

2.3 Identification of bacterial enhancins

The Pfam 36.0 database (Mistry et al., 2021) was searched to ascertain the occurrence and the taxonomic distribution of enhancin proteins, which are metalloproteases known to promote bacterial and viral infections by degrading the polysaccharide layer of the invertebrate PM (Wang and Granados, 1997; Peng et al., 1999; Galloway et al., 2005; Fang et al., 2009; Garcia-Gonzalez and Genersch, 2013; Wu et al., 2019; Nakamura et al., 2021). Identification and characterization of enhancins across Bacteria superkingdom were performed by searching the Peptidase M60, enhancin and enhancin-like (M60-like; PF13402), and Putative mucin or carbohydrate-binding module (Mucin_bdg; PF03272) domains. These two domains are the defining feature of the mucin-degrading enhancins (Wang and Granados, 1997; Nakjang et al., 2012). Candidate proteins were checked individually to reduce the number of false positive entries. The protein structure was assessed using the SMART research tool (Letunic et al., 2021) in Normal Mode, which contains Swiss-Prot, SP-TrEMBL, and stable Ensembl proteomes. Signal peptides were additionally predicted by SignalP-5.0 (cbs.dtu.dk/services/SignalP). Schematic representation of the enhancin proteins was done by entering "M60-like" AND Pfam: Mucin_bdg" in the domain selection and the domain architecture query was restricted to Bacteria. Finally, a Newick tree was generated based on National Center for Biotechnology Information (NCBI) taxonomy (ncbi.nlm.nih.gov) and displayed in iTOL v.6 (Letunic and Bork, 2021).

Nucleotide sequences of the enhancin encoding genes were retrieved from the genomes of the selected bacterial representatives available in the GenBank® database. To detect the *enhancin* gene in the *B. cereus* LTG-1 strain, a PCR assay targeting a 952 bp long fragment was developed. The PCR mixture contained 12.5 µl of 2X DreamTaq PCR Master Mix (Thermo Fischer Scientific, IL, USA), 1 µl of each BcEnhc-F and BcEnhc-R primer (Supplementary Table S1), 5 µl of DNA template, and PCR grade water up to 25 µl. The amplification program consisted of initial denaturation at 95°C for 3 min, followed by 35 cycles of denaturation at 95°C for 30 s, 60°C for 30 s, 72°C for 1 min, and a final elongation at 72°C for 7 min. The resulting PCR product was evaluated by gel electrophoresis and submitted for bidirectional DNA sequencing using the amplification primers (Microsynth AG, Austria).

2.4 Phylogenetic tree reconstruction

Bacterial 16S rRNA gene sequences obtained from bacterial isolates were aligned in BioEdit software v.7.2.5 using ClustalW with the default settings (Hall, 1999). Poorly aligned regions were edited manually, and the phylogeny was calculated by the Maximum Likelihood (ML) method in the bioinformatics software MEGA v.7.0 (Kumar et al., 2016). Best-fit nucleotide substitution model (T92+G+I) was selected according to AICc values (Akaike information criterion corrected), and the tree topology was completed using the Nearest-Neighbor-Interchange (NNI) heuristic model. Internal nodes of the tree were estimated with 1,000 bootstrap replicates. An ML tree of the protein alignment was computed based on the WGM model (Whelan and Goldman, 2001) implemented in MEGA v.7.0 (Kumar et al., 2016). The dataset was assessed with 100 bootstrap replicates.

2.5 Production of recombinant *Bc*Enhancin

A recombinant form of the *B. cereus* enhancin (r*Bc*E) was synthesized by GenScript Biotech, Netherlands. Briefly, the coding sequence of the WBV46172.1 protein without its putative signal peptide was cloned into the pET30a template vector with *Nde*I and *Hin*dIII restriction sites and expressed in the *E. coli* BL21 (DE3) system. The soluble protein with a C-terminal polyhistidine tag was induced at two different expression conditions, 37°C for 4 h and 15°C for 16 h, and then purified in a single step by Ni resin. The expression level of the recombinant protein and purity were analyzed under reducing conditions by SDS-PAGE and Western Blot. The purified r*Bc*E was aliquoted and stored at - 80°C until used for tick feeding.

2.6 Tick capillary feeding and bacterial infection

Depending on the experimental setup, female *I. ricinus* ticks were fed by blood, bacteria suspension, or purified protein using a modified capillary feeding technique (Figure 1) (Kim et al., 2021). Ticks from all groups were first infected with the wild-type *B. afzelii* strain RS 163_11i initially isolated from an *I. ricinus* tick in Serbia (Ćakić et al., 2019). An aliquot of frozen spirochetes was thawed at room temperature, transferred into sterile glass tubes, and incubated in 6 ml of Barbour-Stoenner-Kelly (BSK-H) medium supplemented with 6% rabbit serum (Sigma-Aldrich, St. Louis, MO, USA) at 33°C. *Borrelia* culture was grown until the cells reached a concentration of ~ 1 x 10^7/ml. The spirochete number was estimated by dark field microscopy using a Neubauer counting chamber (Wertheim, Germany) as previously described (Veinović et al., 2016). Sterile 5 µl glass capillaries (Drummond, PA, USA) filled with the culture were placed under a stereomicroscope over the hypostomes of ticks immobilized on a double-sided adhesive tape mounted on a microscopic slide (Supplementary Figure S2). Ticks were carefully removed from the tape after 3 h of feeding, placed in sterile 5 ml tubes with holes, and kept in a desiccator at 22°C and ~ 97% relative

10.3389/fcimb.2024.1476266

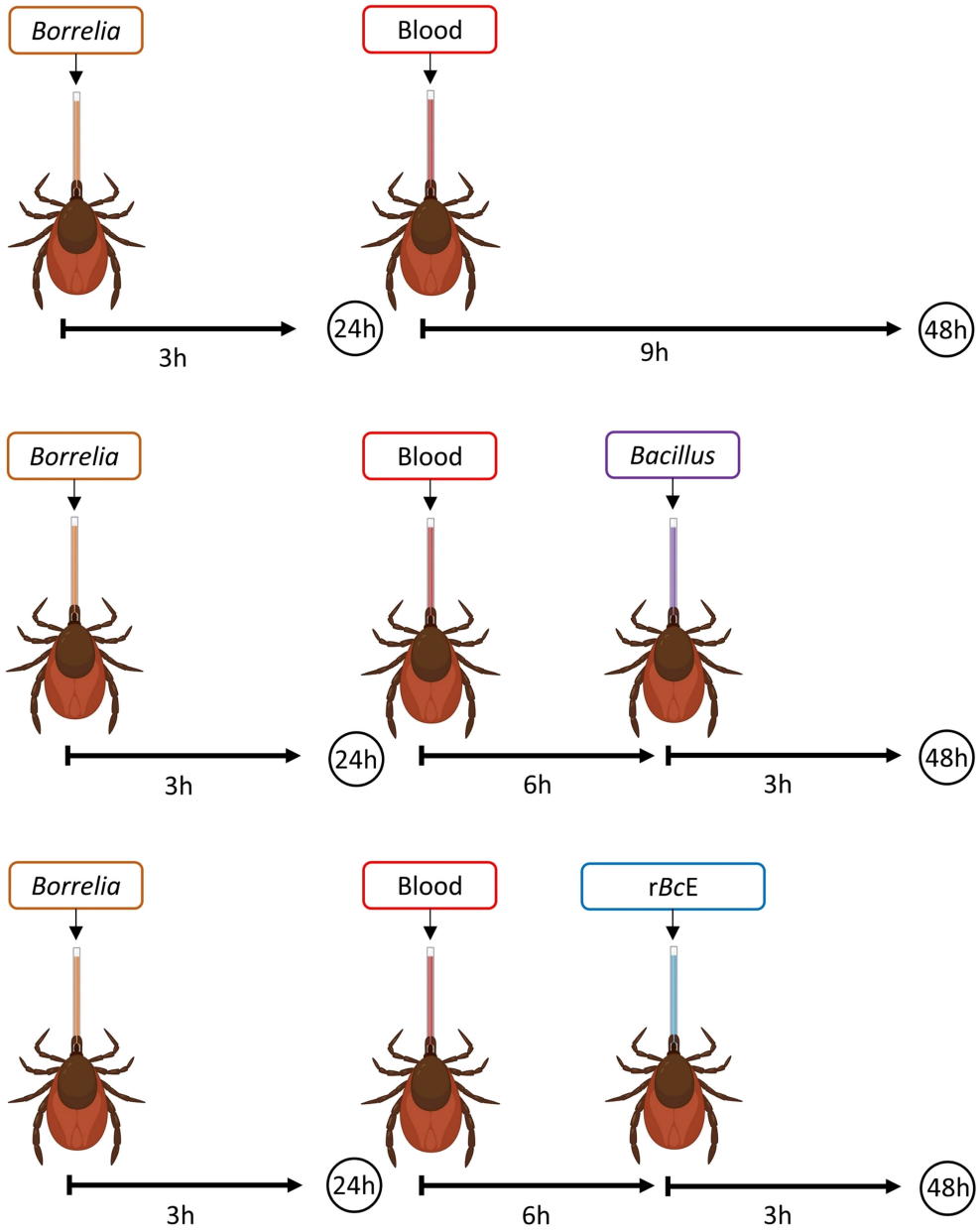

FIGURE 1
A schematic illustration of the experimental design. Ticks were infected with *B. afzelii* RS 163_11i using glass capillaries and after the 24-hour recovery period, they were fed either with *B. cereus* LTG-1 or *B. licheniformis* SP-3 bacteria suspensions or the purified *B. cereus* enhancin (r*Bc*E) protein. Bacterial levels were assessed 48 hours after feeding by qPCR. The figure was created with BioRender.com.

humidity for 24 h. After the 24-h recovery period, ticks were fed either by fresh defibrinated sheep blood (Oxoid, UK) alone or the blood in combination with bacteria suspension or the purified r*Bc*E protein depending on the group (Figure 1). *Bacillus cereus* LTG-1 and *B. licheniformis* SP-3 isolates were used for tick oral infection. The glycerol stocks of the bacteria were inoculated into Luria-Bertani (LB) broth (Carl Roth, Germany) and incubated overnight at 37°C with shaking. The overnight cultures were diluted in LB broth to obtain a standardized OD_{600} of 0.02 and incubated for an extra 2 h. The bacteria suspensions were mixed with the sheep blood (50:50 v/v) and used in two separate feeding experiments. Ticks from the r*Bc*E group received a mixture of the blood and the purified r*Bc*E at the final concentration of 15 µg/ml. This concentration is comparable to the amount of the recombinant enhancin used for mosquito feeding experiments conducted by Wu and colleagues (2019). Control ticks (mock) were fed with r*Bc*E inactivated at 70°C for 30 min. Tick feeding was performed in a humidified chamber in an incubator at 32°C. After feeding, ticks were separated by groups in sterile 5 ml tubes and maintained in the desiccator for 48 h before being processed for analysis.

2.7 Quantification of bacterial loads by qPCR

Prior to dissection, ticks were washed in 70% ethanol and sterile MQ water as described above. The wash-off water was used for DNA extraction and served as a control in downstream analyses. The individual tick guts were digested with proteinase K at 56°C overnight and then subjected to genomic DNA extraction using a QIAamp DNA Mini kit (Qiagen, Germany). The spirochete load was assessed by a probe-based qPCR that targets a 132 bp fragment of the *fla* gene that encodes *Borrelia* flagellin (Schwaiger et al., 2001). An additional qPCR targeting the mitochondrial 16S rRNA gene of *Ixodes* was run for DNA extraction control and data normalization purposes (Becker et al., 2023). Both qPCRs were conducted in 20 µl reactions containing GoTaq Probe qPCR Mastermix (Promega, WI, USA), 10 pmol of each primer, 5 pmol of Taqman probe, 5 µl DNA template, and nuclease-free water. Primer and probe sequences are listed in Supplementary Table 1. All qPCRs were performed in a CFX96 Real-Time PCR cycler (Bio-Rad Laboratories, Germany). The cycling conditions were identical for both PCR assays and consisted of 2 min at 95°C for denaturation, followed by 50 cycles of 15 sec at 60°C and 1 min at 95°C. Two technical replicates were tested, and no template controls were included in each PCR run. Relative abundance of spirochetes was normalized to the tick 16S rRNA reference gene and calculated using the $2^{-\Delta\Delta Ct}$ method (Pfaffl, 2001).

Quantification of total bacteria load in individual tick guts was assessed by a SYBR Green qPCR using the universal 341F/785R primers that target the hypervariable V3-V4 region of the 16S rRNA gene (Klindworth et al., 2013). The data were normalized to the tick 16S rRNA gene using the Ixo16-F/Ixo16S-R primers (Pfaffl, 2001; Becker et al., 2023). The PCRs were performed with the iQ SYBR Green Supermix (Bio-Rad Laboratories, Germany) following the manufacturer's recommendations.

2.8 Bactericidal assay

To assess the potential borreliacidal effect of the purified r*Bc*E, we performed an antimicrobial susceptibility *in vitro* test as previously described (Veinović et al., 2021). Briefly, *B. afzelii* RS 163_11i strain was grown to log phase and the bacterial suspensions (4 x 10^5 spirochetes/ml) were incubated at 33°C either with active or heat-inactivated r*Bc*E protein at three different concentrations (15 µg/ml, 30 µg/ml, and 60 µg/ml) or the ceftriaxone antibiotic (4 µg/ml), which was used as a positive control. Untreated bacterial culture served as a negative control. Proteins and the antibiotic preparations were filtered through 0.22 µm syringe filters (Sartorius Stedim Biotech GmbH, Germany) before incubation. The number, viability (%), and morphology of spirochetes were assessed by dark field microscopy after 24 and 48 h of incubation.

2.9 Whole-mount fluorescence *in situ* hybridization

A modified FISH protocol (Duron et al., 2018) was employed for the visualization of bacteria in tick guts. Whole ticks were fixed in a 4% paraformaldehyde solution 48 h post-feeding. To enable faster penetration of the fixative, the tick cuticula was pierced in several places with a sterile needle. After 3 days of fixation at 4°C, ticks were dissected under a stereomicroscope. The extracted guts were incubated overnight at 46°C in 200 µl of hybridization buffer (36 µl of 5M NaCl, 4 µl of 1M Tris-HCl, 0.02 g of dextran sulfate, 20 µl of blocking agent, 0.2 µl of 10% SDS, 40 µl of formamide, and 100 µl of MQ water) containing the Borr4 (Hammer et al., 2001) oligonucleotide probe labeled with Cy3 dyes at both ends (Supplementary Table S1). Next, the samples were washed with the washing buffer (43 µl of 5M NaCl, 20 µl of 1M Tris-HCl, 10 µl of 0.5M EDTA, 1 µl of 10% SDS, and 926 µl of MQ water) at 48°C for 30 min and additionally with 1 x PBS for 15 min at room temperature to remove the excess probes from the tissue. Counterstaining with DAPI (10 µg/ml in PBS) was performed in the dark for 8 min. Finally, the guts were washed with ice-cold MQ water and placed on a microscope slide, mounted with an antifade mounting media (Citifluor, PA, USA), and covered with a cover slip. The slides were examined with the Leica DMi8 Thunder Epifluorescence microscope (Leica Microsystems, Germany) using 20X dry, 63X glycerol, and 100X oil objective lens. The Leica LAS X microscope software (Leica Thunder Imager, Leica Microsystems, Germany) scanning the DAPI and Cy3 fluorescence channels with the Maximum Intensity Projection of 50 Z-stack images was used for FISH image acquisition.

2.10 Tick sectioning and Periodic acid Schiff's staining

Tick histology and PAS staining were performed at the Department of Clinical Sciences of Veterinary Medicine in Sarajevo following the protocol published by Narasimhan and colleagues (2014). Briefly, formalin-fixed ticks were routinely processed, embedded in paraffin, and cut at 3-6 µm sections. The sections were deparaffinized, stained with PAS (Sigma-Aldrich, MO, USA), and visualized by light microscopy (Olympus BX51, Japan) at 40X magnification. Images were acquired using computer image analysis software (Cell Digital Imaging Software, Olympus, Japan). At least 6-10 sections per tick were examined.

2.11 Gene expression by RT-qPCR

RNA was extracted from pooled tick guts (five guts per pool) using a Total RNA Purification kit (Norgen Biotek, Canada) following the manufacturer's instructions. Prior to extraction, the guts were homogenized in 600 µl of Buffer RL supplemented with β-mercaptoethanol (Sigma-Aldrich, Austria) by passage through 24- and 27-gauge needles (Knorr et al., 2021). The RNA extraction from *B. cereus* LTG-1 culture was done following the protocol for bacterial cells with an additional lysozyme step (Sigma-Aldrich, Austria). Quantification of RNA was accomplished with the Qubit 4 Fluorometer (Thermo Fischer Scientific, IL, USA) and Qubit RNA Broad Range Assay kit (Thermo Fischer Scientific, IL, USA). The

isolates were additionally purified and concentrated with the RNA Clean & Concentrator kit (Zymo Research, CA, USA). Subsequently, the RNA samples free of contaminating DNA (Turbo DNA-free kit, Ambion, USA) were reverse transcribed to cDNA with the High-Capacity cDNA Reverse Transcription kit (Applied Biosystems, CA, USA) and stored at - 20°C until use. To examine whether r*Bc*E affects tick gut immune response, the relative transcript levels of the major immune genes and genes related to the PM formation were determined by RT-qPCR. Primer sequences are listed in Supplementary Table S1. The amplification was carried out in a CFX96 Real-Time PCR cycler (Bio-Rad Laboratories, Germany) with an initial denaturation at 95°C for 5 min followed by 35 cycles at 95°C for 15 sec and 63°C for 30 sec. A melt curve analysis was performed to check the specificity of the resulting amplicons, and a no-template control was included for each gene. The PCR mixture was prepared in a final volume of 20 µl using iQ SYBR Green Supermix (Bio-Rad Laboratories, Germany), 0.8 µl of each primer, 1 µl of cDNA, and nuclease-free water. The relative gene expressions were calculated using the $2^{-\Delta\Delta Ct}$ method (Pfaffl, 2001) and normalized to the levels of the *I. ricinus* elongation factor 1-alpha (*elf-1a*) housekeeping gene.

2.12 Microbiota analysis by 16S rRNA gene-targeted amplicon sequencing

Amplicon sequencing was performed at the Joint Microbiome Facility of the University of Vienna and the Medical University of Vienna (project ID: JMF-2311-10). Briefly, the hypervariable V3-V4 regions of the bacterial 16S rRNA genes were amplified with the primers 341F and 785R containing 16 bp head adapters (H1: 5′-GCTATGCGCGAGCTGC-3′, H2: 5′-TAGCGCACACCTGGTA-3′) in the first PCR step, followed by a second barcoding PCR step performed with 12 bp unique dual barcodes (Herbold et al., 2015; Pjevac et al., 2021). After each amplification, the products were purified and normalized with the SequalPrep™ Normalization Plate kit (Invitrogen), and the second-step amplicons were pooled and concentrated on columns with the innuPREP PCRpure Kit (Analytik Jena, Germany). Sequence library preparation was done using the Illumina TruSeq DNA Nano Kit (Illumina, CA, USA) and libraries were sequenced in paired-end mode (2 × 300 nt; v3 chemistry) on an Illumina MiSeq (Illumina, CA, USA). Next, amplicon pools were extracted from the raw sequencing data applying default parameters in FASTQ workflow in BaseSpace (Illumina), PhiX sequences were decontaminated using BBDuk (BBtools) (Bushnell et al., 2017), and the sequences were demultiplexed with the Python package demultiplex by permitting one mismatch for barcodes and two mismatches for linkers and primers (Herbold et al., 2015; Pjevac et al., 2021). FASTQ reads 1 and 2 were trimmed at 230 bp with allowed expected errors of 4 and 6, respectively, paired-end reads were merged and ASVs were subsequently inferred with the Divisive Amplicon Denoising Algorithm (DADA2) (Callahan et al., 2016a, Callahan et al., 2016b). Taxonomy was assigned with the SINA v.1.6.1 classifier (Pruesse et al., 2012) against the SILVA SSU database SSU Ref NR 99 v.138.1 (doi.org/10.5281/zenodo.3986799). Taxa represented at less than 1% relative abundance were excluded from the analyses to rule out potential environmental contaminants (Narasimhan et al., 2022).

2.13 Statistical analysis

Statistical analyses were performed using GraphPad Prism10 (GraphPad Software Inc., CA, USA) and R v.4.0 statistical software. The differences between the control and experimental groups were analyzed using a nonparametric two-tailed Mann-Whitney *U* test. 16S rRNA data analyses were performed using R packages rstatix v.0.7.0, ampvis v.2.0 (Allaire, 2012), and ggplot2 v.3.3.3 (Wickham, 2009). The Shapiro-Wilk test was performed to test for normality of the data, and the result of this determined whether *t* tests or Wilcoxon tests were used. All *p* values were adjusted via fdr correction. Alpha and beta diversity indices were calculated using the R package vegan v.2.5 (Oksanen et al., 2013). Differences were considered significant if $p < 0.05$.

3 Results

3.1 Bacteria residing in the guts of *I. ricinus* ticks express enhancins

To understand the molecular mechanisms by which tick gut bacteria can antagonize the growth of *Borrelia* species, we first isolated cultivable bacteria from questing *I. ricinus* nymphs, males, and females collected from three locations in Vienna, Austria (Supplementary Figure S1). Overall, 30 bacterial species representing 15 genera were isolated from individual (15.8%) or pooled tick guts (39.6%) and almost half of the isolates belonged to the family Bacillaceae (Figures 2A, B). All isolates were representatives of aerobic and/or facultative anaerobic Gram-positive bacteria commonly found on the skin and in the environment (Supplementary Table S2).

Representatives of five bacterial species identified in the present study for which complete annotated genomes are publicly available, namely *B. cereus*, *Bacillus mycoides*, *Bacillus toyonensis*, *Neobacillus niacini*, and *Curtobacterium flaccumfaciens* were found to contain putative enhancins by Pfam domain and genome analysis (Figure 2A; Supplementary Figure S3). Considering the ability of *B. cereus* enhancins to digest mucins of different arthropods (Fang et al., 2009; Wu et al., 2019), we selected *B. cereus* LTG-1 strain as a model organism for the following tick feeding experiments. Furthermore, *B. cereus* strains are commonly found in *Ixodes* ticks (Martin and Schmidtmann, 1998; Murrell et al., 2003; Kmet and Čaplová, 2019; Rousseau et al., 2021; Yang et al., 2021; Tóth et al., 2023). The capacity of *B. cereus* to produce enhancin appears to be strain-dependent as not all sequenced strains encode the *enhancin* gene (Nakjang et al., 2012). Hence, a PCR assay targeting a 952 bp fragment was used for the gene detection and characterization in our bacterial isolate. Sequence analysis and Basic Local Alignment Search Tool (blast.ncbi.nlm.nih.gov) revealed a 100% homology of the obtained nucleotide sequence with the M60 family metallopeptidase from the *B. cereus* PL22-16A soil

10.3389/fcimb.2024.1476266

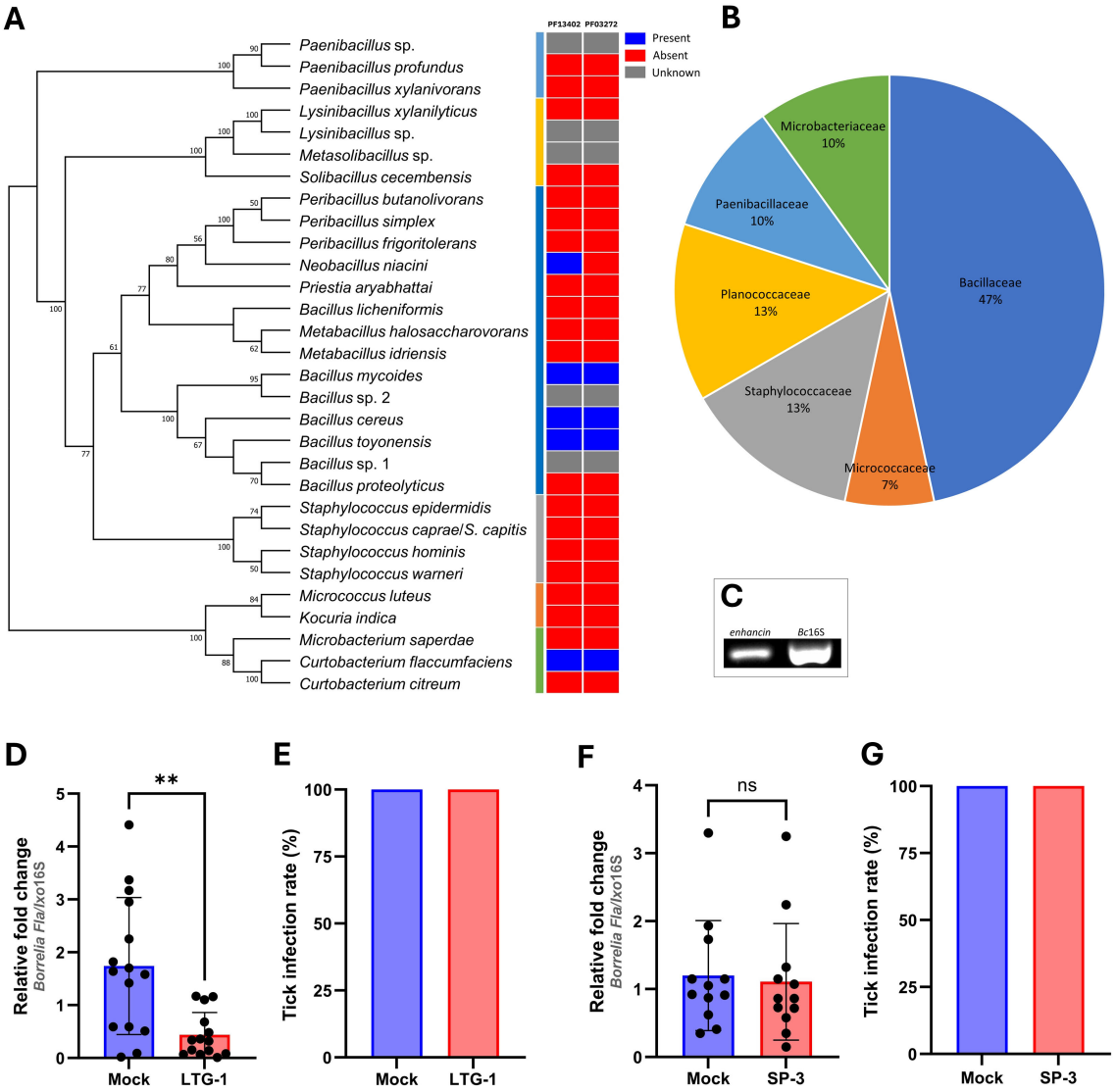

FIGURE 2
An enhancin-containing bacterium affects *Borrelia* colonization in the tick gut. **(A)** Bacteria identified by culture-dependent approach in individual or pooled guts of nymphal, male, and female ticks. An ML bootstrap tree of the 16S rRNA nucleotide sequences of bacterial isolates (1329 bp). The tree with the highest log likelihood (13903.286) is shown. Bootstrap values based on 1,000 replicates are indicated at the nodes (only values higher than 50% are shown). Color strip: Presence and absence of the Peptidase M60, enhancin and enhancin-like (PF13402) and Putative mucin or carbohydrate-binding module (PF03272) conserved domains across the phylogeny of 30 bacterial isolates based on the Pfam domain analysis. **(B)** Prevalence of the bacteria (%) isolated from *I. ricinus* ticks at the family level. **(C)** Expression of *enhancin* in bacteria suspension (*B. cereus* LTG-1) assessed by RT-PCR. **(D, E)** *B. afzelii* load and the infection rate (%) in guts of female *I. ricinus* ticks co-infected with *B. cereus* LTG-1 strain. One dead tick was excluded from the analysis. **(F, G)** *B. afzelii* load and the infection rate (%) in guts of female *I. ricinus* ticks co-infected with *B. licheniformis* SP-3. **(D, F)** Each data point represents an individual gut. Results are presented as mean ± SD of two technical replicates. Normalized Ct values were compared between groups by a nonparametric two-tailed Mann-Whitney *U* test (ns, not significant, $^{**}p \leq 0.01$).

isolate (GenBank® accession number: CP115856.1). Together, these results indicate that bacteria inhabiting *I. ricinus* guts contain putative enhancins and suggest their potential to alter the structural integrity of the tick PM by digesting the mucous-like matrix.

3.2 Coinfection with *B. cereus* LTG-1 reduces *B. afzelii* load in the tick gut

To investigate whether enhancin-containing bacteria can influence *B. afzelii* persistence in the tick vector, infected *I. ricinus* females were fed with *B. cereus* LTG-1 via capillary feeding (Figure 1). Bacteria loads in individual tick guts were assessed 48 h post-feeding by qPCR. Oral introduction of the bacteria suspension, in which the *enhancin* gene was expressed (Figure 2C), reduced *B. afzelii* levels in comparison with the control ticks (Mann Whitney *U* test, $p = 0.0015$, Figure 2D). However, feeding of *B. cereus* LTG-1 was unable to completely clear *B. afzelii* infection (Figure 2E). One tick from the LTG-1 group died after feeding and it was excluded from further analyses. While twelve out of 14 guts from the bacteria-fed ticks were positive by qPCR, none of the control ticks contained detectable DNA of *B. cereus*. This

result suggests that a transient bacterial association is sufficient to reduce *B. afzelii* load. The inability of *B. cereus* LTG-1 to stably colonize *I. ricinus* guts may be due to colonization resistance conferred either by the resident tick microbiota or by host immune defenses. To exclude the possibility that the reduction in *B. afzelii* was due to modulation of the gut microbiome or other factors unrelated to enhancin production, we fed ticks with another tick-associated *Bacillus* species, *Bacillus licheniformis*, which does not encode enhancin (Figure 2A). The spirochete loads and *Borrelia* infection rates were comparable between control ticks and those fed with *B. licheniformis* SP-3 suspension (Mann Whitney *U* test, $p = 0.5223$, Figures 2F, G). Taken together, our results suggest that gut colonization with *B. cereus* LTG-1 inhibits *B. afzelii* growth within the tick vector due at least in part to its secreted *Bc*Enhancin.

3.3 *Bc*Enhancin hinders *B. afzelii* colonization by compromising the structural integrity of the PM

The *Bc*Enhancin protein has a predicted molecular weight of 85.5 kDa and consists of an N-terminal signal peptide and M60-like (E-value: 5.55e-42) and Mucin_bdg (7.9e-36) domains (Figure 3A). The M60-like domain has a typical zinc metallopeptidase motif with an additional catalytic glutamic acid residue (HEXXHX(8,28)E) and it represents a mucin-active part of the protein (Figures 3A, B), whereas Mucin_bdg is the binding domain for enhancins and other similar metalloproteases (Wang and Granados, 1997; Nakjang et al., 2012). *Bc*Enhancin homologs are also found in other bacteria associated with *I. ricinus* ticks (Stojek and Dutkiewicz, 2004; Tveten et al., 2013; Lejal et al., 2021; Rousseau et al., 2021; Guizzo et al., 2022; Tóth et al., 2023) bearing 29.4% to 98.5% similarity at the protein level (Figures 3B, C). To experimentally test the hypothesis that secreted *Bc*Enahncin has the potential to impair *B. afzelii* colonization, we generated a recombinant version of the protein (r*Bc*E) using an *E. coli* BL21 (DE3) expression system and assessed the ability of the purified form to digest the tick PM *in vivo*. Sodium dodecyl-sulfate polyacrylamide gel electrophoresis (SDS-PAGE) and Western blot analyses revealed a single protein of the expected molecular weight with ≥ 90% purity (Figure 3D). The purified r*Bc*E was used for tick feeding (Figure 1) and the spirochete burden was determined by qPCR and FISH. The control group received an equal amount of heat-inactivated r*Bc*E. Ticks fed the purified protein showed significantly decreased *B. afzelii* levels (Mann Whitney *U* test, $p < 0.0001$, Figure 3E) and slightly lower infection rate ($p > 0.05$, Figure 3F) when compared to control ticks. All ticks survived the treatment and qualitative assessment of tick activity after feeding (i.e., mobility and questing activity) did not reveal any apparent deviation from normal tick behavior, suggesting that r*Bc*E does not have observable acute effects on tick fitness. The qPCR results were further confirmed by visualization of the spirochetes in the guts by FISH using a *Borrelia*-specific probe (Hammer et al., 2001). Clusters of spirochetes in the guts of control ticks could be seen in almost every microscopic field of view, whereas guts from r*Bc*E-fed ticks contained only a few scattered bacteria (Figure 3G). Besides the differences in the spirochete number and the spatial organization between the groups, a deviation from the typical flat-wave spirochete morphology was observed in the r*Bc*E group (Figure 3G), which might be indicative of impaired bacteria mobility (DeHart et al., 2021). *In vitro* assessment of the r*Bc*E on pathogen burden, viability, or morphology revealed that the suppressive effect of r*Bc*E is not due to direct bactericidal action (Supplementary Figure S4). To further examine the potential effect of r*Bc*E on the structural integrity of the PM, tick histology sections were stained with the PAS base stain, which specifically detects the glycan-rich layer of the PM in blood-feeding arthropods (Narasimhan et al., 2014; Abraham et al., 2017; Narasimhan et al., 2017; Wu et al., 2019). Ticks fed with r*Bc*E displayed thinner and fragmented PM 24 hours after oral administration in comparison to those treated with inactivated enzyme (Figure 4). Together, this suggests the ability of *Bc*Enhancin to affect *B. afzelii* colonization by impairing the structural organization of the PM and further reinforce the importance of this physical gut barrier for persistence of *Borrelia* within its arthropod vector.

3.4 *Bc*Enhancin treatment induces transcriptional changes in host immune response genes

Because the disruption of the arthropod gut barrier may induce an immune response in the epithelial cells (Kuraishi et al., 2011; Yang et al., 2014; Narasimhan et al., 2017; Rodgers et al., 2017; Talyuli et al., 2023), we sought to examine if specific immune pathways or components are involved in observed *B. afzelii* reduction in ticks. Expression profiles of the selected putative genes representing key factors of the JAK/STAT (*stat*), Toll (*myD88*), and IMD (*xiap*) immune signaling pathways, free radical defense (*nos*), antimicrobial peptides (*DefMT3*, *DefMT4*), and structural components of the PM (*peritrophin-1*, *mucin-2*) (Smith and Pal, 2014) were assessed by RT-qPCR. While transcript levels of *stat*, *xiap*, *nos*, and *mucin-2* were not altered, *myD88* and *peritrophin-1* genes were upregulated in the guts 48 hours after oral administration of the purified r*Bc*E protein. Expression levels of two defensins (*DefMT3*, *DefMT4*) were decreased in treated ticks compared to the mock control (Figure 5). These results imply that the degradation of the PM by *Bc*Enhancin affects the expression profile of the gut immune genes.

3.5 *Bc*Enhancin treatment influences total bacterial load and composition in infected tick guts

As *Bc*Enhancin affected the gut protective barrier and immunity, we speculated that these changes might influence the microbiome composition. To address this, we first quantified the total bacterial burden by 16S rRNA gene-targeted qPCR. Ticks fed with heat-inactivated r*Bc*E had lower bacterial load 48 h after

10.3389/fcimb.2024.1476266

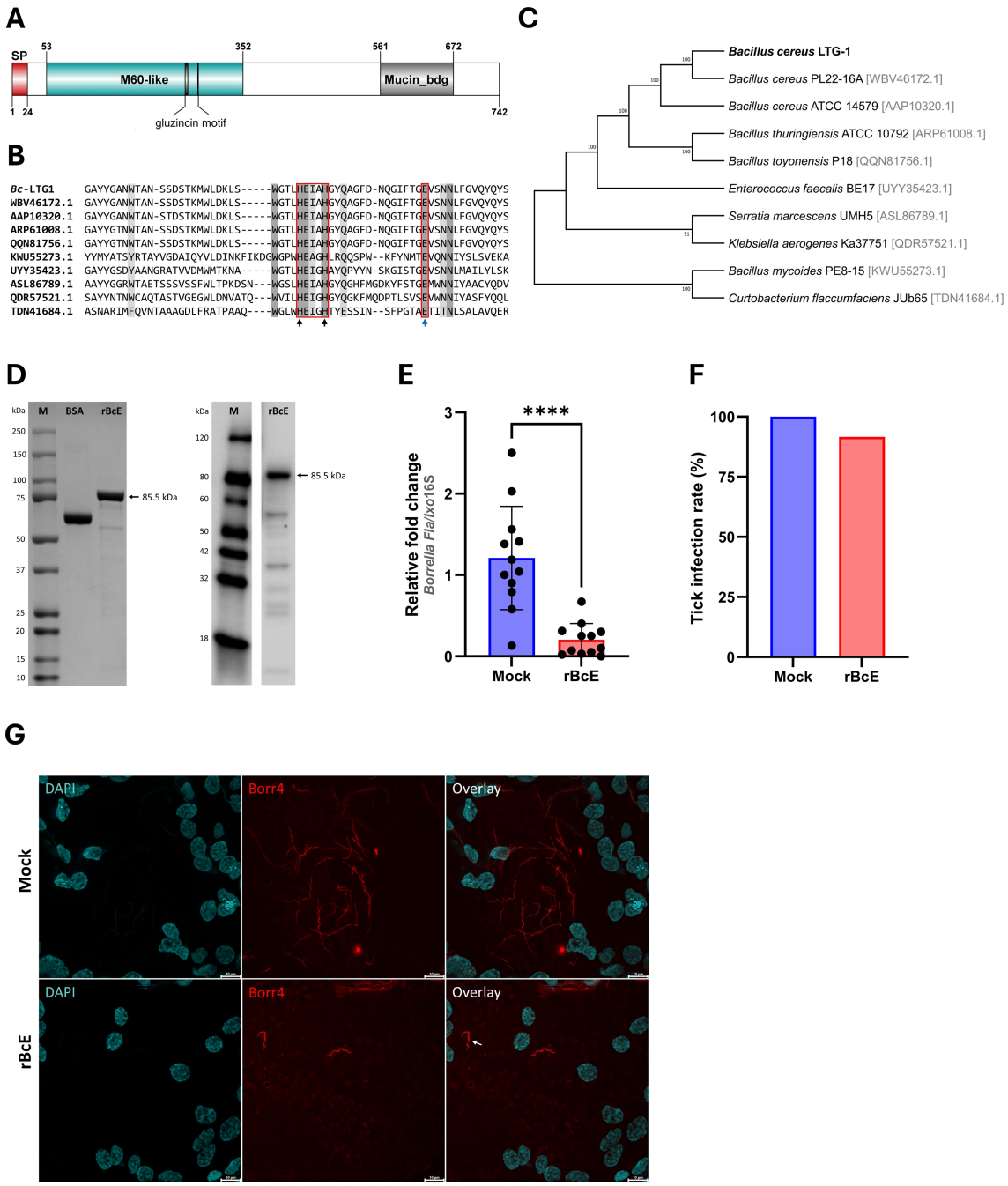

FIGURE 3

*Bc*Enhancin reduces *B. afzelii* growth by compromising the PM structural integrity. **(A)** Domain architecture of the putative *Bc*Enhancin protein. *Bc*Enhancin consists of the N-terminal signal peptide (SP) and two conserved domains. The M60-like domain contains a gluzincin motif (HEXXHX (8,24)E). The protein structure is visualized using DOG 2.0 Illustrator (Ren et al., 2009). **(B)** Partial amino acid sequence alignment of the M60-like domain identified in *I. ricinus*-related bacteria. Identical residues are shaded in dark grey, whereas similar residues are in light grey. The gluzincin with the typical zinc metallopeptidase motif (HEXXH) and the additional glutamate (E) residue is boxed. The arrows indicate the Zn^{+} binding (black) and catalytic (blue) residues. **(C)** An ML tree of the bacterial enhancin proteins based on the WGM model. GenBank® accession numbers for each amino acid sequence are given in the brackets. Numbers at the nodes indicate bootstrap values based on 100 replicates (only values >50% are included). **(D)** Detection of the purified r*Bc*E by SDS-PAGE (left) and Western blot (right) under reducing conditions. Bovine serum albumin (BSA) served as a control in SDS-PAGE. r*Bc*E expression was detected by Western blot using a mouse anti-His monoclonal antibody. **(E, F)** Load of *B. afzelii* and the infection rate (%) in ticks fed by the heat-inactivated (mock) and active form of the r*Bc*E protein. Each data point represents an individual gut. Results are presented as mean ± SD of two technical replicates. Statistical significance was determined by a nonparametric two-tailed Mann-Whitney *U* test (****$p \leq 0.0001$). **(G)** Visualization of the spirochete burden and morphology in guts of female ticks by whole-mount FISH. Images represent five biological replicates per group. The arrow indicates a spirochete with altered morphology. *Scale-bar*: 10 µm.

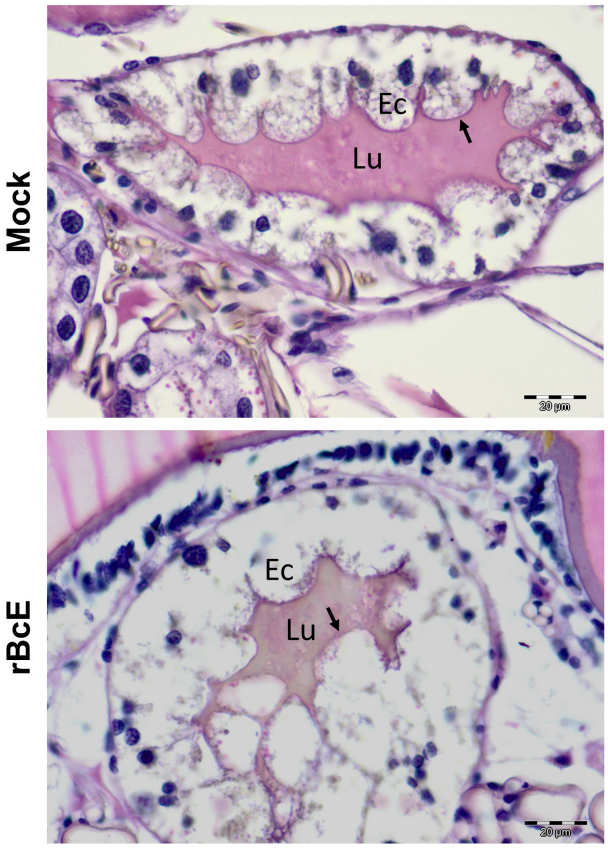

FIGURE 4
PAS staining of the tick gut sections showing the difference in the PM structure between control (mock) and r*Bc*E ticks. Results are shown for one representative of three biological replicates. Arrows indicate the PAS-positive PM layer. Lu, gut lumen; Ec, gut epithelial cell. *Scale-bar*: 20 µm.

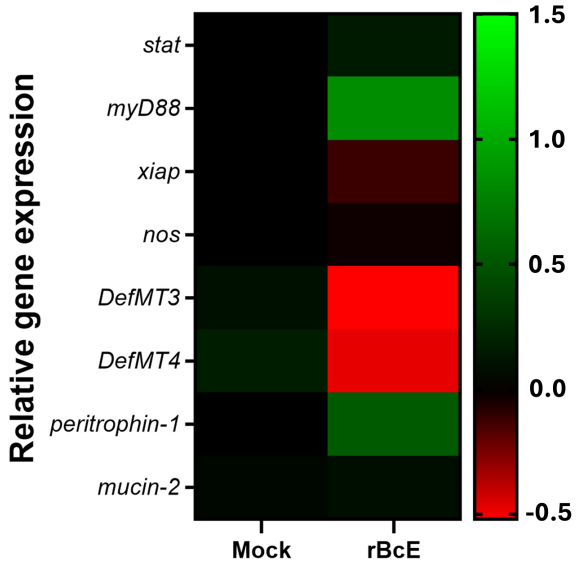

FIGURE 5
Heat map showing alterations in the expression profiles of the representative immune and structural genes between ticks fed with heat-inactivated (mock) or active r*Bc*E protein ($p > 0.05$). Transcription was assessed by RT-qPCR at 48 hours post-feeding and the data were normalized to the tick *elf-1a* housekeeping gene. Data represent mean values of three biological replicates.

feeding compared to those fed with the intact protein, but the difference was not statistically significant (Mann Whitney *U* test, $p = 0.5043$, Figure 6A). Samples were then subjected to 16S rRNA gene amplicon sequencing to investigate the differences in bacterial diversity and composition between the groups. Six samples, two from the control group and four from the r*Bc*E group were excluded from the study due to inadequate reads. Amplicon sequence variants (ASVs) attributed to *Candidatus* Midichloria sp. were also removed from the data set because this endosymbiont primarily resides in ovaries (Olivieri et al., 2019) and we would not expect it to be part of the active gut microbiome. Gut bacterial community composition differed between the groups at both the phylum and the genus level (Figures 6B, C; Supplementary Figures S5A, B). The differences in composition were mainly due to alterations in the relative abundances of *Borrelia*, *Acinetobacter*, *Brevibacterium*, *Flavobacterium*, *Staphylococcus*, *Pseudomonas*, and *Corynebacterium* (Figures 6C; Supplementary Figure S5B). Alpha diversity was significantly different between the groups, with ticks from the r*Bc*E group having a higher Shannon diversity compared to control ticks (Student's *t*-test, adjusted $p = 0.0127$, Figure 6D). Multivariate analysis of variance revealed significant differences in microbiome composition (PerMANOVA, $F = 6.6083$, adjusted $p = 0.0001$) and Principal component analysis (PCA) of microbial relative abundances indicated separation of clusters (Figure 6E). However, the difference in alpha (Student's *t*-test, adjusted $p = 0.854$) and beta (PerMANOVA, $F = 0.9818$, adjusted $p = 0.463$) diversities between the groups was not significant after *Borrelia* ASVs were removed from the dataset (Supplementary Figure S6), suggesting that the alterations in microbiome composition was driven largely by *B. afzelii* abundance.

4 Discussion

Successful pathogen infection and persistence within a tick vector depends on the complex interactions between the host, its microbiome, and the pathogen (Kurokawa et al., 2020). The gut environment is profoundly influenced by residential microbes, which can either promote or antagonize pathogen colonization and its subsequent transmission to the vertebrate host (Kurokawa et al., 2020; Narasimhan et al., 2021; Wu-Chuang et al., 2021). Therefore, understanding the functional consequences of the tripartite interactions and the mechanisms by which certain microbial components of the gut microbiome might affect *Borrelia* infection success is of great research interest and could spur novel strategies to control both LB and its tick vector.

In the present study, we showed that *Bc*Enhancin derived from a tick-associated *Bacillus* bacterium limits *B. afzelii* persistence in *I. ricinus* females by interfering with the structural organization of the PM, further supporting the critical role of this physical barrier in the

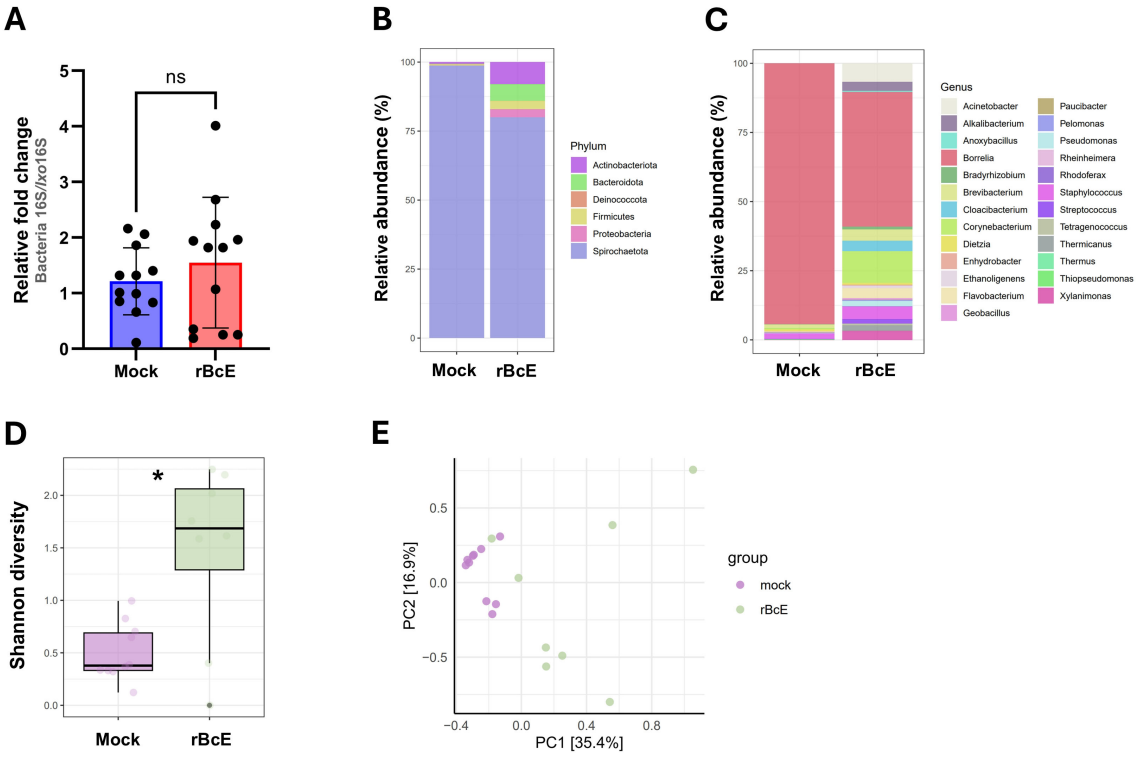

FIGURE 6
The tick PM is important for maintaining gut microbial homeostasis. **(A)** Total bacteria load in the guts of ticks fed with heat-inactivated (mock) or active r*Bc*E protein assessed by conventional PCR using universal 16S rRNA primers. Statistical significance was evaluated by a non-parametric Mann-Whitney *U* test (ns, not significant). **(B, C)** Taxonomic composition and relative abundance of bacterial communities in control and treated ticks at the taxonomic rank of phylum and genus. Only genera with relative abundance > 1% were considered. **(D)** Alpha diversity measured by Shannon diversity index (Student's *t*-test, *$p \leq 0.05$). **(E)** Principal component analysis (PCA) based on Bray-Curtis distances of bacterial communities between the groups, displayed by different colored dots.

protection of spirochetes. The intact PM might be particularly important for *B. afzelii* infection success considering that this species, unlike the North American *B. burgdorferi* strains vectored by *I. scapularis*, remains in the tick gut until it is transmitted to the vertebrate host by regurgitation of spirochetes from the gut lumen (Pospisilova et al., 2019). Its integrity is largely influenced by the gut microbiome, which regulates the expression of peritrophins by the activation of the JAK-STAT signaling pathway (Narasimhan et al., 2014). Our data, however, suggest that *Bc*Enhancin induces structural changes in the PM by degrading the protective mucopolysaccharide layer, as seen by PAS staining of the tick gut sections, but this needs to be further confirmed by *in vitro* digestion assay with recombinant *I. ricinus* mucins. The similar mucin-degrading effect and destruction of the PM have been reported in other arthropods, including mosquitoes exposed to enhancins encoded by *B. cereus*, *Bacillus thuringiensis*, and *Serratia marcescens* (Fang et al., 2009; Wu et al., 2019). These bacterial enhancins also demonstrate the ability to digest intestinal mucins *in vitro* by cleaving the *O*-glycosylated sites (Fang et al., 2009; Wu et al., 2019). Mucins are heavily *O*-glycosylated proteins that, along with peritrophins, line the invertebrate PM and maintain its structural and functional integrity (Wu et al., 2019; Kozelková et al., 2023). Proteomic and transcriptomic profiling of *I. ricinus* guts revealed several putative mucins and peritrophins, some of which were upregulated upon infection with *B. afzelii* (Mahmood et al., 2021; Kozelková et al., 2023). Moreover, borrelial pathogens exploit chitobiose from the tick PM as an energy source and a building block for the bacterial cell wall (DeHart et al., 2021). These results may indicate that *Borrelia* induces the formation of the PM to enhance its colonization and persistence within the tick vector. By contrast, the compromised structure of the PM appears to promote infection with some intracellular tick-borne pathogens, such as *Anaplasma phagocytophilum*, *Theileria* sp., and *Babesia microti* by facilitating the pathogen migration from the gut to salivary glands (Abraham et al., 2017; Jalovecka et al., 2018; Wei et al., 2021). Consistent with these observations, higher abundances of *Bacillus* species in *Anaplasma*-positive *I. ricinus* (Lejal et al., 2021) and *Theileria*-positive *Rhipicephalus microplus* (Adegoke et al., 2020) ticks may suggest that members of this bacterial genus enhance the tick susceptibility to infections, possibly by interacting with the PM.

We also observed changes in the expression profiles of gut immune response genes in ticks with the compromised PM, which might affect *B. afzelii* colonization. The highest transcription level among selected genes was recorded for a gene encoding myD88 adapter protein. MyD88 is a key component of the Toll signaling

pathway, which is predominantly induced by Gram-positive bacteria and fungi in *Drosophila* flies (Michel et al., 2001; Rutschmann et al., 2002), but the importance of Toll activation in controlling bacterial infections in ticks is poorly understood. In this context, the increased expression of *myD88* positively correlated with the increased relative abundance of Gram-positive bacteria such as *Staphylococcus*, *Streptococcus*, *Corynebacterium*, and *Brevibacterium* in r*Bc*E-fed ticks. Narasimhan and colleagues (2017) report similar findings in *I. scapularis* ticks after the abrogation of a gene encoding the PIXR gut protein with a Reeler domain. Specifically, knockdown of *pixr* impaired the structural integrity of the PM, decreased *B. burgdorferi* loads, and resulted in the elevated expression of another transcription factor of the Toll pathway called *dorsal*. Several immune pathways or their components, including myD88 have been shown to be involved in controlling the initial skin colonization by *Borrelia* spirochetes (Bockenstedt et al., 2006), suggesting that the immune response mediated by myD88 or some of the downstream Toll effector molecules might play a role in the clearance of *B. afzelii* from the guts of I. *ricinus*. Interestingly, ticks exposed to r*Bc*E showed decreased expression of two selected defensins that are typically expressed by *I. ricinus* gut cells (Tonk et al., 2014). Metalloproteases produced by certain bacterial and protozoan pathogens are known for their ability to inactivate multiple antimicrobial peptides, including defensins (Belas et al., 2004; Kulkarni et al., 2006). Consequently, it is possible that *Bc*Enhancin suppresses the activity of tick defensins to prevent bacterial cell death.

The breakdown in the integrity of the PM was also associated with a reduced load of *Borrelia*, but the abundances of other taxa were not significantly affected. This result suggests that the PM plays a selective role in limiting *Borrelia* burden in the tick gut, while having little to no effect on bacterial commensals that inhabit the intraperitrophic (luminal) space. According to our observations and those of previous studies (Kariu et al., 2013; Narasimhan et al., 2014; Yang et al., 2014, Yang et al., 2021), we hypothesize that the growth of *Borrelia* spirochetes is inhibited when they are exposed to luminal bacteria and/or their toxins in ticks with an impaired gut barrier.

In summary, our study uncovered the influence of residential gut microbes on tick-spirochete interaction dynamics and confirmed the importance of the PM for *B. afzelii* infection. While this knowledge moves the field beyond a descriptive understanding of the tick gut microbiome, further studies are required to establish a correlative relationship between enhancin-containing bacteria and resistance to *Borrelia* colonization of the tick gut under natural conditions. Our results suggest that targeting structural components of the tick gut holds potential for the development of alternative tools to control LB. Genetic modification of symbiotic or commensal gut-colonizing microbes to express effector molecules that can inhibit pathogen development within the vector has been recently proposed as an efficient strategy for the control of tick-borne diseases (Mazuecos et al., 2023). Therefore, using PM-degrading proteins in paratransgenesis represents a promising option that should be investigated in future studies.

Data availability statement

The datasets presented in this study can be found in online repositories. The names of the repository/repositories and accession number(s) can be found at: https://www.ncbi.nlm.nih.gov/, PRJNA1086846. Nucleotide sequences of the 16S rRNA gene from bacterial isolates have been deposited in GenBank® with accession numbers PP446093-PP446122. The *B. cereus* LTG-1 enhancing gene sequence is available under accession number PP444694.

Ethics statement

The manuscript presents research on animals that do not require ethical approval for their study.

Author contributions

AH: Conceptualization, Data curation, Formal analysis, Funding acquisition, Investigation, Methodology, Project administration, Resources, Visualization, Writing – original draft. GV: Data curation, Formal analysis, Investigation, Methodology, Writing – review & editing. AA: Data curation, Formal analysis, Investigation, Methodology, Writing – review & editing. DS: Formal analysis, Software, Writing – review & editing. MK: Data curation, Investigation, Writing – review & editing. GN: Data curation, Investigation, Writing – review & editing. RS: Data curation, Formal analysis, Investigation, Writing – review & editing. JŠ: Data curation, Formal analysis, Investigation, Writing – review & editing. ST: Formal analysis, Resources, Writing – review & editing. DB: Formal Analysis, Supervision, Writing – review & editing.

Funding

The author(s) declare financial support was received for the research, authorship, and/or publication of this article. This research was funded in whole or in part by the Austrian Science Fund (FWF) [Project ID No.: P 36130]. The work of GV, RS and ST was supported by the Ministry of Science Technological Development and Innovation of the Republic of Serbia (Contract Number 451-03-66/2024-03/200015 with Institute for Medical Research University of Belgrade, National Institute of Republic of Serbia).

Acknowledgments

We thank Dr. Petra Pjevac and Dr. Joana Séneca Silva from the Joint Microbiome Facility of the University of Vienna and Medical University of Vienna, Austria for their support in the 16S rRNA gene amplicon library preparation.

Conflict of interest

The authors declare that the research was conducted in the absence of any commercial or financial relationships that could be construed as a potential conflict of interest.

Publisher's note

All claims expressed in this article are solely those of the authors and do not necessarily represent those of their affiliated organizations, or those of the publisher, the editors and the reviewers. Any product that may be evaluated in this article, or claim that may be made by its manufacturer, is not guaranteed or endorsed by the publisher.

Supplementary material

The Supplementary Material for this article can be found online at: https://www.frontiersin.org/articles/10.3389/fcimb.2024.1476266/full#supplementary-material

References

Abraham, N. M., Liu, L., Jutras, B. L., Yadav, A. K., Narasimhan, S., Gopalakrishnan, V., et al. (2017). Pathogen-mediated manipulation of arthropod microbiota to promote infection. *Proc. Natl. Acad. Sci. U.S.A.* 114, E781–E790. doi: 10.1073/pnas.1613422114

Adegoke, A., Kumar, D., Bobo, C., Rashid, M. I., Durrani, A. Z., Sajid, M. S., et al. (2020). Tick-borne pathogens shape the native microbiome within tick vectors. *Microorganisms* 8. doi: 10.3390/microorganisms8091299

Allaire, J. (2012). *RStudio: Integrated Development for R.* (Boston, MA: RStudio, PBC). Available online at: http://www.rstudio.com.

Becker, N. S., Rollins, R. E., Stephens, R., Sato, K., Brachmann, A., Nakao, M., et al. (2023). *Candidatus* Lariskella arthopodarum endosymbiont is the main factor differentiating the microbiome communities of female and male *Borrelia*-positive *Ixodes persulcatus* ticks. *Ticks Tick Borne Dis.* 14, 102183. doi: 10.1016/j.ttbdis.2023.102183

Belas, R., Manos, J., and Suvanasuthi, R. (2004). *Proteus mirabilis* ZapA metalloprotease degrades a broad spectrum of substrates, including antimicrobial peptides. *Infect. Immun.* 72, 5159–5167. doi: 10.1128/IAI.72.9.5159-5167.2004

Bockenstedt, L. K., Liu, N., Schwartz, I., and Fish, D. (2006). MyD88 deficiency enhances acquisition and transmission of *Borrelia burgdorferi* by *Ixodes scapularis* ticks. *Infect. Immun.* 74, 2154–2160. doi: 10.1128/IAI.74.4.2154-2160.2006

Bushnell, B., Rood, J., and Singer, E. (2017). BBMerge - Accurate paired shotgun read merging via overlap. *PloS One* 12, e0185056. doi: 10.1371/journal.pone.0185056

Ćakić, S., Veinović, G., Cerar, T., Mihaljica, D., Sukara, R., Ružić-Sabljić, E., et al. (2019). Diversity of Lyme borreliosis spirochetes isolated from ticks in Serbia. *Med. Vet. Entomol.* 33, 512–520. doi: 10.1111/mve.12392

Callahan, B. J., McMurdie, P. J., Rosen, M. J., Han, A. W., Johnson, A. J., and Holmes, S. P. (2016a). DADA2: High-resolution sample inference from Illumina amplicon data. *Nat. Methods* 13, 581–583. doi: 10.1038/nmeth.3869

Callahan, B. J., Sankaran, K., Fukuyama, J. A., McMurdie, P. J., and Holmes, S. P. (2016b). Bioconductor workflow for microbiome data analysis: from raw reads to community analyses. *F1000Res.* 5. doi: 10.12688/f1000research.8986.2

DeHart, T. G., Kushelman, M. R., Hildreth, S. B., Helm, R. F., and Jutras, B. L. (2021). The unusual cell wall of the Lyme disease spirochaete *Borrelia burgdorferi* is shaped by a tick sugar. *Nat. Microbiol.* 6, 1583–1592. doi: 10.1038/s41564-021-01003-w

Duron, O., Morel, O., Noël, V., Buysse, M., Binetruy, F., Lancelot, R., et al. (2018). Tick-bacteria mutualism depends on B vitamin synthesis pathways. *Curr. Biol.* 28, 1896–1902.e5. doi: 10.1016/j.cub.2018.04.038

Estrada-Peña, A., Álvarez-Jarreta, J., and Cabezas-Cruz, A. (2018). Reservoir and vector evolutionary pressures shaped the adaptation of *Borrelia*. *Infect. Genet. Evol.* 66, 308–318. doi: 10.1016/j.meegid.2018.03.023

Fang, S., Wang, L., Guo, W., Zhang, X., Peng, D., Luo, C., et al. (2009). Bacillus thuringiensis bel protein enhances the toxicity of Cry1Ac protein to *Helicoverpa armigera* larvae by degrading insect intestinal mucin. *Appl. Environ. Microbiol.* 75, 5237–5243. doi: 10.1128/AEM.00532-09

Gall, C. A., Reif, K. E., Scoles, G. A., Mason, K. L., Mousel, M., Noh, S. M., et al. (2016). The bacterial microbiome of *Dermacentor andersoni* ticks influences pathogen susceptibility. *ISME J.* 10, 1846–1855. doi: 10.1038/ismej.2015.266

Galloway, C. S., Wang, P., Winstanley, D., and Jones, I. M. (2005). Comparison of the bacterial Enhancin-like proteins from *Yersinia* and Bacillus spp. with a baculovirus Enhancin. *J. Invertebr. Pathol.* 90, 134–137. doi: 10.1016/j.jip.2005.06.008

Garcia-Gonzalez, E., and Genersch, E. (2013). Honey bee larval peritrophic matrix degradation during infection with *Paenibacillus* larvae, the aetiological agent of American foulbrood of honey bees, is a key step in pathogenesis. *Environ. Microbiol.* 15, 2894–2901. doi: 10.1111/1462-2920.12167

Grandi, G., Chiappa, G., Ullman, K., Lindgren, P. E., Olivieri, E., Sassera, D., et al. (2023). Characterization of the bacterial microbiome of Swedish ticks through 16S rRNA amplicon sequencing of whole ticks and of individual tick organs. *Parasitol. Vectors* 16, 39. doi: 10.1186/s13071-022-05638-4

Grigoreva, L. A., and Amosova, L. I. (2004). Peritrophic matrix in the midgut of tick females of the genus *Ixodes* (Acari: Ixodidae). *Parazitologiia* 38, 3–11.

Guizzo, M. G., Dolezelikova, K., Neupane, S., Frantova, H., Hrbatova, A., Pafco, B., et al. (2022). Characterization and manipulation of the bacterial community in the midgut of *Ixodes ricinus*. *Parasitol. Vectors* 15, 248. doi: 10.1186/s13071-022-05362-z

Guizzo, M. G., Neupane, S., Kucera, M., Perner, J., Frantová, H., da Silva Vaz, I., et al. (2020). Poor unstable midgut microbiome of hard ticks contrasts with abundant and stable monospecific microbiome in ovaries. *Front. Cell. Infect. Microbiol.* 10. doi: 10.3389/fcimb.2020.00211

Hall, T. A. (1999). BioEdit: a user-friendly biological sequence alignment editor and analysis program for Windows 95/98/NT. *Nucleic Acids Symposium Ser.* 41, 95–98.

Hammer, B., Moter, A., Kahl, O., Alberti, G., and Göbel, U. B. (2001). Visualization of *Borrelia burgdorferi* sensu lato by fluorescence in *situ* hybridization (FISH) on whole-body sections of *Ixodes ricinus* ticks and gerbil skin biopsies. *Microbiol. (Reading)* 147, 1425–1436. doi: 10.1099/00221287-147-6-1425

Herbold, C. W., Pelikan, C., Kuzyk, O., Hausmann, B., Angel, R., Berry, D., et al. (2015). A flexible and economical barcoding approach for highly multiplexed amplicon sequencing of diverse target genes. *Front. Microbiol.* 6. doi: 10.3389/fmicb.2015.00731

Jacquet, M., Genné, D., Belli, A., Maluenda, E., Sarr, A., and Voordouw, M. J. (2017). The abundance of the Lyme disease pathogen *Borrelia afzelii* declines over time in the tick vector *Ixodes ricinus*. *Parasitol. Vectors* 10, 257. doi: 10.1186/s13071-017-2187-4

Jalovecka, M., Hajdusek, O., Sojka, D., Kopacek, P., and Malandrin, L. (2018). The complexity of piroplasms life cycles. *Front. Cell. Infect. Microbiol.* 8. doi: 10.3389/fcimb.2018.00248

Kariu, T., Smith, A., Yang, X., and Pal, U. (2013). A chitin deacetylase-like protein is a predominant constituent of tick peritrophic membrane that influences the persistence of Lyme disease pathogens within the vector. *PloS One* 8, e78376. doi: 10.1371/journal.pone.0078376

Kim, T. K., Tirloni, L., Bencosme-Cuevas, E., Kim, T. H., Diedrich, J. K., Yates, J. R., et al. (2021). *Borrelia burgdorferi* infection modifies protein content in saliva of *Ixodes scapularis* nymphs. *BMC Genomics* 22, 152. doi: 10.1186/s12864-021-07429-0

Kitsou, C., Foor, S. D., Dutta, S., Bista, S., and Pal, U. (2021). Tick gut barriers impacting tick-microbe interactions and pathogen persistence. *Mol. Microbiol.* 116, 1241–1248. doi: 10.1111/mmi.14822

Klindworth, A., Pruesse, E., Schweer, T., Peplies, J., Quast, C., Horn, M., et al. (2013). Evaluation of general 16S ribosomal RNA gene PCR primers for classical and next-generation sequencing-based diversity studies. *Nucleic Acids Res.* 41, e1. doi: 10.1093/nar/gks808

Kmet, V., and Čaplová, Z. (2019). An update on the *Ixodes ricinus* microbiome. *JMBFS.* 8, 1340–1342. doi: 10.15414/jmbfs.2019

Knorr, S., Reissert-Oppermann, S., Tomás-Cortázar, J., Barriales, D., Azkargorta, M., Iloro, I., et al. (2021). Identification and characterization of immunodominant proteins from tick tissue extracts inducing a protective immune response against *Ixodes ricinus* in cattle. *Vaccines (Basel)* 9, 636. doi: 10.3390/vaccines9060636

Kozelková, T., Dyčka, F., Lu, S., Urbanová, V., Frantová, H., Sojka, D., et al. (2023). Insight into the dynamics of the *Ixodes ricinus* nymphal midgut proteome. *Mol. Cell. Proteomics* 22, 100663. doi: 10.1016/j.mcpro.2023.100663

Kulkarni, M. M., McMaster, W. R., Kamysz, E., Kamysz, W., Engman, D. M., and McGwire, B. S. (2006). The major surface-metalloprotease of the parasitic protozoan, *Leishmania*, protects against antimicrobial peptide-induced apoptotic killing. *Mol. Microbiol.* 62, 1484–1497. doi: 10.1111/j.1365-2958.2006.05459.x

Kumar, S., Stecher, G., and Tamura, K. (2016). MEGA7: molecular evolutionary genetics analysis version 7.0 for bigger datasets. *Mol. Biol. Evol.* 33, 1870–1874. doi: 10.1093/molbev/msw054

Kuraishi, T., Binggeli, O., Opota, O., Buchon, N., and Lemaitre, B. (2011). Genetic evidence for a protective role of the peritrophic matrix against intestinal bacterial infection in *Drosophila melanogaster*. *Proc. Natl. Acad. Sci. U.S.A.* 108, 15966–15971. doi: 10.1073/pnas.1105994108

Kurokawa, C., Lynn, G. E., Pedra, J. H. F., Pal, U., Narasimhan, S., and Fikrig, E. (2020). Interactions between *Borrelia burgdorferi* and ticks. *Nat. Rev. Microbiol.* 18, 587–600. doi: 10.1038/s41579-020-0400-5

Landesman, W. J., Mulder, K., Fredericks, L. P., and Allan, B. F. (2019). Cross-kingdom analysis of nymphal-stage *Ixodes scapularis* microbial communities in relation to *Borrelia burgdorferi* infection and load. *FEMS Microbiol. Ecol.* 95, fiz167. doi: 10.1093/femsec/fiz167

Lejal, E., Chiquet, J., Aubert, J., Robin, S., Estrada-Peña, A., Rue, O., et al. (2021). Temporal patterns in *Ixodes ricinus* microbial communities: an insight into tick-borne microbe interactions. *Microbiome* 9, 153. doi: 10.1186/s40168-021-01051-8

Letunic, I., and Bork, P. (2021). Interactive Tree Of Life (iTOL) v5: an online tool for phylogenetic tree display and annotation. *Nucleic Acids Res.* 49, W293–W296. doi: 10.1093/nar/gkab301

Letunic, I., Khedkar, S., and Bork, P. (2021). SMART: recent updates, new developments and status in 2020. *Nucleic Acids Res.* 49, D458–D460. doi: 10.1093/nar/gkaa937

Mahmood, S., Sima, R., Urbanova, V., Trentelman, J. J. A., Krezdorn, N., Winter, P., et al. (2021). Identification of tick *Ixodes ricinus* midgut genes differentially expressed during the transmission of *Borrelia afzelii* spirochetes using a transcriptomic approach. *Front. Immunol.* 11. doi: 10.3389/fimmu.2020.612412

Martin, P. A., and Schmidtmann, E. T. (1998). Isolation of aerobic microbes from *Ixodes scapularis* (Acari: Ixodidae), the vector of Lyme disease in the eastern United States. *J. Econ. Entomol.* 91, 864–868. doi: 10.1093/jee/91.4.864

Mazuecos, L., Alberdi, P., Hernández-Jarguín, A., Contreras, M., Villar, M., Cabezas-Cruz, A., et al. (2023). Frankenbacteriosis targeting interactions between pathogen and symbiont to control infection in the tick vector. *iScience* 26, 106697. doi: 10.1016/j.isci.2023.106697

Michel, T., Reichhart, J. M., Hoffmann, J. A., and Royet, J. (2001). *Drosophila* Toll is activated by Gram-positive bacteria through a circulating peptidoglycan recognition protein. *Nature* 414, 756–759. doi: 10.1038/414756a

Mistry, J., Chuguransky, S., Williams, L., Qureshi, M., Salazar, G. A., Sonnhammer, E. L. L., et al. (2021). Pfam: The protein families database in 2021. *Nucleic Acids Res.* 49, D412–D419. doi: 10.1093/nar/gkaa913

Murrell, A., Dobson, S. J., Yang, X., Lacey, E., and Barker, S. C. (2003). A survey of bacterial diversity in ticks, lice and fleas from Australia. *Parasitol. Res.* 89, 326–334. doi: 10.1007/s00436-002-0722-4

Nakamura, K., Okumura, K., Harada, M., Okamoto, M., Okura, M., and Takamatsu, D. (2021). Peritrophic matrix-degrading proteins are dispensable virulence factors in a virulent *Melissococcus plutonius* strain. *Sci. Rep.* 11. doi: 10.1038/s41598-021-88302-8

Nakjang, S., Ndeh, D. A., Wipat, A., Bolam, D. N., and Hirt, R. P. (2012). A novel extracellular metallopeptidase domain shared by animal host-associated mutualistic and pathogenic microbes. *PloS One* 7, e30287. doi: 10.1371/journal.pone.0030287

Narasimhan, S., Rajeevan, N., Graham, M., Wu, M. J., DePonte, K., Marion, S., et al. (2022). Tick transmission of *Borrelia burgdorferi* to the murine host is not influenced by environmentally acquired midgut microbiota. *Microbiome* 10, 173. doi: 10.1186/s40168-022-01378-w

Narasimhan, S., Rajeevan, N., Liu, L., Zhao, Y. O., Heisig, J., Pan, J., et al. (2014). Gut microbiota of the tick vector *Ixodes scapularis* modulate colonization of the Lyme disease spirochete. *Cell Host Microbe* 15, 58–71. doi: 10.1016/j.chom.2013.12.001

Narasimhan, S., Schuijt, T. J., Abraham, N. M., Rajeevan, N., Coumou, J., Graham, M., et al. (2017). Modulation of the tick gut milieu by a secreted tick protein favors *Borrelia burgdorferi* colonization. *Nat. Commun.* 8, 184. doi: 10.1038/s41467-017-00208-0

Narasimhan, S., Swei, A., Abouneameh, S., Pal, U., Pedra, J. H. F., and Fikrig, E. (2021). Grappling with the tick microbiome. *Trends Parasitol.* 37, 722–733. doi: 10.1016/j.pt.2021.04.004

Oksanen, F. J., Blanchet, G., Friendly, M., Kindt, R., Legendre, P., McGlinn, D., et al. (2013). *vegan: community ecology package. R package version 2.0.* Available online at: http://CRAN.R-project. org/package=vegan.

Olivieri, E., Epis, S., Castelli, M., Varotto Boccazzi, I., Romeo, C., Desirò, A., et al. (2019). Tissue tropism and metabolic pathways of *Midichloria mitochondrii* suggest tissue-specific functions in the symbiosis with *Ixodes ricinus*. *Ticks Tick Borne Dis.* 10, 1070–1077. doi: 10.1016/j.ttbdis.2019.05.019

Pal, U., Kitsou, C., Drecktrah, D., Yaş, Ö.B., and Fikrig, E. (2021). Interactions between ticks and Lyme disease spirochetes. *Curr. Issues Mol. Biol.* 42, 113–144. doi: 10.21775/cimb.042.113

Peng, J., Zhong, J., and Granados, R. (1999). A baculovirus enhancin alters the permeability of a mucosal midgut peritrophic matrix from lepidopteran larvae. *J. Insect Physiol.* 45, 159–166. doi: 10.1016/s0022-1910(98)00110-3

Pfaffl, M. W. (2001). A new mathematical model for relative quantification in real-time RT-PCR. *Nucleic Acids Res.* 29, e45. doi: 10.1093/nar/29.9.e45

Pjevac, P., Hausmann, B., Schwarz, J., Kohl, G., Herbold, C. W., Loy, A., et al. (2021). An economical and flexible dual barcoding, two-step PCR approach for highly multiplexed amplicon sequencing. *Front. Microbiol.* 12. doi: 10.3389/fmicb.2021.669776

Pospisilova, T., Urbanova, V., Hes, O., Kopacek, P., Hajdusek, O., and Sima, R. (2019). Tracking of *Borrelia afzelii* transmission from infected *Ixodes ricinus* nymphs to mice. *Infect. Immun.* 87, e00896–e00818. doi: 10.1128/IAI.00896-18

Pruesse, E., Peplies, J., and Glöckner, F. O. (2012). SINA: accurate high-throughput multiple sequence alignment of ribosomal RNA genes. *Bioinformatics* 28, 1823–1829. doi: 10.1093/bioinformatics/bts252

Ren, J., Wen, L., Gao, X., Jin, C., Xue, Y., and Yao, X. (2009). DOG 1.0: illustrator of protein domain structures. *Cell. Res.* 19, 271–273. doi: 10.1038/cr.2009.6

Riva, A., Rasoulimehrabani, H., Cruz-Rubio, J. M., Schnorr, S. L., von Baeckmann, C., Inan, D., et al. (2023). Identification of inulin-responsive bacteria in the gut microbiota via multi-modal activity-based sorting. *Nat. Commun.* 14. doi: 10.1038/s41467-023-43448-z

Rodgers, F. H., Gendrin, M., Wyer, C. A. S., and Christophides, G. K. (2017). Microbiota-induced peritrophic matrix regulates midgut homeostasis and prevents systemic infection of malaria vector mosquitoes. *PloS Pathog.* 13, e1006391. doi: 10.1371/journal.ppat.1006391

Ross, B. D., Hayes, B., Radey, M. C., Lee, X., Josek, T., Bjork, J., et al. (2018). *Ixodes scapularis* does not harbor a stable midgut microbiome. *ISME J.* 12, 2596–2607. doi: 10.1038/s41396-018-0161-6

Rousseau, R., Vanwambeke, S. O., Boland, C., and Mori, M. (2021). The isolation of culturable bacteria in *Ixodes ricinus* ticks of a Belgian peri-urban forest uncovers opportunistic bacteria potentially important for public health. *Int. J. Environ. Res. Public Health* 18, 12134. doi: 10.3390/ijerph182212134

Rutschmann, S., Kilinc, A., and Ferrandon, D. (2002). Cutting edge: the toll pathway is required for resistance to gram-positive bacterial infections in *Drosophila*. *J. Immunol.* 168, 1542–1546. doi: 10.4049/jimmunol.168.4.1542

Schwaiger, M., Péter, O., and Cassinotti, P. (2001). Routine diagnosis of *Borrelia burgdorferi* (sensu lato) infections using a real-time PCR assay. *Clin. Microbiol. Infect.* 7, 461–469. doi: 10.1046/j.1198-743x.2001.00282.x

Smith, A. A., and Pal, U. (2014). Immunity-related genes in *Ixodes scapularis* - perspectives from genome information. *Front. Cell. Infect. Microbiol.* 4. doi: 10.3389/fcimb.2014.00116

Sperling, J. L. H., Fitzgerald, D., Sperling, F. A. H., and Magor, K. E. (2020). Microbiome composition and *Borrelia* detection in *Ixodes scapularis* ticks at the northwestern edge of their range. *Trop. Med. Infec.t Dis.* 5, 173. doi: 10.3390/tropicalmed5040173

Steere, A. C., Strle, F., Wormser, G. P., Hu, L. T., Branda, J. A., Hovius, J. W., et al. (2016). Lyme borreliosis. *Nat. Rev. Dis. Primers* 2, 16090. doi: 10.1038/nrdp.2016.90

Steinbrink, A., Brugger, K., Margos, G., Kraiczy, P., and Klimpel, S. (2022). The evolving story of *Borrelia burgdorferi* sensu lato transmission in Europe. *Parasitol. Res.* 121, 781–803. doi: 10.1007/s00436-022-07445-3

Stojek, N. M., and Dutkiewicz, J. (2004). Studies on the occurrence of Gram-negative bacteria in ticks: *Ixodes ricinus* as a potential vector of *Pasteurella*. *Ann. Agric. Environ. Med.* 11, 319–322.

Talyuli, O. A. C., Oliveira, J. H. M., Bottino-Rojas, V., Silveira, G. O., Alvarenga, P. H., Barletta, A. B. F., et al. (2023). The *Aedes aEgypti* peritrophic matrix controls arbovirus vector competence through HPx1, a heme-induced peroxidase. *PloS Pathog.* 19, e1011149. doi: 10.1371/journal.ppat.1011149

Tonk, M., Cabezas-Cruz, A., Valdés, J. J., Rego, R. O., Rudenko, N., Golovchenko, M., et al. (2014). Identification and partial characterisation of new members of the *Ixodes ricinus* defensin family. *Gene* 540, 146–152. doi: 10.1016/j.gene.2014.03.002

Tóth, A. G., Farkas, R., Papp, M., Kilim, O., Yun, H., Makrai, L., et al. (2023). *Ixodes ricinus* tick bacteriome alterations based on a climatically representative survey in Hungary. *Microbiol. Spectr.* 11, e0124323. doi: 10.1128/spectrum.01243-23

Tveten, A. K., Riborg, A., and Vadseth, H. T. (2013). DGGE Identification of microorganisms associated with *Borrelia burgdorferi* sensu lato- or *Anaplasma phagocytophilum*-infected *Ixodes ricinus* ticks from Northwest Norway. *Int. J. Microbiol.* 2013, 805456. doi: 10.1155/2013/805456

Veinović, G., Ćakić, S., Mihaljica, D., Sukara, R., Ružić-Sabljić, E., and Tomanović, S. (2021). *In vitro* efficacy of antibiotics against different *Borrelia* isolates. *Acta Microbiol. Immunol. Hung.* 68, 195–202. doi: 10.1556/030.2021.01441

Veinović, G., Ružić-Sabljić, E., Strle, F., and Cerar, T. (2016). Comparison of growth of *Borrelia afzelii*, *Borrelia garinii*, and *Borrelia burgdorferi* sensu stricto at five different temperatures. *PloS One* 11, e0157706. doi: 10.1371/journal.pone.0157706

Wang, P., and Granados, R. R. (1997). An intestinal mucin is the target substrate for a baculovirus enhancin. *Proc. Natl. Acad. Sci. U.S.A.* 94, 6977–6982. doi: 10.1073/pnas.94.13.6977

Wei, N., Cao, J., Zhang, H., Zhou, Y., and Zhou, J. (2021). The tick microbiota dysbiosis promote tick-borne pathogen transstadial transmission in a *Babesia microti*-infected mouse model. *Front. Cell. Infect. Microbiol.* 11. doi: 10.3389/fcimb.2021.713466

Whelan, S., and Goldman, N. (2001). A general empirical model of protein evolution derived from multiple protein families using a maximum-likelihood approach. *Mol. Biol. Evol.* 18, 691–699. doi: 10.1093/oxfordjournals.molbev.a003851

Wickham, H. (2009). *ggplot2: elegant graphics for data analysis. 1st ed* (New York, NY: Springer).

Wu, P., Sun, P., Nie, K., Zhu, Y., Shi, M., Xiao, C., et al. (2019). A gut commensal bacterium promotes mosquito permissiveness to arboviruses. *Cell Host Microbe* 25, 101–112.e5. doi: 10.1016/j.chom.2018.11.004

Wu-Chuang, A., Mateos-Hernández, L., Estrada-Peña, A., Obregon, D., and Cabezas-Cruz, A. (2021). Current debates and advances in tick microbiome research. *Curr. Res. Parasitol. Vector Borne Dis.* 1, 100036. doi: 10.1016/j.crpvbd.2021.100036

Wu-Chuang, A., Mateos-Hernandez, L., Maitre, A., Rego, R. O. M., Šíma, R., Porcelli, S., et al. (2023). Microbiota perturbation by anti-microbiota vaccine reduces the colonization of *Borrelia afzelii* in *Ixodes ricinus*. *Microbiome* 11, 151. doi: 10.1186/s40168-023-01599-7

Yang, X., Koči, J., Smith, A. A., Zhuang, X., Sharma, K., Dutta, S., et al. (2021). A novel tick protein supports integrity of gut peritrophic matrix impacting existence of gut microbiome and Lyme disease pathogens. *Cell. Microbiol.* 23, e13275. doi: 10.1111/cmi.13275

Yang, X., Smith, A. A., Williams, M. S., and Pal, U. (2014). A dityrosine network mediated by dual oxidase and peroxidase influences the persistence of Lyme disease pathogens within the vector. *J. Biol. Chem.* 289, 12813–12822. doi: 10.1074/jbc.M113.538272

Yoon, S. H., Ha, S. M., Kwon, S., Lim, J., Kim, Y., Seo, H., et al. (2017). Introducing EzBioCloud: a taxonomically united database of 16S rRNA gene sequences and whole-genome assemblies. *Int. J. Syst. Evol. Microbiol.* 67, 1613–1617. doi: 10.1099/ijsem.0.001755

Zhu, Z., Gern, L., and Aeschlimann, A. (1991). The peritrophic membrane of *Ixodes ricinus*. *Parasitol. Res.* 77, 635–641. doi: 10.1007/BF00931028

frontiers | Frontiers in Cellular and Infection Microbiology

TYPE Original Research
PUBLISHED 21 November 2024
DOI 10.3389/fcimb.2024.1486426

OPEN ACCESS

EDITED BY
Deepak Kumar,
University of Southern Mississippi,
United States

REVIEWED BY
Max Maurin,
Centre Hospitalier Universitaire de Grenoble,
France
Surendra Raj Sharma,
University of North Carolina at Chapel Hill,
United States

*CORRESPONDENCE
Jie Feng
jfeng@lzu.edu.cn
Tingting Li
litt@lzu.edu.cn

RECEIVED 26 August 2024
ACCEPTED 21 October 2024
PUBLISHED 21 November 2024

CITATION
Gou Y, Liu D, Xin Y, Wang T, Li J, Xi Y, Zheng X, Che T, Zhang Y, Li T and Feng J (2024) Viable but nonculturable state in the zoonotic pathogen *Bartonella henselae* induced by low-grade fever temperature and antibiotic treatment.
Front. Cell. Infect. Microbiol. 14:1486426.
doi: 10.3389/fcimb.2024.1486426

Viable but nonculturable state in the zoonotic pathogen *Bartonella henselae* induced by low-grade fever temperature and antibiotic treatment

Yuze Gou[1,2], Dongxia Liu[1,2], Yuxian Xin[1,2], Ting Wang[1], Jiaxin Li[1], Yiwen Xi[1], Xiaoling Zheng[3], Tuanjie Che[3], Ying Zhang[4,5], Tingting Li[1]* and Jie Feng[1,2]*

[1]Key Laboratory of Preclinical Study for New Drugs of Gansu Province, School of Basic Medical Sciences, Lanzhou University, Lanzhou, China, [2]State Key Laboratory of Veterinary Etiological Biology, College of Veterinary Medicine, Lanzhou University, Lanzhou, China, [3]Department of Scientific Experimental Research, Innovation Center of Functional Genomics and Molecular Diagnostics Technology of Gansu Province, Lanzhou, China, [4]State Key Laboratory for the Diagnosis and Treatment of Infectious Diseases, The First Affiliated Hospital, Zhejiang University School of Medicine, Hangzhou, China, [5]Center for Microbiome and Disease Research, Jinan Microecological Biomedicine Shandong Laboratory, Jinan, China

The zoonotic pathogen *Bartonella henselae* is responsible for diverse human diseases, from mild to life-threatening, but it often eludes detection in culture-based assays. This study investigates the potential of *B. henselae* to enter a viable but nonculturable (VBNC) state when exposed to human fever temperature or antibiotics, with this state confirmed by successful resuscitation. Viability was assessed using SYBR Green I/PI staining and propidium monoazide–quantitative polymerase chain reaction (PMA-qPCR), while culturability was determined through colony-forming unit (CFU) counting on blood agar plates. Resuscitation of VBNC cells was attempted using modified Schneider's medium with 10% defibrillated sheep blood. In the results, *B. henselae* cells entered a VBNC state after 19 days of exposure to 38.8°C. Antibiotics, particularly with bactericidal activity, induced the VBNC state within 4 days treatment. Successful resuscitation confirmed the VBNC state developed via the above two strategies. Transmission electron microscopy (TEM) examination revealed intact cell structures and dense cytosol in VBNC cells, with a significant increase in plasmolytic cells. Notably, VBNC cells demonstrated greater drug tolerance than cells in the stationary phase, which encompassed a substantial portion of persisters. Proteomic analysis revealed the up-regulation of proteins linked to host cell invasion and stress resistance, while proteins related to signaling and cellular processes were down-regulated. Fluorescence *in situ* hybridization (FISH) analysis confirmed that the VBNC state truly boosted *B. henselae*'s invasion of HUVECs. This study highlights *B. henselae*'s capacity to enter a VBNC state under thermal and antibiotic stress, emphasizing the urgent need for advanced diagnostic and therapeutic strategies to effectively target VBNC cells, which complicate diagnosis and treatment.

KEYWORDS

***Bartonella*, *B. henselae*, VBNC, resuscitation, persister, blood-culture-negative endocarditis (BCNE), cat-scratch disease (CSD)**

Introduction

Bartonellae are fastidious vector-borne Gram-negative bacteria responsible for multiple human diseases (Jin et al., 2023). The predominant Bartonelloses in humans are primarily attributed to *Bartonella henselae*, *Bartonella bacilliformis*, and *Bartonella quintana*. Infection with *B. henselae* can result in the prototypical cat-scratch disease (CSD), characterized by fever and regional lymphadenopathy, primarily affecting immunocompromised individuals and occasionally immunocompetent individuals, especially children and adolescents (Pulliainen and Dehio, 2012). In severe cases, *B. henselae* can lead to bacillary angiomatosis, a condition marked by vasoproliferative tumors affecting the skin and internal organs (Pulliainen and Dehio, 2012). Additionally, a broad spectrum of manifestations has been reported in association with persistent infection of *B. henselae*, including asymptomatic bacteremia, which is a distinctive characteristic of *Bartonella* (Massei et al., 2004; Breitschwerdt et al., 2008). The prevalence of *B. henselae* infection is worldwide, with a seroprevalence in China of up to 9.68% (Song Xiu et al., 2020). In the United States, there are estimated 12,500 cases of CSD annually, with the proportion of hospitalized CSD patients increasing from 3.5% in 2005–2007 to 4.2% in 2011–2013 (Nelson et al., 2016). Despite the prevalence, diagnosing *B. henselae* infections remains challenging. Antibody-based serological assays are widely applied for diagnosing *B. henselae* infection. However, these assays present several limitations, including cross-reactivity with other species and organisms, variability in antigen preparations, cutoff titers, and other factors (La Scola and Raoult, 1996; Massei et al., 2004).

Traditional diagnostic methods based on bacterial cultivation (Drummond et al., 2023; Koutantou et al., 2023), often face challenges due to the fastidious nature of *B. henselae*, which is difficult to culture and detect. This limitation can result in diagnostic difficulties, as in blood-culture-negative endocarditis (BCNE) (Okaro et al., 2017). While molecular techniques offer higher detection rates (Prudent et al., 2018; Sayed et al., 2022; Koutantou et al., 2023), they do not confirm the presence of live bacterial cells. Despite the well-established causative relationship between *B. henselae* and certain diseases, the difficulty of isolating *B. henselae* from some infected hosts, combined with the limitations of molecular detection methods, means that these techniques alone cannot fully satisfy Koch's postulates. This difficulty underscores the importance of microbial culture, still considered the gold standard for detecting infectious pathogens. Higher recovery rates from clinical specimens have been achieved by the shell-vial technique, which involves the inoculation of clinical specimens onto confluent cell monolayers on coverslips within shell vials, followed by low-speed centrifugation to enhance bacterial attachment and penetration, with subsequent detection via immunofluorescence, and definitive bacterial identification by PCR (Lagier et al., 2015). In a study of endocarditis patients suspected of *Bartonella* spp. infection, the recovery rate was 44% using a shell vial culture assay, compared to only 4% when directly culturing on Columbia sheep blood agar plates (La Scola and Raoult, 1999). The improved sensitivity for recovering *Bartonella* isolates by shell-vial culture methods suggests that certain factors in the subculture system are essential for the growth of some *Bartonella* isolates, which may enter a viable but nonculturable (VBNC) state and have the potential to revert to a culturable state under appropriate conditions.

The VBNC state is a survival strategy employed by various bacterial species, allowing them to maintain cellular integrity and metabolic activity while remaining undetectable by standard culturing methods (Liu et al., 2023). VBNC bacteria can resuscitate under favorable conditions, potentially leading to recurrent infections and complicating treatment. For example, VBNC *Listeria monocytogenes* can resuscitate and cause listeriosis in vulnerable populations (Lotoux et al., 2022). VBNC cells also exhibit resistance to antibiotics and immune stress (Ayrapetyan et al., 2015b), contributing to persistent infections. The persistence of VBNC pathogens in hosts, especially intracellular pathogens like *Bartonella*, poses significant challenges for accurate diagnosis and risk assessment in clinical settings.

Given these challenges, this study aimed to determine whether *B. henselae* can enter a VBNC state and to characterize these cells in detail. We induced the VBNC state in *B. henselae* using high temperature and antibiotic treatment, mimicking conditions like fever and antimicrobial exposure, and developed a method for resuscitating *B. henselae* VBNC cells, which could greatly improve the diagnosis, detection, and treatment of bartonellosis.

Materials and methods

Bacterial strain and culture conditions

Bartonella henselae strain Houston-1 (ATCC 49882) was cultured in a modified Schneider's medium (Riess et al., 2008; Li et al., 2019). Briefly, 10 mL modified Schneider's medium was composed of 8 mL Schneider's drosophila medium (Gibco, USA), 1 mL heat-inactivated fetal bovine serum (VivaCell, China), and 1 mL 50% sucrose solution. Cultures were incubated at 33°C without shaking. Colony forming units (CFU) were counted after serial 10-fold dilutions on Columbia blood agar plates with 5% defibrinated sheep blood, followed by incubation at 33°C.

Quantification of live *B. henselae* cells via SYBR Green I/PI assay

The viability of *B. henselae* was evaluated using a SYBR Green I/propidium iodide (PI) staining method (Feng et al., 2014; Li et al., 2019). Bacterial samples were stained with SYBR Green I

(Invitrogen, USA) and PI (Solarbio, China), incubated in darkness at room temperature (RT) for 30 minutes, and counted under an IX71 inverted microscope (Olympus, Japan). Dead cells, marked by red fluorescence emitted from PI, were distinguished from live cells, which exhibited green fluorescence due to SYBR Green I binding.

For plate reader analysis, standard samples were prepared by mixing live and 70% isopropanol-killed bacteria in varying ratios. Both these standards and culture samples were stained with SYBR Green I/PI, incubated at RT in darkness for 30 minutes, and analyzed using a fluorescence plate reader. Green and red fluorescence intensities were measured using a fluorescence plate reader (Thermo Fisher Scientific, USA). The percentage of viable *B. henselae* cells in each sample was calculated based on the ratios of green to red fluorescence intensities, providing a quantitative assessment of cell viability under various experimental conditions.

Quantification via PMA-qPCR

Live *B. henselae* cells were quantified using the PMA-qPCR method, following a previously described protocol (Lazou et al., 2019). Briefly, 990 µL aliquots of bacterial cultures were added with 10 µL propidium monoazide (PMA) (Bioscience, China) in Eppendorf tubes and kept at RT for 10 min in darkness with occasional mixing. Samples were then exposed to light for 15 min, followed by centrifugation at 10,000 g for 5 min. DNA was extracted from the cell pellets using QIAamp DNA Mini Kit (Qiagen, Germany). For the calibration standard curve preparation, mixtures of live and 3% H_2O_2-killed bacteria were prepared to create five different ratios of viable cells. These mixtures were treated in parallel with the samples described above. The extracted DNA from each sample, including standards and samples, was mixed with Hieff UNICON Universal Blue qPCR SYBR Green Master Mix (YEASEN, China) and specific primers (Bhe-16s-qF AATCTTGCGACCGTACTCCC, Bhe-16s-qR TCCACGCCGTAAACGATGAA) targeting the *B. henselae* 16S rRNA gene. Quantitative PCR was performed on a QuantStudio (Applied Biosystems). Live *B. henselae* cells were quantified using a PMA-qPCR method (Lazou et al., 2019). The PMA inhibition factor was calculated using the formula 2^(Ct(PMA treated)-Ct(PMA untreated)), and the viability percentage was determined by 100/(PMA inhibition factor) and calibrated using the standard calibration curve.

Induction of VBNC cells

VBNC cells were induced by two methods: culture under fever-like temperature (38.8°C) up to 25 days and treatment with antibiotics at 37°C. The antibiotics tested included gentamicin (15 µg/mL), streptomycin (43 µg/mL), doxycycline (7 µg/mL) and erythromycin (1.44 µg/mL). Cultures were periodically sampled to assess viability and culturability. The drugs were prepared according to the manual of clinical and laboratory standards institute (CLSI) and sterilized with a 0.22 µm filter. Methylene blue was dissolved in DMSO.

Resuscitation of *B. henselae* from the VBNC state

Cultures of *B. henselae* cells in the VBNC state-inducing course were periodically drawn. Samples were then divided into two aliquots. One aliquot from each sample was directly deposited onto blood agar plates, and the second aliquot underwent a resuscitation process. For the aliquot dropped on the blood agar plate, drug removal and resuspension were required for antibiotic-induced VBNC cells in the culture. For the resuscitation, cells were collected by centrifugation (5000×g, 5 min), resuspended in the modified Schneider's medium supplemented with 10% defibrinated sheep blood, and incubated at 33°C for 1 day, followed by plating on Columbia blood agar plate. The successful resuscitation of *B. henselae* in pure VBNC state was achieved when the aliquot gone through resuscitation displayed colonies but the parallel aliquot directly deposited on blood agar plates failed to do so.

Transmission electron microscopy

Bacterial cells were pelleted and fixed with 2.5% glutaraldehyde in 0.1 M sodium cacodylate buffer. After that, the cells were suspended in 2% agarose and cut into cubes. Then, samples were washed and resuspended in 0.1 M sodium cacodylate buffer, and fixed in osmium tetroxide. After staining, samples were washed, dehydrated, and soaked in acetone, followed by immersion in 3:1 acetone: epoxy resin, 1:1 acetone: epoxy resin and pure epoxy resin overnight. Finally, samples were cut into ultrathin sections, stained with uranyl acetate and lead citrate, and visualized with a Hitachi HT7700 transmission electron microscope. Cell size and shape were analyzed using Fiji software (Schindelin et al., 2012).

DIA (data-independent acquisition) proteomic analysis by LC-MS/MS

B. henselae cells were pelleted by centrifugation and washed with PBS to remove residual culture medium. Cell pellets were resuspended in lysis buffer composed of 4% SDS, 100 mM DTT, and 100 mM Tris-HCl (pH 8.0), boiled for 3 min, and were then ultrasonicated, with insoluble cellular debris removed after centrifugation at 16,000 g for 15 min. The resultant clear supernatant was then assayed for protein concentration using the BCA Protein Assay Kit (BeyoTime, China). Protein digestion was conducted by adopting the Filter-Aided Sample Preparation (FASP) technique. LC-MS/MS analyses were performed with an Orbitrap Astral mass spectrometer linked to a Vanquish Neo UHPLC system. Peptides were loaded into a Low-Load µPAC™ Neo HPLC Column (Thermo Scientific). The mobile phase consisted

of (A) water with 0.1% formic acid, and (B) 80% acetonitrile with 0.1% formic acid. We used a DIA method that included a survey scan from 380-980 m/z at resolution 240000 with AGC target of 500% and 5 ms injection time. The energy and timing for the scans were precisely controlled, and the resulting spectra were recorded in two different formats. The DIA MS/MS scans were acquired by Astral from 150-2000 m/z with 2 m/z isolation window and with AGC target of 500% and 3 ms injection time. The spectra of full MS scan and DIA scan were recorded in profile and centroid type, respectively. Data were analyzed using the DIA-NN 1.8.1 (Demichev et al., 2020), and underwent a database search against the GenBank database, specifically targeting the NCBI for *B. henselae* Houston-1 sequence (NC_005956). Results from the database search were refined to ensure a false discovery rate of less than 1% at both the peptide-spectrum match and protein levels. Gene ontology enrichment analysis, heat map figure and volcano figure were executed by using KEGG database (Kanehisa et al., 2017) and statistical language R with ggplot2, pheatmap and EnhencedVolcano packages.

Fluorescence *in situ* hybridization of HUVECs

Prior to infection, log-phase *B. henselae* cultured at 33°C and *B. henselae* VBNC induced by culturing at 38.8°C for 19 days were washed twice with PBS and resuspended in DMEM (F12) medium. Human umbilical vein endothelial cells (HUVECs, CCTCC GDC0635) were washed twice with PBS before being infected with a multiplicity of infection (MOI) of 100 of *B. henselae* either in logarithmic phase or in VBNC state. The plates were centrifuged at 1800 g for 5 min and then incubated in 5% CO_2 at 37°C or 38.8°C. At various post-infection time points, the plates were washed thoroughly with PBS and fixed with 4% paraformaldehyde for 2 h. Following fixation, cells were washed three times with PBS, and then treated with PBS containing 0.1% Triton X-100 for 10 min to permeabilize the cell membrane. Cells were then dehydrated in 50%, 80%, and 100% ethanol, respectively, and hybridized overnight with the BA23 probe (5'-6-FAM-CTATCACCCTCTTTGGTTCG-3') in hybridization buffer (900 mM NaCl, 20% formamide, 0.01% SDS, 20 mM Tris, pH8.0) (Prudent et al., 2017). After hybridization, the cells were washed with washing buffer (0.225 M NaCl, 5 mM EDTA, 0.01% SDS, pH 8.0) and then stained with DAPI for 3 min. Following three washes with ddH_2O, coverslips were sealed and examined using a Zeiss LZM 900 confocal laser scanning microscope.

Results

VBNC formation at elevated temperature

We investigated the impact of temperature on the formation of VBNC cells by assessing cell viability and culturability of *B. henselae* at 38.8°C and 33°C. Culturable cells were determined by CFU counting on blood agar plates, while viable cells were evaluated using SYBR Green I/PI staining and/or PMA-qPCR. The viability measurements from these methods showed a strong linear relationship (Supplementary Figure S1). At 33°C, *B. henselae* cells remained viable from the 2-day logarithmic phase to the 19-day late-stationary phase. However, culturability significantly declined, from 77.3% in 2-day cultures to 1.8% in 19-day cultures (Figure 1A), indicating VBNC cell formation. At 38.8°C, approximately 20%-30% of the cells remained viable after 19 days, but no colonies formed on blood agar plates (Figure 1A), suggesting that the entire population of viable cells had entered a VBNC state.

Overtime, at 33°C, viable and culturable cells were initially comparable, but culturable cells declined markedly by 18- and 19-day, confirming VBNC cell presence. At 38.8°C, viable cells remained relatively constant, but no culturable cells were detected by 18- and 19-day, confirming a pure VBNC state. Resuscitation experiments demonstrated that *B. henselae* could recover from the VBNC state (Figure 1B).

Morphological and physiological changes in *B. henselae* VBNC cells

Bacteria typically undergo a series of changes in morphological structure and physiological characteristics upon entering the VBNC state. In this study, TEM was utilized to observe the morphological adjustments and intracellular content changes in *B. henselae* cells in the VBNC state. We observed that VBNC cells maintained intact cell walls, membranes and abundant intracellular content, with no significant changes in shape or size (Figures 2A–C). However, many VBNC cells exhibited plasmolysis (Figures 2A, D), a morphological abnormality characterized by the cell membrane shrinking away from the cell wall, especially when compared to cells in the logarithmic and stationary phases. The intracellular contents in plasmolytic VBNC cells appeared to be more intensely condensed relative to those in cells from the other two cultures, with a pronounced separation between the cell membrane and the cell wall. These observations suggest that while *B. henselae* VBNC cells retain their overall structural integrity they undergo significant intracellular condensation and membrane detachment, indicative of a stress response and metabolic adjustment characteristic of the VBNC state.

Drug tolerance of *B. henselae* VBNC cells

VBNC cells of various bacterial species exhibit robust competence in surviving antibiotics of multiple classes. We compared the drug susceptibility of VBNC cells cultured at 38.8°C for 19 days with cells cultured at 33°C for 19 days. VBNC cells showed significant tolerance to multiple antibiotics, especially anti-persister drugs like daptomycin and methylene blue (Figure 2E). Meanwhile, the corresponding MIC values for the resuscitated VBNC cells were identical to those of logarithmic-phase cells (Supplementary Table S1), consistent with previous suggestion that VBNC cells are part of drug-tolerant persisters, not drug-resistant mutants (Zhang, 2014; Ayrapetyan et al., 2015a). Notably, over 80% of *B. henselae* cells at 38.8°C developed multi-drug tolerance within just 5 days' culture, while cells at 33°C took 10 days to reach

10.3389/fcimb.2024.1486426

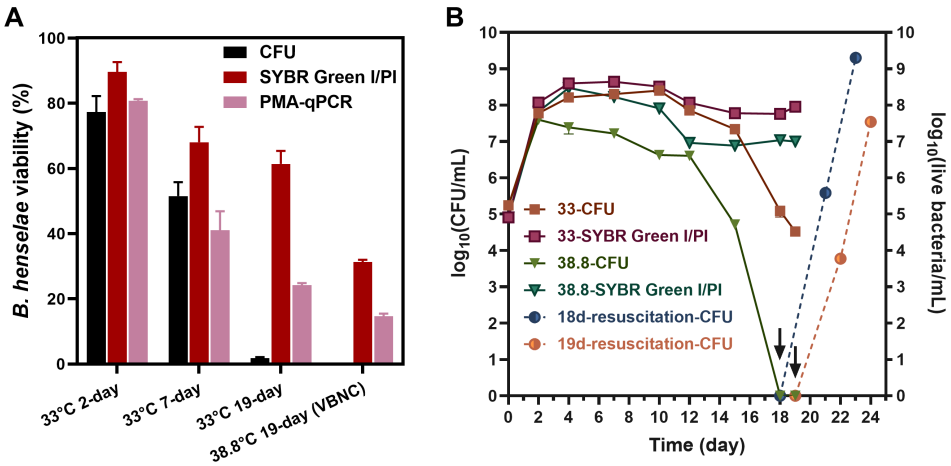

FIGURE 1
Temperature effect on the formation of *B. henselae* VBNC cells. **(A)** Evaluation of culturability and viability for *B. henselae* cells cultured at 33°C and 38.8°C, respectively. Culturable cells were monitored by CFU counting, whereas viable cell counting were monitored by SYBR Green I/PI assay and PMA-qPCR assay. The CFU-based viability for each sample was determined by dividing the CFU count by the total cell count observed under the microscope. Similarly, the SYBR Green I/PI-based viability was calculated by dividing the count of green-stained (live) cells by the total cell count under the microscope. For the PMA-qPCR assay, viability was calculated based on the PMA inhibition factor and calibrated by the calibration curve. **(B)** The entry of VBNC state at 33°C and 38.8°C were monitored over time. The arrows and dash lines represent the resuscitation for 18-day-cultured and 19-day-cultured VBNC bacteria at 38.8°C. All tests were run in triplicates, and all data are averages of biological triplicates ± standard deviation.

similar levels (Figure 2F). The enhanced development of drug-tolerant VBNC cells of *B. henselae* at elevated temperatures poses a significant treatment challenge, particularly under febrile conditions.

Antibiotic-induced VBNC state in *B. henselae*

To explore if antibiotics could also induce VBNC states, we treated *B. henselae* cultures with several clinically used antibiotics at their maximum serum concentrations, defined as the highest concentrations achievable in human serum following administration. Treatment with gentamicin and streptomycin for 4 days led to a slight decrease of viable cells and undetectable levels of culturable cells (Figure 3A), which indicates that *B. henselae* fully transitioned into the VBNC state, as confirmed by successful resuscitation. In contrast, doxycycline and erythromycin led to only a partial transition to the VBNC state after 7 days (Figure 3B), indicating that bactericidal antibiotics (gentamicin and streptomycin) are more effective in inducing the VBNC state than bacteriostatic agents.

Divergent proteomic profiles between VBNC and culturable *B. henselae* cells

To understand the molecular mechanisms governing the VBNC state, we conducted a comparative proteomic analysis between VBNC cells and late-stationary-phase cells. The datasets have been deposited to the iProX partner repository (Chen et al., 2022) with the identifier PXD055316. Out of 1230 identified proteins, 217 showed significant differential expression (p-value < 0.05). Of these, 104 proteins were up-regulated (FC >= 1.5), with 63 exhibiting FC values exceeding 2.0, while 113 were down-regulated (FC <= 0.67), with 45 falling below 0.5 (Figure 4A). Particularly, up-regulated expression of HecB/FhaC family proteins (BH07920, BH06540 and BH06660), filamentous hemagglutinin (FhaB1), the hemin-binding protein (BH02570), TrwL/J, VirB, invasion-associated locus B (IalB), BafA, and superoxide dismutase (SOD) was observed. *B. henselae* VBNC cells also up-regulated molecular chaperones and heat shock proteins, including GroES (HSP10 family), GroEL (HSP60 family), DnaK (HSP70 family), and IbpA (HSP20 family).

Pathways related to energy and lipid metabolism were notably up-regulated, while those associated with nucleotide, amino acid, glycan, cofactor, and vitamin metabolism were down-regulated (Figure 4B), reflecting the metabolic adaptation of VBNC cells.

Rapid invasion of HUVECs by VBNC *B. henselae*

Proteomic analysis revealed that VBNC *B. henselae* upregulates proteins related to adhesion and host cell invasion. Using FISH and confocal scanning microscopy, we found that VBNC cells rapidly invade HUVECs, with internalization observed within 12-18 hours post-infection, whereas no internalization was observed with logarithmic-phase *B. henselae* at the same time points (Figure 4C).

Discussion

Microbial cultivation has long been considered the gold standard for identifying pathogens in clinical samples. However, the existence of VBNC bacteria, which do not grow on routine culture media, complicates clinical diagnosis. For *Bartonella* species,

10.3389/fcimb.2024.1486426

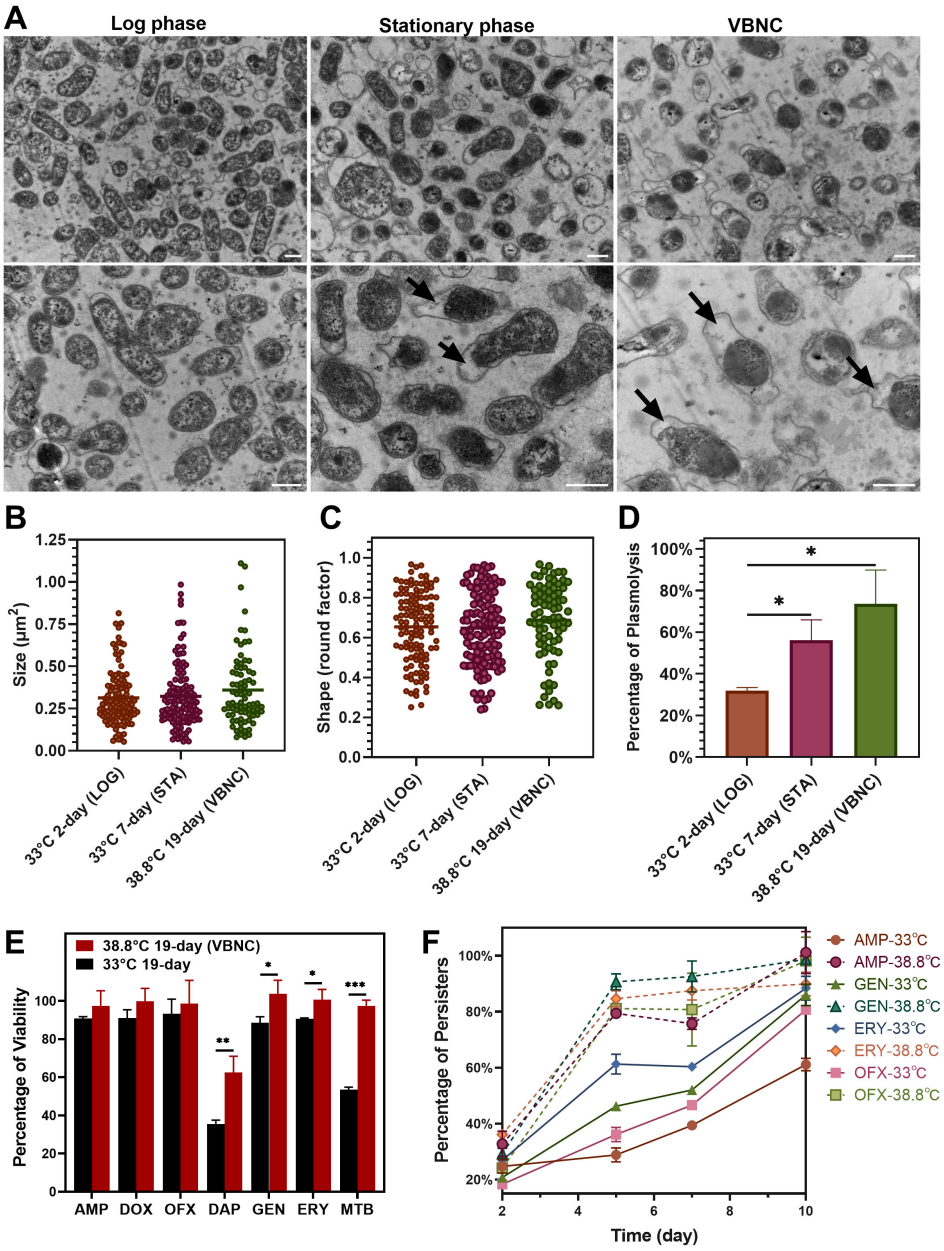

FIGURE 2
Comparison of morphology and drug tolerance of *B. henselae* cells across different states. **(A)** TEM images show the morphology of *B. henselae* in the logarithmic phase (LOG), stationary phase (STA), and VBNC state, with a scale bar of 0.5 μm. ImageJ software was used to analyze bacterial cell size **(B)**, shape **(C)** and the percentage of plasmolysis **(D)**. **(E)** The percentage of viable cells in the population after drug exposure. *B. henselae* cells were separately treated for 10 days with different drugs, including clinically used (ampicillin, doxycycline, ofloxacin, gentamicin, erythromycin) and anti-persister drugs (daptomycin, methylene blue). Over 15-fold MIC for each antibiotic (100 μg/mL) was used to sort out persisters from bacterial populations in cultures. Viable cells were quantified using SYBR Green I/PI staining combined with a plate reader assay. **(F)** The formation of *B. henselae* persisters was monitored over time at 38.8°C and 33°C. Statistical significance between groups was assessed using *t*-tests, with significant differences indicated by asterisks (*P <0.05; **P <0.01; ***P <0.001).

cultivation on blood agar plates is critical for diagnosing infections (La Scola and Raoult, 1999; Okaro et al., 2017). However, cases of "culture-negative" endocarditis caused by *B. henselae* have been reported (Okaro et al., 2017). Furthermore, culture-based tests fail to detect all *Bartonella* in blood samples, with only 69% (11/16) of *Bartonella*-infected samples successfully cultured (Pitassi et al., 2015). Shell-vial culture techniques have improved the recovery rates of *Bartonella* from clinical specimens (Lagier et al., 2015), particularly compared to direct culture on blood agar plates (La Scola and Raoult, 1999), suggesting that *Bartonella* spp. may enter a viable but nonculturable (VBNC) state under certain conditions, which could be one of the causes for the failure in cultivation.

To prove that *B. henselae* can enter a VBNC state under specific conditions, *B. henselae* was cultivated at 38.8°C, a temperature equivalent to the body temperature of cats and dogs and the fever temperature in humans, to induce the VBNC state in this study. We

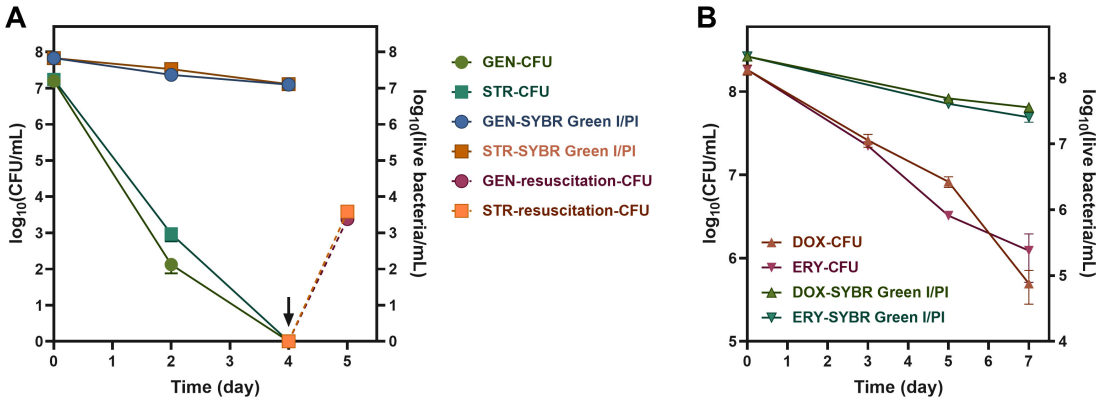

FIGURE 3
Antibiotic induction of *B. henselae* into the VBNC state. The culturability and the viability curve of *B. henselae* treated with bacteriocidal antibiotics **(A)** and bacteriostatic antibiotics **(B)** at 37°C. The arrows and dash lines represent the resuscitation of VBNC cells. The culturable cells and viable cells were monitored by CFU and SYBR Green I/PI assay, respectively. All tests were run in triplicates, and all data are averages of biological triplicates ± standard deviation. GEN, gentamicin; STR, streptomycin; DOX, doxycycline; ERY, erythromycin.

found that *B. henselae* could enter a pure VBNC state after 19 days at 38.8°C, with no culturable cells detected (Figure 1B). The formation of VBNC cells was primarily indicated by discrepancies between the number of culturable cells and the total viable cell count. Culturable cells were routinely quantified through CFU counts on agar plates, while total viable cells were assessed using cell membrane integrity-based methods, such as PMA-qPCR (Kibbee and Ormeci, 2017; Lazou et al., 2019) and SYBR Green I/PI staining (Feng et al., 2018). The viability percentages measured by PMA-qPCR showed a linear correlation with those obtained using SYBR Green I/PI staining combined with plate reader or microscopic analysis (Supplementary Figure S1). However, PMA-qPCR consistently reported lower viability compared to SYBR Green I/PI staining combined with microscopic observation (Figure 1A), indicating a higher signal from dead bacterial cells in PMA-qPCR. It is well-documented that extracellular DNA can lead to overestimations of viable bacterial counts in PMA-qPCR (Lovdal et al., 2011). Although washing bacterial cells may mitigate this bias, the additional washing and centrifugation steps can damage fragile *B. henselae* cells, further complicating the accurate assessment of viability. In this study, SYBR Green I/PI staining was favored for its faster and convenient sample processing, eliminating the need for cell washing and pelleting, and its minimal sample requirements (10 μL), making it an ideal method for the timely assessment of resuscitation.

Clinically used antibiotics, particularly bactericidal ones like gentamicin and streptomycin, also triggered the VBNC state (Figure 3), converting the entire viable population into VBNC state after just 4 days. Over 100 bacterial species have been documented to enter a nonculturable state, with some species, such as *Mycobacterium tuberculosis* (Zhang et al., 2001), *Vibrio vulnificus*, and *Legionella pneumophila*, can resuscitate (Li et al., 2014). Given resuscitation is now a gold standard for verifying the VBNC state (Liu et al., 2023), we developed a specialized medium as described in the Methods section and successfully resuscitated VBNC cells generated by cultivation at 38.8°C or antibiotic treatment, which otherwise failed to grow on regular blood agar plates. The resuscitation method developed here would be promising to improve the diagnostic detection of *B. henselae* in clinical practice, though further studies in clinical settings are needed.

The viability assessment of bacterial cells in this study (PMA-qPCR assay and SYBR Green I/PI assay) relied on membrane integrity, which might misclassify dead cells with intact membrane as VBNC cells (Song and Wood, 2021). However, TEM analysis confirmed that *B. henselae* VBNC cells developed at 38.8°C maintain an intact cell wall, intact inner membrane, and dense cytosol (Figure 2). Notably, substantial shrinkage of the inner membrane away from the cell wall was observed in a large portion of VBNC cells, highlighting its relevance under stress conditions. Similar morphology was reported in *E. coli* in response to nutrient depletion (Shi et al., 2021), and the presence of plasmolysis implies that bacterial cells were alive (Korber et al., 1996). The morphology changes of VBNC *B. henselae* need further study in the future.

The ability of *B. henselae* to enter the VBNC state likely contributes to the frequent failure to isolate the bacterium from hosts, posing challenges for clinical diagnosis and treatment. The generation of a pure VBNC state at an elevated temperature of 38.8°C in our study suggests that *B. henselae* may exist in the VBNC state within infected hosts, such as febrile humans, cats, and dogs, where the normal body temperatures in the latter animal hosts can range from 38.3 to 39.2°C. This hypothesis aligns with the difficulty of isolating *B. henselae* from infected animals (Diniz et al., 2013; Sayed et al., 2022). Additionally, it suggests that fever in patients caused by *B. henselae* infection may also promote the transition to the VBNC state.

VBNC state has been proposed as part of bacterial persistence (Zhang, 2014; Ayrapetyan et al., 2018) for bacterial survival in adverse environments, exhibiting significant convergence in their characteristics and molecular mechanisms, particularly in antibiotic tolerance (Ayrapetyan et al., 2015b). Previous studies demonstrated that stationary-phase cultures contain a large portion of drug-

10.3389/fcimb.2024.1486426

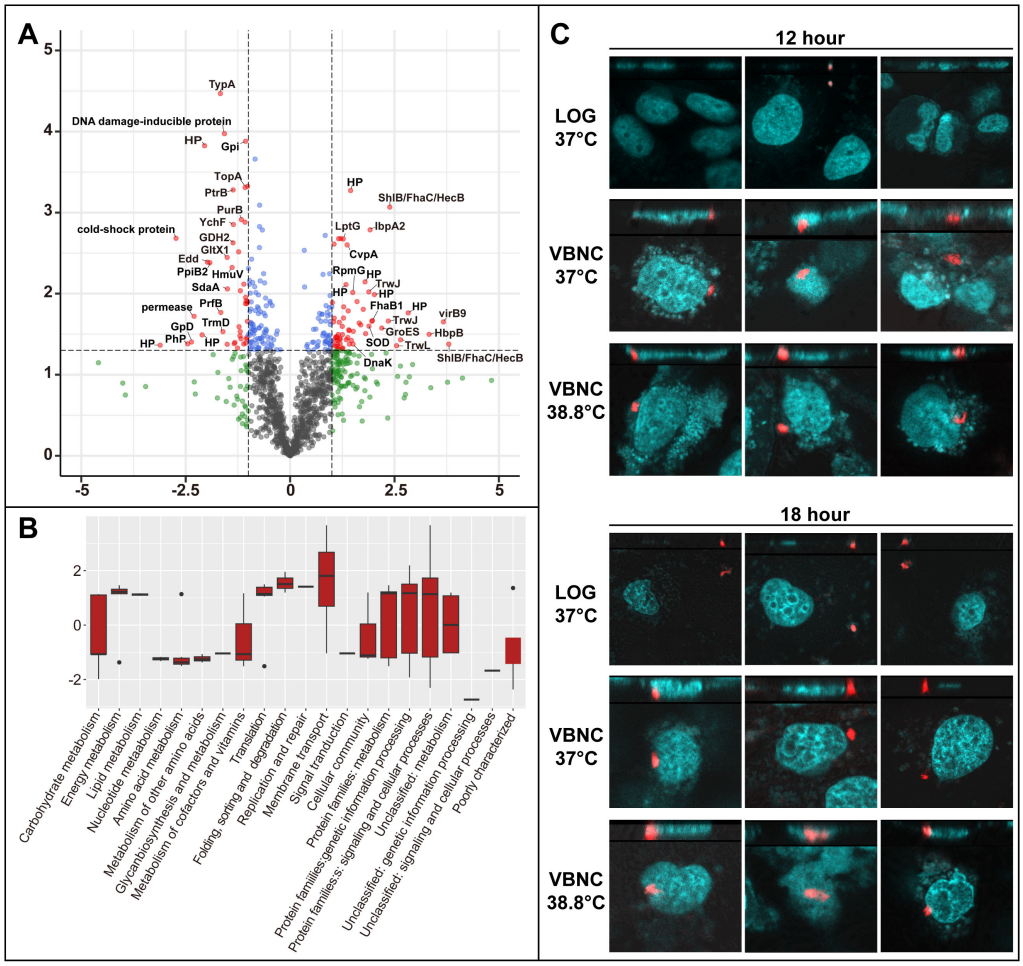

FIGURE 4
Differential protein expression in *B. henselae* VBNC cells and their ability to invade HUVECs. **(A)** Comparison of protein expression in VBNC cells *vs.* late-stationary-phase cells. A volcano plot shows significant protein expression changes in VBNC cells (p-value < 0.05, $\log_2$FC ≥ 1 or $\log_2$FC ≤ -1) marked in red. Other proteins with less pronounced changes are shown in green ($\log_2$FC ≥ 1 or $\log_2$FC ≤ -1, but p-value ≥ 0.05) and blue (p-value < 0.05, but $\log_2$FC between -1 and 1). Protein label abbreviations: HP, hypothetical protein; PhP, phage protein. **(B)** A bar chart depicts the enrichment of Gene Ontology terms among significantly altered proteins (p-value < 0.05, $\log_2$FC ≥ 1 or $\log_2$FC ≤ -1), categorized by KEGG pathways and visualized using R ggplot2 boxplots. For **(A, B)**, VBNC cells were confirmed through a resuscitation assay after 19 days of incubation at 38.8°C, with the control group of *B. henselae* cells cultured at 33°C for 19 days. **(C)** The invasion of HUVECs by *B. henselae* VBNC cells and cells at the logarithmic stage was analyzed at 12 and 18 hours post-infection using FISH combined with confocal scanning microscopy. A multiplicity of infection (MOI) of 100 of *B. henselae* was used either in logarithmic phase or in VBNC state. *B. henselae* cells, labeled with a specific 16S rRNA probe, appear in red, while HUVECs nucleic acids, stained with DAPI, are shown in cyan.

tolerant persisters in various bacterial species, including *B. henselae* (Li et al., 2019). This study found that pure *B. henselae* VBNC cells exhibited enhanced drug tolerance relative to persisters (Figure 2E), especially against anti-persister drugs like daptomycin and methylene blue (Li et al., 2019). Currently, the VBNC state and bacterial persistence are regarded as closely related phenomena along a shared 'dormancy continuum', rather than entirely distinct states (Ayrapetyan et al., 2015b). However, the mechanisms underlying drug tolerance in *B. henselae* during these two forms may be different and require further investigation. High-temperature exposure also significantly accelerated the formation of *B. henselae* persisters (Figure 2F), suggesting that *B. henselae* in infected individuals may be more drug-tolerant, posing substantial challenges for clinical treatment.

Furthermore, clinically used antibiotics were shown to induce the VBNC state in *B. henselae*. Bacterial antibiotics like gentamicin and streptomycin eliminated culturable cells within 4 days (Figure 3A), which is consistent with our previous findings (Li et al., 2019). However, viable cell counts remained high. This, combined with successful resuscitation, unearthed a novel insight: these clinically employed antibiotics can induce *B. henselae* into VBNC state, at least under *in vitro* conditions. Even bacteriostatic antibiotics like doxycycline and erythromycin, also converted a portion of *B. henselae* cells to VBNC state (Figure 3B). Therefore, the current antibiotic treatment for *B. henselae*-infected individuals may have paradoxical effect of killing some growing bacteria while promoting VBNC cell formation, which can contribute to persistent and/or chronic infection. These findings advance our understanding of the impact of antibiotic treatment for

Bartonella infections, urging the need to develop more effective treatments to combat the persister forms of this emerging human pathogen, especially the VBNC form.

The molecular mechanisms underlying VBNC formation in bacteria remain incompletely understood (Liu et al., 2023), though key genes and pathways, including those related to stress response, membrane proteins, toxin-antitoxin systems, and cell division, have been identified (Dong et al., 2020). Proteomic analysis in this study revealed that 17.6% of identified proteins were significantly altered in *B. henselae* VBNC cells compared to culturable cells. Notably, up-regulated proteins involved in hemin and iron uptake, such as FhaB1 and the hemin-binding proteins (Sander et al., 2000), suggest an iron deficiency in VBNC cells. This iron deficiency is supported by the resuscitation process, where sheep blood, rich in heme iron, promoted the recovery of VBNC cells to a culturable state. However, the specific contribution of sheep blood in the resuscitation process is a complex issue. Future studies should focus on identifying the key factors involved in the resuscitation of *B. henselae* VBNC cells, including the evaluation of various iron components.

Beyond their role in facilitating hemin and/or iron uptake, the HecB/FhaC proteins and hemin-binding proteins are also responsible for mediating *B. henselae* adhesion to host cells (Franz and Kempf, 2011). More proteins involved in host cell adhesion and invasion were up-regulated in VBNC cells (Figure 4; Supplementary Table S2; Supplementary Figure S2), including TrwL/J, VirB, and IalB. The Trw and VirB systems, which are Type 4 secretion system (T4SS), play critical roles in the adhesion of *Bartonella* to host cells (Jin et al., 2023), whereas IalB protein is implicated in erythrocyte invasion. The increased expression of these proteins in VBNC cells are likely responsible for facilitating the entry and invasion of *B. henselae* into host cells. FISH analysis in this study indeed confirmed that *B. henselae* in the VBNC state could invade HUVECs within 12-18 hours, whereas no invasion was observed for logarithmic-phase *B. henselae* during this same period (Figure 4C). Typically, actively growing bacteria require at least 24-30 hours to invade HUVECs (Dehio et al., 1997; Schmid et al., 2004). This suggests that VBNC *B. henselae* may have a faster invasion capability compared to its logarithmic-phase counterpart. This rapid invasion provides an effective strategy for countering environmental stress and evading the host immune clearance.

Another up-regulated protein in VBNC cells was BafA, a *Bartonella*-produced mitogen that exhibits pro-angiogenic activity through vascular endothelial growth factor receptor-2 (VEGFR-2) on the cell surface, resulting in the proliferation of *Bartonella*-infected vascular endothelial cells through activating the mitogen-activated protein kinase (MAPK) pathway (Tsukamoto et al., 2020). Other up-regulated proteins in VBNC cells included molecular chaperones and heat shock proteins (Figure 4A; Supplementary Figure S2), which are likely critical for maintaining the stability and folding of proteins in the VBNC state, thereby ensuring bacterial survival under unfavorable conditions. The down-regulation of cold shock proteins (Figure 4A) aligns with VBNC induction under high temperatures. SOD, an enzyme that eliminates reactive oxygen species, was also up-regulated, possibly aiding *B. henselae* VBNC cells survival at elevated temperatures.

Pathways involved in energy metabolism, lipid metabolism, and protein synthesis were up-regulated, while those related to the metabolism of nucleotides, amino acids, glycans, cofactors, and vitamins were down-regulated (Figure 4B). This metabolic shift suggests that *B. henselae* VBNC cells maintain essential functions for survival while down-regulating less critical pathways, characteristics of VBNC states (Liu et al., 2023) that share similarities with bacterial persister pathways (Zhang, 2014; Niu et al., 2024).

In conclusion, this study investigated *B. henselae*'s ability to enter the VBNC state and invade host cells efficiently. *B. henselae* can fully enter the VBNC state under fever-mimicking temperature (38.8°C) and antibiotic treatment, exhibiting enhanced drug tolerance and specific morphological and proteomic adjustments. The evidence suggests that bacteria in the VBNC state are not just a theoretical risk but may actively contribute to host pathogenesis, relapsing infections, and antibiotic failure. These findings underscore the diagnostic challenges posed by *B. henselae* in the VBNC state and emphasize the need for improving treatment strategies and developing effective culture methods to recover *B. henselae* isolates from patients.

Data availability statement

The original contributions presented in the study are publicly available. This data can be found here: ProteomeXchange website: http://proteomecentral.proteomexchange.org/cgi/GetDataset?ID=PXD055316 and iProX: https://www.iprox.cn//page/project.html?id=IPX0009557000.

Ethics statement

Ethical approval was not required for the studies on humans in accordance with the local legislation and institutional requirements because only commercially available established cell lines were used.

Author contributions

YG: Data curation, Methodology, Validation, Writing – original draft. DL: Data curation, Methodology, Validation, Writing – original draft. YXX: Data curation, Methodology, Validation, Writing – original draft. TW: Data curation, Methodology, Writing – review & editing. JL: Data curation, Methodology, Writing – review & editing. YWX: Data curation, Methodology, Writing – review & editing. XZ: Data curation, Formal analysis, Writing – review & editing. TC: Conceptualization, Writing – review & editing. YZ: Conceptualization, Writing – review & editing. TL: Conceptualization, Data curation, Formal analysis, Investigation, Writing – original draft, Writing – review & editing. JF: Conceptualization, Funding acquisition, Investigation, Writing – original draft, Writing – review & editing.

Funding

The author(s) declare financial support was received for the research, authorship, and/or publication of this article. This study

was funded by the Science and Technology Project of Gansu Province (No. 24CXGA022), the National Natural Science Foundation of China (No. 81902099) and the State Key Laboratory of Veterinary Etiological Biology, Lanzhou Veterinary Research Institute, Chinese Academy of Agricultural Sciences (No. SKLVEB2020KFKT005). The funders had no role in study design, data collection or analysis, decision to publish, or preparation of the manuscript.

Conflict of interest

The authors declare that the research was conducted in the absence of any commercial or financial relationships that could be construed as a potential conflict of interest.

Publisher's note

Supplementary material

The Supplementary Material for this article can be found online at: https://www.frontiersin.org/articles/10.3389/fcimb.2024.1486426/full#supplementary-material

References

Ayrapetyan, M., Williams, T. C., Baxter, R., and Oliver, J. D. (2015a). Viable but nonculturable and persister cells coexist stochastically and are induced by human serum. *Infect. Immun.* 83, 4194–4203. doi: 10.1128/IAI.00404-15

Ayrapetyan, M., Williams, T. C., and Oliver, J. D. (2015b). Bridging the gap between viable but non-culturable and antibiotic persistent bacteria. *Trends Microbiol.* 23, 7–13. doi: 10.1016/j.tim.2014.09.004

Ayrapetyan, M., Williams, T., and Oliver, J. D. (2018). Relationship between the viable but nonculturable state and antibiotic persister cells. *J. bacteriol.* 200 (20), e00249–18. doi: 10.1128/JB.00249-18

Breitschwerdt, E. B., Maggi, R. G., Nicholson, W. L., Cherry, N. A., and Woods, C. W. (2008). Bartonella sp. bacteremia in patients with neurological and neurocognitive dysfunction. *J. Clin. Microbiol.* 46, 2856–2861. doi: 10.1128/JCM.00832-08

Chen, T., Ma, J., Liu, Y., Chen, Z., Xiao, N., Lu, Y., et al. (2022). iProX in 2021: connecting proteomics data sharing with big data. *Nucleic Acids Res* 50 (D1), D1522–D1527. doi: 10.1093/nar/gkab1081

Dehio, C., Meyer, M., Berger, J., Schwarz, H., and Lanz, C. (1997). Interaction of Bartonella henselae with endothelial cells results in bacterial aggregation on the cell surface and the subsequent engulfment and internalisation of the bacterial aggregate by a unique structure, the invasome. *J. Cell Sci.* 110, 2141–2154. doi: 10.1242/jcs.110.18.2141

Demichev, V., Messner, C. B., Vernardis, S. I., Lilley, K. S., and Ralser, M. (2020). DIA-NN: neural networks and interference correction enable deep proteome coverage in high throughput. *Nat. Methods* 17, 41–44. doi: 10.1038/s41592-019-0638-x

Diniz, P. P., Morton, B. A., Tngrian, M., Kachani, M., Barron, E. A., Gavidia, C. M., et al. (2013). Infection of domestic dogs in Peru by zoonotic bartonella species: a cross-sectional prevalence study of 219 asymptomatic dogs. *PloS Negl. Trop. Dis.* 7, e2393. doi: 10.1371/journal.pntd.0002393

Dong, K., Pan, H., Yang, D., Rao, L., Zhao, L., Wang, Y., et al. (2020). Induction, detection, formation, and resuscitation of viable but non-culturable state microorganisms. *Compr. Rev. Food Sci. Food Saf.* 19, 149–183. doi: 10.1111/1541-4337.12513

Drummond, M. R., Dos Santos, L. S., de Almeida, A. R., Lins, K. A., Barjas-Castro, M. L., Diniz, P., et al. (2023). Comparison of molecular methods for Bartonella henselae detection in blood donors. *PloS Negl. Trop. Dis.* 17, e0011336. doi: 10.1371/journal.pntd.0011336

Feng, J., Wang, T., Zhang, S., Shi, W., and Zhang, Y. (2014). An optimized SYBR green I/PI assay for rapid viability assessment and antibiotic susceptibility testing for *borrelia burgdorferi*. *PloS One* 9, e111809. doi: 10.1371/journal.pone.0111809

Feng, J., Yee, R., Zhang, S., Tian, L., Shi, W., Zhang, W., et al. (2018). A rapid growth-independent antibiotic resistance detection test by SYBR green/propidium iodide viability assay. *Front. Med.* 5, 127. doi: 10.3389/fmed.2018.00127

Franz, B., and Kempf, V. A. (2011). Adhesion and host cell modulation: critical pathogenicity determinants of Bartonella henselae. *Parasit Vectors* 4, 54. doi: 10.1186/1756-3305-4-54

Jin, X., Gou, Y., Xin, Y., Li, J., Sun, J., Li, T., et al. (2023). Advancements in understanding the molecular and immune mechanisms of Bartonella pathogenicity. *Front. Microbiol.* 14. doi: 10.3389/fmicb.2023.1196700

Kanehisa, M., Furumichi, M., Tanabe, M., Sato, Y., and Morishima, K. (2017). KEGG: new perspectives on genomes, pathways, diseases and drugs. *Nucleic Acids Res.* 45, D353–D361. doi: 10.1093/nar/gkw1092

Kibbee, R. J., and Ormeci, B. (2017). Development of a sensitive and false-positive free PMA-qPCR viability assay to quantify VBNC Escherichia coli and evaluate disinfection performance in wastewater effluent. *J. microbiol. Methods* 132, 139–147. doi: 10.1016/j.mimet.2016.12.004

Korber, D. R., Choi, A., Wolfaardt, G. M., and Caldwell, D. E. (1996). Bacterial plasmolysis as a physical indicator of viability. *Appl. Environ. Microbiol.* 62, 3939–3947. doi: 10.1128/aem.62.11.3939-3947.1996

Koutantou, M., Kambas, K., Makka, S., Fournier, P. E., Raoult, D., and Angelakis, E. (2023). Limitations of serological diagnosis of typical cat scratch disease and recommendations for the diagnostic procedure. *Can. J. Infect. Dis. Med. Microbiol.* 2023, 4222511. doi: 10.1155/2023/4222511

Lagier, J. C., Edouard, S., Pagnier, I., Mediannikov, O., Drancourt, M., and Raoult, D. (2015). Current and past strategies for bacterial culture in clinical microbiology. *Clin. Microbiol. Rev.* 28, 208–236. doi: 10.1128/Cmr.00110-14

La Scola, B., and Raoult, D. (1996). Serological cross-reactions between Bartonella quintana, Bartonella henselae, and Coxiella burnetii. *J. Clin. Microbiol.* 34, 2270–2274. doi: 10.1128/jcm.34.9.2270-2274.1996

La Scola, B., and Raoult, D. (1999). Culture of Bartonella quintana and Bartonella henselae from human samples: a 5-year experience, (1993 to 1998). *J. Clin. Microbiol.* 37, 1899–1905. doi: 10.1128/JCM.37.6.1899-1905.1999

Lazou, T. P., Iossifidou, E. G., Gelasakis, A. I., Chaintoutis, S. C., and Dovas, C. I. (2019). Viability quantitative PCR utilizing propidium monoazide, spheroplast formation, and campylobacter coli as a bacterial model. *Appl. Environ. Microbiol.* 85 (20), e01499–19. doi: 10.1128/AEM.01499-19

Li, T., Feng, J., Xiao, S., Shi, W., Sullivan, D., and Zhang, Y. (2019). Identification of FDA-Approved Drugs with Activity against Stationary Phase Bartonella henselae. *Antibiot. (Basel)* 8, 50. doi: 10.3390/antibiotics8020050

Li, L., Mendis, N., Trigui, H., Oliver, J. D., and Faucher, S. P. (2014). The importance of the viable but non-culturable state in human bacterial pathogens. *Front. Microbiol.* 5. doi: 10.3389/fmicb.2014.00258

Liu, J. Y., Yang, L., Kjellerup, B. V., and Xu, Z. B. (2023). Viable but nonculturable (VBNC) state, an underestimated and controversial microbial survival strategy. *Trends Microbiol.* 31, 1013–1023. doi: 10.1016/j.tim.2023.04.009

Lotoux, A., Milohanic, E., and Bierne, H. (2022). The viable but non-culturable state of listeria monocytogenes in the one-health continuum. *Front. Cell Infect. Microbiol.* 12. doi: 10.3389/fcimb.2022.849915

Lovdal, T., Hovda, M. B., Bjorkblom, B., and Moller, S. G. (2011). Propidium monoazide combined with real-time quantitative PCR underestimates heat-killed Listeria innocua. *J. microbiol. Methods* 85, 164–169. doi: 10.1016/j.mimet.2011.01.027

Massei, F., Messina, F., Gori, L., Macchia, P., and Maggiore, G. (2004). High prevalence of antibodies to Bartonella henselae among Italian children without evidence of cat scratch disease. *Clin. Infect. Dis.* 38, 145–148. doi: 10.1086/379824

Nelson, C. A., Saha, S., and Mead, P. S. (2016). Cat-scratch disease in the United States 2005-2013. *Emerg. Infect. Dis.* 22, 1741–1746. doi: 10.3201/eid2210.160115

Niu, H., Gu, J., and Zhang, Y. (2024). Bacterial persisters: molecular mechanisms and therapeutic development. *Signal Transduct Target Ther.* 9, 174. doi: 10.1038/s41392-024-01866-5

Okaro, U., Addisu, A., Casanas, B., and Anderson, B. (2017). Bartonella species, an emerging cause of blood-culture-negative endocarditis. *Clin. Microbiol. Rev.* 30, 709–746. doi: 10.1128/CMR.00013-17

Pitassi, L. H., de Paiva Diniz, P. P., Scorpio, D. G., Drummond, M. R., Lania, B. G., Barjas-Castro, M. L., et al. (2015). Bartonella spp. bacteremia in blood donors from Campinas, Brazil. *PloS Negl. Trop. Dis.* 9, e0003467. doi: 10.1371/journal.pntd.0003467

Prudent, E., La Scola, B., Drancourt, M., Angelakis, E., and Raoult, D. (2018). Molecular strategy for the diagnosis of infectious lymphadenitis. *Eur. J. Clin. Microbiol. Infect. Dis.* 37, 1179–1186. doi: 10.1007/s10096-018-3238-2

Prudent, E., Lepidi, H., Audoly, G., La Scola, B., Fournier, P. E., Edouard, S., et al. (2017). Bartonella henselae is usually not viable in lymph nodes of patients with cat scratch disease. *Eur. J. Clin. Microbiol. Infect. Dis.* 36, 2207–2213. doi: 10.1007/s10096-017-3047-z

Pulliainen, A. T., and Dehio, C. (2012). Persistence of Bartonella spp. stealth pathogens: from subclinical infections to vasoproliferative tumor formation. *FEMS Microbiol. Rev.* 36, 563–599. doi: 10.1111/j.1574-6976.2012.00324.x

Riess, T., Dietrich, F., Schmidt, K. V., Kaiser, P. O., Schwarz, H., Schafer, A., et al. (2008). Analysis of a novel insect cell culture medium-based growth medium for Bartonella species. *Appl. Environ. Microbiol.* 74, 5224–5227. doi: 10.1128/AEM.00621-08

Sander, A., Kretzer, S., Bredt, W., Oberle, K., and Bereswill, S. (2000). Hemin-dependent growth and hemin binding of Bartonella henselae. *FEMS Microbiol. Lett.* 189, 55–59. doi: 10.1111/j.1574-6968.2000.tb09205.x

Sayed, A. S. M., Alsaadawy, R. M., Ali, M. M., Abd El-Hamid, R. F., Baty, R. S., and Elmahallawy, E. K. (2022). Serological and molecular detection of bartonella henselae in cats and humans from Egypt: current status and zoonotic implications. *Front. Vet. Sci.* 9. doi: 10.3389/fvets.2022.859104

Schindelin, J., Arganda-Carreras, I., Frise, E., Kaynig, V., Longair, M., Pietzsch, T., et al. (2012). Fiji: an open-source platform for biological-image analysis. *Nat. Methods* 9, 676–682. doi: 10.1038/nmeth.2019

Schmid, M. C., Schulein, R., Dehio, M., Denecker, G., Carena, I., and Dehio, C. (2004). The VirB type IV secretion system of Bartonella henselae mediates invasion, proinflammatory activation and antiapoptotic protection of endothelial cells. *Mol. Microbiol.* 52, 81–92. doi: 10.1111/j.1365-2958.2003.03964.x

Shi, H., Westfall, C. S., Kao, J., Odermatt, P. D., Anderson, S. E., Cesar, S., et al. (2021). Starvation induces shrinkage of the bacterial cytoplasm. *Proc. Natl. Acad. Sci. U.S.A.* 118, e2104686118. doi: 10.1073/pnas.2104686118

Song, S., and Wood, T. K. (2021). [amp]]lsquo;Viable but non-culturable cells' are dead. *Environ. Microbiol.* 23, 2335–2338. doi: 10.1111/1462-2920.15463

Song Xiu, P., Zhang Hai, B., Liu Qi, Y., Sun Ji, M., Xu, L., Gu Shao, H., et al. (2020). Seroprevalence of *bartonella henselae* and identification of risk factors in China. *Biomed. Environ. Sci.* 33, 72–75. doi: 10.3967/bes2020.011

Tsukamoto, K., Shinzawa, N., Kawai, A., Suzuki, M., Kidoya, H., Takakura, N., et al. (2020). The Bartonella autotransporter BafA activates the host VEGF pathway to drive angiogenesis. *Nat. Commun.* 11, 3571. doi: 10.1038/s41467-020-17391-2

Zhang, Y. (2014). Persisters, persistent infections and the Yin-Yang model. *Emerg. Microbes Infect.* 3, 1. doi: 10.1038/emi.2014.3

Zhang, Y., Yang, Y., Woods, A., Cotter, R. J., and Sun, Z. (2001). Resuscitation of dormant Mycobacterium tuberculosis by phospholipids or specific peptides. *Biochem. Biophys. Res. Commun.* 284, 542–547. doi: 10.1006/bbrc.2001.4993

frontiers | Frontiers in Cellular and Infection Microbiology

TYPE Correction
PUBLISHED 07 January 2025
DOI 10.3389/fcimb.2024.1544596

OPEN ACCESS

APPROVED BY
Frontiers Editorial Office,
Frontiers Media SA, Switzerland

*CORRESPONDENCE
Jie Feng
jfeng@lzu.edu.cn
Tingting Li
litt@lzu.edu.cn

RECEIVED 13 December 2024
ACCEPTED 16 December 2024
PUBLISHED 07 January 2025

CITATION
Gou Y, Liu D, Xin Y, Wang T, Li J, Xi Y, Zheng X, Che T, Zhang Y, Li T and Feng J (2025) Corrigendum: Viable but nonculturable state in the zoonotic pathogen *Bartonella henselae* induced by low-grade fever temperature and antibiotic treatment.
Front. Cell. Infect. Microbiol. 14:1544596.
doi: 10.3389/fcimb.2024.1544596

Corrigendum: Viable but nonculturable state in the zoonotic pathogen *Bartonella henselae* induced by low-grade fever temperature and antibiotic treatment

Yuze Gou[1,2], Dongxia Liu[1,2], Yuxian Xin[1,2], Ting Wang[1], Jiaxin Li[1], Yiwen Xi[1], Xiaoling Zheng[3], Tuanjie Che[3], Ying Zhang[4,5], Tingting Li[1]* and Jie Feng[1,2]*

[1]Key Laboratory of Preclinical Study for New Drugs of Gansu Province, School of Basic Medical Sciences, Lanzhou University, Lanzhou, China, [2]State Key Laboratory of Veterinary Etiological Biology, College of Veterinary Medicine, Lanzhou University, Lanzhou, China, [3]Department of Scientific Experimental Research, Innovation Center of Functional Genomics and Molecular Diagnostics Technology of Gansu Province, Lanzhou, China, [4]State Key Laboratory for the Diagnosis and Treatment of Infectious Diseases, The First Affiliated Hospital, Zhejiang University School of Medicine, Hangzhou, China, [5]Center for Microbiome and Disease Research, Jinan Microecological Biomedicine Shandong Laboratory, Jinan, China

KEYWORDS

***Bartonella*, *B. henselae*, VBNC, resuscitation, persister, blood-culture-negative endocarditis (BCNE), cat-scratch disease (CSD)**

A Corrigendum on

Viable but nonculturable state in the zoonotic pathogen *Bartonella henselae* induced by low-grade fever temperature and antibiotic treatment

By Gou Y, Liu D, Xin Y, Wang T, Li J, Xi Y, Zheng X, Che T, Zhang Y, Li T and Feng J (2024) *Front. Cell. Infect. Microbiol.* 14:1486426. doi: 10.3389/fcimb.2024.1486426

In the published article, there was an error in affiliation 1. Instead of "Key Laboratory of Preclinical Study for New Drugs of Gansu Province, School of Basic Medical Sciences, Lanzhou, China", it should be "Key Laboratory of Preclinical Study for New Drugs of Gansu Province, School of Basic Medical Sciences, Lanzhou University, Lanzhou, China".

The authors apologize for this error and state that this does not change the scientific conclusions of the article in any way. The original article has been updated.

Publisher's note

All claims expressed in this article are solely those of the authors and do not necessarily represent those of their affiliated organizations, or those of the publisher, the editors and the reviewers. Any product that may be evaluated in this article, or claim that may be made by its manufacturer, is not guaranteed or endorsed by the publisher.

frontiers | Frontiers in Cellular and Infection Microbiology

TYPE Original Research
PUBLISHED 13 December 2024
DOI 10.3389/fcimb.2024.1496925

OPEN ACCESS

EDITED BY
Omid Teymournejad,
University of Illinois Chicago, United States

REVIEWED BY
Stephen Lu,
National Institute of Allergy and Infectious Diseases (NIH), United States
Pablo Colunga-Salas,
Universidad Veracruzana, Mexico

*CORRESPONDENCE
Veronika Rusňáková Tarageľová
veronika.taragelova@savba.sk

RECEIVED 15 September 2024
ACCEPTED 20 November 2024
PUBLISHED 13 December 2024

CITATION
Rusňáková Tarageľová V, Derdáková M, Selyemová D, Chvostáč M, Mangová B, Didyk YM, Koči J, Kolenčík S, Víchová B, Peťko B, Stanko M and Kazimírová M (2024) Two decades of research on *Borrelia burgdorferi* sensu lato in questing *Ixodes ricinus* ticks in Slovakia. *Front. Cell. Infect. Microbiol.* 14:1496925. doi: 10.3389/fcimb.2024.1496925

Two decades of research on *Borrelia burgdorferi* sensu lato in questing *Ixodes ricinus* ticks in Slovakia

Veronika Rusňáková Tarageľová[1]*, Markéta Derdáková[1], Diana Selyemová[1], Michal Chvostáč[1], Barbara Mangová[1], Yuliya M. Didyk[1,2], Juraj Koči[1], Stanislav Kolenčík[3], Bronislava Víchová[4], Branislav Peťko[5], Michal Stanko[4] and Mária Kazimírová[1]

[1]Institute of Zoology, Slovak Academy of Sciences, Bratislava, Slovakia, [2]Schmalhausen Institute of Zoology of the National Academy of Sciences of Ukraine, Kyiv, Ukraine, [3]Faculty of Natural Sciences, Comenius University in Bratislava, Bratislava, Slovakia, [4]Institute of Parasitology, Slovak Academy of Sciences, Košice, Slovakia, [5]Department of Epizootiology, Parasitology and Protection of One Health, University of Veterinary Medicine and Pharmacy, Košice, Slovakia

Introduction: In Europe, *Borrelia burgdorferi* sensu lato (s.l.), the causative agent of Lyme borreliosis is transmitted by the castor bean tick, *Ixodes ricinus*. In the last decades, global changes affect the spread of ticks and also their bionomics. The aim of this study was summarization of a large dataset obtained during 20 years of research.

Methods: The research was carried out in 1999-2019 at 16 localities in Slovakia that were continuously monitored. In total, 17,249 questing *I. ricinus* ticks were tested for the presence of *B. burgdorferi* s.l.

Results: The total prevalence of infected ticks was 18.8% (3,248/17,249), with 15.1% (1,557/10,302) infected nymphs and 24.3% (1,691/6,947) infected adults. Nine species of *B. burgdorferi* s.l. were identified. *Borrelia afzelii* (37.1%), *B. garinii/bavariensis* (24.7%), and *B. valaisiana* (15.4%) were the most frequent and were present at all study sites, followed by *B. lusitaniae* (12.6%), *B. burgdorferi* sensu stricto (4.1%) and *B. spielmanii* (1.6%). *Borrelia bavariensis* was confirmed only in four samples (0.1%), however, detection of this species has been performed only since 2017. *Borrelia bissettii* and *B. kurtenbachii* were both recorded in one case. The total prevalence differed significantly among four habitat types (urban, suburban, natural, agricultural). The highest infection prevalence was confirmed in natural habitat (22.0%), the lowest in urban habitat (13.2%). In addition, molecular analysis was carried out on part of the collected ticks previously morphologically identified as *I. ricinus*. The analysis did not confirm the occurrence of *Ixodes inopinatus* in Slovakia.

Conclusion: Long-term monitoring of the abundance and spread of ticks as well as the prevalence and genetic variability of tick-borne pathogens can reveal the impact of global climatic and socio-economic changes on different habitats, including natural foci of tick-borne pathogens.

KEYWORDS

***Borrelia*, prevalence, species diversity, habitat, long-term trends**

1 Introduction

Ticks transmit a wider range of pathogenic microorganisms than any other arthropod group (Durden, 2006). In humans, the diseases caused by these agents include Lyme borreliosis (LB), spotted fever group rickettsioses, human granulocytic anaplasmosis, tick-borne encephalitis, babesiosis, and others. Many of these diseases have emerged (or re-emerged) within the past decades (e.g. LB, anaplasmosis, rickettsioses, neoehrlichiosis). New foci of tick-borne disease (TBD) can be formed due to climatic changes and spread of ticks to new areas in the north and higher altitudes (Lindgren et al., 2000; Gray et al., 2009; Rusňáková Tarageľová et al., 2016).

Ixodes ricinus is the main vector of pathogenic microorganisms in Europe (Rizzoli et al., 2014), including *Borrelia* spirochaetes (Lindgren and Jaenson, 2006). Members of the *Borrelia burgdorferi* sensu lato (s.l.) complex are the causative agents of LB which is the most common TBD in areas of Eurasia with moderate climate (Stanek et al., 2012). This group comprises of more than 20 species transmitted by ticks from the *Ixodes ricinus* s.l. complex (Margos et al., 2019). *Borrelia afzelii*, *Borrelia garinii*, *Borrelia bavariensis*, *Borrelia spielmanii* and *Borrelia burgdorferi* sensu stricto (s.s.) are considered pathogenic for humans (Stanek et al., 2012). Genetic variability within the *B. burgdorferi* s.l. complex is associated with different clinical outcome in patients (van Dam et al., 1993) as well as with different reservoir hosts (Humair and Gern, 2000). Research on *B. burgdorferi* s.l. eco-epidemiology has a long history in Slovakia (rev. in Stanko et al., 2022). *Borrelia* prevalence in questing ticks was found to vary from 4.4% in northern Slovakia (Pangrácová et al., 2013) and up to 53.2% in eastern Slovakia (Venczel et al., 2016). The presence of nine species was confirmed, with *B. afzelii* and/or *B. garinii* as the most prevalent. Less frequent and rare species such as *Borrelia valaisiana, B. burgdorferi* sensu stricto (s.s.), *B. spielmanii, B. bavariensis, B. bissettii*, and *B. kurtenbachii* were reported as well (rev. in Stanko et al., 2022; Kazimírová et al., 2023). The prevalence of *Borrelia lusitaniae* was found to be low in Central Europe (Hubálek and Halouzka, 1997; Gern et al., 1999), nevertheless, natural foci with dominance of this species were confirmed in some areas of Slovakia (Rusňáková Tarageľová et al., 2016).

In order to find out whether there are changes in *Borrelia* prevalence and species distribution over the years, long-term monitoring of the prevalence, occurrence and species distribution is necessary. The main aim of this study is the evaluation of changes in the *B. burgdorferi* s.l. prevalence and diversity of species of the *B. burgdorferi* s.l. complex in selected sites of Slovakia during the period from 1999 to 2019.

Ixodes inopinatus described by Estrada-Peña et al. (2014) was confirmed in dry areas of the Mediterranean region in Spain, Portugal, Morocco, Algeria and Tunisia. This tick species morphologically resembles *I. ricinus*. Its occurrence has been confirmed also outside the Mediterranean region (Chitimia-Dobler et al., 2018) and it is possible that in the past many individuals of *I. inopinatus* were mistakenly classified as *I. ricinus*. However, the recent study of Rollins et al. (2023) calls into question the occurrence of *I. inopinatus* in Central Europe.

Hauck et al. (2019) confirmed the presence of *Borrelia* spp., *Rickettsia* spp. and *Anaplasma phagocytophilum* in *I. inopinatus*, while, compared to *I. ricinus*, a considerably higher prevalence of *Borrelia* was recorded in *I. inopinatus*. Molecular screening of selected ticks that were collected in Slovakia would clarify whether *I. inopinatus* also occurs there and participates, together with *I. ricinus*, in the maintenance and transmission of tick-borne pathogens.

2 Materials and methods

2.1 Tick sampling and study sites

Questing ticks were collected by flagging the vegetation at 16 study sites in Slovakia during 1999-2019 (Figure 1). Feeding ticks were collected from birds captured in Drienovec in 2019 (Šujanová et al., 2022). Chosen study locations represented different types of habitats: urban, suburban, natural and agricultural (Supplementary Table S1). The research was done in western Slovakia (WS): four study sites in Bratislava (the campus of the Slovak Academy of Sciences - SAS, Železná studnička, Horský park, Podunajské Biskupice), Malacky, Záhorská Ves, Jurský Šúr, Vrbovce, Fúgelka, Trenčín and in eastern Slovakia (ES): Košice, Rozhanovce, Zádiel, Drienovec, Brzotín. Study sites at Martinské hole Mountains represent a region of northern Slovakia (NS).

Urban habitat is represented by three sites: Horský park and the campus of the SAS in Bratislava, and the castle park in the centre of Malacky town. All these parks are fenced.

Suburban habitat is represented by five sites: Železná studnička and Podunajské Biskupice (both in Bratislava), Jurský Šúr nature reserve, Trenčín and Košice. These sites are not fenced and pass into open country or forest.

Natural habitat is represented by Fúgelka, Martinské hole, Drienovec, Zádiel and Brzotín.

Agricultural habitat is represented by Vrbovce, Záhorská Ves and Rozhanovce.

2.2 Identification of ticks

Questing and several bird-feeding ticks were morphologically identified to species, life stages and sex using standard keys (Nosek and Sixl, 1972; Slovák, 2010). To confirm the identification of ticks and find out whether *I. inopinatus* (Estrada-Peña et al., 2014) occurs in Slovakia, the mitochondrial 16S rRNA locus and nuclear gene TROSPA were amplified and sequenced. The sequences were compared via BLASTn (Altschul et al., 1990) searches to sequences available in GenBank (Mangold et al., 1998; Noureddine et al., 2011; Norte et al., 2021). To amplify each gene, published primers and protocols were used according to Mangold et al. (1998) for 16S rRNA and Noureddine et al. (2011) for TROSPA. Obtained sequences were

10.3389/fcimb.2024.1496925

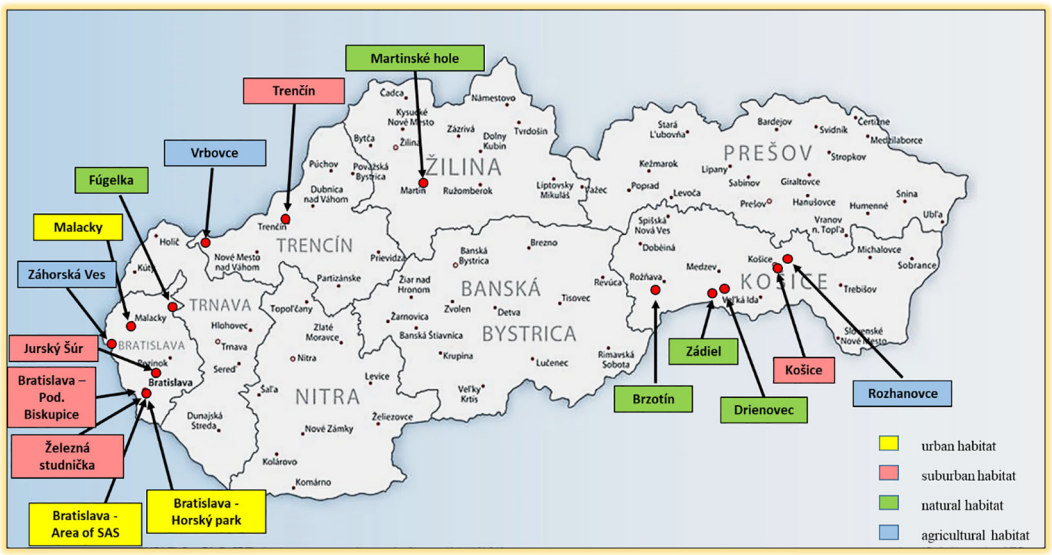

FIGURE 1
Study sites in Slovakia with the type of habitat.

compared with sequences for *I. ricinus* and *I. inopinatus* mentioned in the previous research (16S rRNA, GenBank PopSet: 309318023; TROSPA, GenBank PopSet; 309318631 and 309318389) (Noureddine et al., 2011; Poli et al., 2020).

2.3 Genomic DNA isolation and PCR detection of *B. burgdorferi* s.l.

DNA was isolated from individual ticks by using the alkaline hydrolysis method (Guy and Stanek, 1991) and/or by using commercial kits: DNeasy Blood & Tissue Kit (Qiagen, Germany) and/or Macherey-Nagel NucleoSpin®Tissue kit (Düren, Germany), following the manufacturer protocols. To confirm the presence of the tick DNA a 620-bp fragment of tick mitochondrial gene cytochrome *b* was amplified in randomly selected samples (Black and Roehrdanz, 1998) or total DNA was measured with a Nanodrop 2000c (Thermo Scientific, Wilmington, USA). Samples were stored at -20°C. Isolated DNA was screened for the presence of *B. burgdorgferi* s.l. by several PCR methods as described in previous publications (Derdáková et al., 2003; Hanincová et al., 2003a, 2003b; Taragel'ová et al., 2008; Chvostáč et al., 2018; Vaculová et al., 2019; Mtierová et al., 2020; Kazimírová et al., 2023). A positive (DNA from *Borrelia*-positive tick that was previously sequenced) and a negative control (Nuclease-Free Water, Qiagen, Germany instead of DNA) were used in each PCR reaction. The PCR products from the conventional PCRs were electrophoresed in a 1.5% agarose gel stained with GoodView™ Nucleic Acid stain (SBS Genetech, Beijing, China) and visualised with a UV transilluminator. The list of used PCR assays is summarised in Supplementary Table S2. *Borrelia*-positive samples were further genotyped by RLB (reverse line blot) (Rijpkema et al., 1995; Hanincová et al., 2003a, 2003b; Taragel'ová et al., 2008) or by RFLP (restriction fragment length polymorphism) (Derdáková et al., 2003; and/or sequencing (Chvostáč et al., 2018; Vaculová et al., 2019; Kazimírová et al., 2023). Selected positive samples were further analysed using MLST (multilocus sequence typing) according to the protocol by Margos et al. (2008) and (Mtierová et al., 2020). Samples positive for *B. garinii* have been sequenced for the identification of *B. bavariensis* prevalence only since 2017.

Temporal changes in the prevalence and genetic variability were evaluated only at study sites that had been monitored for at least five years.

2.4 PCR product purification, Sanger sequencing

Purification of PCR products for Sanger sequencing was done by NucleoSpin Gel and PCR Clean-up (Machery-Nagel, Düren, Germany). The sequencing in both the forward and reverse direction was performed in Eurofins Genomics (Eurofins Genomics Germany GmbH, Ebersberg, Germany) and by SeqMe (SEQme s.r.o., Dobříš, Czech Republic). The complementary strands of each sequenced product were manually assembled into consensus sequences. The sequences were compared with GenBank entries using the basic local alignment search tool algorithm (www.ncbi.nlm.nih.gov/blast) and aligned with representative homologous sequences using the Clustal W implemented in the MEGA software version 11 (Tamura et al., 2021).

2.5 Statistical analysis

Within the monitored years, the collections were not uniform, therefore we statistically evaluated only multi-year collections at the same sites (5 and more collection years). Statistical differences in *B. burgdorferi* s.l. prevalence between study years and between four

different habitat types were evaluated by t-test using updated PAST 3 system package (Hammer et al., 2001). Chi-square test was used to analyse the proportions of collected nymphs and adult ticks and the prevalence levels for significant independence. The level of significance was set at $p < 0.05$. Ninety-five percent confidence intervals (95% CI) for each proportion were calculated using an online calculator (Sergeant, 2018) at the website https://epitools.ausvet.com.au/ciproportion. The program outputs include the estimated proportion plus upper and lower limits of the specified confidence interval, using Wilson Score interval method (Brown et al., 2001). Correlations between prevalence of *B. burgdorferi* s.l. species and habitat types were evaluated by Multivariate - Principal component analysis (PCA) using updated PAST 3 system package (Hammer et al., 2001).

3 Results

3.1 Questing ticks

In total, 17,249 *I. ricinus* ticks, including 10,302 nymphs and 6,947 adults were analysed from all study sites.

Questing adult ticks were significantly more abundant than nymphs at two sites in Bratislava: Podunajské Biskupice ($\chi^2 = 30.70$, $p < 0.05$), Železná studnička ($\chi^2 = 31.42$, $p < 0.05$) and in Záhorská Ves ($\chi^2 = 13.11$, $p < 0.05$) as well as at Martinské hole ($\chi^2 = 27.82$, $p < 0.05$) and in Košice ($\chi^2 = 17.47$, $p < 0.05$). On the contrary, nymphs were significantly more abundant at 10 sites: Vrbovce ($\chi^2 = 30.92$, $p < 0.05$), Malacky ($\chi^2 = 230.12$, $p < 0.05$), Šúr ($\chi^2 = 6.45$, $p < 0.05$), Fúgelka ($\chi^2 = 432.77$, $p < 0.05$), Bratislava – SAS ($\chi^2 = 435.62$, $p < 0.05$), Bratislava – Horský park ($\chi^2 = 53.82$, $p < 0.05$), Trenčín ($\chi^2 = 32.11$, $p < 0.05$), Rozhanovce ($\chi^2 = 464.82$, $p < 0.05$), Brzotín ($\chi^2 = 12.46$, $p < 0.05$), Drienovec ($\chi^2 = 190.75$, $p < 0.05$). At site Zádiel the nymphs/adults ratio was balanced (Table 1).

3.2 Molecular identification of ticks

Randomly selected samples of tick DNA collected at Bratislava - Železná studnička, Malacky, Vrbovce, Martinské hole, Drienovec and Košice were sequenced (Table 2). Only samples with high quality sequences were included in the further analysis (n = 46). Sequenced samples from Drienovec (n = 16) represented ticks fed on birds: 3 ticks from *Turdus merula* (n = 2), 6 ticks from *Turdus philomelos* (n = 4), 3 ticks from *Erithacus rubecula* (n = 2), 1 tick from *Fringilla coelebs* (n = 1), 1 tick from *Coccothraustes coccothraustes* (n = 1), 1 tick from *Garrulus glandarius* (n = 1), 1 tick from *Parus major* (n = 1). Sequenced samples from other study sites were represented by ticks collected from vegetation. Morphological identification matched sequencing results, *I. ricinus* was confirmed in all tested samples. All our sequenced samples had 100% query coverage, E-value = 0, and 100% identity with more than one sample of *Ixodes ricinus* (KF197124.1 - Italy, KJ414457.1 – Belgium, GU074645.1 – France, OY973598.1) from the GenBank.

3.3 Prevalence of *B. burgdorferi* s.l.

A total of 17,249 *I. ricinus* ticks, including 10,302 nymphs and 6,947 adults were tested for the presence of *B. burgdorferi* s.l. The total prevalence of infected ticks was 18.8% (3248/17249) (95% CI: 18.3-19.4), with 15.1% (1557/10302) (95% CI: 14.4-15.8) infected nymphs and 24.3% (1691/6947) (95% CI: 23.4-25.4) infected adults. The differences in total prevalence among nymphs and adult ticks were not significant ($\chi^2 = 2.15$, $p = 0.14$). The lowest infection prevalence was detected at site Bratislava – SAS (6.6%, 95% CI: 5.6-7.8), the highest at site Záhorská Ves (33.9%, 95% CI: 30.7 – 37.2) (Table 1). Significantly higher infection prevalence in nymphs than adults was recorded at Vrbovce ($\chi^2 = 7.63$, $p < 0.05$). On the contrary, significantly higher infection prevalence in adult ticks than in nymphs was found at three sites: Záhorská Ves ($\chi^2 = 11.25$, $p < 0.05$), Martinské hole ($\chi^2 = 6.59$, $p < 0.05$) and Zádiel ($\chi^2 = 4.72$, $p < 0.05$). At the other sites no significant differences were recorded.

3.4 Species of *B. burgdorferi* s.l. identified in ticks

A total of 3,158 (97.2%) PCR-positive samples were successfully genotyped. Nine species of *B. burgdorferi* s.l. were identified (Table 3; Supplementary Figure S1). *Borrelia afzelii* (37.1%), *B. garinii/bavariensis* (24.7%), *B. valaisiana* (15.4%) were the most frequent and were present at all study sites. *Borrelia afzelii* was the dominant species at ten sites (Bratislava: Železná studnička, Horský park, SAS and Podunajské Biskupice, Záhorská Ves, Malacky, Vrbovce, Rozhanovce, Brzotín, Drienovská mokraď). The highest proportion of ticks harbouring this species was detected in Malacky (19.2%). *Borrelia garinii/bavariensis* was dominant at sites Fúgelka (18.7%) and Košice (18.0%) while *B. valaisiana* was the most frequent species at sites Záhorská Ves (13.0%) and Jurský Šúr (12.1%). *Borrelia burgdorferi* s.s. (4.1%) was found at majority of sites with the exception of Vrbovce, Jurský Šúr and Drienovská mokraď. This species was the most frequent in Košice (31.3%). *Borrelia spielmanii* (1.6%) appeared sporadically at three sites in Bratislava, in Malacky, Jurský Šúr, Fúgelka and at three sites in Eastern Slovakia with the dominance in Bratislava SAS and Malacky (25.5% each). *Borrelia lusitaniae* (12.6%) was recorded at all sites with the exception of Brzotín. This species considerably dominated in the Martinské hole area (73.7%). We confirmed the presence of *B. bavariensis* only in four ticks: 2 nymphs and 1 male from Malacky (0.1%) and one female from Fúgelka (0.03%).

Co-infections with two, three and/or four species were detected in 4.3% of infected ticks. Among mixed infections, *B. garinii* + *B. valaisiana* was the most frequent (56.3%) followed by *B. afzelii* mixed with *B. valaisiana* (10.4%) and *B. garinii* (8.9%). Prevalence of other species combinations ranged from 1.5 to 6.7%. *Borrelia bissettii* and *Borrelia kurtenbachii* (in mixed infection with *B. burgdorferi* s.s., *B. garinii* and *B. valaisiana*) were detected in one tick from Malacky and in one tick from Rozhanovce, respectively (Hanincová et al., 2003a; Kazimírová et al., 2023). The proportions of eleven types of detected co-infections is shown in Figure 2.

10.3389/fcimb.2024.1496925

TABLE 1 Prevalence of *B. burgdorferi* s.l. in *Ixodes ricinus* ticks at study sites in Slovakia.

Type of habitat	Study site	No. of positive/ tested adults (%)	95% CI	No. of positive/ tested nymphs (%)	95% CI	No. of positive/ tested total ticks (%)	95% CI
Urban	Bratislava – Horský park	23/110 (20.9)	14.4-29.4	32/249 (12.9)	9.3-17.6	55/359 (15.3)	12.0-19.4
	Bratislava – SAS	38/531 (7.2)	5.3-9.7	94/1463 (6.4)	6.3-7.8	132/1994 (6.7)	5.6-7.8
	Malacky	171/682 (25.1)	22.0-28.5	224/1369 (16.4)	14.5-18.4	395/2051 (19.3)	17.6-21.0
	Total	232/1323 (17.5)	15.6-19.7	350/3081 (11.4)	10.3-12.5	582/4404 (13.2)	12.3-14.3
Suburban	Bratislava – Železná studnička	217/1286 (16.9)	14.9-19.0	94/1017 (9.2)	7.6-11.2	311/2303 (13.5)	12.2-15.0
	Bratislava - Podunajské Biskupice	76/236 (32.2)	26.6-38.4	28/130 (21.5)	15.3-29.4	104/366 (28.4)	24.0-33.2
	Jurský Šúr	84/258 (32.6)	27.1-38.5	74/319 (23.2)	18.9-28.1	158/577 (27.4)	23.9-31.2
	Košice	239/892 (26.8)	24.0-29.8	123/724 (17.0)	14.4-19.9	362/1616 (22.4)	20.4-24.5
	Trenčín	12/43 (27.9)	16.8-42.7	28/114 (24.6)	17.6-33.2	40/157 (25.5)	19.3-32.8
	Total	628/2715 (23.1)	21.6-24.8	347/2304 (15.1)	13.7-16.6	975/5019 (19.4)	18.4-20.5
Natural	Fúgelka	83/632 (13.1)	10.7-16.0	263/1619 (16.2)	14.5-18.1	346/2251 (15.4)	13.9-16.9
	Martinské hole	390/1057 (36.9)	34.0-39.9	148/828 (17.9)	15.4-20.6	538/1885 (28.5)	26.6-30.6
	Drienovec	67/249 (26.9)	21.8-32.7	169/667 (25.3)	22.2-28.8	236/916 (25.8)	23.0-28.7
	Zádiel	21/86 (24.4)	16.6-34.5	10/88 (11.4)	6.3-19.7	31/174 (17.8)	12.8-24.2
	Brzotín	10/34 (29.4)	16.8-46.2	14/70 (20.0)	12.3-30.8	24/104 (23.1)	16.0-32.1
	Total	571/2058 (27.7)	25.6-29.7	604/3272 (18.5)	17.2-19.8	1175/5330 (22.1)	21.0-23.2
Agricultural	Záhorská Ves	208/456 (45.6)	41.1-50.2	66/353 (18.7)	15.0-23.1	274/809 (33.9)	30.7-37.2
	Vrbovce	9/109 (8.3)	4.4-15.0	50/208 (24.0)	18.7-30.3	59/317 (18.6)	14.7-23.3
	Rozhanovce	43/286 (15.0)	11.4-19.6	140/1084 (12.9)	11.1-15.0	183/1370 (13.4)	11.7-15.3
	Total	260/851 (30.6)	27.6-33.7	256/1645 (15.6)	13.9-17.4	516/2496 (20.7)	19.1-22.3
Total		1691/6947 (24.3)	23.4-25.4	1557/10302 (15.1)	14.4-15.8	3248/17249 (18.8)	18.3-19.4

TABLE 2 List of *Ixodes* ticks molecularly identified to species (16S, TROSPA).

Study site	Year of ticks collection	Tick developmental stage/sex	No. of sequenced samples
Železná studnička	2017, 2018	5F	5
Malacky	2017, 2018	2N, 3F	5
Vrbovce	2017, 2018	2N, 1F, 2M	5
Martinské hole	2016	7F, 3M	10
Drienovec	2019	5L,11N**	16
Košice	2017, 2018	5N	5
Total		5L, 20N, 16F, 5M	46

L, larva; N, nymph; F, female; M, male; **bird-feeding ticks.

3.5 Changes in the infection prevalence and diversity of *B. burgdorferi* s.l. species during the monitored years

3.5.1 Železná studnička (suburban habitat, six years monitored)

The total infection prevalence was 13.5% (95% CI: 12.2-15.0). The lowest prevalence was recorded in 2013 (8.1%, 95% CI: 6.5-11.3) and in 2017 tick positivity increased (26.1%, 95% CI: 19.0-34.6). Differences in the prevalence of infected ticks were significant between study years ($t = 6.26$, $p < 0.05$). *Borrelia afzelii* predominated in all studied years except for 2013 when *B. valaisiana* and *B. garinii*/*B. bavariensis* dominated. *Borrelia lusitaniae* was recorded during three study years (2011, 2012, 2013), *B. burgdorferi* s.s. in 2012, 2013 and 2019 (Figure 3).

TABLE 3 Number of positive *Ixodes ricinus* ticks and prevalence of *B. burgdorferi* s.l. species at study sites in Slovakia.

Species / Study sites	*B. afzelii*	*B. garinii*/*B. bavariensis*	*B. burgdorferi* s.s.	*B. valaisiana*	*B. lusitaniae*	*B. spielmanii*	*B. bavariensis*	*mixed infections**	Total
BA-ŽS (%)	130 (43.9)	77 (26.0)	8 (2.7)	48 (16.2)	22 (7.4)	9 (3.0)	-	2 (0.7)	296
BA-HP (%)	18 (34.6)	17 (32.7)	4 (7.7)	10 (19.2)	1 (1.9)	2 (3.8)	-	0	52
BA-SAS (%)	40 (30.3)	32 (24.2)	10 (7.6)	23 (17.4)	13 (9.8)	13 (9.8)	-	1 (0.8)	132
BA-PB (%)	65 (62.5)	21 (20.2)	1 (1.0)	10 (9.6)	2 (1.9)	0	-	5 (4.8)	104
Záh. Ves (%)	128 (46.7)	30 (10.9)	8 (2.9)	63 (23.0)	25 (9.1)	0	-	20 (7.3)	274
Malacky (%)	225 (63.2)	64 (18.0)	10 (2.8)	38 (10.7)	3 (0.8)	13 (3.7)	3 (0.8)	19* (5.3)	375
Vrbovce (%)	29 (59.2)	8 (16.3)	0	6 (12.2)	2 (4.1)	0	-	4 (8.2)	49
Jurský Šúr (%)	13 (8.2)	66 (41.8)	0	59 (37.3)	1 (0.6)	1 (0.6)	-	18 (11.4)	158
Fúgelka (%)	120 (35.0)	146 (42.6)	9 (2.6)	44 (12.8)	14 (4.1)	2 (0.6)	1 (0.3)	7 (2.0)	343
Trenčín (%)	7 (17.5)	18 (45.0)	4 (10.0)	10 (25.0)	1 (2.5)	0	-	0	40
Mart. hole (%)	113 (21.5)	62 (11.8)	19 (3.6)	28 (5.3)	294 (55.9)	0	-	10 (1.9)	526
Košice (%)	83 (24.4)	140 (41.2)	41 (12.1)	50 (14.7)	1 (0.3)	1 (0.3)	-	24 (7.1)	340
Rozhanovce (%)	62 (36.3)	40 (23.4)	14 (8.2)	37 (21.6)	13 (7.6)	5 (2.9)	-	9** (3.5)	180
Zádiel (%)	4 (12.9)	2 (6.5)	2 (6.5)	14 (45.2)	2 (6.5)	5 (16.1)	-	2 (6.5)	31
Brzotín (%)	10 (47.6)	6 (28.6)	1 (4.8)	4 (19.0)	0	0	-		21
Drienovec (%)	126 (53.4)	49 (20.8)	0	42 (17.8)	5 (2.1)	0	-	14 (5.9)	236
Total (%)	1173	779	131	486	399	51	4	135	3158
Prevalence	37.1%	24.7%	4.1%	15.4%	12.6%	1.6%	0.1%	4.3%	

BA-PB, Bratislava - Podunajské Biskupice; BA-SAS, Bratislava – Slovak Academy of Sciences; BA-HP, Bratislava – Horský park; BA-ŽS, Bratislava – Železná studnička. *one tick infected with *B. bissettii*; **one tick infected with *B. kurtenbachii*.

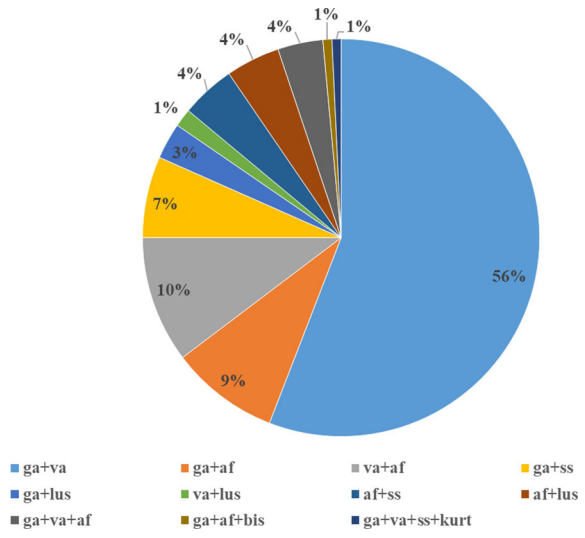

FIGURE 2
Borrelia burgdorferi s.l. species in mixed infections. ga - *B. garinii*, va - *B. valaisiana*, af - *B. afzelii*, ss - *B. burgdorferi* s.s., lus - *B. lusitaniae*, bis - *B. bissettii*, kurt - *B. kurtenbachii*.

3.5.2 Malacky (urban park, nine years monitored)

The total infection prevalence was 19.3% (95% CI: 17.6 – 21.0), whereas differences in the prevalence of infected ticks were significant between study years (t = 6.41, p < 0.05). The lowest prevalence of *Borrelia*-positive ticks was recorded in 2004 (5.1%, 95% CI: 3.6-7.1). *Borrelia afzelii* was dominant in all study years. *Borrelia garinii/B. bavariensis* was the second most frequent species during the years 1999, 2008, 2017, and 2019. *Borrelia valaisiana* had a higher representation only in 2001-2002 and 2004. *Borrelia lusitaniae* was detected only in samples collected in 2007. *Borrelia burgdorferi* s.s. and *B. spielmanii* were detected in a low percentage in several years. At this site, *B. bavariensis* was confirmed in three ticks (2017, 2018, 2019) (Figure 4).

3.5.3 Martinské hole (natural habitat, 11 years monitored)

Prevalence of infected ticks fluctuated between study years (14.7%, 95% CI: 9.9-21.2; 46.1%, 95% CI: 38.9-53.4). The total infection prevalence was 28.5% (95% CI: 26.6-30.6). Differences in the prevalence of infected ticks were significant between study years (t = 8.56, p < 0.05). *Borrelia lusitaniae* clearly dominated in six years (2004, 2006-2007, 2009, 2010-2011). From 2013 the proportion of ticks infected with this species gradually decreased. *Borrelia burgdorferi* s.s. was detected in a small number of ticks during the monitored period with the exception of the last two years. *Borrelia garinii/B. bavariensis* predominated in 2017-2019. *Borrelia valaisiana* was recorded in a low percentage during all study years with the exception of 2008 (Figure 5).

3.5.4 Drienovská mokrad̆ (natural habitat, five years monitored)

The total infection prevalence was 25.8% (95% CI: 23.0-28.7). Differences in the prevalence of infected ticks were not significant between the study years (t = 14.63, p < 0.05). *Borrelia afzelii* was the dominant species in four years (2013, 2017-2019), followed by *B. garinii/B. bavariensis* and *B. valaisiana* which were dominant in 2002. *Borrelia lusitaniae* was found only in 2019 (Figure 6).

3.5.5 Rozhanovce (agricultural habitat, six years monitored)

The total infection prevalence was 13.4% (95% CI: 11.7-15.3). Differences in the prevalence of infected ticks were significant between study years (t = 5.17, p < 0.05). The most frequent species were *B. afzelii* (2007, 2008, 2011, 2012), *B. garinii/B. bavariensis* (predominant in 2013) and *B. valaisiana* (2007).

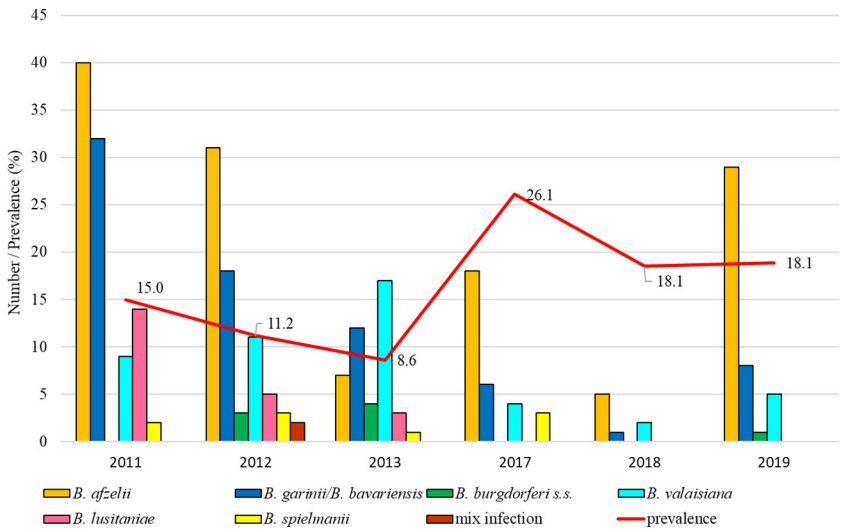

FIGURE 3
Total infection prevalence and representation of *B. burgdorferi* s.l. species in Bratislava - Železná studnička.

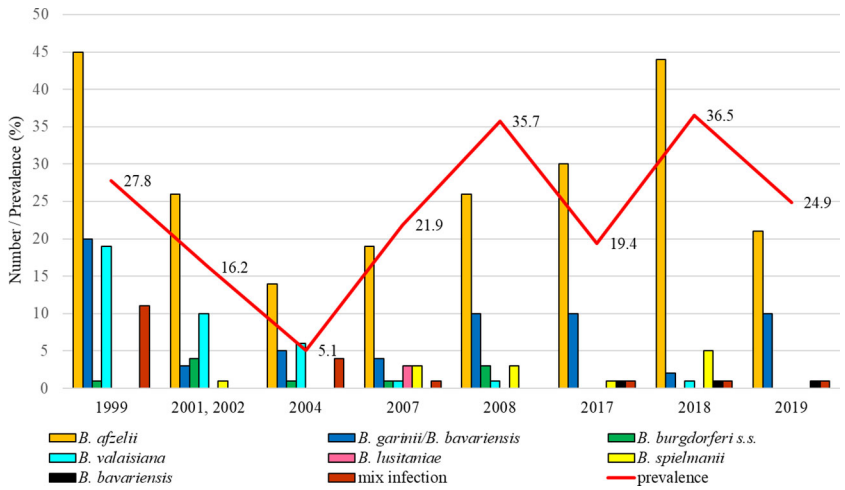

FIGURE 4
Total infection prevalence and representation of *B. burgdorferi* s.l. species in Malacky.

Borrelia burgdorferi s.s. was detected in 2007, 2011, 2012 (with evident increase) and 2013 (Figure 7).

3.5.6 Košice (suburban habitat, nine years monitored)

Total infection prevalence was 22.4% (95% CI: 20.4-24.5). Differences in the prevalence of infected ticks were significant between study years ($t = 7.51$, $p < 0.05$). The lowest proportion of *Borrelia*-positive ticks was recorded in 2003 (13.1%, 95% CI: 9.3-18.3). From this year the infection prevalence was increasing up to 37.2% (95% CI: 28.8-46.4) in 2018. In the first studied year *B. burgdorferi* s.s. predominated (31.7%) and *B. garinii/B. bavariensis* was the most frequent in 2003, 2004, 2005 and 2017. *Borrelia afzelii* dominated in 2013 and 2018. *Borrelia valaisiana* was recorded in all years with the exception of 2003 and 2004 (Figure 8).

3.6 Prevalence of *Borrelia burgdorferi* s.l. in ticks from four habitat types

The total prevalence differed significantly among four habitat types (Table 1) ($t = 9.66$, $p < 0.05$). The highest prevalence was confirmed in the natural habitat (22.0%), the lowest in the urban habitat (13.2%).

Borrelia afzelii predominated in all habitats, but had the highest affinity to urban and agricultural habitats. *Borrelia valaisiana* and *B.*

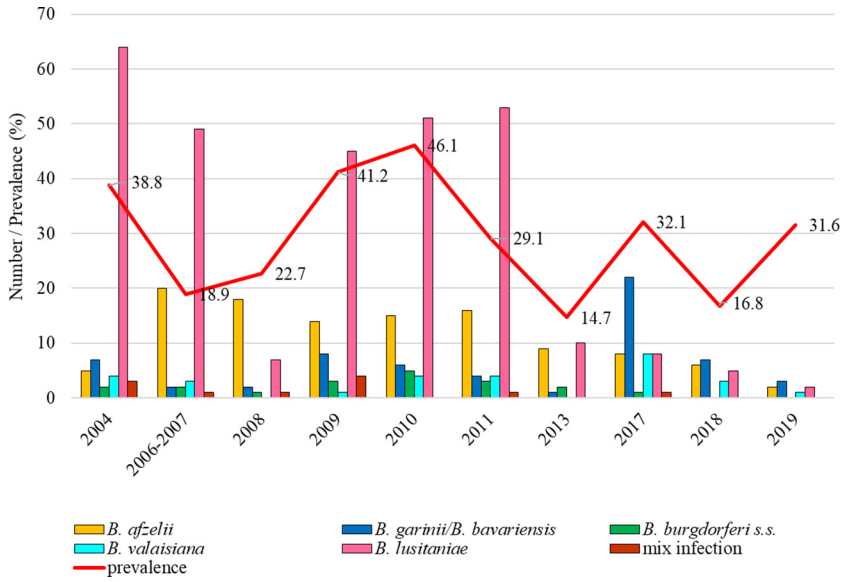

FIGURE 5
Total infection prevalence and representation of *B. burgdorferi* s.l. species in Martinské hole.

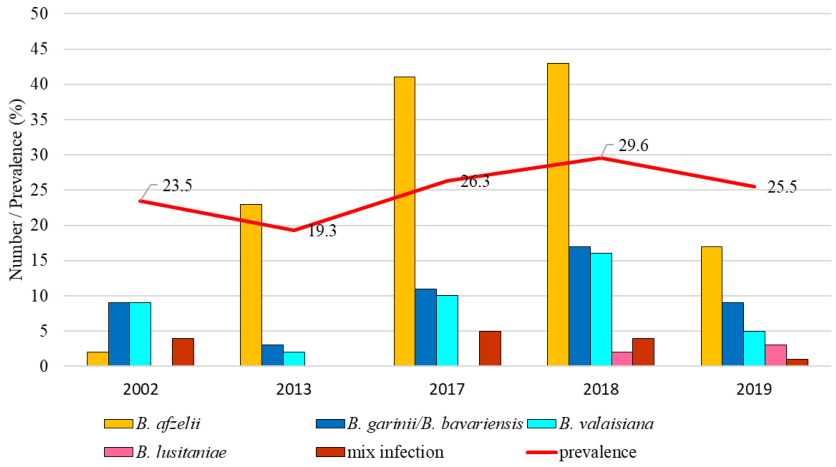

FIGURE 6
Total infection prevalence and representation of *B. burgdorferi* s.l. species in Drienovská mokraď.

garinii/*B. bavariensis* were the most frequent species (33.0%) at suburban sites, which was also confirmed by PCA analysis (Table 4; Figure 9). *Borrelia lusitaniae* was positively associated with the natural habitat. However, it is not possible to draw definitive conclusions based on the PCA analysis in case of *B. burgdorferi* s.s. and *B. spielmanii*. To confirm the correlation, it is necessary to obtain more samples of both agents.

4 Discussion

4.1 *Ixodes ricinus/Ixodes inopinatus*

Some studies indicate the presence of *I. inopinatus* ticks not only in dry Mediterranean regions, but also at sites in Central Europe (CE) (Chitimia-Dobler et al., 2018; Toma et al., 2021). Its occurrence was recorded in several regions of Germany (Chitimia-Dobler et al., 2017; Hauck et al., 2019), sympatric occurrence with *I. ricinus* in Romania, in western Austria and southeastern Germany (Chitimia-Dobler et al., 2018). Natural hosts include foxes, sheep and lizards (Estrada-Peña et al., 2014; Chitimia-Dobler et al., 2018). The species was recently recorded on migratory birds (Toma et al., 2021). On the other hand, the situation with regards to the presence of this tick species in CE is complicated (Kahl and Gray, 2023) and some studies suggest that it does not occur in CE (Rollins et al., 2023). Published data about *I. inopinatus* described by Estrada-Peña et al. (2014) raise the question of whether this species also occurs in Slovakia. Based on published data, we sequenced randomly selected samples of ticks that were morphologically determined as *I. ricinus*. Our preliminary analyses have not confirmed the presence of *I. inopinatus* in Slovakia.

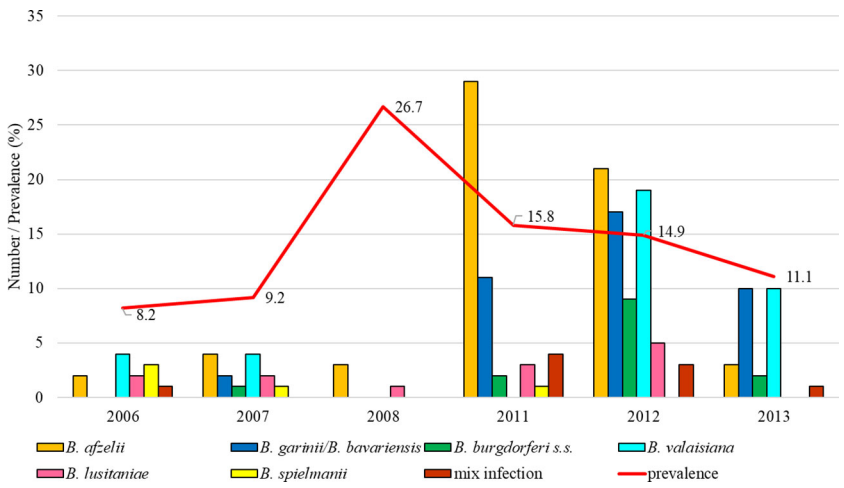

FIGURE 7
Total infection prevalence and representation of *B. burgdorferi* s.l. species in Rozhanovce.

10.3389/fcimb.2024.1496925

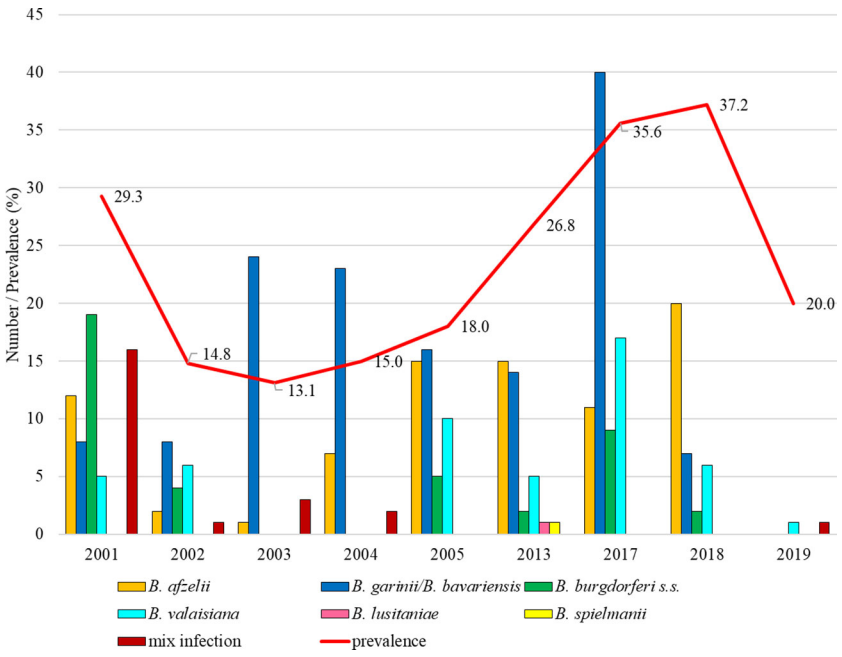

FIGURE 8
Total infection prevalence an representation of *B. burgdorferi* s.l. species in Košice.

4.2 *Borrelia burgdorferi* s.l.

Borrelia burgdorferi s.l. complex is the subject of many epidemiological studies in Europe (Rauter and Hartung, 2005; Strnad et al., 2017; Estrada-Peña et al., 2018). Global warming and climate change in Central Europe (CE) has an impact on the geographic distribution and seasonal activity of ticks and pathogens they carry as well as on the occurrence and population density of their hosts (Lindgren et al., 2000; Nuttall, 2022).

Long-term studies on the prevalence of *B. burgdorferi* s.l. are rare although monitoring of changes in the prevalence and species diversity at the same sites can provide precious information on the impact of global changes on ticks and tick-borne pathogens. In the present study, we summarised data on the infection prevalence and distribution of species of the *B. burgdorferi* s.l. complex in questing *I. ricinus* ticks from 16 study sites in Slovakia and from over 20 years (1999-2019). The large package of data shows considerable spatial variability within the *B. burgdorferi* s.l. complex even in such

TABLE 4 Number of positive *Ixodes ricinus* ticks and prevalence of *B. burgdorferi* s.l. species in urban/suburban/natural/agricultural habitats.

Habitat	No. of positive/tested ticks (%)	*B. afzelii* (%)	*B. garinii*/*B. bavariensis* (%)	*B. valaisiana* (%)	*B. lusitaniae* (%)	*B. spielmanii* (%)	*B. burgdorferi* s.s. (%)
Urban	582/4404 (13.2)	283 (48.6)	113 (19.4)	71 (12.2)	17 (2.9)	28 (4.8)	24 (4.1)
Suburban	975/5019 (19.4)	298 (30.6)	322 (33.0)	177 (18.2)	27 (2.8)	11 (1.1)	54 (5.5)
Natural	1175/5330 (22.0)	343 (29.2)	266 (22.6)	132 (11.2)	315 (26.8)	7 (0.6)	31 (2.6)
Agricultural	516/2496 (20.7)	219 (42.4)	78 (15.1)	106 (20.5)	40 (7.8)	5 (1.0)	22 (4.3)

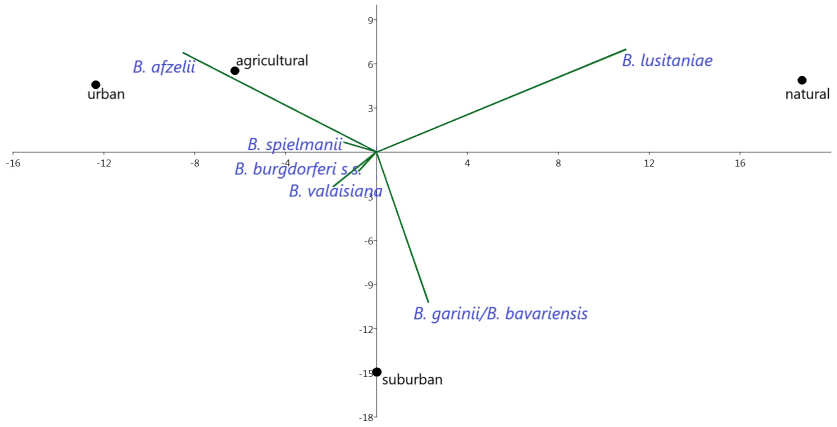

FIGURE 9
Correlations between prevalence of *B. burgdorferi* s.l. species and habitat types.

a small geographic area as Slovakia. In addition, marked temporal differences in the prevalence of infected ticks were observed at the same localities. These results are consistent with other European studies on spatial and temporal changes in *Borrelia* prevalence (e.g. Hönig et al., 2015; Okeyo et al., 2020; Hartemink et al., 2021; Medlock et al., 2022; Glass et al., 2023).

The abundance of *I. ricinus* is influenced by many factors and varies depending on the month/time of collection, as well as on changes that occur at individual sites over the years (for example, clearing of dense undergrowth in city parks, mowing of grassy areas etc.). Usually, nymphs are spread more uniformly than adult ticks and larvae (Gray et al., 2021). The relative abundance of questing *I. ricinus* nymphs in a three-year study from five selected central European countries was found to be associated with climatic conditions, but mainly with the Normalized Difference Vegetation Index, and did not significantly depend on land use categories (Rosà et al., 2018). In Slovakia, the highest density of nymphs was found in green urban sites, whereas by summarizing data from all studied countries and habitat types (urban, suburban, natural, agricultural), density of nymphs was highest in the natural habitats (Rosà et al., 2018). In our analysed datasets, nymphs were more abundant at ten study sites whereas adult ticks prevailed at five study sites. We recorded a higher overall infection prevalence of *B. burgdorferi* s.l. (18.8%) compared to the meta-analyses for Central Europe: 13.7% (Rauter and Hartung, 2005) and 12.3% (Strnad et al., 2017). The prevalence of *Borrelia*-infected nymphs (15.1%) in Slovakia was higher than 10.1% and 11.8% in the datasets from 1984-2003 (Rauter and Hartung, 2005) and from 2010-2016 (Strnad et al., 2017), respectively. The situation was similar for adult ticks with 24.3% positive ticks in 1999-2019 (our study) in contrast to previous studies - 18.6% (Rauter and Hartung, 2005) and 14.9% (Strnad et al., 2017). In contrast, the overall *Borrelia* prevalence in nymphs based on data from Slovakia, Germany and Italy for 2011-2013 was 19.3% (Rosà et al., 2018).

In our study, the lowest infection prevalence was recorded in urban areas (13.2%) while in a long-term study from the city of Hanover (Germany) the prevalence of infected ticks was as high as 25.5% (Glass et al., 2023). In comparison with urban sites of Slovakia, higher *Borrelia* prevalence was recorded in suburban, natural and agricultural sites which have more diverse vertebrate hosts composition (Rizzoli et al., 2014; Kazimírová et al., 2023). Spatial and temporal changes in the borrelial prevalence even within small geographical areas were reported from Slovakia, e.g., by Pangrácová et al. (2013) and Kazimírová et al. (2023). Depending on the location and habitat type, prevalence of infected ticks ranged from 1.0% to 27.8% (nymphs) and from 0% to 49.4% (adults). Total prevalence was found to range between 0% and 38.3% in urban/suburban sites, between 8.0% and 29.4% in natural sites and between 32.3% and 38.1% in agricultural sites and ecotones (see Kazimírová et al., 2023).

The distribution of *B. burgdorferi* s.l. species in a site depends on the presence of appropriate reservoir hosts (Wolcott et al., 2021; Steinbrink et al., 2022; Estrada-Peña et al., 2024). In total, nine species were identified in our study. *Borrelia afzelii*, *B. garinii*/*bavariensis* and *B. valaisiana* were the most frequent and were confirmed at all study sites. These results are consistent with data from other European studies (Strnad et al., 2017; Mysterud et al., 2019). In the suburban habitat, bird-associated species (*B. garinii* and *B. valaisiana*) prevailed, which may be related to the high number of songbirds in urban forest parks. *Borrelia lusitaniae* was confirmed in 12.8% positive samples from Slovakia, which is a higher proportion than 7% in the study of Strnad et al. (2017). This was caused by a high proportion of *B. lusitaniae*-positive ticks (73.7%) from a natural focus in a mountain region in Slovakia, Martinské hole Mts., that is not typical of Central Europe (Rusňáková Tarageľová et al., 2016). According to our results, this species has an affinity to the natural habitat, but the results are skewed by high number of *B. lusitaniae*-positive ticks from one study site only. By our previous methodology, identification of *B. bavariensis* was not possible, but we assume that confirmed infections with *B. garinii* might have included this species. The presence of *B. bavariensis* was confirmed in Slovakia by Hamšíková

et al. (2017) and in a former study as the *B. garinii* ospA serotype 4 (Lenčáková et al., 2006). The rare species *B. bissettii* and *B. kurtenbachii* have been detected in Slovakia only once, and in coinfections with other *Borrelia* species (Hanincová et al., 2003b; Kazimírová et al., 2023).

Global changes are affecting all components of the natural foci of tick-borne diseases (Gray et al., 2009). Changes in the diversity of *Borrelia* species at the monitored sites in Slovakia were probably due to the influence of several factors:

a. spectrum and/or abundance of competent reservoir hosts for *B. burgdorferi* s.l.;
b. changes in the environment (natural and/or due to human activities);
c. various methodologies for the detection of *B. burgdorferi* s.l.;
d. unequal numbers of collected ticks in individual years and study sites.

As *B. afzelii* is associated with rodents, increasing/decreasing of the prevalence of this species may be driven by natural fluctuations in rodent population densities (Glass et al., 2023) as well as by changes in the species composition of the rodent communities. For example, high population densities of the common vole (*Microtus arvalis*), the major reservoir host for *B. afzelii* (Radzijevskaja et al., 2013), were registered Europe-wide (Jacob et al., 2020; Heroldová et al., 2021), and the striped field mouse (*Apodemus agrarius*) is currently expanding its range (Tulis et al., 2023). In years with low population densities of rodents, song birds being reservoirs of *B. garinii* and *B. valaisiana* may become the major feeding hosts and sources of infection for *I. ricinus*, especially in urban and suburban areas (Rizzoli et al., 2014). *Borrelia lusitaniae* dominated at Martinské hole until 2013, but since then its prevalence has been decreasing. At this location, a large area of the forest was destroyed, so the composition of tick hosts has probably changed.

5 Conclusions

The analysis of a large dataset of *B. burgdorferi* s.l. infections in questing *I. ricinus* nymphs and adults collected during over 20 years from a number of sites representing different habitat types of Slovakia revealed (1) the presence of infected ticks in all explored sites, (2) spatial and temporal differences in the prevalence of infections and in the diversity of *Borrelia* species. Nine species were found to occur, with *B. afzelii* and *B. garinii* prevailing. Presence of human-pathogenic *Borrelia* species was confirmed in all studied sites. Depending on the site, these comprised *B. afzelii* and *B. garinii, B. burgdorferi* s.s, *B. bavariensis* and *B. spielmanii*. Urban/suburban green areas and parks have been identified as foci for circulation of pathogenic *Borrelia* species and represent areas with high epidemiological risk. Long-term monitoring of the presence and prevalence of *Borrelia* infections in ticks is needed to unravel new foci of the pathogens and confirm the maintenance of existing foci in a changing environment.

Data availability statement

The original contributions presented in the study are included in the article/Supplementary Material. Further data are publicly available and can be found here: https://doi.org/10.6084/m9.figshare.27967431.v1. Further inquiries can be directed to the corresponding author.

Ethics statement

The manuscript presents research on animals that do not require ethical approval for their study.

Author contributions

VR: Conceptualization, Data curation, Funding acquisition, Investigation, Methodology, Project administration, Resources, Validation, Writing – original draft, Writing – review & editing. MD: Conceptualization, Data curation, Funding acquisition, Investigation, Methodology, Supervision, Validation, Writing – review & editing. DS: Funding acquisition, Investigation, Methodology, Validation, Writing – review & editing. MC: Formal analysis, Investigation, Methodology, Writing – review & editing. BM: Formal Analysis, Investigation, Methodology, Visualization, Writing – review & editing. YD: Investigation, Methodology, Writing – review & editing. JK: Investigation, Methodology, Writing – review & editing. SK: Methodology, Writing – review & editing. BV: Writing – review & editing. BP: Methodology, Writing – review & editing. MS: Methodology, Writing – review & editing. MK: Conceptualization, Funding acquisition, Methodology, Resources, Validation, Writing – original draft, Writing – review & editing.

Funding

The author(s) declare that financial support was received for the research, authorship, and/or publication of this article. This study was financially supported by the Scientific Grant Agency of Ministry of Education and SAS, by the projects VEGA no. 2/0137/21, no. 2/0004/22 and Slovak Research and Development Agency of the Ministry of Education, Science, Research and Sport of the Slovak Republic APVV-22-0372.

Acknowledgments

We thank Klára Hanincová, Tatiana Košťálová, Lenka Mahríková, Elena Ondrisková, Ivana Cíglerová, Katarína Cabadajová, Zuzana Čužiová, Tatiana Mikušová, Jasna Kraljik, Zuzana Hamšíková, Lucia Blaňarová, Renáta Ivanová, and Radovan Václav, for the tick collections and laboratory work.

Conflict of interest

The authors declare that the research was conducted in the absence of any commercial or financial relationships that could be construed as a potential conflict of interest.

Publisher's note

All claims expressed in this article are solely those of the authors and do not necessarily represent those of their affiliated organizations, or those of the publisher, the editors and the reviewers. Any product that may be evaluated in this article, or claim that may be made by its manufacturer, is not guaranteed or endorsed by the publisher.

Supplementary material

The Supplementary Material for this article can be found online at: https://www.frontiersin.org/articles/10.3389/fcimb.2024.1496925/full#supplementary-material

References

Altschul, S. F., Gish, W., Miller, W., Myers, E. W., and Lipman, D. J. (1990). Basic local alignment search tool. *J. Mol. Biol.* 215, 403–410. doi: 10.1016/S0022-2836(05)80360-2

Black, W. C., and Roehrdanz, R. L. (1998). Mitochondrial gene order is not conserved in arthropods: Prostriate and metastriate tick mitochondrial genomes. *Mol. Biol. Evol.* 15, 1772–1785. doi: 10.1093/oxfordjournals.molbev.a025903

Brown, L. D., Cai, T. T., and DasGupta, A. (2001). Interval estimation for a binomial proportion. *Stat. Sci.* 16, 101–133. doi: 10.1214/ss/1009213286

Chitimia-Dobler, L., Bestehorn, M., Bröker, M., Borde, J., Molcanyi, T., Andersen, N. S., et al. (2017). Morphological anomalies in *Ixodes ricinus* and *Ixodes inopinatus* collected from tick-borne encephalitis natural foci in Central Europe. *Exp. Appl. Acarol.* 72, 379–397. doi: 10.1007/s10493-017-0163-5

Chitimia-Dobler, L., Rieß, R., Kahl, O., Wölfel, S., Dobler, G., Nava, S., et al. (2018). *Ixodes inopinatus* – occurring also outside the Mediterranean region. *Ticks Tick Borne Dis.* 9, 196–200. doi: 10.1016/j.ttbdis.2017.09.004

Chvostáč, M., Špitalská, E., Václav, R., Vaculová, T., Minichová, L., and Derdáková, M. (2018). Seasonal patterns in the prevalence and diversity of tick-borne *Borrelia burgdorferi* sensu lato, *Anaplasma phagocytophilum* and *Rickettsia* spp. in an urban temperate forest in South Western Slovakia. *Int. J. Environ. Res. Public Health* 15, 994. doi: 10.3390/ijerph15050994

Derdáková, M., Beati, L., Peťko, B., Stanko, M., and Fish, D. (2003). Genetic variability within *Borrelia burgdorferi* sensu lato genospecies established by PCR-single-strand conformation polymorphism analysis of the rrfA-rrlB intergenic spacer in *Ixodes ricinus* ticks from the Czech Republic. *Appl. Environ. Microbiol.* 69, 509–516. doi: 10.1128/AEM.69.1.509-516.2003

Durden, L. A. (2006). "Taxonomy, host associations, life cycles and vectorial importance of ticks parasitizing small mammals," in *Micromammals and Macroparasites. From Evolutionary Ecology to Management*. Eds. S. Morand, B. R. Krasnov and R. Poulin (Springer Verlag, Tokyo), 91–102.

Estrada-Peña, A., Cutler, S., Potkonjak, A., Vassier-Tussaut, M., Van Bortel, W., Zeller, H., et al. (2018). An updated meta-analysis of the distribution and prevalence of *Borrelia burgdorferi* s.l. in ticks in Europe. *Int. J. Health Geogr.* 17, 41. doi: 10.1186/s12942-018-0163-7

Estrada-Peña, A., Nava, S., and Petney, T. (2014). Description of all the stages of *Ixodes inopinatus* n. sp. (Acari: Ixodidae). *Ticks Tick Borne Dis.* 5, 734–743. doi: 10.1016/j.ttbdis.2014.05.003

Estrada-Peña, A., Sprong, H., and Wijburg, S. R. (2024). A crucial nexus: Phylogenetic *versus* ecological support of the life-cycle of *Ixodes ricinus* (Ixodoidea: Ixodidae) and Borrelia spp. amplification. *Curr. Res. Parasitol. Vector Borne Dis.* 6, 100198. doi: 10.1016/j.crpvbd.2024.100198

Gern, L., Hu, C. M., Kocianová, E., Výrosteková, V., and Řeháček, J. (1999). Genetic diversity of *Borrelia burgdorferi* sensu lato isolates obtained from *Ixodes ricinus* ticks collected in Slovakia. *Eur. J. Epidemiol.* 15, 665–669. doi: 10.1023/a:1007660430664

Glass, A., Springer, A., Raulf, M. K., Fingerle, V., and Strube, C. (2023). 15-year *Borrelia* prevalence and species distribution monitoring in *Ixodes ricinus*/*inopinatus* populations in the city of Hanover, Germany. *Ticks Tick Borne Dis.* 14, 102074. doi: 10.1016/j.ttbdis.2022.102074

Gray, J. S., Dautel, H., Estrada-Peña, A., Kahl, O., and Lindgren, E. (2009). Effects of climate change on ticks and tick-borne diseases in europe. *Interdiscip. Perspect. Infect. Dis.* 2009, 593232. doi: 10.1155/2009/593232

Gray, J., Kahl, O., and Zintl, A. (2021). What do we still need to know about *Ixodes ricinus*? *Ticks Tick Borne Dis.* 12, 101682. doi: 10.1016/j.ttbdis.2021.101682

Guy, E. C., and Stanek, G. (1991). Detection of *Borrelia burgdorferi* in patients with Lyme disease by the polymerase chain-reaction. *J. Clin. Pathol.* 44, 610–611. doi: 10.1136/jcp.44.7.610

Hammer, Ø., Harper, D. A. T., and Ryan, P. D. (2001). PAST: paleontological statistics software package for education and data analysis. *Palaeontol. Electron.* 4, 9. Available at: http://palaeo-electronica.org/2001_1/past/issue1_01.htm.

Hamšíková, Z., Coipan, C., Mahríková, L., Minichová, L., Sprong, H., and Kazimírová, M. (2017). *Borrelia miyamotoi* and co-infection with *Borrelia afzelii* in *Ixodes ricinus* ticks and rodents from Slovakia. *Microb. Ecol.* 73, 1000–1008. doi: 10.1007/s00248-016-0918-2

Hanincová, K., Schäfer, S. M., Etti, S., Sewell, H. S., Tarageľová, V., Žiak, D., et al. (2003a). Association of *Borrelia afzelii* with rodents in Europe. *Parasitology* 126, 11–20. doi: 10.1017/s0031182002002548

Hanincová, K., Tarageľová, V., Koči, J., Schäfer, S. M., Hails, R., Ullmann, A. J., et al. (2003b). Association of *Borrelia garinii* and *B. valaisiana* with songbirds in Slovakia. *Appl. Environ. Microbiol.* 69, 2825–2830. doi: 10.1128/AEM.69.5.2825-2830.2003

Hartemink, N., van Vliet, A. J. H., Gort, G., Gassner, F., Jacobs, F., Fonville, M., et al. (2021). Seasonal patterns and spatial variation of *Borrelia burgdorferi* (*sensu lato*) infections in *Ixodes ricinus* in the Netherlands. *Parasitol. Vectors.* 14, 121. doi: 10.1186/s13071-021-04607-7

Hauck, D., Springer, A., Pachnicke, S., Schunack, B., Fingerle, V., and Strube, C. (2019). *Ixodes inopinatus* in northern Germany: occurrence and potential vector role for *Borrelia* spp., *Rickettsia* spp., and *Anaplasma phagocytophilum* in comparison with *Ixodes ricinus*. *Parasitol. Res.* 118, 3205–3216. doi: 10.1007/s00436-019-06506-4

Heroldová, M., Sipos, J., Suchomel, J., and Zejda, J. (2021). Influence of crop type on common vole abundance in Central European agroecosystems. *Agric. Ecosyst. Environ.* 315, 107443. doi: 10.1016/j.agee.2021.107443

Hönig, V., Svec, P., Halas, P., Vavruskova, Z., Tykalova, H., Kilian, P., et al. (2015). Ticks and tick-borne pathogens in South Bohemia (Czech Republic)–spatial variability in *Ixodes ricinus* abundance, *Borrelia burgdorferi* and tick-borne encephalitis virus prevalence. *Ticks Tick Borne Dis.* 6, 559–567. doi: 10.1016/j.ttbdis.2015.04.010

Hubálek, Z., and Halouzka, J. (1997). Distribution of *Borrelia burgdorferi* sensu lato genomic groups in Europe, a review. *Eur. J. Epidemiol.* 13, 951–957. doi: 10.1023/a:1007426304900

Humair, P., and Gern, L. (2000). The wild hidden face of Lyme borreliosis in Europe. *Microbes Infect.* 2, 915–922. doi: 10.1016/s1286-4579(00)00393-2

Jacob, J., Imholt, C., Caminero-Saldaña, C., Couval, G., Giraudoux, P., Herrero-Cófreces, S., et al. (2020). Europe-wide outbreaks of common voles in 2019. *J. Pest Sci.* 93, 703–709. doi: 10.1007/s10340-020-01200-2

Kahl, O., and Gray, J. S. (2023). The biology of *Ixodes ricinus* with emphasis on its ecology. *Ticks Tick Borne Dis.* 14, 102114. doi: 10.1016/j.ttbdis.2022.102114

Kazimírová, M., Mahríková, L., Hamšíková, Z., Stanko, M., Golovchenko, M., and Rudenko, N. (2023). Spatial and temporal variability in prevalence rates of members of the *Borrelia burgdorferi* species complex in *Ixodes ricinus* ticks in urban, agricultural and sylvatic habitats in Slovakia. *Microorganisms.* 11, 1666. doi: 10.3390/microorganisms11071666

Lenčáková, D., Hizo-Teufel, C., Peťko, B., Schulte-Spechtel, U., Stanko, M., Wilske, B., et al. (2006). Prevalence of *Borrelia burgdorferi* s.l. OspA types in *Ixodes ricinus* ticks from selected localities in Slovakia and Poland. *Int. J. Med. Microbiol.* 296 Suppl 40, 108–118. doi: 10.1016/j.ijmm.2005.12.012

Lindgren, E., and Jaenson, T. G. T. (2006). *Lyme borreliosis in Europe: Influences of Climate and Climate Change, Epidemiology, Ecology and Adaptation Measures* (Copenhagen: World Health Organization).

Lindgren, E., Tälleklint, L., and Polfeldt, T. (2000). Impact of climatic change on the northern latitude limit and population density of the disease transmitting European tick *Ixodes ricinus*. *Environ. Health Perspect.* 108, 119–123. doi: 10.1289/ehp.00108119

Mangold, A. J., Bargues, M. D., and Mas-Coma, S. (1998). Mitochondrial 16S rDNA sequences and phylogenetic relationships of species of *Rhipicephalus* and other tick

genera among Metastriata (Acari: Ixodidae). *Parasitol. Res.* 84, 478–484. doi: 10.1007/s004360050433

Margos, G., Fingerle, V., and Reynolds, S. (2019). *Borrelia bavariensis*: vector switch, niche invasion, and geographical spread of a tick-borne bacterial parasite. *Front. Ecol. Evol.* 7. doi: 10.3389/fevo.2019.00401

Margos, G., Gatewood, A. G., Aanensen, D. M., Hanincová, K., Terekhova, D., Vollmer, S. A., et al. (2008). MLST of housekeeping genes captures geographic population structure and suggests a European origin of *Borrelia burgdorferi*. *Proc. Natl. Acad. Sci. U.S.A.* 105, 8730–8735. doi: 10.1073/pnas.0800323105

Medlock, J. M., Vaux, A. G. C., Gandy, S., Cull, B., McGinley, L., Gillingham, E., et al. (2022). Spatial and temporal heterogeneity of the density of *Borrelia burgdorferi*-infected *Ixodes ricinus* ticks across a landscape: A 5-year study in southern England. *Med. Vet. Entomol.* 36, 356–370. doi: 10.1111/mve.12574

Mtierová, Z., Derdáková, M., Chvostáč, M., Didyk, Y. M., Mangová, B., Rusňáková Tarageľová, V., et al. (2020). Local population structure and seasonal variability of *Borrelia garinii* genotypes in *Ixodes ricinus* ticks, Slovakia. *Int. J. Environ. Res. Public Health* 17, 3607. doi: 10.3390/ijerph17103607

Mysterud, A., Stigum, V. M., Jaarsma, R. I., and Sprong, H. (2019). Genospecies of *Borrelia burgdorferi* sensu lato detected in 16 mammal species and questing ticks from northern Europe. *Sci. Rep.* 9, 5088. doi: 10.1038/s41598-019-41686-0

Norte, A. C., Boyer, P. H., Castillo-Ramirez, S., Chvostáč, M., Brahami, M. O., Rollins, R. E., et al. (2021). The population structure of *Borrelia lusitaniae* is reflected by a population division of its *Ixodes* vector. *Microorganisms.* 9, 933. doi: 10.3390/microorganisms9050933

Nosek, J., and Sixl, W. (1972). Central-European ticks (Ixodoidea). Key for determination. *Mitt. Abt. Zool.* 1, 61–92. Landesmus. Joanneum.

Noureddine, R., Chauvin, A., and Plantard, O. (2011). Lack of genetic structure among Eurasian populations of the tick *Ixodes ricinus* contrasts with marked divergence from north-African populations. *Int. J. Parasitol.* 41, 183–192. doi: 10.1016/j.ijpara.2010.08.010

Nuttall, P. A. (2022). Climate change impacts on ticks and tick-borne infections. *Biologia* 77, 1503–1512. doi: 10.1007/s11756-021-00927-2

Okeyo, M., Hepner, S., Rollins, R. E., Hartberger, C., Straubinger, R. K., Marosevic, D., et al. (2020). Longitudinal study of prevalence and spatio-temporal distribution of *Borrelia burgdorferi* sensu lato in ticks from three defined habitats in Latvia 1999–2010. *Environ. Microbiol.* 22, 5033–5047. doi: 10.1111/1462-2920.15100

Pangrácová, L., Derdáková, M., Pekárik, L., Hviščová, I., Víchová, B., Stanko, M., et al. (2013). *Ixodes ricinus* abundance and its infection with the tick-borne pathogens in urban and suburban areas of Eastern Slovakia. *Parasitol. Vectors* 6, 238. doi: 10.1186/1756-3305-6-238

Poli, P., Lenoir, J., Plantard, O., Ehrmann, S., Røed, K. H., Leinaas, H. P., et al. (2020). Strong genetic structure among populations of the tick *Ixodes ricinus* across its range. *Ticks Tick Borne Dis.* 11, 101509. doi: 10.1016/j.ttbdis.2020.101509

Radzijevskaja, J., Paulauskas, A., Rosef, O., Petkevicius, S., Mazeika, V., and Rekasius, T. (2013). The propensity of voles and mice to transmit *Borrelia burgdorferi* sensu lato infection to feeding ticks. *Vet. Parasitol.* 197, 318–325. doi: 10.1016/j.vetpar.2013.06.008

Rauter, C., and Hartung, T. (2005). Prevalence of *Borrelia burgdorferi* sensu lato genospecies in *Ixodes ricinus* ticks in Europe: a metaanalysis. *Appl. Environ. Microbiol.* 71, 7203–7216. doi: 10.1128/AEM.71.11.7203-7216.2005

Rijpkema, S. G. T., Molkenboer, M. J. C. H., Schouls, L. M., Jongejan, F., and Schellekens, J. F. P. (1995). Simultaneous detection and genotyping of three genomic groups of *Borrelia burgdorferi* sensu lato in Dutch *Ixodes ricinus* ticks by characterization of the amplified intergenic spacer region between 5S and 23S ribosomal RNA genes. *J. Clin. Microbiol.* 33, 3091–3095. doi: 10.1128/jcm.33.12.3091-3095.1995

Rizzoli, A., Silaghi, C., Obiegala, A., Rudolf, I., Hubálek, Z., Földvári, G., et al. (2014). *Ixodes ricinus* and its transmitted pathogens in urban and peri-urban areas in Europe: New hazards and relevance for public health. *Front. Publ. Health* 2. doi: 10.3389/fpubh.2014.00251

Rollins, E., Margos, G., Brachmann, A., Krebs, S., Mouchet, A., Dingemanse, N. J., et al. (2023). German *Ixodes inopinatus* samples may not actually represent this tick species. *Int. J. Parasitol.* 53, 751–761. doi: 10.1016/j.ijpara.2023.06.007

Rosà, R., Andreo, V., Tagliapietra, V., Baráková, I., Arnoldi, D., Hauffe, H. C., et al. (2018). Effect of climate and land use on the spatio-temporal variability of tick-borne bacteria in Europe. *Int. J. Environ. Res. Publ. Health* 15, 732. doi: 10.3390/ijerph15040732

Rusňáková Tarageľová, V., Mahríková, L., Selyemová, D., Václav, R., and Derdáková, M. (2016). Natural foci of *Borrelia lusitaniae* in a mountain region of Central Europe. *Ticks Tick Borne Dis.* 7, 350–356. doi: 10.1016/j.ttbdis.2015.12.006

Sergeant, E. S. G. (2018). *Epitools Epidemiological Calculators* (Ausvet). Available at: http://epitools.ausvet.com.au.

Slovák, M. (2010). Pictorial key to the adults of ticks (Acari: Ixodida) of the Slovakia fauna. *Entomofauna carpathica* 22, 8–13.

Stanek, G., Wormser, G. P., Gray, J., and Strle, F. (2012). Lyme borreliosis. *Lancet* 379, 461–473. doi: 10.1016/S0140-6736(11)60103-7

Stanko, M., Derdáková, M., Špitalská, E., and Kazimírová, M. (2022). Ticks and their epidemiological role in Slovakia: from the past till present. *Biologia.* 77, 1575–1610. doi: 10.1007/s11756-021-00845-3

Steinbrink, A., Brugger, K., Margos, G., Kraiczy, P., and Klimpel, S. (2022). The evolving story of *Borrelia burgdorferi* sensu lato transmission in Europe. *Parasitol. Res.* 121, 781–803. doi: 10.1007/s00436-022-07445-3

Strnad, M., Hönig, V., Růžek, D., Grubhoffer, L., and Rego, R. O. M. (2017). Europe-wide meta-analysis of *Borrelia burgdorferi* sensu lato prevalence in questing *Ixodes ricinus* ticks. *Appl. Environ. Microbiol.* 83, e00609–e00617. doi: 10.1128/AEM.00609-17

Šujanová, A., Čužiová, Z., and Václav, R. (2022). The infection rate of bird-feeding *Ixodes ricinus* ticks with *Borrelia garinii* and *B. valaisiana* varies with host haemosporidian infection status. *Microorganisms.* 11, 60. doi: 10.3390/microorganisms11010060

Tamura, K., Stecher, G., and Kumar, S. (2021). MEGA11: molecular evolutionary genetics analysis version 11. *Mol. Biol. Evol.* 38, 3022–3027. doi: 10.1093/molbev/msab120

Tarageľová, V., Koči, J., Hanincová, K., Kurtenbach, K., Derdáková, M., Ogden, N. H., et al. (2008). Blackbirds and song thrushes constitute a key reservoir of *Borrelia garinii*, the causative agent of borreliosis in Central Europe. *Appl. Environ. Microbiol.* 74, 1289–1293. doi: 10.1128/AEM.01060-07

Toma, L., Mancuso, E., d'Alessio, S. G., Menegon, M., Spina, F., Pascucci, I., et al. (2021). Tick species from Africa by migratory birds: a 3-year study in Italy. *Exp. Appl. Acarol.* 83, 147–164. doi: 10.1007/s10493-020-00573-4

Tulis, F., Ševčík, M., Jánošíková, R., Baláž, I., Ambros, M., Zvaríková, L., et al. (2023). The impact of the striped field mouse's range expansion on communities of native small mammals. *Sci. Rep.* 13, 753. doi: 10.1038/s41598-022-26919-z

Vaculová, T., Derdáková, M., Špitalská, E., Václav, R., Chvostáč, M., and Rusňáková Tarageľová, V. (2019). Simultaneous occurrence of *Borrelia miyamotoi*, *Borrelia burgdorferi* sensu lato, *Anaplasma phagocytophilum* and *Rickettsia helvetica* in *Ixodes ricinus* ticks in urban foci in Bratislava, Slovakia. *Acta Parasitol.* 64, 19–30. doi: 10.2478/s11686-018-00004-w

van Dam, A. P., Kuiper, H., Vos, K., Widjojokusumo, A., de Jongh, B. M., Spanjaard, L., et al. (1993). Different genospecies of *Borrelia burgdorferi* are associated with distinct clinical manifestations of Lyme borreliosis. *Clin. Infect. Dis.* 17, 708–717. doi: 10.1093/clinids/17.4.708

Venczel, R., Knoke, L., Pavlovic, M., Dzaferovic, E., Vaculová, T., Silaghi, C., et al. (2016). A novel duplex real-time PCR permits simultaneous detection and differentiation of *Borrelia miyamotoi* and *Borrelia burgdorferi* sensu lato. *Infection.* 44, 47–55. doi: 10.1007/s15010-015-0820-8

Wolcott, K. A., Margos, G., Fingerle, V., and Becker, N. S. (2021). Host association of *Borrelia burgdorferi* sensu lato: A review. *Ticks Tick Borne Dis.* 12, 101766. doi: 10.1016/j.ttbdis.2021.101766

frontiers | Frontiers in Cellular and Infection Microbiology

TYPE Original Research
PUBLISHED 16 December 2024
DOI 10.3389/fcimb.2024.1494450

OPEN ACCESS

EDITED BY
Omid Teymournejad,
University of Illinois Chicago, United States

REVIEWED BY
Chinmay V. Tikhe,
Johns Hopkins University, United States
Erich Loza Telleria,
Charles University, Czechia

*CORRESPONDENCE
Kevin R. Macaluso
kmacaluso@southalabama.edu

†PRESENT ADDRESSES
Chanida Fongsaran,
Department of Pathology, University of Texas Medical Branch, Galveston, TX, United States,
Victoria I. Verhoeve,
Department of Biology, West Virginia University, Morgantown, WV, United States,
Krit Jirakanwisal,
Department of Pathology, University of Texas Medical Branch, Galveston, TX, United States,
Emma K. Harris,
Center for Vector-Borne Infectious Diseases, Colorado State University, Fort Collins, CO, United States,
Kevin R. Macaluso,
Department of Microbiology and Immunology, Frederick P. Whiddon College of Medicine, University of South Alabama, Mobile, AL, United States

‡These authors have contributed equally to this work and share first authorship

RECEIVED 10 September 2024
ACCEPTED 14 November 2024
PUBLISHED 16 December 2024

CITATION
Fongsaran C, Verhoeve VI, Jirakanwisal K, Harris EK and Macaluso KR (2024) Identification and characterization of a Relish-type NF-κB, DvRelish, in *Dermacentor variabilis* in response to *Rickettsia rickettsii* infection. *Front. Cell. Infect. Microbiol.* 14:1494450. doi: 10.3389/fcimb.2024.1494450

Identification and characterization of a Relish-type NF-κB, DvRelish, in *Dermacentor variabilis* in response to *Rickettsia rickettsii* infection

Chanida Fongsaran[†‡], Victoria I. Verhoeve[†‡], Krit Jirakanwisal[‡], Emma K. Harris[‡] and Kevin R. Macaluso*[‡]

Department of Pathobiological Sciences, School of Veterinary Medicine, Louisiana State University, Baton Rouge, LA, United States

Ixodid ticks serve as hosts and transmission vectors for several obligate intracellular bacteria, including members of the spotted fever group (SFG) of *Rickettsia*. Although ticks generate an immune response to bacterial insults, many of the signaling molecules associated with the response and how they may contribute to vector competence for *Rickettsia* are undefined. In this study, we isolated a full-length *dvrelish* transcript from *Dermacentor variabilis*, which encoded a Relish-type NF-κB. The presence of a canonical Rel homology domain (RHD) consistent with NF-κB proteins suggested a role in tick immune response for DvRelish. The expression of DvRelish was confirmed in tick tissues and fluorescent microscopy of tick hemocytes indicated increased expression following infection with *Rickettsia* as compared to a non-tick-borne bacterial pathogen. To further determine the effect of *dvRelish* gene knockdown on rickettsial infection, we used RNA interference-mediated gene knockdown in *D. variabilis* and demonstrated that transcription of *dvRelish* was decreased after 24 h post-injection of siRNA. We then assessed the response of *D. variabilis* when exposed to *Rickettsia rickettsii* and determined that transcription of *dvRelish* was inversely associated with rickettsial loads at 48 h post-exposure. Further studies are required to broaden the understanding of differential immune responses in ticks to SFG *Rickettsia* infection and elucidate the role played by the arthropod immune system in vector competence.

KEYWORDS

Relish, tick, *Rickettsia*, NF-κB, immune response

Introduction

Ixodid ticks cause harm to vertebrate hosts through blood feeding and the transmission of disease-causing agents including viruses, protozoan parasites, and bacteria. As Gram-negative, obligate intracellular bacteria, the spotted fever group (SFG) of *Rickettsia* infect ticks and can be transmitted vertically between life cycle stages and horizontally from feeding ticks to vertebrate hosts. The duality in transmission routes is unique to the tick–SFG *Rickettsia* relationship, and the route employed is thought to be guided by the pathogenic nature of the *Rickettsia* (Perlman et al., 2006). The American dog tick, *Dermacentor variabilis*, is a vector and reservoir of *Rickettsia rickettsii*, the etiologic agent of Rocky Mountain spotted fever (RMSF). In addition to potentially lethal infection of humans, *R. rickettsii* can be pathogenic to the tick vector. Deleterious effects of *R. rickettsii* infection in *D. variabilis* ticks including reduced feeding, fecundity, and molting success have been previously reported (Niebylski et al., 1999; Schumacher et al., 2016; Harris et al., 2017). A fitness phenotype has been associated with rickettsial infection in *D. variabilis*, yet as rickettsiae are transmitted vertically, the tick response to rickettsial infection and the survival of rickettsiae are balanced.

Similar to other eukaryotes, ticks encode the signaling pathways that regulate the innate immune response such as toll, immunodeficiency (IMD), and Janus kinase/signal transducers and activators of transcription (JAK-STAT) (Gulia-Nuss et al., 2016; Sonenshine and Macaluso, 2017). Through a process originally described in *Drosophila melanogaster*, the expression of the antimicrobial peptide (AMP) genes depends on two members of the nuclear factor-κB (NF-κB) family of inducible transactivators: Dorsal-related immunity factors (DIFs) and Relish. Relish is responsive to Gram-negative bacterial infections (Ferrandon et al., 2007). For ticks, evidence of immune signaling pathways, including NF-κB, were identified in *Ixodes scapularis* (Smith and Pal, 2014; Gulia-Nuss et al., 2016). Specifically, sequences for a toll-like receptor with leucine-rich repeats, a Dorsal-type NF-κB and its regulating partner Cactus, a Relish-type NF-κB, and Caspar, a negative regulator of the IMD pathway, are present (Smith and Pal, 2014). Shaw et al. (2017) showed that lipids derived from *Borrelia burgdorferi* and *Anaplasma* species stimulate the IMD pathway in *I. scapularis* and *Dermacentor andersoni*, ultimately controlling the bacterial load in the tick. Components of the immune regulatory pathways, including the transcription factor Relish, have been identified in other tick species, including *Rhipicephalus microplus*, and are responsive to tick infection with *Anaplasma marginale* (Capelli-Peixoto et al., 2017). While receptors for initiation of the IMD pathway have not been identified in ticks, the unfolded protein response and a CD36-like protein called croquemort are alternates by which the IMD pathway is induced in *I. scapularis* (Sidak-Loftis et al., 2022; O'Neal et al., 2023). While the response of tick vectors to transiently infecting bacterial pathogens has been examined, the response to vertically transmitted pathogens such as SFG *Rickettsia* remains unresolved.

To understand the immune response in ticks during SFG *Rickettsia* infection, this study identified and characterized Relish-type NF-κB in *D. variabilis*. The results indicate that *D. variabilis* respond to *R. rickettsii* infection through the expression and activation of a Relish-type NF-κB protein. To further characterize the function of Relish-type NF-κB gene in *D. variabilis*, RNAi-mediated gene silencing was employed and the impact on rickettsial infection was observed. This study demonstrates that Relish-type NF-κB is involved in *D. variabilis* tick response to *R. rickettsii* infection and deepens the understanding of the functional roles of Relish-type NF-κB during the tick immune response.

Material and methods

Identification of a partial *dvrelish* transcript using previously published high-throughput sequencing databases

For the purpose of identifying previously unidentified *D. variabilis* transcripts with homology to Relish-type NF-κB proteins, a homology cloning approach was designed. Conserved domain searches of previously sequenced high-throughput sequence datasets and rapid amplification of cDNA ends-PCR (RACE-PCR) were used. A Blast search of the Genbank databases using the characterized Relish amino acid sequences from *D. melanogaster* (accession: Q94527), *Aedes aegypti* (accession: Q8MV44), and *Carcinoscorpius rotundicauda* (accession: ABC75034) as the query sequence returned no previously sequenced and annotated NF-κB gene transcript or protein sequence for *D. variabilis*. Three 454 pyrosequencing databases from published studies were previously released to NCBI's Sequence Read Archive (Jaworski et al., 2010; Bissinger et al., 2011; Sonenshine et al., 2011) and consisted of unannotated partial transcripts isolated and sequenced from uninfected *D. variabilis* tissues, and whole *D. variabilis* injected with Gram-negative and Gram-positive bacteria, fungi, and ticks infected with intracellular *Anaplasma phagocytophilum* via feeding on an infected animal (accessions: SRX001954, SRX001955, and SRX018179). The sequencing datasets were combined and served as a local database for Blast (v2.2.27). The presence of partial transcripts containing domains characteristic of Relish-type NF-κB proteins was identified using the following domain alignments from the Conserved Domain Database (NCBI): (1) Rel homology domains (RHDs) (cd07++884 RHD-n_Relish); (2) immunoglobulin/plexin/transcription factor (IPT) domains (cd01177 IPT_NFkappaB); and (3) ankyrin repeats (cd00204 ANK). A reverse position-specific Blast (RPS-Blast) was performed using conserved domain database alignments for each of the canonical domains described above as the query. Identified partial transcripts were then used for primer design, transcript isolation, and cDNA library synthesis using the SMARTer RACE 5′/3′ cDNA synthesis kit (Clontech).

Infection of *D. variabilis* with *R. rickettsii* and sample preparation

A colony of *Rickettsia*-free *D. variabilis* was maintained on rats, guinea pigs, and rabbits, as previously described (Macaluso et al., 2001). *Rickettsia rickettsii* (str. Shelia Smith) were maintained and

propagated in Vero cells with Dulbecco's modified Eagle's medium (DMEM) (Invitrogen) supplemented with 5% fetal bovine serum (Hyclone). Cells were maintained in a 34°C incubator with 5% CO_2. For rickettsial isolation, bacteria were partially purified when cells were ≥80% infected (Sunyakumthorn et al., 2008). Cells were lifted from a single infected T-75 flask and lysed with 10 passages through a 27-gauge needle. The resultant lysate was then centrifuged for 10 min at 275 × *g* at 4°C. The supernatant, which contained rickettsiae, was then passed through a 2-µm filter to remove host cell debris. Bacterial viability was determined using the Baclight viability staining kit (Invitrogen). Rickettsiae were enumerated with a Petroff-Hausser bacterial counting chamber on a Leica fluorescent microscope. Enumerated rickettsiae (2.5×10^8) were subsequently resuspended in 10 µL of sterile phosphate-buffered saline (PBS).

Unfed, virgin female *D. variabilis* were injected with *R. rickettsii* (str. Shelia Smith). Prior to injection with rickettsiae, ticks were surface-sterilized with 5-min incubations of 0.1% bleach and 70% ethanol, and three times with distilled water. The ticks were then immobilized with tape, dorsal side down and injected into the hemocoel cavity via the coxae of the third left leg. Five unfed adult females were injected with 2 µL of *R. rickettsii* solution with a 33-gauge Hamilton needle. Ticks were maintained in a humidified environmental chamber at 27°C. At 1 h post-exposure, ticks were removed from the incubator and dissected in sterile PBS. Additionally, five uninfected, surface-sterilized ticks were dissected. Salivary glands, gut, ovaries, and hemolymph from infected ticks, and separately tissues from uninfected ticks, were combined for RNA extraction in 300 µL of TRIzol reagent (ThermoFisher). Prior to RNA isolation, tissues were homogenized using a TissueLyzer and 3-mm stainless steel beads (QIAGEN) in a 1.7-mL microcentrifuge tube for 4 min at 25 Hz/s. RNA was isolated as per the manufacturer's instructions and stored at −80°C until used. Total RNA (1 µg) was treated with 2 units of Turbo DNase (Ambion) before cleanup and concentration with the Clean and Concentrator-5 kit (Zymo). Total RNA was subsequently reverse-transcribed using the iScript cDNA synthesis kit, including no reverse transcriptase reactions to identify DNA contamination.

RACE-cDNA library synthesis, RACE-PCR, cloning, and sequencing

Total RNA (1 µg) was used for 5′- and 3′-enriched RACE-cDNA library synthesis using the SMARTer RACE 5′/3′ kit (Clontech) as per the manufacturer's protocols. Primers were designed using Primer3 (Koressaar and Remm, 2007; Untergasser et al., 2012) from a partial *D. variabilis* transcript identified through RPS-Blast with homology to Relish-type RHD and are listed in Table 1. Each specific primer was combined with the Universal Primer Mix (Clontech) that amplifies the 5′ or 3′ adaptor in each library for PCR amplification. Traditional PCR with an additional round of cycling was performed with each RACE-PCR library and the appropriate direction-specific and transcript-specific primer. RACE-PCR was performed using the Advantage cDNA PCR kit (Clontech) with 1 µL of each library as template in separate PCR reactions. The thermocycling conditions consisted of 1 cycle at 95°C for 10 min, amplification for 40 cycles with denaturing at 95°C for 30 s, annealing at 45°C for 1 min, and extension at 72°C for 3 min. A final extension was performed for 10 min at 72°C. For the additional rounds of PCR, 0.5 µL of the previous reaction was used as the template for the next reaction. PCR reactions were visualized with a 1.5% agarose gel (GenePure) and SYBRSafe DNA gel stain (Invitrogen). All bands amplified were cloned using the TOPO TA Cloning kit with pCR4-TOPO (Invitrogen) per the manufacturer's instructions. Plasmids were isolated using the Fast Plasmid Mini kit (Eppendorf) according to the manufacturer's instructions. Plasmid inserts were sequenced using the dye terminator method on an Applied Biosystems 3130 Genetic Analyzer in GeneLab at Louisiana State University (LSU). Inserts were analyzed with MacVector (v14.5.0) and aligned with the isolated partial transcript sequence derived from traditional PCR with Clustal W.

Analysis of the isolated *dvrelish* transcript

The full-length transcript, *dvrelish*, was aligned to previously isolated Relish-type NF-κB transcript sequences in other model organisms including the fruit fly *D. melanogaster* (accession: Q94527), the mosquito *Aedes aegypti* (accession: Q8MV44), and the horseshoe crab *C. rotundicauda* (accession: ABC75034) using MacVector (v14.5.0). Nucleotide and translated amino acid alignments were used to determine percent identities. A conserved domain search was performed using the Conserved Domain Database (NCBI) to identify all domains present on the transcript. The Open Reading Frame Finder (NCBI) was used to determine the correct open reading frame of the transcript. The cNLS mapper (Kosugi et al., 2009) was used to determine the presence of a nuclear localization sequence.

Anti-DvRelish peptide antibody production

The production of an anti-DvRelish peptide antibody was commercially produced by YenZym Antibodies. Briefly, two peptides from the RHD of dvrelish were chosen and linked to the keyhole limpet hemocyanin (KLH) carrier protein separately. The two peptides used for immunization were as follows: CESSTQQRKTYPT KLENYNTQ-amide (DvRelish amino acids 47–67) and CYRRKIESLQPSQEEQRQLQ-amide (DvRelish amino acids 131–149). These peptides were chosen as candidates because they were predicted to be both hydrophilic and expressed on the surface of the protein. A rabbit was immunized with the combination of the two KLH-conjugated peptides in Freund's complete adjuvant. After 2 months, the rabbit was inoculated with a secondary booster of both peptides. Serum was collected and the specificity of the produced antibodies in serum was determined by enzyme-linked immunosorbent assay. Antibody was then purified by high-performance liquid chromatography and delivered from the company at 0.24 mg/mL of purified mono-specific polyclonal IgG.

TABLE 1 Primers used for the isolation of full-length *dvrelish* transcript.

Primer name	Primer sequence (5′-3′)	Purpose	Reference
IPTDV_43F	TGCACATCTGACTCCTGGAA	Initial isolation	This study
IPTDV_233R	ACAAAGGCTGGAAAGCTCAG	Initial isolation	This study
IPTLeggo211>5′	GACTATGGCCACCTGATGGT	5′ RACE-PCR	This study
RelishLeggo1925>3′	TGCCTTGTGACCCTTCTGA	3′ RACE-PCR	This study
RelishLeggo1247>3′	TGCAAGGCGGATACTCTACC	Sequencing	This study
RelishLeggo1797>3′	TGCTGACCTTTCACTTGTGG	Sequencing	This study
RelishLeggo2358>3′	CGGTCAAAAGTGGTGGAAGT	Sequencing	This study

Detection of DvRelish in tick tissue lysate

Uninfected adult females were dissected and tissues were placed in RIPA buffer with Complete Mini EDTA-free protease inhibitor cocktail (Roche) and homogenized using a sonicating probe (Sonic Dismembranator, Fisher) with 25% amplitude for 5 s, five times, on ice. The protein concentration in the tissue lysate was quantified using the DC Assay (Bio-Rad) per the manufacturer's instructions. Tick protein (25 µg per lane) was separated with a Mini-ProteanX 4%–15% Tris-Glycine mini-gel (Bio-Rad). Separated proteins were transferred onto a 0.45-µm pore nitrocellulose membrane using a Trans-Blot semi-dry transfer cell at 25 V for 25 min. The membrane was blocked with 5% BSA in tris-buffered saline with 0.5% Tween 20 (TBST). Primary anti-DvRelish antibody (1:100) in 5% BSA in TBST was followed by secondary donkey anti-rabbit Li-Cor 800CW antibody (1:15,000). Peptide competition was performed with anti-DvRelish antibody (1:100) supplemented with 1 µg of each peptide the antibody was raised against. Blots were visualized with a Li-Cor Odyssey imager.

To confirm the antibody specificity, unfed female *D. variabilis* whole tick tissue was separated by SDS-PAGE. Bands of interest identified concurrently by Western blot at 100 and 70 kDa were excised from a 6% Tris-glycine gel with a clean scalpel blade. Samples were digested prior to mass spectrometry analysis with porcine pancreas-derived trypsin (Sigma-Aldrich). Digested samples were submitted for MALDI-TOF/TOF mass spectrometry on a Bruker UltrafleXtreme MALDI-TOF/TOF MS system (Bruker Daltonics) at the LSU Chemistry Department. For identification of submitted samples, reported sample peptide masses were compared to predicted masses for the putative amino acid sequence of DvRelish. *In silico* trypsin digestion analysis of the putative DvRelish amino acid sequence was performed with one missed cleavage allowed using the PeptideMass predictor program from the Swiss Institute of Bioinformatics ExPAsy website (Wilkins et al., 1997).

DvRelish RHD construction, transfection of HEK293T/17 cells, and peptide characterization

The insert fragment was amplified using the primers shown in Table 2 to generate insert fragments containing the 5′-*Bgl*II and 3′-*BamH*I recognition sites, KOZAK sequence, and 6×His tag. The human embryonic kidney cell line HEK293T/17 (ATCC CRL-11268) was transfected with eukaryotic expression vectors (pAcGFP1-C1) (Clontech) harboring the RHD, using Lipofectamine 3000 (Invitrogen). Briefly, 4×10^6 HEK293T/17 cells were seeded into 60-mm tissue culture dishes and maintained under standard conditions for 24 h. Mixtures of Lipofectamine 3000 (10 µL) and 5 µg of pAcGFP1-C1 with/without truncated *DvRelish* plasmids in Opti-MEM Reduced Serum Medium (Invitrogen) were incubated at room temperature for 15 min and then added onto HEK293T/17 culture plates. After 20 h post-transfection, the culture medium was replaced with fresh medium and transfected cells were collected at 48 h after transfection. Subsequently, the

TABLE 2 Primers used to construct the DvRelish RHD for gene expression analysis and siRNA generation.

Primer name	Primer sequence (5′-3′)	Purpose	Reference
NheI-RHD_F[a,b]	cta**gctagc**cgccaccatgcaccatcaccatcaccatATGCCTATC	RHD construction	This study
BamHI-IPT_R[a,b]	cgc**ggatcc**ttaAGGCAGATAGGTGAACTCAA	RHD construction	This study
siDvRelish2_Antisense[c]	aaGACTGCTGTTTTGTTACAGcctgtctc	siRNA	This study
siDvRelish2_Sense[c]	aaCTGTAACAAAACAGCAGTCcctgtctc	siRNA	This study
siGFP_Antisense[c]	aaATTTTCTGTCAGTGGAGAGcctgtctc	siRNA	This study
siGFP_Sense[c]	aaCTCTCCACTGACAGAAAATcctgtctc	siRNA	This study

[a]Engineered restriction enzyme sites are highlighted in bold text and underlined.
[b]Lowercase: vector sequence, upper case: insert sequence in pAcGFP-C1.
[c]Uppercase: target sequence.

culture medium was removed, and cells were washed twice with 1× PBS. For 60-mm tissue culture dishes, 500 µL of lysis buffer (50 mM Tris-HCl, pH 7.4, 150 mM NaCl, and 1% Nonidet P-40) containing protease inhibitor cocktail (Bio Basic Inc.) was added and the cells were harvested and transferred to a 1.5-mL microcentrifuge tube. The collected cells were incubated on ice for 15 min and then the cell debris was removed by centrifugation at 2,500 × *g*, 4°C for 15 min. Total protein was collected from the supernatant and transferred to a new microcentrifuge tube. The proteins were applied to a Capturem™ His-Tagged Purification Miniprep column (Takara) and performed according to the manufacturer's instructions. Recombinant DvRelish expression was analyzed via SDS-PAGE and Western blot. SDS-PAGE was performed using 4%–12% Mini-PROTEAN® TGX™ Precast Protein Gels (Bio-Rad). Then, the protein was transferred to 0.45 µM pore nitrocellulose (Bio-Rad) using a Trans-Blot SD semi-dry transfer apparatus (Bio-Rad). For Western blot analysis, the membranes were incubated with a mouse monoclonal 6× anti-His monoclonal antibody (1:5,000; Takara, Clontech) or a rabbit polyclonal anti-DvRelish peptide antibody (1:1,000; Yenzyme), followed by a secondary antibody of donkey anti-mouse Li-Cor 680 CW (1:20,000; Li-Cor) or a donkey anti-rabbit Li-Cor 800 CW antibody (1:15,000). Western blots were imaged using a Li-Cor Odyssey imager (Li-Cor).

Electrophoretic mobility shift assay of recombinant *dvRelish* RHD

Recombinant *DvRelish* RHD in HEK293T cells were resuspended in 500 µL of cell lysis buffer (20 mM Tris, pH 7.4, 150 mM NaCl, 1% Nonidet P-40, 0.5% sodium deoxycholate, and 0.1% SDS) containing protease inhibitors. The cell suspensions were lysed in an ice-water bath during sonication for 5 min. The lysate was centrifuged at 12,000 × *g* for 10 min at 4°C, and the pellet was discarded. Electrophoretic mobility shift assay (EMSA) was performed according to the manufacturer's instructions from Odyssey EMSA Kit (LI-COR). Briefly, 10 µg of r*DvRelish* RHD proteins was incubated with 10× Binding buffer, 1 µg/µL Poly (dI·dc), 25 mM DTT, and IRDye 700 NF-κB oligonucleotide. The mixture was incubated at room temperature for 30 min in the dark. The sample was then mixed with 10× Orange loading dye and loaded onto 4% Native gels for electrophoresis. To evaluate the binding, the gel was imaged with the Odyssey Infrared Imaging System.

DvRelish expression in hemocyte samples for fluorescent microscopy

Bacteria were used to assess DvRelish expression in tick hemocytes. *R. rickettsii* was purified via sucrose gradient. Briefly, infected cells were lysed by repeated passage through a needle, followed by centrifugation to separate *Rickettsia* over a 20% sucrose cushion and kept at −80°C in SPG buffer (218 mM sucrose, 3.8 mM KH_2PO_4, 7.2 mM K_2HPO_4, and 4.9 mM L-glutamate, pH 7.2) (Chan et al., 2011). Total concentration of rickettsiae was quantified via endpoint dilution assay as previously described (Esteves et al., 2020). Overnight cultures of *Pseudomonas aeruginosa* (ATCC 25873) were grown in a 37°C shaking incubator in trypic soy broth (Invitrogen) and assessed for viability and enumerated using the Baclight viability staining kit, as described previously. Bacteria were pelleted via centrifugation at 4°C for 10 min at 16,000 × *g* and resuspended in sterile PBS.

Five unfed adult *D. variabilis* female ticks per group were injected 10^7 P. *aeruginosa* (ATCC 27853) or 10^7 *R. rickettsii*. The ticks were surface-sterilized and immobilized dorsal side-down using tape and injected as mentioned previously. After 1 h, hemolymph was collected from the coxal–trochanteral joint and smeared on a glass slide. The slide was air-dried, fixed in 4% paraformaldehyde with 4% sucrose in PBS for 10 min, washed with PBS, permeabilized with 0.1% Triton X-100 in PBS for 15 min, blocked with 3% BSA in PBS for 1 h, and then washed twice with 0.03% Triton X-100 in PBS. Hemocytes were incubated with anti-DvRelish peptide antibody (1:50) at 4°C for 1 h. Following incubation, the cells were washed three times and then incubated with an FITC-conjugated goat anti-rabbit antibody (1:100) for 1 h at room temperature. Samples incubated without primary anti-DvRelish antibodies serve as a control for off-target secondary antibody binding. After the final wash, the cells were mounted with VECTASHIELD mounting medium containing DAPI (Vector Laboratories) and examined using an Olympus FLUOVIEW confocal microscope.

Knockdown and expression of *dvRelish* and quantitative reverse transcription PCR

siRNA templates were designed from target sites on DvRelish (Genbank accession number KJ484815.1) and the green fluorescent protein (Genbank accession number U62637.1). The sequences were subjected to siRNA template design to generate DNA oligonucleotides sequences for the Silencer® siRNA Construction Kit (Ambion). siRNA templates were synthesized following the Silencer® siRNA Construction Kit (Ambion) protocol and the concentrations were determined using a NanoDrop® ND-1000 UV-Vis Spectrophotometer (Thermo Fisher Scientific).

For microinjection, five unfed adult female ticks were surface-sterilized and immobilized as previously described. Each tick was injected with 1 µL of PBS containing either 250 or 500 ng of siRNA using a 33-gauge Hamilton needle and a 5-µL glass syringe into the coxae of the third left leg. Ticks were placed in a humidified incubator set at 27°C under 90% humidity for 24 h. The following day, the surviving ticks were injected with 1 µL containing 10^7 bacterial suspension using a 33-gauge Hamilton needle and a 5-µL glass syringe into the coxae of the third left leg. Ticks were incubated in a 27°C humidified environmental chamber for 12, 24, and 48 h post-exposure.

Total RNA was extracted from adult *D. variabilis* tissues (combined: salivary glands, gut, ovary, and hemolymph) using TRIzol reagent (Molecular Research Center) following standard protocols. Following quantification of RNA via a NanoDrop ND-1000 UV-Vis Spectrophotometer, 2 units of TurboDNase

(Invitrogen) was added and incubated at 37°C for 30 min. RNA was purified and concentrated using the Clean and Concentrator-5 Kit (Zymo Research) and eluted in 20 µL of DNase/RNase-free water. Total purified RNA (250 ng) was used with the iScript™ cDNA Synthesis Kit (Bio-Rad). No reverse transcriptase reactions (water was added instead of reverse transcriptase) were performed to assess residual DNA by qPCR.

Gene expression was quantified by qPCR on a LightCycler (Roche). The amplification reaction was performed in triplicate in a final volume of 35 µL using 10 µM of specific primers and probes (Table 3) and 5 µL of cDNA as template and iTaq Universal Probes Master Mix (Bio-Rad). Ten microliters of the qPCR reaction mix was assessed in triplicate on a 384-well plate and amplified using a Light Cycler 480 Real-Time PCR system (Roche). The qPCR conditions consisted of an initial cycle at 95°C for 3 min for denaturation, followed by 45 cycles at 95°C for 15 s for denaturation, 60°C for 1 min for annealing, and 72°C for 1 s for extension, followed by cooling down to 40°C for 30 s. Serial dilutions of the pCR4-TOPO plasmid containing amplicons for each primer set genes were assessed in parallel, serving as a standard for concentration analysis. Serial diluted standards with known copy numbers, as well as environmental and negative (PCR water) controls, were included along with experimental samples for each set of reactions.

Statistical analysis

All data are presented as mean ± standard error of the mean (SEM). Statistical significance between two groups was determined by *t*-test with a *p*-value ≤ 0.05 considered significant. Additionally, comparative differences among multiple experimental groups were analyzed by analysis of variance (ANOVA), followed by the Tukey's *post-hoc* test with a *p*-value ≤ 0.05 considered significant. All statistical analyses were performed using the GraphPad Prism Software.

Results

Isolation of a partial *dvrelish* transcript and completion of full-length transcript via RACE-PCR

The RPS-Blast of the *D. variabilis* 454 pyrosequencing database resulted in one partial transcript with an RHD, one partial transcript with an IPT domain, and two partial transcripts with ankyrin repeats. The sequences for RHD-containing and IPT-containing transcripts were utilized for primer design for PCR. Both primer sets were used in traditional PCR with cDNA from uninfected ticks and *D. variabilis* infected with *R. rickettsii*. Resultant amplicons were cloned and sequenced. No partial transcripts with homology to previously identified Relish-type NF-κB were identified in cDNA libraries from uninfected *D. variabilis*. Traditional PCR using cDNA from *R. rickettsii*-infected *D. variabilis* as template resulted in the amplification of two partial transcripts with identity to known NF-κB transcripts. However, only the primer set specific for IPT domains was successful in amplifying the intended target whereas the RHD-specific primers instead amplified an alternative RHD characteristic of another RHD-containing NF-κB protein, Dorsal. Primers for RACE-PCR with both 5′ and 3′ enriched libraries were then designed with at least 100 nucleotides to overlap RACE-PCR amplicons with traditional PCR amplicons. These primers were paired with the universal primer mix (UPM) primers specific to the 5′ or 3′ adaptor, which was ligated during the RACE-library preparation. Amplicons were not immediately visualized with 40 cycles of PCR; thus, 0.5 µL of first-round reactions was used as the template for a second round of 40 cycles of PCR. All amplicons visualized were cloned into pCR4-TOPO and sequenced. Amplification of the 5′-end of the *dvrelish* transcript occurred with additional rounds of RACE-PCR with primer IPTLeggo211>5′. A single band overlapped with the known partial transcript after sequencing with M13 Forward and M13 Reverse primers and completed the 5′

TABLE 3 Primers and probes for qPCR.

Primer name	Primer sequence (5′-3′)	Reference
DvRelish-187_Fw	AACTACAATACACAGTTACCCCAT	This study
DvRelish-293_Rv	ACTGTAACAAAACAGCAGTCTT	This study
DvRelish-HEX	HEX/TC ATG TCC A/ZEN/T CGT ATC ACC ATG CGA/3IABkFQ/	This study
DvActin-1424For	CTTTGTTTTCCCGAGCAGAG	Sunyakumthorn et al. (2012)
DvActin-1572Rev	CCAGGGCAGTAGAAGACGAG	Sunyakumthorn et al. (2012)
DvActin-Cy5	Cy5/TC ATG TCC A/TAO/T CGT ATC ACC ATG CGA/3IAbRQSp/	This study
ompBRr1370F	ATAACCCAAGACTCAAACTTTGGTA	Jiang et al. (2005)
ompBRr1494r	GCAGTGTTACCGGGATTGCT	Jiang et al. (2005)
RrompB-FAM	FAM/CGCGATCTTAAAGTTCCTAATGCTATAACCCTTACCG ATCGCG	Harris et al. (2017)

sequencing of the *dvrelish* transcript. Amplification of the 3′-end of *dvrelish* transcript occurred with RelishLeggo1925>3′ and the UPM with additional rounds of RACE-PCR and sequencing of all amplicons. One large amplicon of approximately 2,500 base pairs (bp) overlapped with the previously known sequence. Complete sequencing of the cloned amplicon was performed with primer walking. Primers RelishLeggo1247>3′, RelishLeggo1797>3′, and RelishLeggo2358>3′ were used for the sequencing, completing the 3′-end of the transcript. The full-length transcript was deposited into Genbank under the accession KJ484815.

Analysis of isolated *dvrelish* transcript

A schematic representing the domain architecture was determined through searches with the Conserved Domain Database, ORF finder, and cNLS mapper for the putative-translated transcript and is presented in Figure 1A. The full-length *dvrelish* transcript was 3,138 nucleotides in length with an ORF that starts at base 409 through the stop codon beginning at base 3031. The putative translated ORF is 873 amino acids long. The conserved domain search determined the presence of a RHD (amino acids 20–193), an IPT domain (amino acids 197–300), a nuclear localization sequence (amino acids 307–317), and five ankyrin repeats (amino acids 520–751).

The percent identities for the nucleotide alignment and translated amino acid alignment are listed in Figure 1B. In general, the nucleotides align slightly better than the amino acid sequences. The closest nucleotide and amino acid sequence were from the horseshoe crab, *C. rotundicauda*, with nucleotide and amino acid identities of 36.1% and 23.3%, respectively. Compared to the *I. scapularis* p105-like transcript (ISCW018935), which does not contain the canonical inhibitory ankyrin repeats, there is 58.4% nucleotide identity, and 35.8% translated amino acid identity across the conserved regions. The translated amino acid sequence of the transcript aligned to Relish-type NF-κB proteins of other model organisms. The nucleotide sequence is minimally conserved with other arthropods, including the mosquito vector *A. aegypti*. The transcript sequence encoding the *Drosophila* NF-κB contains multiple stretches of nucleotides within the RHD and IPT domains that are not encoded in the mosquito or horseshoe crab Relish NF-κB transcripts. Additionally, the horseshoe crab Relish-type NF-κB transcript encodes numerous additional stretches of nucleotides present in the C-terminal ankyrin repeat domains that were previously identified as linker sequence (Fan et al., 2008). In stark contrast, the transcript encoding *dvrelish* contains only two linker sequences.

Interestingly, while the putative translated amino acid sequence of *dvrelish* has minimal amino acid identity to other arthropods, the conserved domain search reveals that the RHD, IPT, and ankyrin repeats are highly conserved (Figure 1C). The recognized domains and their specific amino acid sequence correspond to structures that are integral to the function of Relish-type NF-κB proteins. DNA binding sites and ankyrin repeat binding sites throughout the RHD and IPT were conserved in DvRelish.

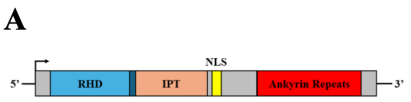

B

Organism	Percent nucleotide identity	Percent amino acid identity
Drosophila melanogaster	33.2	18.7
Aedes aegypti	35.7	18.5
Carcinoscorpius rotundicauda	36.1	23.3

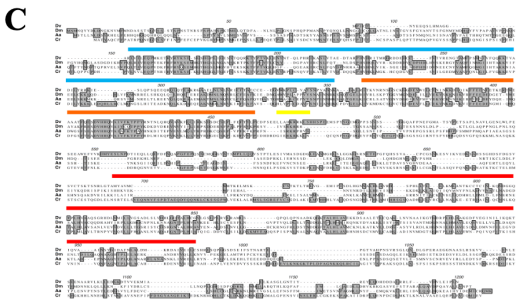

FIGURE 1
(A) Schematic representation of the *dvrelish* transcript. RHD represents the Rel homology domain; IPT represents the immunoglobulin, plexin, transcription factor domain; and NLS represents nuclear localization sequence. **(B)** Percent identity of isolated *dvrelish* transcript and putative translated DvRelish protein as compared to the Relish-type NF-κB of other model organisms. **(C)** Multiple sequence comparison of Relish-type NF-κB translated amino acid sequence. *dvrelish* was translated and aligned to Relish-type NF-κB molecules of *Drosophila melanogaster* (accession: Q94527), *Aedes aegypti* (accession: Q8MV44), and *Carcinoscorpus rotundicauda* (accession: ABC75034). The conserved domains are represented by boxes on the alignment. Specifically, the Rel homology domain is labeled from amino acid (AA) 156 to 351, the IPT domain is labeled from AA 361 to 463, the nuclear localization sequence is labeled from AA 470 to 479, and the ankyrin repeat domain is labeled from AA 689 to 983. Shading with the amino acid alignment indicates identities across the aligned sequences. DBS represents regions corresponding to DNA binding sites. ABS represents regions corresponding to ankyrin binding sites.

Detection of DvRelish in tick tissue lysate

DvRelish expression was queried in *D. variabilis* tissues. All tissues of the tick were homogenized and centrifuged to remove insoluble tick materials. Tick protein (25 µg) was probed via Western blot with anti-DvRelish antibody, resulting in the recognition of multiple protein bands (Figure 2). A peptide competition assay was performed to determine the specificity of anti-DvRelish binding. The addition of 1 µg of each peptide to the primary DvRelish incubation resulted in the loss of signal at 100 and 70 kDa. The secondary antibody only control was performed, yielding non-specific binding of the donkey anti-rabbit 800CW antibody to tick tissues. Despite non-specific binding to *D. variabilis* proteins, the peptide competition assay demonstrated that the anti-DvRelish antibody recognized two proteins at 100 and 70 kDa. Both proteins were identified by mass spectrometry and the resultant peptide masses were compared to the masses predicted for DvRelish by *in silico* trypsin analysis. The predicted DvRelish peptide masses corresponded with 18 identified peptide masses and with 9 peptide masses identified within the 70-kDa protein. Additionally, the 70-kDa protein masses identified by mass spectrometry corresponded with only three predicted masses with a translated partial putative *dvdorsal* transcript corresponding to a Dorsal-type NF-κB protein previously isolated. Together, these data confirm the recognition of DvRelish via the anti-DvRelish antibody at 100 kDa and the N-terminal DvRelish at 70 kDa.

rDvRelish expression and purification

For EMSA, the DvRelish RHD was cloned in vector plasmid (pAcGFP-C1) with N-terminal 6×His tag. The DvRelish expression plasmid was transfected into HEK293T cells using Lipofectamine 3000. The transfected cells were detected with fluorescence microscopy (Supplementary Figure 1) and total protein lysates were collected and purified by His-tagged column, followed by Western blot analysis. The recombinant protein was detected with both anti-His (Figure 3A) and anti-DvRelish (Figure 3B) antibodies. These results suggest that the recombinant DvRelish protein is expressed.

Electrophoretic mobility shift assay

We further characterized DvRelish via EMSA. Recombinantly expressed DvRelish RHD was incubated with fluorescently labeled NF-κB consensus DNA motif probes. In the control experiments, no protein/DNA complex or only pAcGFP-C1 vector (Figure 4,

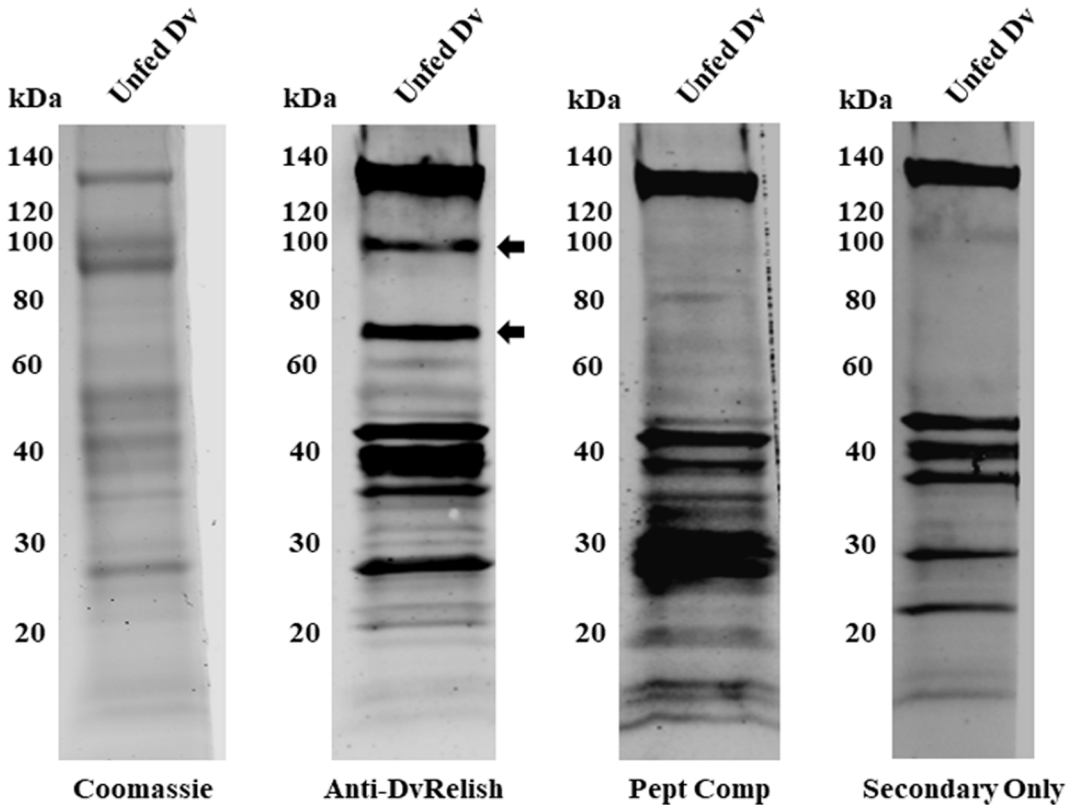

FIGURE 2
Expression of DvRelish in *D. variabilis* tissues. Expression of DvRelish in 25 µg of protein from unfed adult female *D. variabilis* tissue lysate. DvRelish was recognized via Western blot with anti-DvRelish antibody. A peptide competition assay (Pept Comp) decreased recognition of proteins at 100 and 70 kDa.

10.3389/fcimb.2024.1494450

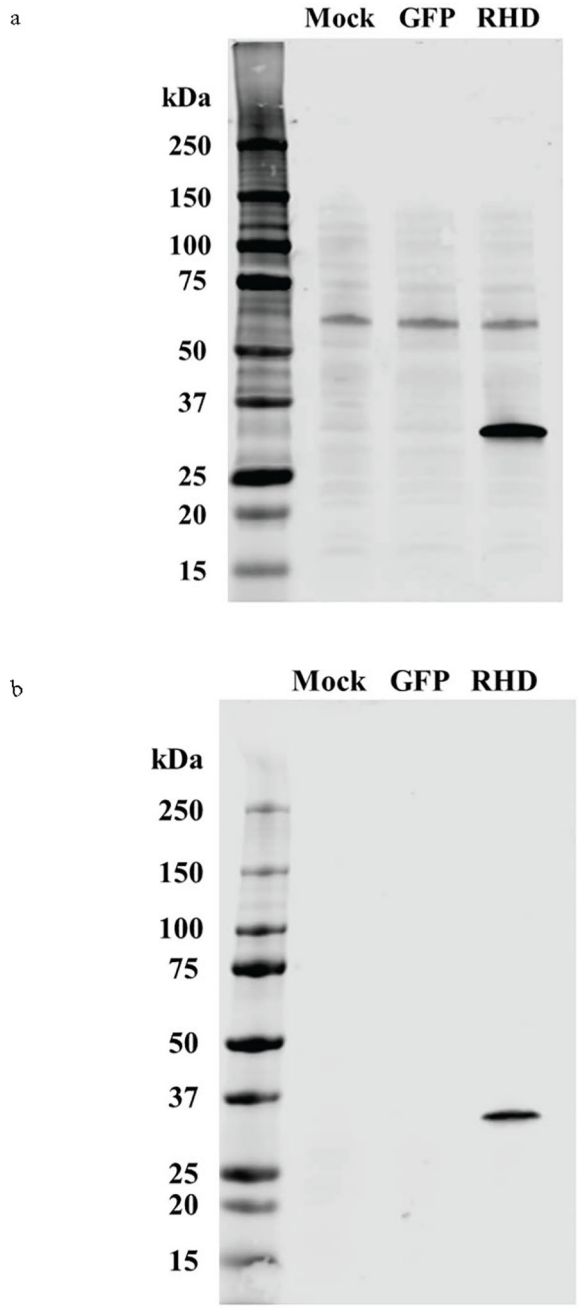

FIGURE 3
Western blot analysis of recombinant expression and protein purification of DvRelish. The rDvRelish expression plasmid with N-terminal 6×His tag was used to transfect HEK293T cells. The lysates were resolved on a 4%–12% SDS-PAGE gel. Lane 1 contained lysate from cells transfected without the vector plasmid (mock). Lane 2 contained lysate from cells transfected with the vector plasmid (pAcGFP-C1). Lane 3 contained rDvRelish RHD protein with 6×His tag. The membrane was probed with anti-His antibodies **(A)** and customized antibodies targeting DvRelish peptides **(B)**.

lanes 1-2), nonspecific binding was not observed. The EMSA results showed that the DvRelish RHD could bind to the NF-κB DNA motifs (Figure 4 lanes 3–5), demonstrating the DNA-binding capacity of the transfected Relish protein. This suggests that the recombinant DvRelish RHD has an interaction with NF-κB motif. DvRelish could function as a transcription factor to activate κB motifs and regulate the expression of immune-related genes in *D. variabilis*.

Immunofluorescence assay of *D. variabilis* hemocytes

Because hemocytes are an important site of AMP production, the hemocytes of unfed *D. variabilis* females were collected and spotted onto slides for IFA to detect DvRelish expression and nuclear localization in the presence of bacterial infection. To further explore the response of *D. variabilis* hemocytes to *R. rickettsii*, adult unfed *D. variabilis* females were injected with either 10^7 *R. rickettsii* or *P. aeruginosa*. Following exposure for 1 h, the hemolymph was collected, and the cells were stained with anti-DvRelish as previously described. DvRelish was present within the cytoplasm of the hemocytes in both *R. rickettsii*-injected and *P. aeruginosa*-injected but not in control hemocytes (Figure 5). While qualitative, the intensity of *R. rickettsii* treatment is greater than that observed in the *P. aeruginosa*-treated hemocytes.

Functional knockdown of DvRelish via RNA-mediated interference

We sought to determine whether expression of *dvrelish* in *D. variabilis* ticks could be downregulated via siRNA-mediated gene silencing. Adult, unfed *D. variabilis* females were injected with 250 ng, 500 ng, or PBS as a control and incubated for 24 h. The expression of DvRelish mRNA was analyzed by qPCR. The results showed that there was reduced expression of DvRelish transcript with 500 ng of siRNA at 24 h post-injection (Figure 6A).

To determine the effect of the reduced expression of DvRelish during the tick response to *R. rickettsii* infection, adult, unfed *D.*

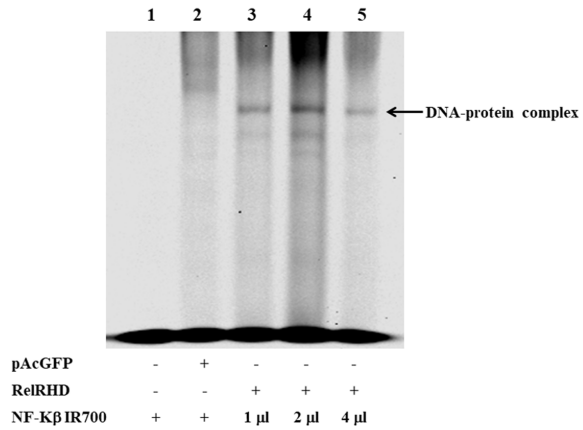

FIGURE 4
EMSA analysis demonstrating recombinant DvRelish RHD binding to kB motifs. EMSA was performed using 5′IR700 consensus NF-κB probes to assess binding specificity. The gel image shows that the recombinant protein specifically binds to κB motifs. Lanes 1 and 2 serve as control for non-specific binding. Lanes 3, 4, and 5 show rDvRelish RHD binding to κB motifs 50, 100, and 200 fmol, respectively. The arrowhead indicates the DNA–protein complex.

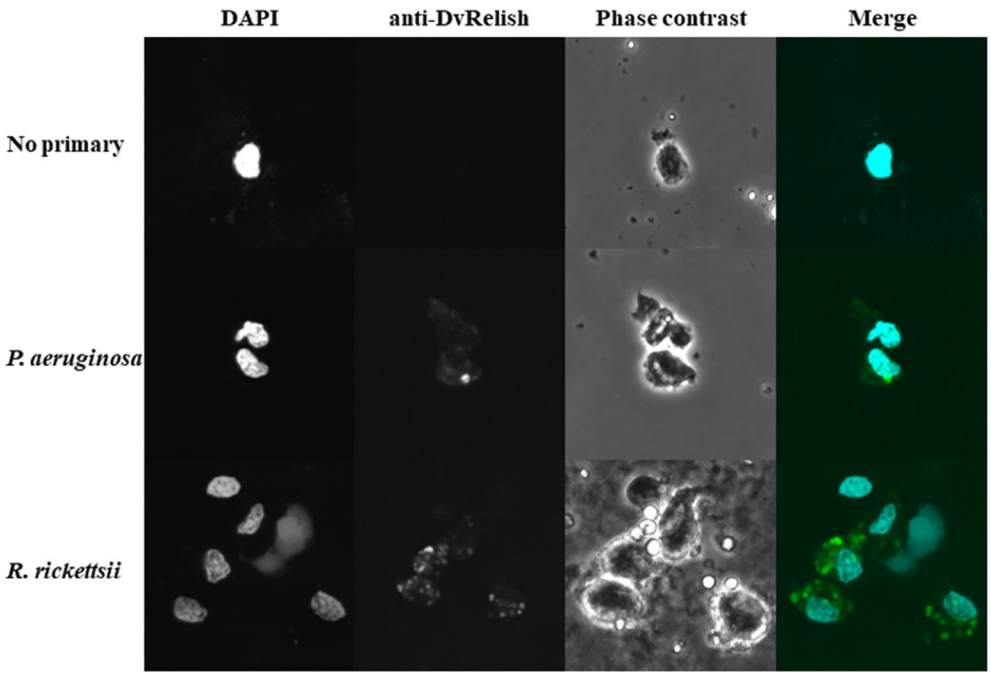

FIGURE 5
Immunofluorescence detection of tick hemocytes. Expression of DvRelish and nuclear localization in response to injected bacteria. Adult, unfed *D. variabilis* females were exposed to *R. rickettsii* or *P. aeruginosa*. After 1 h of exposure, hemolymph was collected, and hemocytes were strained with DAPI to visualize nuclear localization. DvRelish expression was detected using an anti-rabbit FITC-conjugated secondary antibody.

variabilis females were injected 500 ng of siRNAs directed against *dvrelish*, GFP, or PBS as a control and incubated for 24 h. Ticks were then injected with 10^7 *R. rickettsii* or PBS. Following exposure for 12, 24, and 48 h, ticks were collected to determine the expression of *dvRelish*. Expression of DvRelish mRNA was determined by qPCR and normalized to *dvactin* at the selected time points (Figures 6B–D). The results showed that the transcriptional expression levels were not significantly different at 12 hpe, and exposure to *R. rickettsii* did not impact the transcription of *dvrelish* (Figure 6B). At 24 hpe, *dvrelish* transcription was significantly reduced in unexposed ticks compared to ticks injected with GFP or PBS only and to ticks that were exposed to *R. rickettsii* (Figure 6C). At 48 hpe, siRelish had no impact on *dvrelish* transcription in the unexposed ticks, but a significant reduction in transcription was observed in the siRelish-treated ticks exposed to *R. rickettsii* (Figure 6D). These observations suggest that siRelish had an effect through 24 h and the exposure to *R. rickettsii* had a variable impact on the transcription of *dvrelish* expression in ticks. When examining rickettsial load in ticks exposed to either siRelish or controls, no differences in rickettsial load was observed through 24 h, while *dvrelish* knockdown resulted in increased *R. rickettsii* load at 48 hpe (Figure 6E). Together, these results showed that when *dvrelish* transcription is unchanged, rickettsial loads are also unchanged; however, if *dvrelish* is lower, rickettsial loads are greater.

Discussion

Ticks serve as vectors for a number of obligate intracellular bacteria. Within the Rickettsiales, members of the SFG *Rickettsia* are unique by employing ticks as both reservoir hosts and vectors to transit to vertebrate hosts (Sonenshine and Macaluso, 2017). The progression of infection is not fully characterized for SFG *Rickettsia* in ticks. If ingested while a female tick takes a bloodmeal, rickettsiae infect the midgut and then transit to other tick tissues, including the hemolymph, salivary glands, and ovaries. As tick hemocytes are free floating in tick hemolymph, it is likely that infection occurs for cells independent of the cell-to-cell spread observed in monoculture. If infection of the ovaries or salivary glands occurs, SFG *Rickettsia* can be transmitted to progeny (vertical) or new hosts (horizontal) (Sonenshine and Macaluso, 2017). For *Dermacentor ticks*, infection with *R. rickettsii* can result in reduced tick fitness (Niebylski et al., 1999; Schumacher et al., 2016; Harris et al., 2017). Furthermore, a differential transcriptional response, including immune components, is activated in ticks when infected with SFG *Rickettsia* (Mulenga et al., 2003; Macaluso et al., 2003; Sunyakumthorn et al., 2013; Martins et al., 2019; Guizzo et al., 2022).

In the current study, the immune factor Relish-type NF-κB was examined in *D. variabilis*. The successful isolation of a full-length transcript of *dvrelish* identified a putative transcription factor responsive to Gram-negative bacteria, as described in other arthropods (Hetru and Hoffmann, 2009). Because there is no genome sequenced for *D. variabilis*, RACE was employed to fully characterize the molecule given the limited transcriptomes with evidence of partial NF-kB transcripts. Identifying the full transcript and its untranslated regions may also provide evidence of regulatory mechanisms for future studies. The *dvrelish* transcript is produced at a low level and only the cDNA from *Rickettsia*-infected *D. variabilis*

10.3389/fcimb.2024.1494450

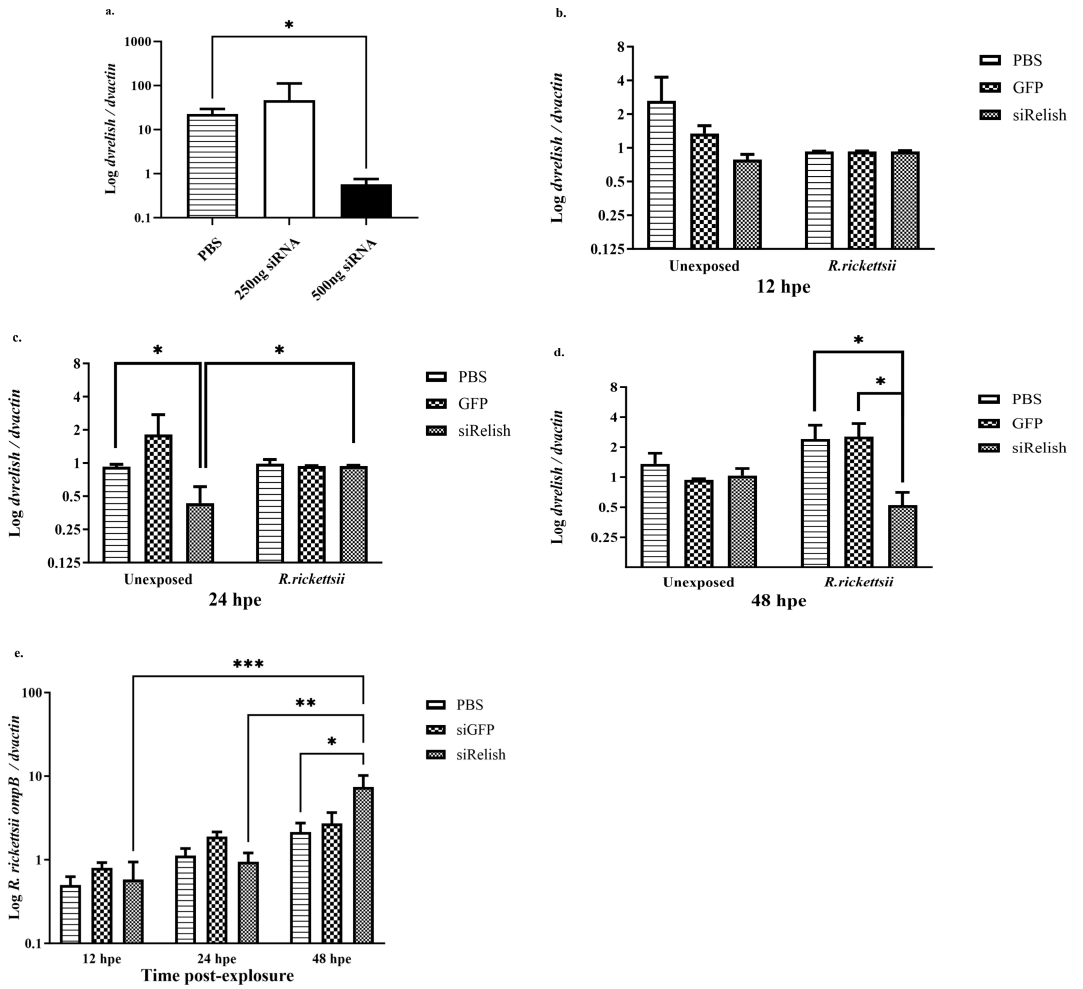

FIGURE 6
(A) Expression of DvRelish mRNA in *D. variabilis* ticks after Relish gene silencing. DvRelish was successfully knocked down using 500 ng of siRNA. **(B–D)** With siRNA, DvRelish mRNA expression was measured in unexposed ticks and *R. rickettsii* exposed ticks at 12, 24, and 48 h post-exposure. The transcription level of the *dvrelish* gene was determined by RT-qPCR and normalized against *dvactin*. **(E)** *R. rickettsii ompB* mRNA levels were assessed after gene knockdown by RT-qPCR and normalized against *dvactin*. Data are presented as mean relative expression, with error bars representing the standard error of the mean (SEM). Statistical significance for DvRelish gene silencing was determined using a *t*-test, with *p*-values ≤ 0.05 considered significant. Statistical significance for siRNA DvRelish in unexposed and *R. rickettsii*-exposed ticks was determined using a two-way ANOVA with Tukey's *post-hoc* test, with a *p*-value ≤ 0.05 considered significant. *$p < 0.05$, **$p < 0.01$, and ***$p < 0.001$.

contained detectable amounts of *dvrelish* transcript. This was not unexpected as infection in arthropods induces the increased transcription of immune-related genes, including those encoding NF-κB proteins (Meister et al., 2005; Tanaka et al., 2007; Antonova et al., 2009). To obtain full-length transcript, RACE-PCR was employed as has been done for other *Dermacentor* genes (Mulenga et al., 2004; Sunyakumthorn et al., 2012; Petchampai et al., 2014). Within the sequence, conserved domain searches identified the RHD of *dvrelish* as Relish type, as opposed to Dorsal/Dif-type. While the nucleotide and amino acid identities are low compared to other model arthropods, the amino acids responsible for the protein function of Relish-type NF-κB are highly conserved in the RHD, IPT domain, and ankyrin repeats. In *Drosophila*, the conserved domains of NF-κB allow for binding to DNA, dimerization, and the binding of the encoded ankyrin repeats for sequestration in the cytoplasm of cells (Hetru and Hoffmann, 2009). While an NF-κB protein has been annotated in the *I. scapularis* genome, the sequence does not contain a critical canonical domain of the ankyrin repeats (Smith and Pal, 2014; Rosa et al., 2016). Dorsal-type NF-κB proteins are unique in having a separate inhibitory protein that sequesters the protein in the cytoplasm; however, Relish proteins have encoded ankyrin repeats, which act as the inhibitory domain (Hetru and Hoffmann, 2009). Once activated, the inhibitory N-terminal portion of the protein is cleaved, the nuclear localization sequence is exposed, and it is translocated into the nucleus of the cell. The presence of encoded ankyrin repeats supports the classification of *dvrelish* as encoding a putative Relish-type NF-κB protein.

To further characterize DvRelish, protein expression was assessed in uninfected, unfed adult female *D. variabilis*. Two protein bands of interest were specifically recognized, and both were analyzed by mass spectrometry. Peptide competition assays confirmed the specificity of the antibody used for detection. The identification of both the full-length DvRelish protein and the cleaved N-terminal DvRelish demonstrated basal levels of expression of DvRelish in tick tissues. Relish-type NF-κB proteins are known to be expressed at basal levels in

model arthropods, and after immune activation, both mRNA transcription and protein translation are increased (Meister et al., 2005; Fan et al., 2008; Tanji et al., 2010). Previous reports also suggest that immune responsive transcription factors are active in ticks infected with SFG *Rickettsia* (Mulenga et al., 2003; Macaluso et al., 2003; Sunyakumthorn et al., 2013; Martins et al., 2019; Guizzo et al., 2022). The influence of signaling mechanisms controlling tissue-specific and bacteria-specific immune responses and how these responses mediate the dissemination of SFG *Rickettsia* in their tick vectors require further study.

Next, we examined the activation mechanisms associated with DvRelish. The canonical Relish of *Drosophila* is a modular protein consisting of two domains, RHD and IκB. The RHD domain enters the nucleus and activates the expression of AMP genes as active transcriptional mediators (Stoven et al., 2003; Meister et al., 2005). Relish was described to be similar to mammalian NF-κB molecules, p105 and p100, which contain the RHD domain (Dushay et al., 1996). Furthermore, activation of Relish can induce immunity and embryogenesis, suggesting that similar proteins were present in primordial immune systems (Dushay et al., 1996). However, Dif, Dorsal, and Relish can form different homo- and heterodimeric combinations that have distinct DNA-binding affinities (Han and Ip, 1999). In the *Drosophila* IMD pathway, after the phosphorylation of Relish, the Rel moiety migrates to the nucleus where it regulates the expression of genes encoding AMPs and many other proteins (De Gregorio et al., 2002; Ferrandon et al., 2007). To assess the DNA binding of DvRelish, we generated rDvRHD for use in an EMSA. Binding of DvRelish RHD to κB motifs suggests that DvRelish is a transcription factor and activates κB motifs to regulate the expression of immune-regulated genes. A direct association between DvRelish binding to κB motifs and abundance of tick AMPs was not investigated in the current study but should be examined.

Because tick hemocytes are important in AMP production (Johns et al., 2001; Hynes et al., 2008), we explored differential expression of DvRelish during bacterial insult. We utilized *P. aeruginosa* as a non-tick-associated bacteria to contrast the tick-borne *R. rickettsii*. Qualitative analysis indicated increased expression of DvRelish in hemocytes from *R. rickettsii*-exposed ticks, compared to *P. aeruginosa*-exposed ticks at 1 hpi. Several variables may account for observed differences including time and origin of stimulation. The expression of Relish-type NF-κB proteins has been previously visualized in cultured *Drosophila* cells indicating nuclear translocation in as little as 10 min post-stimulation with *E. coli* peptidoglycan (PGN) (Stoven et al., 2003). As purified PGN of Gram-positive and Gram-negative bacteria has been shown to elicit AMP production via NF-κB signaling (Hedengren-Olcott et al., 2004), the variance in nuclear translocation of DvRelish in *D. variabilis* hemocytes may be due to differential patterns of induction of NF-κB proteins in ticks as compared to other arthropods. While further analyses including confirmation that hemocytes were infected with bacteria is needed, these results suggest that *R. rickettsii* can induce the expression of Relish-type NF-κB in *D. variabilis* hemocytes.

In arthropods, the role of Relish has been characterized using Relish deletion mutants and resulted in increased host susceptibility to bacterial and fungal infection (Hedengren et al., 1999). In the current study, we hypothesized that if DvRelish is critical for the tick innate immune response to infection, silencing the expression of *dvrelish* gene would increase the number of *R. rickettsii* in the ticks. First, the expression of *dvrelish* was confirmed to be significantly reduced in *D. variabilis* with 500 ng of siRNA at 6 h post-injection. Then, to test the hypothesis, siRNA-treated ticks were exposed to *R. rickettsii* and *dvrelish* transcription and rickettsial load were assessed over 48 h. At 48 h post-exposure, there was a significant decrease in *dvrelish* transcription in the treated groups, compared to no siRNA or the non-specific GFP-siRNA control. The reduced *dvrelish* transcription corresponded with increased rickettsial load at 48 h compared to control treatments. The results are consistent with what has been reported for *Anaplasma marginale* infection in *Rhipicephalus microplus*, where RNA-mediated silencing of Relish was associated with significantly greater *A. marginale* loads (Capelli-Peixoto et al., 2017). Overall, the data suggest an inverse relationship between Relish function and rickettsial loads.

The tick immune response and vector interactions with SFG *Rickettsia* have been recently reviewed (Fogaça et al., 2021; Kim, 2022). In the current study, a full-length *dvrelish* transcript was isolated and partially characterized in the tick *D. variabilis*. Further study is needed to examine the signaling that induces DvRelish and the tissue-associated immune molecules that are produced as a result of activation. For example, in *D. andersoni*, blocking IRE1α, an upstream inducer of Relish, led to increased bacterial loads in tick midgut and salivary glands (Sidak-Loftis et al., 2022). While *A. marginale* infection did not induce changes in Relish transcription in *R. microplus* midguts and salivary glands, knockdown of Relish was associated with a decrease in the AMP microplusin and an increase in bacterial loads in these tissues. The tick species and tissue-specific nature are intriguing as it has been reported that basal levels of AMPs are present in the tick midgut (Guizzo et al., 2024), whereas in *Amblyomma maculatum*, infection with *Rickettsia parkeri* induces transcription of more than 11,000 immune-related genes, including Relish, in tick hemocytes (Adegoke et al., 2023). The current study provides novel insight into a unique tick–pathogen system that can serve as a basis to better understand how SFG *Rickettsia* navigate the tick immune response to persist within vector populations.

Data availability statement

The datasets presented in this study can be found in online repositories. The names of the repository/repositories and accession number(s) can be found below: https://www.ncbi.nlm.nih.gov/genbank/, KJ484815.

Ethics statement

The manuscript presents research on animals that do not require ethical approval for their study.

Author contributions

CF: Conceptualization, Data curation, Formal analysis, Investigation, Methodology, Validation, Visualization, Writing – original draft, Writing – review & editing. VV: Conceptualization, Data curation, Formal analysis, Investigation, Methodology, Software, Validation, Visualization, Writing – original draft, Writing – review & editing. KJ: Investigation, Methodology, Writing – review & editing. EH: Investigation, Methodology, Writing – review & editing. KM: Conceptualization, Funding acquisition, Project administration, Supervision, Writing – review & editing.

Funding

The author(s) declare financial support was received for the research, authorship, and/or publication of this article. The research was supported by the National Institutes of Health (NIH) (to KM, AI077784).

Acknowledgments

We thank Natthida Petchampai and Sean Riley for technical assistance with the study. A portion of this study was a component of a dissertation by VV.

Conflict of interest

The authors declare that the research was conducted in the absence of any commercial or financial relationships that could be construed as a potential conflict of interest.

Publisher's note

Supplementary material

The Supplementary Material for this article can be found online at: https://www.frontiersin.org/articles/10.3389/fcimb.2024.1494450/full#supplementary-material

SUPPLEMENTARY FIGURE 1
Expression of DvRelish Rel homology domain (RHD) in transfected HEK293T cells. HEK293T cells transfected with DvRelish-pAcGFP. The transfected cells were visualized under fluorescence microscope.

References

Adegoke, A., Ribeiro, J. M. C., Brown, S., Smith, R. C., and Karim, S. (2023). *Rickettsia parkeri* hijacks tick hemocytes to manipulate cellular and humoral transcriptional responses. *Front. Immunol.* 14. doi: 10.3389/fimmu.2023.1094326

Antonova, Y., Alvarez, K. S., Kim, Y. J., Kokoza, V., and Raikhel, A. S. (2009). The role of NF-kappaB factor REL2 in the Aedes aEgypti immune response. *Insect Biochem. Mol. Biol.* 39, 303–314. doi: 10.1016/j.ibmb.2009.01.007

Bissinger, B. W., Donohue, K. V., Khalil, S. M., Grozinger, C. M., Sonenshine, D. E., Zhu, J., et al. (2011). Synganglion transcriptome and developmental global gene expression in adult females of the American dog tick, Dermacentor variabilis (Acari: Ixodidae). *Insect Mol. Biol.* 20, 465–491. doi: 10.1111/j.1365-2583.2011.01086.x

Capelli-Peixoto, J., Carvalho, D. D., Johnson, W. C., Scoles, G. A., Fogaça, A. C., Daffre, S., et al. (2017). The transcription factor Relish controls Anaplasma marginale infection in the bovine tick Rhipicephalus microplus. *Dev. Comp. Immunol.* 74, 32–39. doi: 10.1016/j.dci.2017.04.005

Chan, Y. G., Riley, S. P., Chen, E., and Martinez, J. J. (2011). Molecular basis of immunity to rickettsial infection conferred through outer membrane protein B. *Infect. Immun.* 79, 2303–2313. doi: 10.1128/IAI.01324-10

De Gregorio, E., Spellman, P. T., Tzou, P., Rubin, G. M., and Lemaitre, B. (2002). The Toll and Imd pathways are the major regulators of the immune response in Drosophila. *EMBO J.* 21, 2568–2579. doi: 10.1093/emboj/21.11.2568

Dushay, M. S., Asling, B., and Hultmark, D. (1996). Origins of immunity: Relish, a compound Rel-like gene in the antibacterial defense of Drosophila. *Proc. Natl. Acad. Sci. U S A.* 93, 10343–10347. doi: 10.1073/pnas.93.19.10343

Esteves, E., Fongsaran, C., Langohr, I. M., Riley, S. P., Labruna, M. B., Daffre, S., et al. (2020). Comparative analysis of infection by *rickettsia rickettsii* sheila smith and taiaçu strains in a murine model. *Pathogens.* 9, 744. doi: 10.3390/pathogens9090744

Fan, Z. H., Wang, X. W., Lu, J., Ho, B., and Ding, J. L. (2008). Elucidating the function of an ancient NF-kappaB p100 homologue, CrRelish, in antibacterial defense. *Infect. Immun.* 76, 664–670. doi: 10.1128/IAI.00948-07

Ferrandon, D., Imler, J. L., Hetru, C., and Hoffmann, J. A. (2007). The Drosophila systemic immune response: sensing and signalling during bacterial and fungal infections. *Nat. Rev. Immunol.* 7, 862–874. doi: 10.1038/nri2194

Fogaça, A. C., Sousa, G., Pavanelo, D. B., Esteves, E., Martins, L. A., Urbanová, V., et al. (2021). Tick immune system: what is known, the interconnections, the gaps, and the challenges. *Front. Immunol.* 12. doi: 10.3389/fimmu.2021.628054

Guizzo, M. G., Budachetri, K., Adegoke, A., Ribeiro, J. M. C., and Karim, S. (2022). *Rickettsia parkeri* infection modulates the sialome and ovariome of the Gulf coast tick, Amblyomma maculatum. *Front. Microbiol.* 13. doi: 10.3389/fmicb.2022.1023980

Guizzo, M. G., Frantová, H., Lu, S., Kozelková, T., Číhalová, K., Dyčka, F., et al. (2024). The immune factors involved in the rapid clearance of bacteria from the midgut of the tick Ixodes ricinus. *Front. Cell Infect. Microbiol.* 14. doi: 10.3389/fcimb.2024.1450353

Gulia-Nuss, M., Nuss, A. B., Meyer, J. M., Sonenshine, D. E., Roe, R. M., Waterhouse, R. M., et al. (2016). Genomic insights into the Ixodes scapularis tick vector of Lyme disease. *Nat. Commun.* 7, 10507. doi: 10.1038/ncomms10507

Han, Z. S., and Ip, Y. T. (1999). Interaction and specificity of Rel-related proteins in regulating Drosophila immunity gene expression. *J. Biol. Chem.* 274, 21355–21361. doi: 10.1074/jbc.274.30.21355

Harris, E. K., Verhoeve, V. I., Banajee, K. H., Macaluso, J. A., Azad, A. F., and Macaluso, K. R. (2017). Comparative vertical transmission of Rickettsia by Dermacentor variabilis and Amblyomma maculatum. *Ticks Tick Borne Dis.* 8, 598–604. doi: 10.1016/j.ttbdis.2017.04.003

Hedengren, M., Asling, B., Dushay, M. S., Ando, I., Ekengren, S., Wihlborg, M., et al. (1999). Relish, a central factor in the control of humoral but not cellular immunity in Drosophila. *Mol. Cell.* 4, 827–837. doi: 10.1016/s1097-2765(00)80392-5

Hedengren-Olcott, M., Olcott, M. C., Mooney, D. T., Ekengren, S., Geller, B. L., and Taylor, B. J. (2004). Differential activation of the NF-kappaB-like factors Relish and Dif in Drosophila melanogaster by fungi and Gram-positive bacteria. *J. Biol. Chem.* 279, 21121–21127. doi: 10.1074/jbc.M313856200

Hetru, C., and Hoffmann, J. A. (2009). NF-kappaB in the immune response of Drosophila. *Cold Spring Harb. Perspect. Biol.* 1, a000232. doi: 10.1101/cshperspect.a000232

Hynes, W. L., Stokes, M. M., Hensley, S. M., Todd, S. M., and Sonenshine, D. E. (2008). Using RNA interference to determine the role of varisin in the innate immune system of the hard tick Dermacentor variabilis (Acari: Ixodidae). *Exp. Appl. Acarol.* 46, 7–15. doi: 10.1007/s10493-008-9158-6

Jaworski, D. C., Zou, Z., Bowen, C. J., Wasala, N. B., Madden, R., Wang, Y., et al. (2010). Pyrosequencing and characterization of immune response genes from the American dog tick, Dermacentor variabilis (L.). *Insect Mol. Biol.* 19, 617–630. doi: 10.1111/j.1365-2583.2010.01037.x

Jiang, J., Blair, P. J., Felices, V., Moron, C., Cespedes, M., Anaya, E., et al. (2005). Phylogenetic analysis of a novel molecular isolate of spotted fever group Rickettsiae from northern Peru: Candidatus Rickettsia andeanae. *Ann. N Y Acad. Sci.* 1063, 337–342. doi: 10.1196/annals.1355.054

Johns, R., Sonenshine, D. E., and Hynes, W. L. (2001). Identification of a defensin from the hemolymph of the American dog tick, Dermacentor variabilis. *Insect Biochem. Mol. Biol.* 31, 857–865. doi: 10.1016/s0965-1748(01)00031-5

Kim, H. K. (2022). *Rickettsia*-host-tick interactions: knowledge advances and gaps. *Infect. Immun.* 90, e0062121. doi: 10.1128/iai.00621-21

Koressaar, T., and Remm, M. (2007). Enhancements and modifications of primer design program Primer3. *Bioinformatics.* 23, 1289–1291. doi: 10.1093/bioinformatics/btm091

Kosugi, S., Hasebe, M., Tomita, M., and Yanagawa, H. (2009). Systematic identification of cell cycle-dependent yeast nucleocytoplasmic shuttling proteins by prediction of composite motifs. *Proc. Natl. Acad. Sci. U S A.* 106, 10171–10176. doi: 10.1073/pnas.0900604106

Macaluso, K. R., Mulenga, A., Simser, J. A., and Azad, A. F. (2003). Differential expression of genes in uninfected and rickettsia-infected Dermacentor variabilis ticks as assessed by differential-display PCR. *Infect. Immun.* 71, 6165–6170. doi: 10.1128/IAI.71.11.6165-6170.2003

Macaluso, K. R., Sonenshine, D. E., Ceraul, S. M., and Azad, A. F. (2001). Infection and transovarial transmission of rickettsiae in Dermacentor variabilis ticks acquired by artificial feeding. *Vector Borne Zoonotic Dis.* 1, 45–53. doi: 10.1089/153036601750137660

Martins, L. A., Malossi, C. D., Galletti, M. F. B. M., Ribeiro, J. M., Fujita, A., Esteves, E., et al. (2019). The Transcriptome of the Salivary Glands of *Amblyomma aureolatum* Reveals the Antimicrobial Peptide Microplusin as an Important Factor for the Tick Protection Against *Rickettsia rickettsii* Infection. *Front. Physiol.* 10. doi: 10.3389/fphys.2019.00529

Meister, S., Kanzok, S. M., Zheng, X. L., Luna, C., Li, T. R., Hoa, N. T., et al. (2005). Immune signaling pathways regulating bacterial and malaria parasite infection of the mosquito Anopheles Gambiae. *Proc. Natl. Acad. Sci. U S A.* 102, 11420–11425. doi: 10.1073/pnas.0504950102

Mulenga, A., Macaluso, K. R., Simser, J. A., and Azad, A. F. (2003). Dynamics of Rickettsia-tick interactions: identification and characterization of differentially expressed mRNAs in uninfected and infected Dermacentor variabilis. *Insect Mol. Biol.* 12, 185–193. doi: 10.1046/j.1365-2583.2003.00400.x

Mulenga, A., Simser, J. A., Macaluso, K. R., and Azad, A. F. (2004). Stress and transcriptional regulation of tick ferritin HC. *Insect Mol. Biol.* 13, 423–433. doi: 10.1111/j.0962-1075.2004.00502.x

Niebylski, M. L., Peacock, M. G., and Schwan, T. G. (1999). Lethal effect of Rickettsia rickettsii on its tick vector (Dermacentor andersoni). *Appl. Environ. Microbiol.* 65, 773–778. doi: 10.1128/AEM.65.2.773-778.1999

O'Neal, A. J., Singh, N., Rolandelli, A., Laukaitis, H. J., Wang, X., Shaw, D. K., et al. (2023). Croquemort elicits activation of the immune deficiency pathway in ticks. *Proc. Natl. Acad. Sci. U S A.* 120, e2208673120. doi: 10.1073/pnas.2208673120

Perlman, S. J., Hunter, M. S., and Zchori-Fein, E. (2006). The emerging diversity of *Rickettsia*. *Proc. Biol. Sci.* 273, 2097–2106. doi: 10.1098/rspb.2006.3541

Petchampai, N., Sunyakumthorn, P., Guillotte, M. L., Thepparit, C., Kearney, M. T., Mulenga, A., et al. (2014). Molecular and functional characterization of vacuolar-ATPase from the American dog tick Dermacentor variabilis. *Insect Mol. Biol.* 23, 42–51. doi: 10.1111/imb.12059

Rosa, R. D., Capelli-Peixoto, J., Mesquita, R. D., Kalil, S. P., Pohl, P. C., Braz, G. R., et al. (2016). Exploring the immune signaling pathway-related genes of the cattle tick Rhipicephalus microplus: From molecular characterization to transcriptional profile upon microbial challenge. *Dev. Comp. Immunol.* 59, 1–14. doi: 10.1016/j.dci.2015.12.018

Schumacher, L., Snellgrove, A., and Levin, M. L. (2016). Effect of Rickettsia rickettsii (Rickettsiales: Rickettsiaceae) Infection on the Biological Parameters and Survival of Its Tick Vector-Dermacentor variabilis (Acari: Ixodidae). *J. Med. Entomol.* 53, 172–176. doi: 10.1093/jme/tjv166

Shaw, D. K., Wang, X., Brown, L. J., Chávez, A. S., Reif, K. E., Smith, A. A., et al. (2017). Infection-derived lipids elicit an immune deficiency circuit in arthropods. *Nat. Commun.* 8, 14401. doi: 10.1038/ncomms14401

Sidak-Loftis, L. C., Rosche, K. L., Pence, N., Ujczo, J. K., Hurtado, J., Fisk, E. A., et al. (2022). The unfolded-protein response triggers the arthropod immune deficiency pathway. *mBio.* 13, e0070322. doi: 10.1128/mbio.00703-22

Smith, A. A., and Pal, U. (2014). Immunity-related genes in Ixodes scapularis–perspectives from genome information. *Front. Cell Infect. Microbiol.* 4. doi: 10.3389/fcimb.2014.00116

Sonenshine, D. E., Bissinger, B. W., Egekwu, N., Donohue, K. V., Khalil, S. M., and Roe, R. M. (2011). First transcriptome of the testis-vas deferens-male accessory gland and proteome of the spermatophore from Dermacentor variabilis (Acari: Ixodidae). *PLoS One* 6, e24711. doi: 10.1371/journal.pone.0024711

Sonenshine, D. E., and Macaluso, K. R. (2017). Microbial invasion vs. Tick immune regulation. *Front. Cell Infect. Microbiol.* 7. doi: 10.3389/fcimb.2017.00390

Stoven, S., Silverman, N., Junell, A., Hedengren-Olcott, M., Erturk, D., Engstrom, Y., et al. (2003). Caspase-mediated processing of the Drosophila NF-kappaB factor Relish. *Proc. Natl. Acad. Sci. U S A.* 100, 5991–5996. doi: 10.1073/pnas.1035902100

Sunyakumthorn, P., Bourchookarn, A., Pornwiroon, W., David, C., Barker, S. A., and Macaluso, K. R. (2008). Characterization and growth of polymorphic Rickettsia felis in a tick cell line. *Appl. Environ. Microbiol.* 74, 3151–3158. doi: 10.1128/AEM.00025-08

Sunyakumthorn, P., Petchampai, N., Grasperge, B. J., Kearney, M. T., Sonenshine, D. E., and Macaluso, K. R. (2013). Gene expression of tissue-specific molecules in ex vivo Dermacentor variabilis (Acari: Ixodidae) during rickettsial exposure. *J. Med. Entomol.* 50, 1089–1096. doi: 10.1603/me12162

Sunyakumthorn, P., Petchampai, N., Kearney, M. T., Sonenshine, D. E., and Macaluso, K. R. (2012). Molecular characterization and tissue-specific gene expression of Dermacentor variabilis α-catenin in response to rickettsial infection. *Insect Mol. Biol.* 21, 197–204. doi: 10.1111/j.1365-2583.2011.01126.x

Tanaka, H., Matsuki, H., Furukawa, S., Sagisaka, A., Kotani, E., Mori, H., et al. (2007). Identification and functional analysis of Relish homologs in the silkworm, Bombyx mori. *Biochim. Biophys. Acta* 1769, 559–568. doi: 10.1016/j.bbaexp.2007.07.001

Tanji, T., Yun, E. Y., and Ip, Y. T. (2010). Heterodimers of NF-kappaB transcription factors DIF and Relish regulate antimicrobial peptide genes in Drosophila. *Proc. Natl. Acad. Sci. U S A.* 107, 14715–14720. doi: 10.1073/pnas.1009473107

Untergasser, A., Cutcutache, I., Koressaar, T., Ye, J., Faircloth, B. C., Remm, M., et al. (2012). Primer3–new capabilities and interfaces. *Nucleic Acids Res.* 40, e115. doi: 10.1093/nar/gks596

Wilkins, M. R., Lindskog, I., Gasteiger, E., Bairoch, A., Sanchez, J. C., Hochstrasser, D. F., et al. (1997). Detailed peptide characterization using PEPTIDEMASS–a World-Wide-Web-accessible tool. *Electrophoresis.* 18, 403–408. doi: 10.1002/elps.1150180314

frontiers | Frontiers in Immunology

TYPE Original Research
PUBLISHED 03 April 2025
DOI 10.3389/fimmu.2025.1479862

OPEN ACCESS

EDITED BY
Deepak Kumar,
University of Southern Mississippi,
United States

REVIEWED BY
Zhuo Ma,
Albany College of Pharmacy and Health Sciences, United States
Jyotirmayee Dey,
KIIT University, India

*CORRESPONDENCE
Farzad Badmasti
fbadmasti2008@gmail.com

RECEIVED 12 August 2024
ACCEPTED 17 March 2025
PUBLISHED 03 April 2025

CITATION
Moradkasani S, Esmaeili S, Asadi Karam MR, Mostafavi E, Shahbazi B, Salek Farrokhi A, Chiani M and Badmasti F (2025) Development of a multi-epitope vaccine from outer membrane proteins and identification of novel drug targets against *Francisella tularensis*: an *In Silico* approach. *Front. Immunol.* 16:1479862. doi: 10.3389/fimmu.2025.1479862

Development of a multi-epitope vaccine from outer membrane proteins and identification of novel drug targets against *Francisella tularensis*: an *In Silico* approach

Safoura Moradkasani[1,2], Saber Esmaeili[1,2,3], Mohammad Reza Asadi Karam[4], Ehsan Mostafavi[1,3], Behzad Shahbazi[5,6], Amir Salek Farrokhi[7], Mohsen Chiani[8] and Farzad Badmasti[9]*

[1]WHO Collaborating Centre for Vector-Borne Diseases, Department of Epidemiology and Biostatistics, Research Centre for Emerging and Reemerging Infectious Diseases, Pasteur Institute of Iran, Tehran, Iran, [2]Student Research Committee, Pasteur Institute of Iran, Tehran, Iran, [3]National Reference Laboratory for Plague, Tularemia and Q Fever, Research Centre for Emerging and Reemerging Infectious Diseases, Pasteur Institute of Iran, Akanlu, KabudarAhang, Hamadan, Iran, [4]Department of Molecular Biology, Pasteur Institute of Iran, Tehran, Iran, [5]School of Pharmacy, Semnan University of Medical Sciences, Semnan, Iran, [6]Nervous System Stem Cells Research Center, Semnan University of Medical Sciences, Semnan, Iran, [7]Department of Immunology, Pasteur Institute of Iran, Tehran, Iran, [8]Department of Nanobiotechnology, Pasteur Institute of Iran, Tehran, Iran, [9]Department of Bacteriology, Pasteur Institute of Iran, Tehran, Iran

Background: *Francisella tularensis* is a category A potential thread agent, making the development of vaccines and countermeasures a high priority. Therefore, identifying new vaccine candidates and novel drug targets is essential for addressing this significant public health concern.

Methods: This study presents an *in silico* analysis of two strategies against *F. tularensis* infection: the development of a multi-epitope vaccine (MEV) and the identification of novel drug targets. Outer membrane proteins (OMPs) were predicted using subcellular localization tools and immunogenicity was evaluated using a reverse vaccinology pipeline. Epitopes from these OMPs were combined to create candidate MEV for prophylactic protection. Concurrently, cytoplasmic proteins were subjected to rigorous analysis to identify potential novel drug targets.

Results: Of 1,921 proteins, we identified 12 promising protein vaccine candidates from *F. tularensis* OMPs and proposed a multi-epitope vaccine (MEV) designed using seven immunodominant epitopes derived from four of these OMPs, including two hypothetical proteins (WP_003026145.1 and WP_003029346.1), an OmpA family protein (WP_003020808.1), and PD40 (WP_003021546.1). In addition, we proposed 10 novel drug targets for *F. tularensis*: Asp-tRNA (Asn)/Glu-tRNA (Gln) amidotransferase subunit GatC (WP_003017413.1), NAD(P)-binding protein (WP_042522581.1), 30S ribosomal protein S16 (WP_003023081.1), Class I SAM-dependent methyltransferase (WP_003022345.1), haloacid dehalogenase (WP_003014157.1), uroporphyrinogen-III synthase (WP_003022220.1), and four

hypothetical proteins (WP_003017784.1, WP_003020080.1, WP_003020066.1, and WP_003022350.1).

Conclusion: This study designed an MEV and proposed novel drug targets to address tularemia, offering broad protection against various *F. tularensis* strains. MEV, with favorable physicochemical properties, showed strong potential through molecular docking and dynamic simulations. Immune simulations suggest that it may elicit robust responses against pathogens. The identification of novel drug targets can lead to the discovery of new antimicrobial agents. However, further *in vitro* and *in vivo* studies are required to validate their efficacy and capability.

KEYWORDS

***Francisella tularensis*, tularemia, multi-epitope vaccine, reverse vaccinology, drug target**

1 Introduction

Tularemia is an acute zoonotic disease caused by *Francisella tularensis*, a Gram-negative intracellular coccobacillus that poses a significant threat to human health (1). The disease is primarily caused by two subspecies: *F. tularensis* subsp. *tularensis* (type A) and *F. tularensis* subsp. *holarctica* (type B), with type A being the most virulent (2). Without antibiotic treatment, tularemia can lead to a mortality rate as high as 30% (3). Recognizing its potential as a bioweapon, the Centers for Disease Control and Prevention (CDC) classifies *F. tularensis* as a Category A bioterrorism agent, underscoring the urgent need for effective medical countermeasures (3). The main antibiotics used to treat tularemia include fluoroquinolones, tetracyclines, and aminoglycosides (4). However, *F. tularensis* exhibits resistance to several commonly used antibiotics including penicillin, polymyxin B, erythromycin, azithromycin, and carbapenems (4, 5). Given these challenges, ongoing research on novel molecular structures with unique mechanisms of action, supported by microbial genome analysis, is essential for identifying new drug targets, particularly for pathogens that are difficult to culture (6).

Despite extensive efforts, an approved vaccine for human tularemia remains elusive, primarily because of the complex immune evasion strategies employed by *F. tularensis* (7). Although B-cells generate antibodies, these are insufficient for complete protection. The intracellular nature of the bacterium significantly limits the effectiveness of the humoral response, emphasizing the critical role of T-cells, particularly the CD4+ and CD8+ subsets, in providing long-lasting immunity. T-cells contribute to bacterial clearance through cytokine production and the coordination of the immune response, underscoring the need for robust T-cell-mediated immunity. Given the limitations of traditional vaccines and the intricate immune response required to combat *F. tularensis* effectively, the development of a subunit vaccine that elicits strong coordinated T-cell and B-cell responses is essential. This strategy focuses on harnessing key immunodominant epitopes to activate both arms of the immune system to counteract the immune evasion mechanisms of bacteria and deliver comprehensive protection (8). Although conventional multi-antigen vaccines have limitations, peptide-based multi-epitope vaccines (MEVs) represent significant advancements. By leveraging *in silico* methods, MEVs can efficiently identify and target immunodominant epitopes, thereby addressing many shortcomings inherent in traditional vaccine approaches (9, 10). Traditional vaccine development is typically time-consuming and costly and requires extensive *in vivo* and *in vitro* testing (11). However, advances in computational biology and bioinformatics have revolutionized this process, enabling the rapid design of highly effective vaccine constructs and significantly reducing dependence on labor-intensive traditional laboratory methods (12). Reverse vaccinology is a transformative computational approach that leverages genomic data to design vaccine candidates, without the need for pathogen cultivation. By analyzing protein sequences, this method identifies multiple epitopes that trigger both cellular and humoral immune responses, while minimizing side effects (13, 14). Unlike traditional methods, it uncovers both known and novel antigens, opens new pathways for immune interventions, and enhances our understanding of pathogen-host interactions (15). Epitope-based immune-derived vaccines (IDVs) offer significant safety and efficacy advantages over conventional vaccines, particularly against complex pathogens, such as *F. tularensis*, which employs advanced immune evasion strategies. IDVs enhance T-cell responses, which are crucial for long-lasting immunity (16). Reverse vaccinology has successfully prioritized and designed vaccine targets for various pathogens (17–21). MEVs have emerged as effective solutions that incorporate key epitopes to stimulate stronger immune responses, thereby offering superior protection against infectious diseases (22).

In light of these considerations, our study proposes a comprehensive, two-pronged approach to combat tularemia. The

first objective is to design an MEV that not only elicits a strong immune response but also effectively targets the unique challenges posed by this intracellular pathogen. By focusing on key immunodominant epitopes, we aimed to activate both T-cell and B-cell pathways, creating a balanced immune response that addresses the complexities of immune evasion by *F. tularensis*. The second objective was to identify new drug targets, potentially leading to novel therapeutic options for the treatment of tularemia. This integrated approach holds significant promise for the development of effective vaccines and therapeutics. By combining cutting-edge computational methods with deep immunological insights, our research aims to pave the way for innovative strategies for preventing and treating tularemia.

2 Materials and methods

2.1 Design of multi-epitope subunit

2.1.1 Genomic sequence retrieval

A total of 686 *F. tularensis* strains with complete genome sequences were retrieved from the GenBank database (https://www.ncbi.nlm.nih.gov/genbank/), and their proteomes were extracted for core/pan-genome analysis with BPGA software (Bacterial Pan Genome Analysis Tool), version 1.3 (23) based on the USEARCH algorithm. The BPGA analysis of these 686 strains revealed that *F. tularensis* had an open pan-genome and there was a significant genomic diversity within *F. tularensis*. Based on these findings, the *F. tularensis* strain 2017317779 was selected as the reference strain. This strain was classified as *F. tularensis* type A and was isolated from the lung tissue of a patient with tularemia in the USA in 2017 (24). The protein-coding sequences of this strain were annotated and used for further analysis.

2.1.2 Prediction of subcellular localization

The subcellular localization of all *F. tularensis* strain 2017317779 (GenBank: CP073122), used as a reference strain, was predicted using both of PSORTb v3.0.3 (www.psort.org/psortb/) and CELLO version 2.5 (http://cello.life.nctu.edu.tw/) for more accuracy. The results were confirmed with the TMHMM Server v2.0 web tool (https://services.healthtech.dtu.dk/service.php?TMHMM-2.0) (25–27). At this stage, only the surface-exposed proteins including extracellular and outer membrane proteins (OMPs) of *F. tularensis* strain 2017317779 (GenBank: CP073122) were considered for further analysis.

2.1.3 Determination of the overall antigenicity and allergenicity

The antigenicity of the putative immunogenic targets was assessed using the VaxiJen web tool (http://www.ddg-pharmfac.net/vaxijen/VaxiJen/VaxiJen.html), with a cutoff value of ≥ 0.5. This tool utilizes Auto-Cross Covariance (ACC) transformation, converts sequences into uniform vectors based on the chemical properties of proteins, and provides predictions with an accuracy ranging from 70% to 89% (28). To evaluate allergenicity, we employed the AlgPred 2.0 server (https://webs.iiitd.edu.in/raghava/algpred2/batch.html), using a cutoff value of ≥ 0.5. This server integrates six distinct methodologies: (i) IgE mapping, (ii) MEME/Mast motif analysis, (iii) support vector machine (SVM) modules based on both amino acid and dipeptide compositions, (iv) BLAST searches against allergen-representative proteins (ARPs), and (v) a hybrid approach that combines all parameters. While MEME/Mast analysis, BLAST, and IgE mapping indicated non-allergenicity, the SVM modules and hybrid approach suggested potential allergenicity. To ensure a comprehensive evaluation, we performed an additional allergenicity assessment using AllerTOP v2.0 (https://www.ddg-pharmfac.net/AllerTOP/), which corroborated the non-allergenic nature of these proteins. Based on the combined results from both servers, we concluded that vaccine candidates are likely non-allergenic (29, 30).

2.1.4 Homology analysis of immunogenic targets against the human proteome

All selected proteins were analyzed for sequence similarity to the human proteome (*Homo sapiens*, Taxid: 9606) using the PSI-BLAST tool in the BLASTp database (https://blast.ncbi.nlm.nih.gov/Blast.cgi?SIDE=protein). Proteins with significant similarities were excluded to prevent cross-reactivity.

2.1.5 Prevalence of putative immunogenic targets among *F. tularensis* strains

The prevalence and conservation of proteins among these strains were assessed to induce a strong immune response against all *F. tularensis* strains. Homologs of each immunogenic target in the 686 *F. tularensis* strains were retrieved using BLASTp and aligned using MegaX software (31). Proteins with a prevalence > 90% were selected for further analysis (32).

2.1.6 Linear B-cell, T-cell epitopes, and quartile scoring

The VICMpred database (https://webs.iiitd.edu.in/raghava/vicmpred/submission.html) was used to categorize the functional roles of the proteins into four distinct classes: virulence, cellular processes, metabolic molecules, and unknown (33). To identify linear B-cell epitopes in the selected proteins, we used the BepiPred-2.0 tool (https://services.healthtech.dtu.dk/service.php?BepiPred-2.0), with a threshold of ≥ 0.6 (34). The B-cell epitope ratio was calculated by dividing the number of amino acids in the identified epitopes by the total amino acid count for each protein. Subsequently, TepiTool (http://tools.iedb.org/tepitool/), a resource from the Immune Epitope Database (IEDB), was used to predict binding sites for human MHC I and MHC II. For MHC I, binding sites were chosen from the top 5% of peptides, prioritizing those prevalent in the reference HLA allele set for the normal human population (35). The MHC II binding site ratio was calculated by dividing the number of MHC II binding sites by the total amino acid content in each protein. A quartile scoring method was then applied to evaluate each protein based on three indicators: functional class, MHC II binding site ratio, and B-cell epitope

ratio. The overall score for each protein was calculated by summing the individual scores of these indicators. Finally, proteins in the top quartile with the highest cumulative scores were selected.

2.1.7 Protein domain search and predicting of physiochemical characteristics of immunogenic targets

The Conserved Domain Database (CDD) (https://www.ncbi.nlm.nih.gov/Structure/cdd/cdd.shtml) and EggNOG (http://eggnog5.embl.de/#/app/home) were used to identify the functional domains and classification of the proteins. CDD, a part of the NCBI Entrez query system, annotates the location of conserved domains in protein sequences (36, 37). The Expasy ProtParam online tool (https://web.expasy.org/protparam/) was used to calculate the molecular weights and theoretical isoelectric points of the selected proteins (38).

2.1.8 Tertiary structure prediction and characterization of the conformational B-cell epitopes

The Swiss Model (https://swissmodel.expasy.org/) was used to predict the 3D structures of the selected proteins (39). To assess and validate the quality and stability of these models, we used the ProSA-web server (https://prosa.services.came.sbg.ac.at/prosa.php) and ERRAT (https://saves.mbi.ucla.edu/results?Job%20=1243713,%20p=errat) to detect potential errors (40, 41). Conformational B-cell epitopes were identified using the ElliPro server (http://tools.iedb.org/ellipro/) at a threshold of ≥ 0.8. The predicted epitopes were then visualized on the protein surface using Jmol software, with each epitope represented by different colors for clarity (42).

2.1.9 Analysis of protein-protein interactions

The STRING software (https://string-db.org/) server was used to analyze the interaction network of proteins with unknown functions (43). In this analysis, interactions with high confidence scores > 0.7 were considered to minimize false-positive and false-negative results (44).

2.1.10 Prediction and selection of optimal epitopes for vaccine target

B-lymphocytes are crucial in humoral immunity and produce antibodies that detect and neutralize pathogens. To identify potential vaccine targets, the selected protein sequences were scanned for linear B-cell epitopes using the Kolaskar-Tongaonkar algorithm within the Antibody Epitope Prediction tool hosted on the Immune Epitope Database (IEDB) analysis server (http://tools.iedb.org) (35). The predicted B-cell epitopes were evaluated for MHC I processing compatibility, focusing on the most prevalent HLA alleles in Iran, using the IEDB server (35). The VaxiJen web tool (http://www.ddg-pharmfac.net/vaxijen/VaxiJen/VaxiJen.html) was used to predict the antigenicity of putative immunogenic epitopes, with a cut-off value of ≥ 0.5. Additionally, AlgPred 2.0 serve (https://webs.iiitd.edu.in/raghava/algpred2/batch.html) was employed with a cut-off value ≥ 0.5 to investigate the allergenicity of these epitopes. Epitope conservation and hydropathicity were determined using the IEDB analysis server (http://tools.iedb.org/conservancy/). Epitopes that were antigenic and non-allergenic showed > 90% conservation, and the lowest hydropathicity scores were selected as potential candidates for subunit vaccine development.

2.1.11 Structural construction and validation of the vaccine candidate

Effective vaccine design requires appropriate antigenic peptide folding and linker incorporation to maintain epitope integrity, prevent unintended junctional epitopes, and enhance immunogenicity. Without suitable linkers, multi-epitope vaccines may generate unwanted proteins or epitopes, reducing their effectiveness and stability (45). To construct an MEV against *F. tularensis*, linear B-cell epitopes were fused using flexible GPGPG linkers. These flexible linkers, composed of small amino acids, such as glycine and serine, ensure adequate separation between epitope domains and minimize junctional epitope formation, allowing the protein domains to move freely and facilitating proper protein folding. Flexible linkers are also advantageous for enhancing antibody accessibility to epitopes and improving the folding efficiency (46, 47). To optimize antigenicity, epitope shuffling techniques were used to identify the best epitope arrangement with the highest antigenicity score. The 3D structures of the selected proteins were predicted using the Swiss Model (https://swissmodel.expasy.org/) (39). The quality and stability of the 3D models were further evaluated using the ProSA-web (https://prosa.services.came.sbg.ac.at/prosa.php) and ERRAT (https://saves.mbi.ucla.edu/results?Job%20=1243713,%20p=errat) servers to detect structural errors (40, 41). Furthermore, the affinities of the multi-epitope vaccine against human Toll-like receptor 2 (TLR2, PDB: 2Z7X), human Toll-like receptor 4 (TLR4 PDB: 3FXI), HLA-DR-B (PBD: 3PDO_B), and HLA-A chain A (PDB:8XG2_A) were evaluated using the HDOCK web tool (http://hdock.phys.hust.edu.cn/) (48). The interactions of the docked complexes were visualized and validated using the PDBsum server (https://www.ebi.ac.uk/thornton-srv/databases/pdbsum/) (49).

2.1.12 Evaluation of allergenicity, antigenicity, solubility, and physicochemical properties of MEV

To assess the allergenicity of the vaccine construct, we utilized the AlgPred 2.0 server (https://webs.iiitd.edu.in/raghava/algpred2/batch.html) with a cut-off value ≥ 0.5. Allergenicity analysis was performed using AllerTOP v. 2.0 (https://www.ddg-pharmfac.net/AllerTOP/). Both tools consistently indicated that the vaccine construct is non-allergenic, thus mitigating the risk of allergic reactions during vaccination protocols (29, 30). Next, we evaluated the antigenicity of MEV using the VaxiJen server tool (http://www.ddg-pharmfac.net/vaxijen/VaxiJen/VaxiJen.html) (28). Subsequently, the Protein-Sol server (https://protein-sol.manchester.ac.uk/) was employed to predict the solubility of the engineered MEV, where scores above 0.45 indicate solubility (50). Further characterization of MEV included the prediction of major physicochemical characteristics using the ExPASy ProtParam web tool (https://web.expasy.org/protparam/) (38). This tool provides insights into the molecular weight (Mw), theoretical isoelectric point (pI), amino acid composition, *in vitro* and *in*

vivo protein half-life, aliphatic index, instability index, and grand average of hydropathicity (GRAVY) score (51). These parameters are essential to understand the stability, solubility, and potential effectiveness of MEVs as vaccine candidates.

2.1.13 Reverse translation and *in silico* cloning

To ensure codon compatibility and optimize the vaccine construct for expression, we used the Java Codon Adaptation Tool (https://www.jcat.de/) (52). This tool refines codon usage specifically for expression in *Escherichia coli* K12, following the recommended guidelines. For optimal expression, it is important that the protein sequence maintains a GC content between 30–70% and achieves a Codon Adaptation Index (CAI) value above 0.8 (52). Once the sequence was optimized, we performed *in silico* cloning of the finalized MEV model using the SnapGene v7.2 software (https://www.snapgene.com/resources). This software enabled a virtual cloning process, allowing insertion of the optimized vaccine construct into a vector suitable for expression studies and preparation for experimental validation.

2.1.14 Simulations for evaluating the immune response of the vaccine construct

The C-ImmSim tool (https://kraken.iac.rm.cnr.it/C-IMMSIM/) employs position-specific scoring matrices to simulate and predict the intensity of immune responses triggered by vaccines over different time intervals (53). This model helps researchers to understand how vaccine timing and administration influence immune dynamics, which is crucial for optimizing vaccination strategies and evaluating the effectiveness of vaccine candidates.

2.1.15 Molecular dynamics simulation

Molecular dynamics (MD) simulations provide crucial insights into the structural stability and functionality of vaccines in a simulated cytosolic environment. In this study, we explored the interactions between MEV, TLR2, and TLR4 using a 100-nanosecond MD simulation conducted using GROMACS version 2018. The MEV and receptors were situated in a dodecahedral solvent box containing TIP3P water molecules. To simulate physiological conditions, some water molecules were randomly substituted with sodium (Na^+) and chloride (Cl^-) ions. The system was then subjected to energy minimization, followed by equilibration under constant volume (NVT) and pressure (NPT) conditions to ensure system stability. Throughout the simulation, the particle mesh Ewald (PME) method was employed to compute electrostatic interactions, and LINCS constraints were applied to maintain the hydrogen bond lengths. This methodology enabled us to accurately simulate the interactions between MEV and TLRs over 100 nanoseconds (54).

2.2 Identification of novel drug targets

2.2.1 Detection of cytoplasmic protein sequences

Cytoplasmic protein sequences of *F. tularensis* strain 2017317779 were determined using PSORTb version 3.0.3 (http://www.psort.org/psortb/) and CELLO v. 2.5 (http://cello.life.nctu.edu.tw/) (25–27). Given their crucial roles in cellular processes, cytoplasmic proteins are promising targets for small-molecule drug targeting (55).

2.2.2 Selecting human non-similar protein sequences

The homology of the selected proteins to the human proteome (*Homo sapiens*, taxid:9606) was evaluated using PSI-BLAST (https://blast.ncbi.nlm.nih.gov/) to identify proteins similar to those in humans. Proteins that demonstrated significant similarities were excluded from further analysis. Additionally, the MITOMASTER database (http://mammag.web.uci.edu/twiki/bin/view/Mitomaster) was used to assess the similarity between selected proteins and human mitochondrial proteins (55). This precaution ensured that the chosen proteins were distinct from those present in human mitochondria, reinforcing their potential as candidates for further investigation.

2.2.3 Identification of unique metabolic pathway proteins

The KAAS server from the Kyoto Encyclopedia of Genes and Genomes (KEGG) database (https://www.genome.jp/kaas-bin/kaas_main) and BLASTp analysis were employed to identify non-homologous to host proteins that are crucial for the study (56). Protein sequences with distinct pathways from the host were selected for analysis, ensuring that only the proteins involved in specific host pathways were included. This approach focuses on unique biological interactions and processes.

2.2.4 Detection of essential proteins

The DEG 15.2 server contains all crucial proteins involved in key functions of bacterial life, as determined by experimental studies (57). Essential proteins were identified using Genome BLAST with a coverage > 90% and an identity > 80% from the DEG database (http://origin.tubic.org/deg/public/index.php/index).

2.2.5 Identifying novel therapeutic targets

To highlight the uniqueness of the selected proteins as pharmacological targets, we analyzed the remaining candidates from earlier stages using the DrugBank database (https://www.drugbank.ca/structures/search/bonds/sequence) (58). This evaluation assessed their druggability and reinforced their potential as novel therapeutic candidates based on well-established criteria. The proteins were systematically screened against all known drug targets in DrugBank and those didn't exhibit any proposed drugs, were classified as novel drug targets.

2.2.6 Identification of proteins non-similar to the host microbiome

The aim of examining the lack of similarity between the *F. tularensis* metabolic pathway proteins and those from beneficial host microorganisms was to ensure their distinctiveness. We used the NCBI BLAST server for sequence comparisons (See

Supplementary Data 1 for details on gut microbiota) (59). Proteins exhibiting significant similarities with the host microbiome proteins were excluded from the study.

2.2.7 Prediction of functional domains of novel drug targets

Functional domains of the proteins were identified using the Conserved Domain Database (CDD) (https://www.ncbi.nlm.nih.gov/Structure/cdd/cdd.shtml) based on the NCBI Entrez query and EggNOG (http://eggnog5.embl.de/#/app/home) (36, 37).

2.2.8 Analysis of protein-protein interactions

To analyze the interaction network of hypothetical proteins related to distinct drug targets, STRING 11.5 server (https://string-db.org) was employed (43). Interactors with high confidence scores > 0.7 were included in the protein network to mitigate false-positive and false-negative results. Eliminating the query protein resulted in changes in the number of edges (interconnections) and nodes (interconnected proteins), highlighting its influence on biological processes in the organism (44).

3 Results

3.1 Design of MEV

3.1.1 Sequence retrieval

The core-to-pan protein ratio was low and the core-pan plot appeared almost open (Figure 1A). Consequently, using the core proteome was deemed unsuitable, leading to the decision to utilize the entire genome of the *F. tularensis* strain 2017317779 (24). The KEGG distribution plot demonstrated that most core, accessory, and unique genes were involved in the metabolism of this pathogen (Figure 1B). Based on these findings, the proteome of the *F. tularensis* strain 2017317779 was retrieved from the UniProt database (http://www.uniprot.org/). The workflow for identifying new immunogenic targets and designing multi-epitope vaccines against *F. tularensis* is illustrated in Figure 2A.

3.1.2 Prediction of subcellular localization

All 1,921 proteins in the reference strain were analyzed using PSORTb, CELLO, and TMHMM. In total, 361 proteins were identified as OMPs located in the extracellular space.

3.1.3 Prediction of antigenicity and allergenicity

A total of 123 antigenic proteins were identified, of which 116 were determined to be non-allergenic.

3.1.4 Selecting non-homologous proteins from the human proteome

All 116 proteins were evaluated for homology with *Homo sapiens* (taxid: 9606). This analysis revealed that 101 proteins were non-homologous, while 15 proteins were homologous; thus, 15 homologous proteins were excluded.

3.1.5 Prevalence of putative immunogenic targets among circulating *F. tularensis* strains

The frequency of 101 selected proteins was assessed in the 686 F. *tularensis* strains. Five proteins exhibited a low prevalence (< 90%) among these strains and were subsequently excluded from the study.

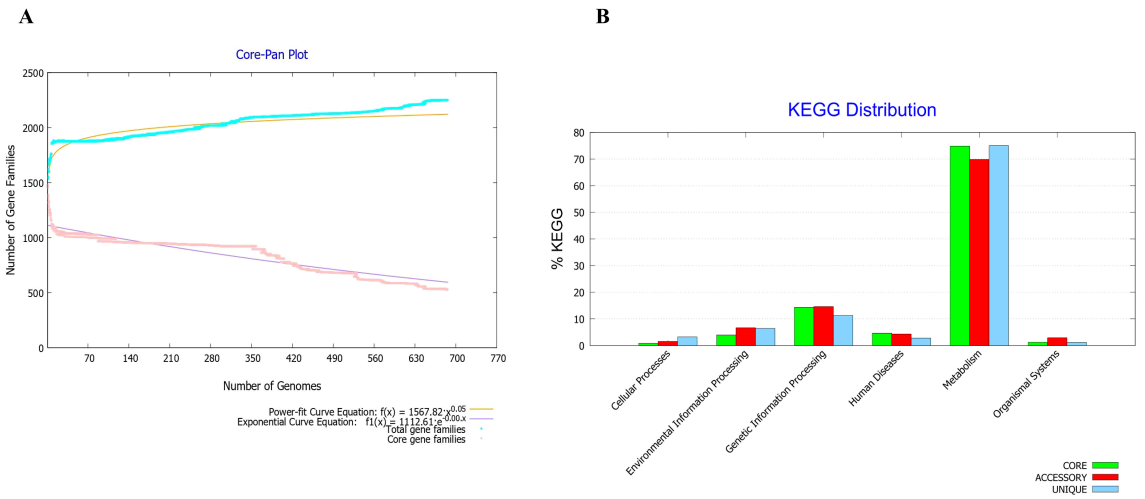

FIGURE 1
Core-proteome analysis of *F. tularensis* strains using BPGA software v 1.3. **(A)** The core-pan plot of 686 F. *tularensis* strains identified 2,249 core proteins. This analysis also demonstrated significant genomic diversity within the *F. tularensis* species. **(B)** Clusters of Orthologous Groups (COGs) analysis showed that the majority of core proteins are involved in key biological functions, including secondary metabolism, genetic and environmental information processing, cellular processes, organismal systems, and human disease pathways.

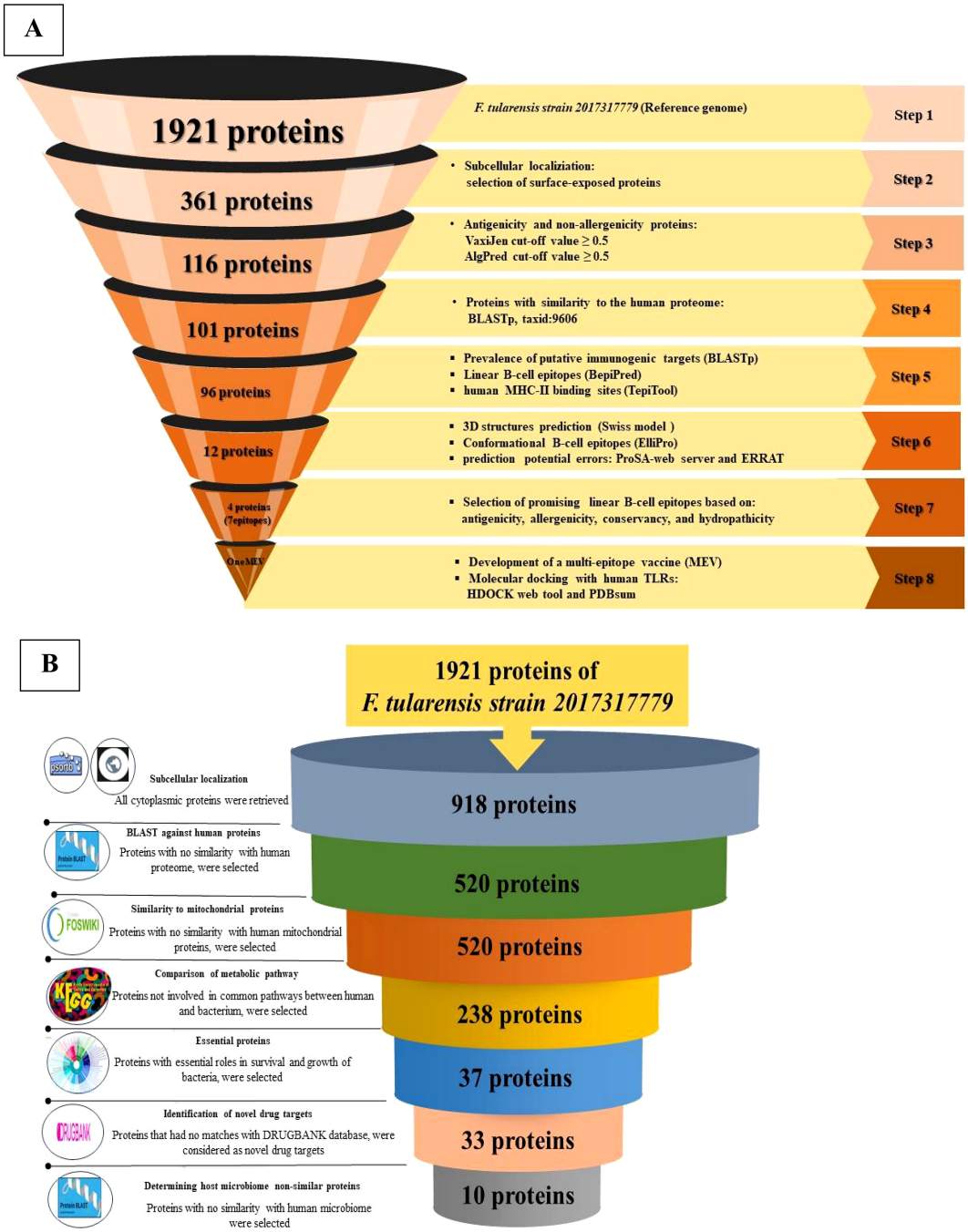

FIGURE 2
Schematic overview of the selection and validation process for putative immunogenic targets, MEV, and novel drug targets. **(A)** This panel illustrates the sequential flow of the reverse vaccinology strategy employed to design an MEV for *F. tularensis*. The schematic includes a comprehensive overview of the software, databases, web tools, and specific cut-off criteria utilized throughout the workflow. **(B)** This panel presents the workflow for identifying novel drug targets in *F. tularensis*. It delineates the various software applications, databases, web tools, and cut-off criteria that were systematically applied during the target identification process in *F. tularensis*.

3.1.6 Quartile score-refined proteins: their conserved domains and physicochemical properties

Using the quartile method, 12 immunogenic targets were identified from the 96 candidate proteins (Figure 3). These targets were scored within the top 25% of properties associated with successful vaccine development. Notably, four proteins were associated with cell wall, membrane, and envelope biogenesis, which are crucial for bacterial survival and serve as potential targets for immune attack. The identified proteins were FopA (WP_003023303.1), OmpA family protein (WP_003020808.1), and a hypothetical protein (WP_003026145.1). Notably, another

10.3389/fimmu.2025.1479862

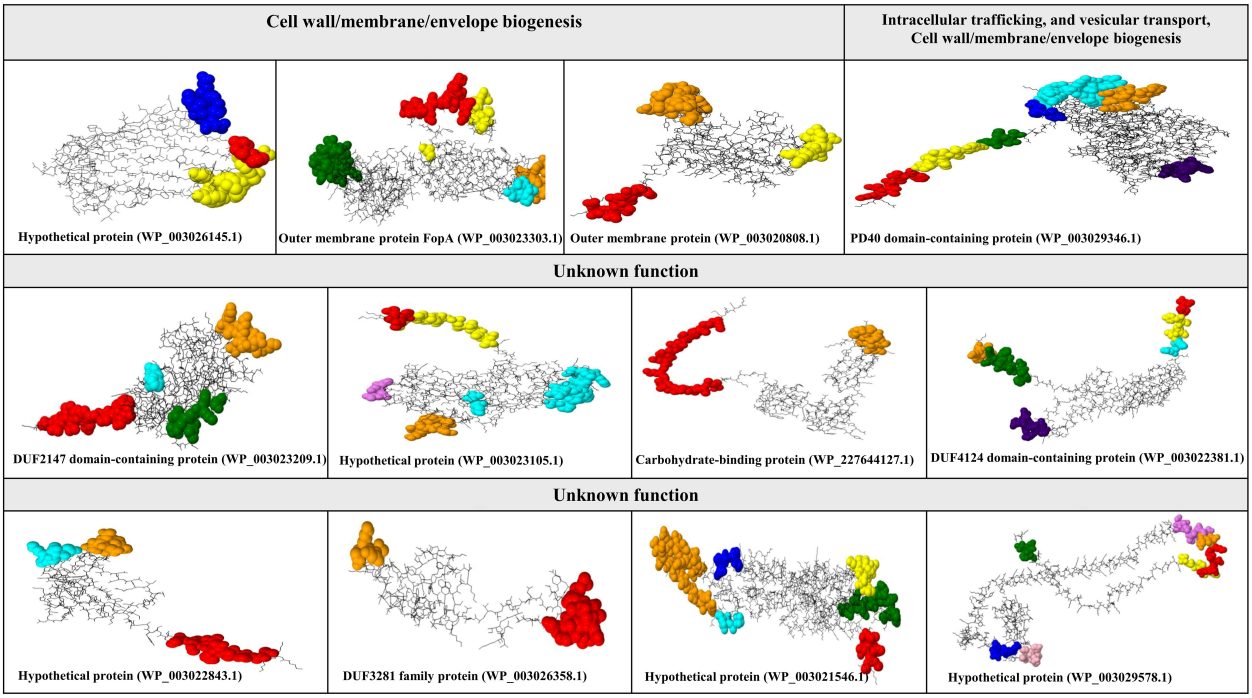

FIGURE 3
Characterization of conformational B-cell epitopes in putative immunogenic targets against *F. tularensis*. This figure illustrates the identification and mapping of conformational B-cell epitopes on the tertiary structures of potential immunogenic targets against *F. tularensis*. Conformational B-cell epitopes were determined using ElliPro and visualized with Jamal software. Each color represents a unique conformational epitope, allowing for easy differentiation and highlighting of the spatial distribution within the protein structure.

hypothetical protein (WP_003029346.1) plays a dual role in intracellular trafficking and cell wall biogenesis, suggesting its potential involvement in immune responses. In addition, eight proteins with unknown functions were identified, including hypothetical proteins (WP_003023105.1, WP_003029578.1, WP_003022843.1), PD40 (WP_003021546.1), DUF2147 (WP_003023209.1), DUF3281 (WP_003026358.1), DUF4124 (WP_003022381.1), and a carbohydrate-binding protein (WP_227644127.1) (Figure 3). All identified proteins had molecular weights less than 110 kDa.

3.1.7 Tertiary structure prediction and characterization of conformational B-cell epitopes

The structures predicted by SWISS-MODEL were validated using Verify 3D, PROSA, and ERRAT analyses, which confirmed the accurate folding of all 12 proteins (Supplementary Data 2). Conformational epitopes were identified and visualized based on the predicted tertiary structures. The number of conformational epitopes for the 12 putative immunogenic targets is as follows: hypothetical protein (WP_003026145.1) (three epitopes), outer membrane protein FopA (WP_003023303.1) (five epitopes), OmpA family protein (WP_003020808.1) (three epitopes), hypothetical protein (WP_003029346.1) (seven epitopes), DUF2147 (WP_003023209.1) (four epitopes), hypothetical protein (WP_003023105.1) (five epitopes), carbohydrate-binding protein (WP_227644127.1) (two epitopes), DUF4124 (WP_003022381.1) (six epitopes), hypothetical protein (WP_003022843.1) (three epitopes), DUF3281 (WP_003026358.1) (two epitopes), PD40 (WP_003021546.1) (six epitopes), and hypothetical protein (WP_003029578.1) (seven epitopes). See Figure 3. Additional details are provided in Supplementary Table 1.

3.1.8 Protein-protein interaction networks

Based on the STRING database, the functions of eight candidate vaccine proteins DUF2147 (WP_003023209.1), hypothetical protein (WP_003023105.1), DUF4124 (WP_003022381.1), carbohydrate-binding protein (WP_227644127.1), hypothetical protein (WP_003022843.1), DUF3281 (WP_003026358.1), PD40 (WP_003021546.1), and hypothetical protein (WP_003029578.1) were not determined. The protein with accession number WP_003023209.1, interacts with the DNA mismatch repair protein (FTT_0486, mutL), several hypothetical proteins (FTT_0066, FTT_1537c, ORF FTT_0485, FTT_0220c, FTT_0045, FTT_1704, and FTT_1349), lipase/acyltransferase (FTT_0023c), and disulfide bond formation protein B (FTT_0107c, *dsbB*). The protein, with accession number WP_003021546.1, interacts with serine hydroxymethyltransferase (SHMT) and deoxyribodipyrimidine photolyase (PhrB). The protein with accession number WP_003023105.1 interacts with an outer membrane lipoprotein (FTT_0198, Blc) and a hypothetical protein (FTT_0200). The proteins with accession numbers WP_003022381.1, and WP_003022843.1 interacted with two

10.3389/fimmu.2025.1479862

hypothetical proteins (Figure 4). The string database did not predict the interactions for hypothetical protein (WP_003029578.1), carbohydrate-binding protein (WP_227644127.1), and DUF3281 (WP_003026358.1).

3.1.9 Multi-epitope vaccine construct processing

Of the 12 proteins, seven B-cell epitopes containing T-cell epitopes from four proteins exhibited promising properties for inclusion in the final vaccine construct (Table 1). Epitopes were linked using a GPGPG linker. The vaccine sequence was converted into FASTA format and evaluated against various criteria, including antigenicity, non-allergenicity, non-toxicity, and solubility. A schematic representation of the final multi-epitope vaccine peptide is shown in Figure 5. The SAVES 6.0 server provided an ERRAT score of 100, and the vaccine demonstrated 84.6% Ramachandran-favored residues with 15.4% in additional allowed regions. The antigenicity score of MEV predicted by the VaxiJen server was 1.061. AlgPred 2.0 and AllerTOP v2.0, were confirmed to be non-allergenic. The selected vaccine candidate exhibited the highest solubility scores, with a value of 0.914. MEV has a low molecular weight (21.27 kDa) and demonstrates extreme thermotolerance, as indicated by its high aliphatic index (61.34). The theoretical pI of MEV was 4.81, and it was recognized as hydrophilic owing to a negative GRAVY score (-0.946). The instability index of the vaccine candidate was 35.9, which categorizes it as a stable polypeptide. The estimated half-life of MEV is 4.4 hours in mammalian reticulocytes *in vitro*, and >10 h in *E. coli in vivo*. The results of protein-protein docking showed that the MEV-TLR-2 complex featured 10 hydrogen bonds and 154 unbound contacts, whereas the MEV-TLR-4 complex exhibited seven hydrogen bonds, three salt bridges, and 132 unbound contacts. The MEV demonstrated nearly equal interactions with TLR-2 (docking score: -235.03 kcal/mol, confidence score: 0.8456, and ligand RMSD: 57.67 Å) and TLR-4 (docking score: -215.94 kcal/mol, confidence score: 0.7890, and ligand RMSD: 42.13 Å). For the HLA interactions, protein-protein docking results showed that the MEV-HLA-A complex featured 3 hydrogen bonds and 179 unbound contacts, with a docking score of -241.44 kcal/mol, a confidence score of 0.8616 and ligand RMSD of 32.93 Å. In comparison, the MEV-HLA-DR-B complex exhibited 6 hydrogen bonds, 1 salt bridge, and 179 unbound contacts, with a docking score of -253.63 kcal/mol, a confidence score of 0.8882, and ligand RMSD of 34.59 Å. The detailed vaccine-receptor interactions are shown in Figure 6.

3.1.10 *In silico* cloning of the design

To optimize processivity and expression in *E. coli*, the MEV sequence was subjected to rigorous reverse translation using the *E. coli* K12 codon table. The Codon Adaptation Index (CAI) was calculated as 0.95. This index quantifies how well codon usage in a sequence matches the codon usage bias of the host organism, with a value of 1.0, indicating perfect adaptation. The sequence also exhibited a GC content of 52.05%, which falls within the favorable range (30-70%) for expression in *E. coli*. Subsequently, using the SnapGene software, the vaccine sequence was inserted into a highly efficient ATOH1_Puc18 expression plasmid vector (Figure 7).

TABLE 1 Seven promising epitopes from four selected *F. tularensis* OMPs were used in the MEV.

Protein (Accession number)	Start	End	length	Epitope	Antigenicity	Ag (Score)	Allergenicity	Conservancy %
Hypothetical protein (WP_003026145.1)	52	72	21	DKGVGEINNSSSVSPNNIAGV	Ag	0.6682	non-allergen	100
Hypothetical protein (WP_003029346.1)	60	86	27	NHNAKLQANDTIKYEIKQKQNIPWKSL	Ag	0.8526	non-allergen	100
OmpA family protein (WP_003020808.1)	23	75	53	STRPDNSDLIKDKYAGVDSSQALEMSSQIYGSDKLSSDQVEQMKKELMNINCR	Ag	0.6334	non-allergen	100
PD40 (WP_003021546.1)	20	50	31	ADDLNAKIVNESVTKYSNNVETDADTINTNSP	Ag	1.2715	non-allergen	100
	230	245	16	YNINSKDAATAIEFND	Ag	1.0516	non-allergen	100
	255	263	9	IKSLQGSDT	Ag	1.0523	non-allergen	100
	402	416	15	IHYQHNDDNKIDHLD	Ag	0.7518	non-allergen	100

Start: The starting amino acid position of the epitope within the protein sequence; End: The ending amino acid position of the epitope within the protein sequence, Length: The number of amino acids in the epitope sequence; Antigenicity: Indicates if the epitope is recognized as an antigen; Antigenicity Score: A numerical score reflecting the strength of the epitope's antigenic potential, with higher scores indicating greater antigenicity; Allergenicity: Indicates whether the epitope is considered an non-allergen; Conservancy (%): The percentage of conservation of the epitope across different species or strains.

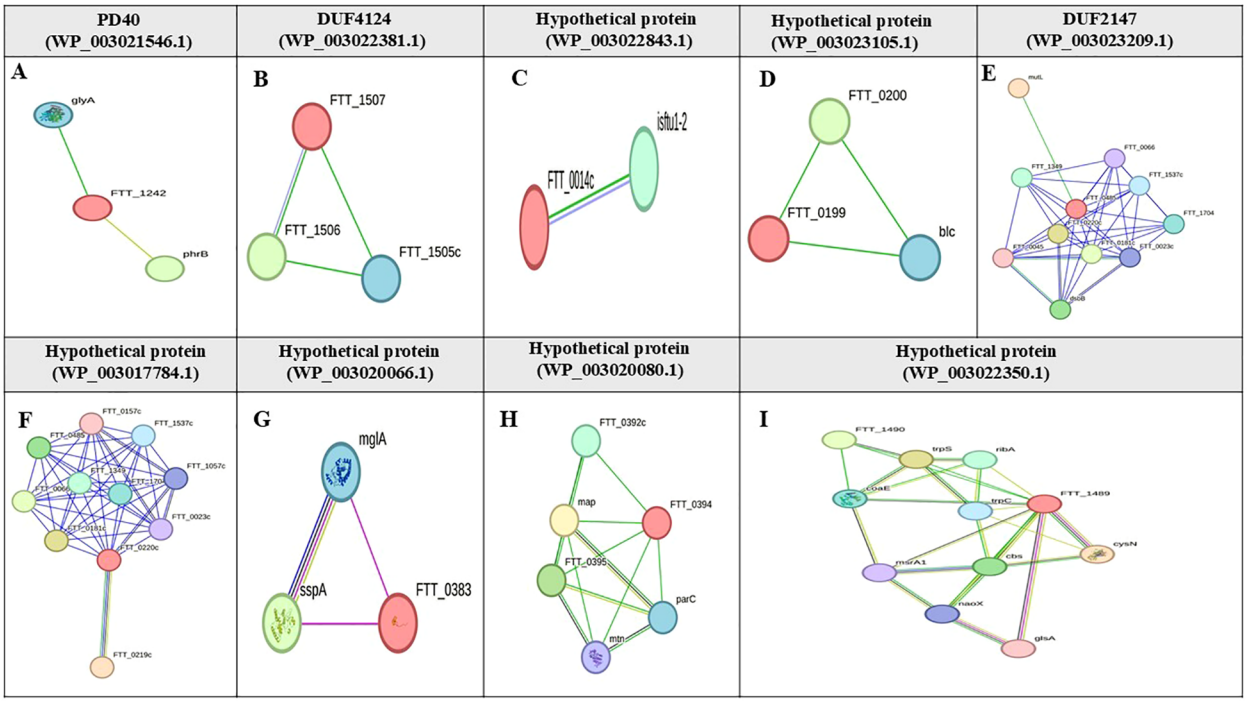

FIGURE 4
Protein-protein interaction network of hypothetical proteins in *F. tularensis*. This figure shows the STRING interaction networks for various hypothetical proteins in *F. tularensis*: **(A)** PD40 (WP_003021546.1), **(B)** DUF4124 (WP_003022381.1), **(C)** Hypothetical protein (WP_003022843.1), **(D)** Hypothetical protein (WP_003023105.1), **(E)** DUF2147 (WP_003023209.1), **(F)** Hypothetical protein (WP_003017784.1), **(G)** Hypothetical protein (WP_003020066.1), **(H)** Hypothetical protein (WP_003020080.1), and **(I)** Hypothetical protein (WP_003022350.1). Target proteins are highlighted in red font. Nodes are empty for proteins with unknown 3D structures and filled for those with known or predicted structures. Edges represent protein-protein associations and are classified by interaction type; light blue edges indicate interactions from curated databases; purple edges signify experimentally validated interactions; green edges represent predicted interactions based on gene neighborhood; red edges indicate gene fusions; blue edges are derived from gene co-occurrence. Additional sources of interaction include yellow edges for text mining; black edges for co-expression; gray edges for protein homology.

3.1.11 Immune simulation of predicted vaccine construct

The vaccine construct peaked rapidly after injection, and then declined, indicating a rapid initial immune response. IgM was the first antibody to respond to MEV and peaks shortly after MEV exposure. Subsequently, IgG antibodies (IgG1 + IgG2) were raised, and the elevation of these two antibodies was critical for long-term immunity. The combined IgM and IgG response showed a broad peak, indicating a sustained antibody presence to combat the antigen (Figure 8A). The initial immune response appears to be driven by IFN-γ, TGF-β, and IL-2, as their levels peaked at around day 5-6. This was followed by a peak in IL-12 and IL-10 levels on day 6-7, suggesting their involvement in sustaining and regulating immune response (Figure 8B). TC cells (CD4 T-cells and CD8 T-cells) peaked around day 10-15, and after 32 days, TC cells populations exhibited decline in concentration (Figure 8C). The population of natural killer (NK) cells peaked around days 7-10 and declines over 35 days (Figure 8D). The initial drop in the total and resting dendritic cell (DC) populations may be attributed to an early response to external injection of the vaccine construct (Figure 8E). This decline was followed by recovery, indicating an adaptive mechanism that restores the cell populations to a stable state. These dynamics highlight the effective engagement of dendritic cells in processing and presenting vaccine antigens, which are essential for a successful immunization response. These results suggest that the vaccine candidate successfully activated the immune system while maintaining the overall stability of the dendritic cell populations. Following the injection of the vaccine candidate, the macrophage populations exhibited dynamic changes, indicative of an effective immune response (Figure 8F).

3.1.12 Molecular dynamic simulation

MD simulations have proven invaluable in guiding experimental validation by analyzing conformational changes, stability variations, and the overall evolution of complex systems under cytosol-like conditions. These simulations allowed for the assessment of parameters such as the RMSD, root mean square fluctuation (RMSF), and radius of gyration. RMSD is a critical metric for evaluating the stability of receptor-ligand complexes. In our MD simulation study, the RMSD graph revealed the MEV, MEV_TLR-2 complex, and MEV_TLR-4 complex exhibited stable interactions, as shown in Figure 9A. Furthermore, we quantified the RMSF of the complexes to assess their flexibility across amino acid residues. Figure 9B illustrates that the RMSF values for the MEV, MEV_TLR-2 complex, and MEV_TLR-4 complex were similar, indicating similar flexibility. Additionally, we analyzed the radius of gyration (Rg) to evaluate the mobility and overall flexibility of the complexes. The gyration graph shown in Figure 9C corroborates the RMSD findings.

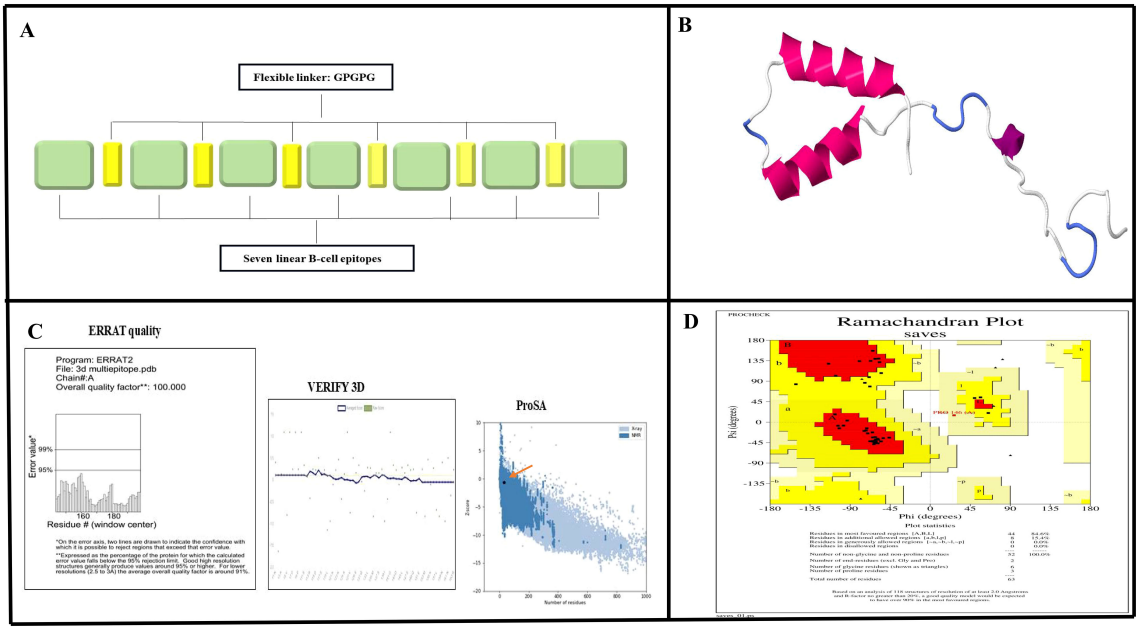

FIGURE 5
Prediction and validation of the MEV structure. **(A)** Schematic diagram illustrating the arrangement of MEV components, featuring linear B-cell epitopes interconnected by GPGPG flexible linkers. **(B)** Predicted tertiary structure of MEV generated using SWISS-MODEL. **(C)** Validation results for the predicted structure, showing an ERRAT quality score of 100% and successful verification through VERIFY3D analysis. Additionally, a Z-score of -0.61, obtained from Pros A, indicates the model's reliability. **(D)** Ramachandran plot analysis revealed that 84.6% of the residues are in favored regions, 15.4% in allowed regions, and 0% in disallowed regions, further confirming the accuracy of the structure.

3.2 Identification of novel drug targets

3.2.1 Detection of cytoplasmic protein sequences: proteins with no similarities to the host

All proteins from the reference strain (1921 proteins) were analyzed using PSORTb and CELLO. A total of 918 cytoplasmic proteins were identified. Using PSI-BLAST, 520 proteins showed no similarity to human proteins, while 398 proteins were excluded due to their similarity with the human proteome. None of the proteins exhibited similarities with human mitochondrial proteins.

3.2.2 Identification of unique metabolic pathway proteins

Following BLAST analysis using the KAAS database, we identified 282 of the 520 non-homologous proteins that were involved in metabolic pathways common to humans and were consequently excluded from further analysis. The remaining 238 non-homologous proteins were retained for subsequent analyses.

3.2.3 Selecting essential protein sequences

Antibacterial agents are often designed to target and inhibit critical gene products, making essential proteins particularly effective therapeutic targets (60). A total of 37 proteins were identified as significant hits using a dataset of essential bacterial proteins from the DEG 15.2 database. These proteins are essential for the survival of *F. tularensis*, underscoring their potential as targets for therapeutic intervention (61). Targeting the unique genetic components specific to microbes can be particularly advantageous for developing species-specific treatments.

3.2.4 Identify novel drug targets

Among the 37 F. *tularensis* proteins identified as significant hits from the DEG 15.2 database, four proteins showed similarities to targets of FDA-approved or experimental drugs listed in the DrugBank database and were therefore excluded from further analysis. The remaining 33 proteins were selected for further investigation.

3.2.5 Determining host microbiome non-similar proteins

In the final analysis, 10 pathogen proteins were identified using microbiome BLAST, which showed no similarity to the human microbial flora (Table 2). Therefore, these proteins have been proposed as exclusive drug targets for combating various *F. tularensis* strains.

3.2.6 Protein-protein interactions

Based on CDD and EggNOG analyses, the functions of six drug target proteins were detected, whereas four hypothetical proteins (WP_003017784.1, WP_003020066.1, WP_003020080.1, and WP_003022350.1) lacked identifiable functions (Table 2). Based on the STRING database results, hypothetical proteins (WP_003017784.1) interacts closely with the cytochrome b561 family protein (FTT_0219c), lipase/acyltransferase proteins (FTT_0023c), Type IV pili lipoprotein (FTT_1057c), conserved

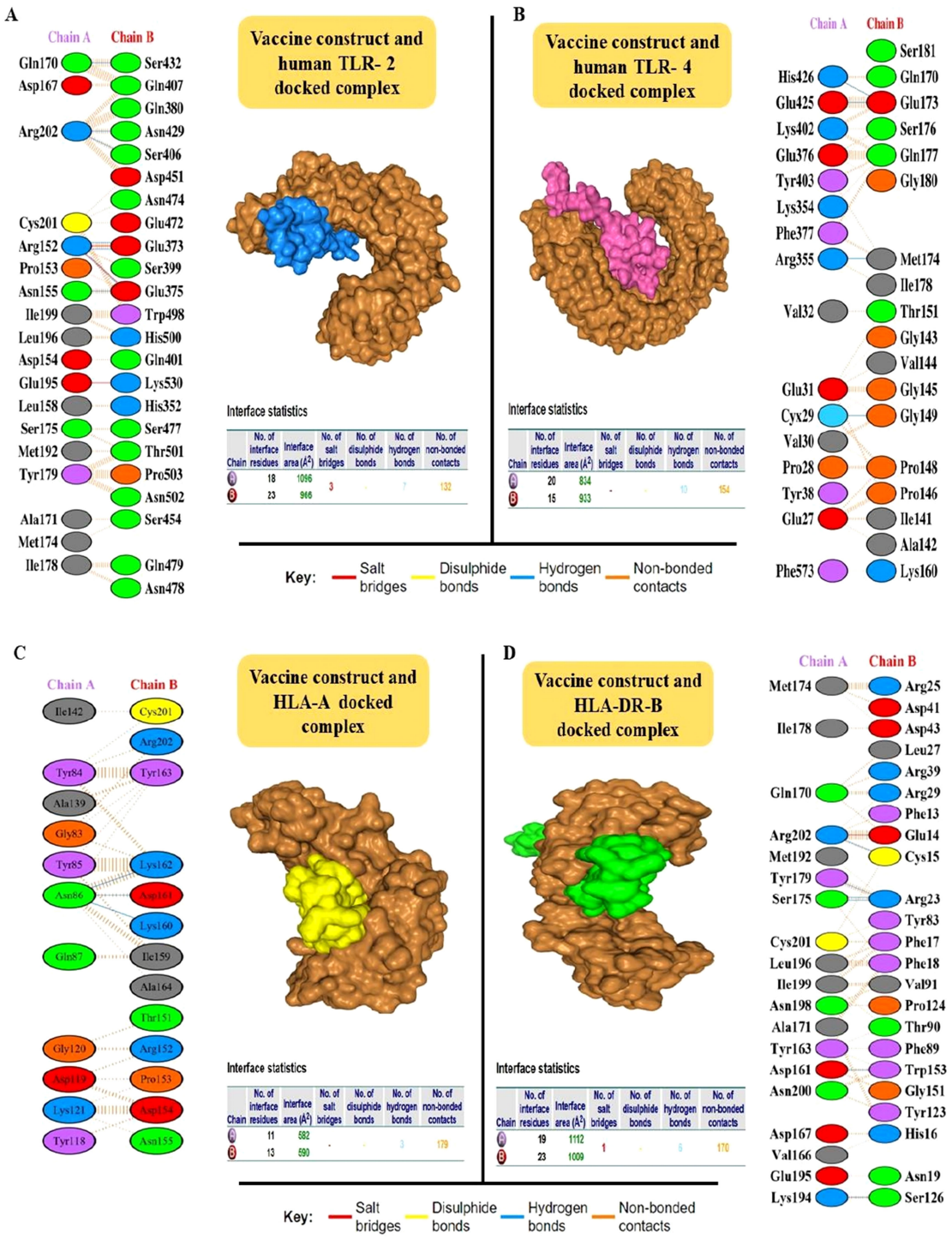

FIGURE 6
Interaction analysis of the MEV construct with Toll-Like Receptors (TLRs) using HDOCK was visualized using the PDBsum server. The fully docked complexes and residue-by-residue interactions are detailed. **(A)** The MEV-TLR-2 interaction is shown, with the vaccine construct (ligand) in blue and the TLR-2 receptor in brown. The complex formed 10 hydrogen bonds and 154 non-bonded contacts. **(B)** The MEV-TLR-4 interaction is depicted with the vaccine construct (ligand) in pink and TLR-4 in brown. This complex feature seven hydrogen bonds, three salt bridges, and 132 non-bonded contacts. **(C)** The MEV-HLA-A interaction is shown, with the vaccine construct (ligand) in yellow and the HLA-A receptor in brown. The complex formed 3 hydrogen bonds and 179 non-bonded contacts. **(D)** The MEV-HLA-DR-B interaction is shown, with the vaccine construct (ligand) in green and the HLA-DR-B receptor in brown. The complex formed 6 hydrogen bonds, 1 salt bridge and 179 non-bonded contacts.

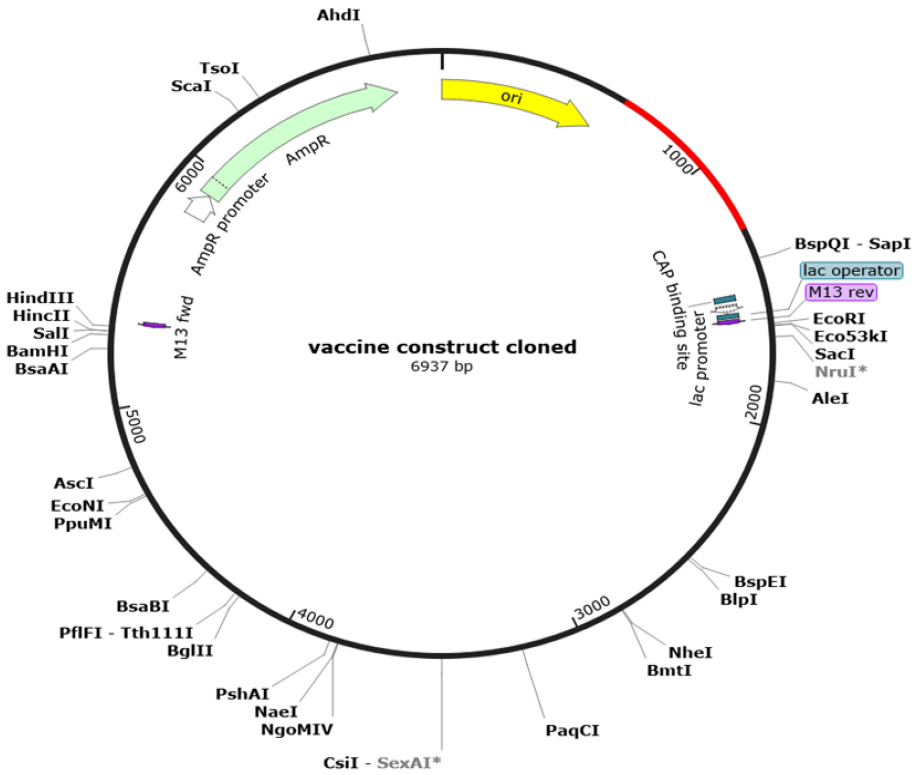

FIGURE 7
Results of *in Silico* restriction cloning. Computational restriction cloning of the reverse-translated MEV candidate fragment into the ATOH1_Puc18 expression plasmid vector was performed using SnapGene 7.2. The black ring represents the vector backbone, while the red arrow indicates the reverse-translated MEV fragment.

hypothetical protein (FTT_1537c), LicB-like transmembrane protein (FTT_0157c), conserved membrane protein similar to Q9X885 (FTT_0181c), a conserved hypothetical protein similar to AAP58972.1 (Q7X3I5) from *F. novicida* (FTT_1704), and two hypothetical proteins (FTT_0485, FTT_0066). Hypothetical protein (WP_003020066.1) shows an expression correlation with stringent starvation protein A (FTT_0458) and is similar to the macrophage growth locus A protein from *F. novicida* (FTT_1275). Hypothetical protein (WP_003020080.1) interacts with a hypothetical protein (FTT_0392c), methionine aminopeptidase (FTT_0393), 5'-methylthioadenosine/S-adenosylhomocysteine nucleosidase (FTT_0397), and DNA topoisomerase IV subunit A (FTT_0396). Hypothetical protein (WP_003022350.1) interacts with Tryptophanyl-tRNA synthetase (TrpS), antiporter protein (FTT_1490), Dephospho-CoA kinase (CoaE), Adenylylsulfate kinase (MsrA1), and Choloylglycine hydrolase (Cbs) (Figure 4).

4 Discussion

Single-antigen vaccines against tularemia are insufficient to provide comprehensive protection, highlighting the necessity for multi-antigen strategies (62–65). Multi-antigen vaccines that incorporate various proteins typically offer improved efficacy by activating broader immune responses (66–68). For example, a tri-antigen vaccine (DnaK, OmpA, and Tul4) generated appropriate antibody responses, but showed low protective efficacy (69). This indicates that while antibodies play a crucial role, effective protection also relies on strong T-cell responses and optimal combinations of antigens. A deeper understanding of these factors is essential for designing more effective vaccines.

In this study, we designed an MEV using immunodominant epitopes from *F. tularensis* OMPs to stimulate both B-cell and T-cell responses to protect against tularemia (70). It has been shown that OMP immunization provides the highest level of protection against tularemia in animal models (66). The membrane components of *F. tularensis* have demonstrated protective efficacy in both prophylactic and post-exposure therapeutic models of tularemia (66, 71, 72). Additionally, a study using a reverse vaccinology approach identified surface proteins as target immunogens for antibody-based immunotherapies against tularemia (73). Reverse vaccinology is a powerful technique for identifying immunogenic and surface-exposed proteins (74, 75), thus enabling the discovery of novel vaccine candidates that traditional methods may miss. An example of such success is the 4CMenB vaccine (Bexsero), the first approved vaccine against *Neisseria meningitidis* serogroup B (MenB) (76, 77). These examples highlight the importance of including a mix of antigens to achieve a protective immune response (78).

Our proposed MEV includes seven immunogenic epitopes from four OMPs, selected for their high antigenicity, solubility, thermostability, and optimal half-life. *In silico* analysis indicated

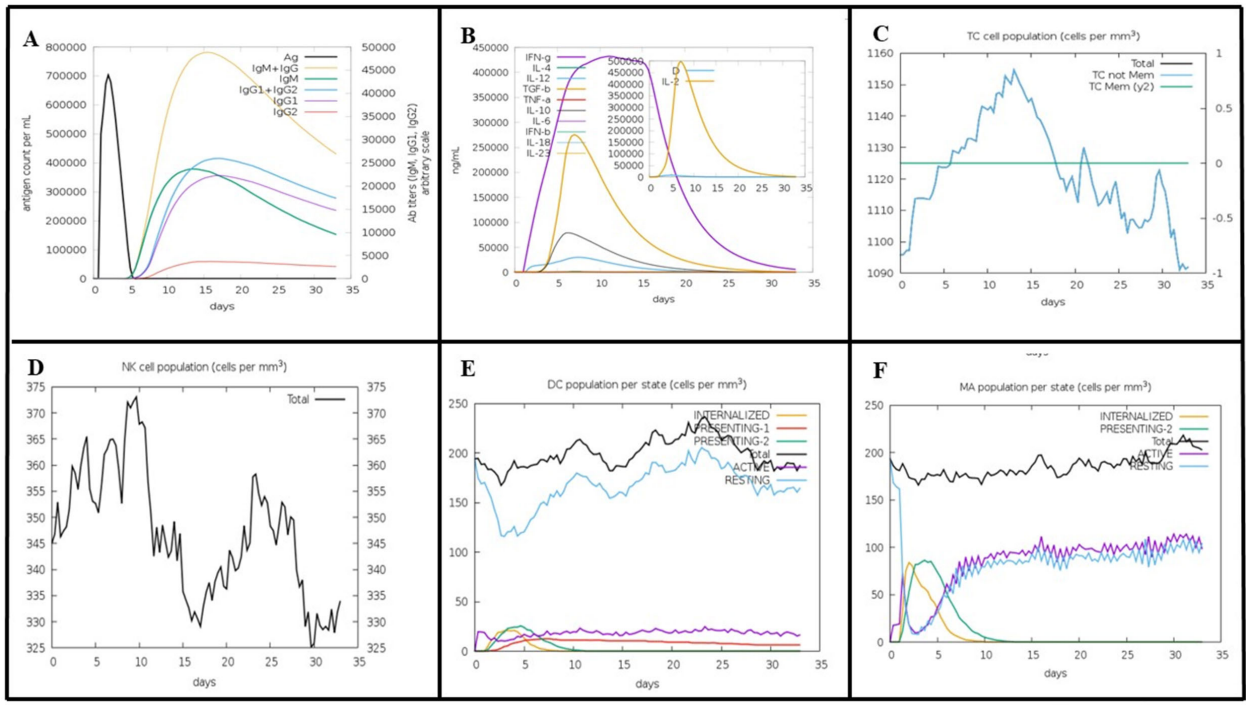

FIGURE 8
Predicted Immune Response to MEV Vaccine Construct Using the C-ImmSim Tool. **(A)** MEV elicits a rapid immune response with an initial IgM peak, followed by sustained levels of IgG (IgG1 + IgG2), indicating prolonged immunity. **(B)** Early cytokine response, dominated by IFN-γ, TGF-β, and IL-2, peaks on days 5-6, with IL-12 and IL-10 contributing to immune regulation on days 6-7. **(C)** T-cells (CD4 and CD8) peak around days 10-15, then gradually decline by day 32. **(D)** NK cells reach peak levels between days 7-10, followed by a gradual decrease over 35 days. **(E)** The initial decrease in dendritic cells reflects the early activation in response to MEV. Intern, internalized antigen; Pres II, presenting on MHC II; Dup, mitotic cycle; anergic, anergic; resting, inactive.

effective expression and purification in *E. coli*, suggesting a cost-effective manufacturing process (79). The docking results indicated that the MEV construct strongly interacted with both TLR-2 and TLR-4, as well as HLA-A and HLA-DR-B, key receptors for initiating immune responses. The stable binding observed with both Class I and Class II MHC molecules is crucial for eliciting T cell-mediated adaptive immunity. These findings suggest that MEV has the potential to stimulate both the innate and adaptive immune pathways, thereby providing broad protection. This design yielded a stable and reproducible MEV, supported by docking and MD simulations, as well as the known roles of TLR2 (80), suggesting that the MEV vaccine construct has the potential to trigger a robust and multifaceted immune response and could be safe for human use. The simulations indicated a strong immune response to *F. tularensis* infection, suggesting a long-lasting immunity. The involvement of immune cells, such as macrophages, T-cells, and NK cells, along with signaling molecules, such as IL-2, IFN-γ, and IL-12, indicates a comprehensive immune response. These results align with those of studies highlighting the roles of IL-2, TNF-α, IFN-γ, and IL-12 in the management of *F. tularensis* infection (81–83). Additionally, the presence of antibodies (IgM and IgG2) suggests mechanisms such as macrophage phagocytosis and complement activation, further supporting MEV's multi-faceted approach (84). However, while the simulation highlighted increased immune cell populations, the absence of activation markers raises concerns regarding the accuracy of predicting functional immune engagement and vaccine efficacy. The recruitment of T-cells or macrophages does not ensure their active participation in the immune response. Activation markers such as CD80/CD86 and MHC are crucial for verifying that antigen-presenting cells (APCs) effectively communicate with T-cells, priming them for action. Without these markers, the immune response may remain suboptimal, potentially compromising the overall protective efficacy of the vaccine (85). This underscores the importance of further validation through both *in vitro* and *in vivo* studies to confirm the functional activation of immune cells.

To overcome the limitations of core proteins and achieve broad-spectrum protection, we employed a two-pronged strategy. First, we targeted vaccine candidates with high prevalence (> 90%) across a wide range of pathogenic *F. tularensis* strains, which were identified using a highly virulent strain as a reference. Second, we prioritized epitopes that exhibited complete sequence conservation (100 %). This comprehensive approach has the potential to develop a vaccine capable of providing robust protection against a broad spectrum of tularemia-causing *F. tularensis* strains. Supporting this strategy, a study by Subrat Kumar Swain et al. demonstrated that the strategic combination of B-cell and T-cell epitopes effectively induces a strong and durable immune response, thereby establishing both cellular and humoral immunity (86). This dual-epitope strategy enhanced the ability of the vaccine to elicit a well-rounded and long-lasting immune response against *F. tularensis* strains.

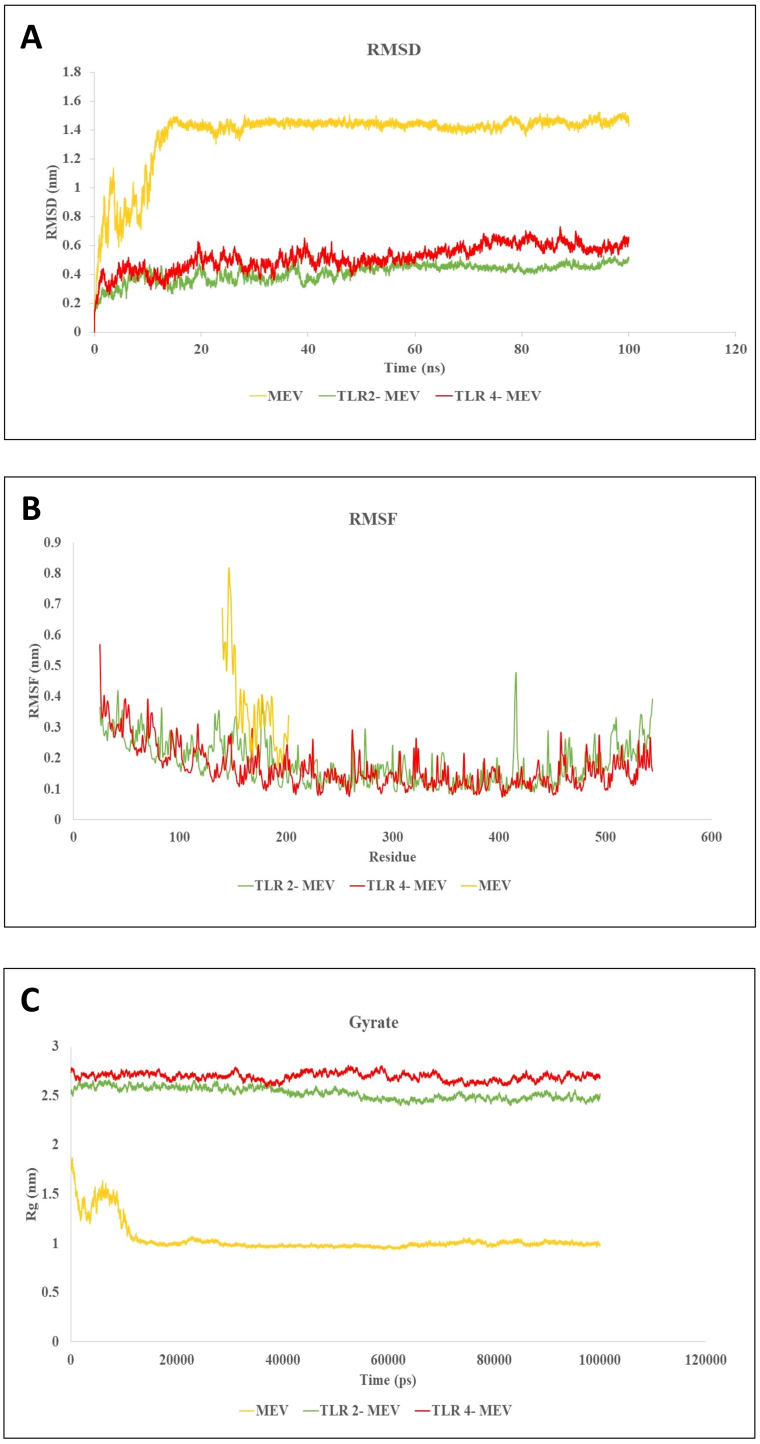

FIGURE 9
Molecular dynamics simulations of MEV and its Complexes with TLR-2 and TLR-4. **(A)** RMSD plot showing the stability of the MEV molecule and the MEV_TLR-2 and MEV_TLR-4 complexes throughout the simulation, with equilibrium RMSD values indicating stable interactions. **(B)** RMSF plot illustrating residue flexibility, where higher RMSF values represent more flexible regions and lower values denote rigidity across the MEV, MEV_TLR-2, and MEV_TLR-4 systems. **(C)** Radius of gyration (Rg) plot reflecting the shape and compactness of each system over time. Stable Rg values indicate consistent molecular shapes, while fluctuations indicate conformational changes. These simulations offer insights into the stability, flexibility, and structural evolution of MEV molecules and their interactions with TLR receptors under cytosolic conditions.

TABLE 2 The shortlist of 10 novel drug targets against *F. tularensis*.

No.	Accession number)	EggNOG and CCD	Gut microbiota BLAST*
1	WP_003017413.1	Asp-tRNA (Asn)/Glu-tRNA (Gln) amidotransferase subunit GatC	–
2	WP_003023081.1	30S ribosomal protein S16	–
3	WP_003017784.1	Hypothetical protein	–
4	WP_003014157.1	Haloacid dehalogenase	–
5	WP_003020066.1	Hypothetical protein	–
6	WP_003020080.1	Hypothetical protein	–
7	WP_003022220.1	uroporphyrinogen-III synthase	–
8	WP_042522581.1	NAD(P)-binding protein	–
9	WP_003022345.1	class I SAM-dependent methyltransferase	–
10	WP_003022350.1	Hypothetical protein	–

*: Minus symbol indicates no significant similarity was found with gut microbiota proteins.

Abbas Khan et al. employed structural proteomics to design a multi-epitope vaccine for tularemia, using *F. novicida*, a less virulent strain (87). In contrast, our approach focused on *F. tularensis* type A, isolated from a patient with tularemia, ensuring greater relevance for vaccine development. This differs, from the findings of Khan et al, who identified only four potential targets in *F. novicida* (87). This discrepancy highlights the potential strain-specific variations in immunogenic targets. Of the 12 proteins identified in our study, only four contained suitable epitopes for MEV design. This demonstrates that a protein may be antigenic and exhibit other essential vaccine candidate properties, yet still lack suitable epitopes for eliciting protective immunity. For instance, FopA was identified as a vaccine candidate in our study but did not provide any suitable epitopes. Similarly, previous studies have shown that FopA does not elicit protective immunity against tularemia in animal models (88).

This study identified ten promising drug development targets that are crucial for the survival and metabolism of *F. tularensis*, thus making them ideal candidates for novel treatments. The targets included Asp-tRNA (Asn)/Glu-tRNA (Gln) amidotransferase subunit GatC (WP_003017413.1), NAD(P)-binding protein (WP_042522581.1), 30S ribosomal protein S16 (WP_003023081.1), Class I SAM-dependent methyltransferase (WP_003022345.1), haloacid dehalogenase (WP_003014157.1), and uroporphyrinogen-III synthase (WP_003022220.1). Four hypothetical proteins (WP_003017784.1, WP_003020080.1, WP_003020066.1, WP_003022350.1). These targets offer significant potential for developing new therapeutic interventions. Among these, GatC (WP_003017413.1), an amidotransferase subunit, is essential for bacteria to thrive in host cells. Inhibition of GatC can effectively prevent infection by halting bacterial proliferation (89). The NAD(P)-binding protein (WP_042522581.1) is another promising target. This vital coenzyme is involved in numerous biochemical processes, with approximately 5.4% of the proteins in the UniProtKB/Swiss-Prot database being annotated as NAD(P)-binding. These proteins, such as ADP-ribosylating toxins and poly-ADP-ribose polymerases, are recognized as therapeutic targets. Inhibition of NAD(P)-binding proteins can disrupt crucial redox and non-redox reactions within a pathogen, thereby crippling its metabolic functions (90). 30S ribosomal protein S16 (WP_003023081.1) plays a critical role in protein synthesis. Targeting bacterial ribosomes has been a successful antibiotic strategy, exemplified by drugs such as linezolid, tetracycline, and chloramphenicol (91–93). Class I SAM-dependent methyltransferase (WP_003022345.1) is also a promising target because of its vital role in cellular processes, such as gene expression, protein function, and cell signaling. Inhibition of these enzymes could disrupt these critical functions, hindering the ability of the bacterium to operate (94). Haloacid dehalogenase (WP_003014157.1), a HAD-like phosphatase, performs various cellular functions including primary and secondary metabolism, enzyme activity or protein assembly regulation, cell housekeeping, and nutrient uptake. Targeting this enzyme can disrupt the essential processes (95). Uroporphyrinogen III synthase (WP_003022220.1) is a cytosolic enzyme involved in heme biosynthesis, catalyzing the formation of uroporphyrinogen III from hydroxymethylbilane. Targeting this enzyme can interfere with the heme biosynthesis pathway in bacteria (96). In the present study, we identified four hypothetical proteins with unknown functions as potential vaccine targets. Understanding the roles of these proteins could open new avenues for treatment, underscoring the importance of further research to uncover novel therapeutic possibilities.

5 Conclusion

Tularemia demands the development of novel vaccine candidates, identification of new drug targets, and the adoption of modern strategies for effective management. In this study, we identified ten proteins involved in key cellular processes and pathways as potential immunogenic targets, including GatC, NAD(P)-binding protein, 30S ribosomal protein S16, Class I SAM-dependent methyltransferase, haloacid dehalogenase, uroporphyrinogen-III synthase, and four hypothetical proteins, which warrant further investigation. To address the challenges posed by *F. tularensis* and improved prophylactic measures, we designed an MEV. Rational design and proven safety of MEVs have accelerated the development of more stable, efficient, and broad-spectrum vaccine candidates that target a range of pathogens and cancers. This rapidly advancing field of immunoinformatics offers great potential for reducing time and resource expenditure, speeding up vaccine discovery, and making it an area ripe for further exploration. Our proposed MEV was predicted to be non-allergenic and to exhibit favorable physicochemical properties. Molecular docking studies combined with molecular dynamics simulations demonstrated the ability of the vaccine to form strong and stable interactions with immune receptors. Immune simulations further suggested the potential of this vaccine to elicit robust immune responses. While the construct shows promise as a safe and effective solution for combating tularemia, comprehensive

in vitro and *in vivo* studies are essential to assess its efficacy under native conditions. The promising results of the computational analyses will be experimentally evaluated to confirm by the authors soon.

Data availability statement

The genome of Francisella tularensis is accessible at https://www.ncbi.nlm.nih.gov/datasets/genome/?taxon=263. The article files will be made available upon publication, and additional materials can be found in the Supplementary Information Files.

Ethics statement

The ethical considerations of the study were approved by the Ethical Committee of the Pasteur Institute of Iran (IR.PII.REC.1403.008).

Author contributions

SM: Conceptualization, Methodology, Software, Writing – original draft, Investigation. SE: Conceptualization, Data Curation, Writing – review & editing, Investigation, Project administration, Resources, Validation, Supervision, Funding acquisition. MA: Conceptualization, Data Curation, Writing – review & editing, Investigation, Project administration, Resources, Validation, Supervision, Funding acquisition. EM: Conceptualization, Data Curation, Writing – review & editing, Investigation. BS: Methodology, Software, Writing – original draft. AS: Conceptualization, Data Curation, Writing – review & editing, Investigation. MC: Conceptualization, Data Curation, Writing – review & editing, Investigation. FB: Conceptualization, Methodology, Software, Data Curation, Writing – review & editing, Investigation, Project administration, Resources, Validation, Supervision, Funding acquisition.

Funding

The author(s) declare that financial support was received for the research and/or publication of this article. This study is part of a Ph.D. thesis supported by the Pasteur Institute of Iran (Grant number: 66002217) and is based on research funded by the Iran National Science Foundation (INSF) (Project number: 4034040).

Conflict of interest

The authors declare that the research was conducted in the absence of any commercial or financial relationships that could be construed as a potential conflict of interest.

Publisher's note

Supplementary material

The Supplementary Material for this article can be found online at: https://www.frontiersin.org/articles/10.3389/fimmu.2025.1479862/full#supplementary-material

References

1. Mulligan MJ, Stapleton JT, Keitel WA, Frey SE, Chen WH, Rouphael N, et al. Tularemia vaccine: Safety, reactogenicity, "Take" skin reactions, and antibody responses following vaccination with a new lot of the Francisella tularensis live vaccine strain - A phase 2 randomized clinical Trial. *Vaccine*. (2017) 35:4730–7. doi: 10.1016/j.vaccine.2017.07.024

2. Oyston PC, Quarry JE. Tularemia vaccine: past, present and future. *Antonie Van Leeuwenhoek*. (2005) 87:277–81. doi: 10.1007/s10482-004-6251-7

3. Dennis DT, Inglesby TV, Henderson DA, Bartlett JG, Ascher MS, Eitzen E, et al. Tularemia as a biological weapon: medical and public health management. *JAMA*. (2001) 285:2763–73. doi: 10.1001/jama.285.21.2763

4. Boisset S, Caspar Y, Sutera V, Maurin M. New therapeutic approaches for treatment of tularaemia: a review. *Front Cell Infect Microbiol*. (2014) 4:40. doi: 10.3389/fcimb.2014.00040

5. Bina XR, Wang C, Miller MA, Bina JE. The Bla2 β-lactamase from the live-vaccine strain of Francisella tularensis encodes a functional protein that is only active against penicillin-class β-lactam antibiotics. *Arch Microbiol*. (2006) 186:219–28. doi: 10.1007/s00203-006-0140-6

6. Belete TM. Novel targets to develop new antibacterial agents and novel alternatives to antibacterial agents. *Hum Microbiome J*. (2019) 11:100052. doi: 10.1016/j.humic.2019.01.001

7. Wawszczak M, Banaszczak B, Rastawicki W. Tularaemia - a diagnostic challenge. *Ann Agric Environ Med*. (2022) 29:12–21. doi: 10.26444/aaem/139242

8. Roberts LM, Powell DA, Frelinger JA. Adaptive immunity to Francisella tularensis and considerations for vaccine development. *Front Cell Infect Microbiol*. (2018) 8:115. doi: 10.3389/fcimb.2018.00115

9. Rappuoli R, Bottomley MJ, D'Oro U, Finco O, De Gregorio E. Reverse vaccinology 2.0: Human immunology instructs vaccine antigen design. *J Exp Med*. (2016) 213:469–81. doi: 10.1084/jem.20151960

10. Dey J, Mahapatra SR, Raj TK, Kaur T, Jain P, Tiwari A, et al. Designing a novel multi-epitope vaccine to evoke a robust immune response against pathogenic multidrug-resistant Enterococcus faecium bacterium. *Gut Pathog*. (2022) 14:21. doi: 10.1186/s13099-022-00495-z

11. De Brito RCF, Cardoso JMO, Reis LES, Vieira JF, Mathias FAS, Roatt BM, et al. Peptide vaccines for Leishmaniasis. *Front Immunol*. (2018) 9:1043. doi: 10.3389/fimmu.2018.01043

12. Sharma R, Rajput VS, Jamal S, Grover A, Grover S. An immunoinformatics approach to design a multi-epitope vaccine against Mycobacterium tuberculosis exploiting secreted exosome proteins. *Sci Rep*. (2021) 11:13836. doi: 10.1038/s41598-021-93266-w

13. D'Mello A, Ahearn CP, Murphy TF, Tettelin H. ReVac: a reverse vaccinology computational pipeline for prioritization of prokaryotic protein vaccine candidates. *BMC Genomics*. (2019) 20:981. doi: 10.1186/s12864-019-6195-y

14. Shey RA, Ghogomu SM, Esoh KK, Nebangwa ND, Shintouo CM, Nongley NF, et al. In-silico design of a multi-epitope vaccine candidate against

onchocerciasis and related filarial diseases. *Sci Rep*. (2019) 9:4409. doi: 10.1038/s41598-019-40833-x

15. Dey J, Mahapatra SR, Singh PK, Prabhuswamimath SC, Misra N, Suar M. Designing of multi-epitope peptide vaccine against Acinetobacter baumannii through combined immunoinformatics and protein interaction-based approaches. *Immunol Res*. (2023) 71:639–62. doi: 10.1007/s12026-023-09374-4

16. Kanampalliwar AM. Reverse vaccinology and its applications. *Methods Mol Biol*. (2020) 2131:1–16. doi: 10.1007/978-1-0716-0389-5_1

17. Jalal K, Abu-Izneid T, Khan K, Abbas M, Hayat A, Bawazeer S, et al. Identification of vaccine and drug targets in Shigella dysenteriae sd197 using reverse vaccinology approach. *Sci Rep*. (2022) 12:251. doi: 10.1038/s41598-021-03988-0

18. Khan K, Jalal K, Uddin R. An integrated in silico based subtractive genomics and reverse vaccinology approach for the identification of novel vaccine candidate and chimeric vaccine against XDR Salmonella typhi H58. *Genomics*. (2022) 114:110301. doi: 10.1016/j.ygeno.2022.110301

19. Nosrati M, Behbahani M, Mohabatkar H. Towards the first multi-epitope recombinant vaccine against Crimean-Congo hemorrhagic fever virus: A computer-aided vaccine design approach. *J BioMed Inform*. (2019) 93:103160. doi: 10.1016/j.jbi.2019.103160

20. Srivastava S, Kamthania M, Kumar Pandey R, Kumar Saxena A, Saxena V, Kumar Singh S, et al. Design of novel multi-epitope vaccines against severe acute respiratory syndrome validated through multistage molecular interaction and dynamics. *J Biomol Struct Dyn*. (2019) 37:4345–60. doi: 10.1080/07391102.2018.1548977

21. Tosta SFO, Passos MS, Kato R, Salgado Á, Xavier J, Jaiswal AK, et al. Multi-epitope based vaccine against yellow fever virus applying immunoinformatics approaches. *J Biomol Struct Dyn*. (2021) 39:219–35. doi: 10.1080/07391102.2019.1707120

22. Nguyen TL, Kim H. Discovering peptides and computational investigations of a multiepitope vaccine target Mycobacterium tuberculosis. *Synth Syst Biotechnol*. (2024) 9:391–405. doi: 10.1016/j.synbio.2024.03.010

23. Chaudhari NM, Gupta VK, Dutta C. BPGA-an ultra-fast pan-genome analysis pipeline. *Sci Rep*. (2016) 6:24373. doi: 10.1038/srep24373

24. Bachert BA, Richardson JB, Mlynek KD, Klimko CP, Toothman RG, Fetterer DP, et al. Development, phenotypic characterization and genomic analysis of a Francisella tularensis panel for tularemia vaccine testing. *Front Microbiol*. (2021) 12:725776. doi: 10.3389/fmicb.2021.725776

25. Ashkenazy H, Erez E, Martz E, Pupko T, Ben-Tal N. ConSurf 2010: calculating evolutionary conservation in sequence and structure of proteins and nucleic acids. *Nucleic Acids Res*. (2010) 38:W529–W33. doi: 10.1093/nar/gkq399

26. Yu NY, Wagner JR, Laird MR, Melli G, Rey S, Lo R, et al. PSORTb 3.0: improved protein subcellular localization prediction with refined localization subcategories and predictive capabilities for all prokaryotes. *Bioinformatics*. (2010) 26:1608–15. doi: 10.1093/bioinformatics/btq249

27. Yu CS, Lin CJ, Hwang JK. Predicting subcellular localization of proteins for Gram-negative bacteria by support vector machines based on n-peptide compositions. *Protein Sci*. (2004) 13:1402–6. doi: 10.1110/ps.03479604

28. Doytchinova IA, Flower DR. VaxiJen: a server for prediction of protective antigens, tumour antigens and subunit vaccines. *BMC Bioinf*. (2007) 8:4. doi: 10.1186/1471-2105-8-4

29. Sharma N, Patiyal S, Dhall A, Pande A, Arora C, Raghava GP. AlgPred 2.0: an improved method for predicting allergenic proteins and mapping of IgE epitopes. *Briefings Bioinf*. (2021) 22:bbaa294. doi: 10.1093/bib/bbaa294

30. Dimitrov I, Flower DR, Doytchinova I eds. AllerTOP-a server for in silico prediction of allergens. In: *BMC bioinformatics*. BioMed Central. doi: 10.1186/1471-2105-14-s6-s4

31. Kumar S, Stecher G, Li M, Knyaz C, Tamura K. MEGA X: molecular evolutionary genetics analysis across computing platforms. *Mol Biol evolution*. (2018) 35:1547. doi: 10.1093/molbev/msy096

32. Yariv B, Yariv E, Kessel A, Masrati G, Chorin AB, Martz E, et al. Using evolutionary data to make sense of macromolecules with a "face-lifted" ConSurf. *Protein Sci*. (2023) 32:e4582. doi: 10.1002/pro.v32.3

33. Saha S, Raghava GP. VICMpred: an SVM-based method for the prediction of functional proteins of Gram-negative bacteria using amino acid patterns and composition. *Genomics Proteomics Bioinf*. (2006) 4:42–7. doi: 10.1016/S1672-0229(06)60015-6

34. Paul S, Sidney J, Sette A, Peters B. TepiTool: A pipeline for computational prediction of T cell epitope candidates. *Curr Protoc Immunol*. (2016) 114:18.9.1–.9.24. doi: 10.1002/0471142735.2016.114.issue-1

35. Ghashghaie A, Alimoghaddam K, Ostadali MR, Khansari L, Sadraee M, Mirrasekhian E, et al. Allele frequencies of HLA class-I loci in the normal Iranian population. *Int J hematology-oncology Stem Cell Res*. (2009) 3(3):18–20.

36. Marchler-Bauer A, Derbyshire MK, Gonzales NR, Lu S, Chitsaz F, Geer LY, et al. CDD: NCBI's conserved domain database. *Nucleic Acids Res*. (2015) 43:D222–6. doi: 10.1093/nar/gku1221

37. Huerta-Cepas J, Szklarczyk D, Heller D, Hernández-Plaza A, Forslund SK, Cook H, et al. eggNOG 5.0: a hierarchical, functionally and phylogenetically annotated orthology resource based on 5090 organisms and 2502 viruses. *Nucleic Acids Res*. (2019) 47:D309–d14. doi: 10.1093/nar/gky1085

38. Foroutan M, Ghaffarifar F, Sharifi Z, Dalimi A. Vaccination with a novel multi-epitope ROP8 DNA vaccine against acute Toxoplasma gondii infection induces strong B and T cell responses in mice. *Comp Immunol Microbiol Infect Dis*. 69:101413. doi: 10.1016/j.cimid.2020.101413

39. Schwede T, Kopp J, Guex N, Peitsch MC. SWISS-MODEL: an automated protein homology-modeling server. *Nucleic Acids Res*. (2003) 31:3381–5. doi: 10.1093/nar/gkg520

40. Prajapat R, Marwal A, Gaur R. Recognition of errors in the refinement and validation of three-dimensional structures of AC1 proteins of begomovirus strains by using ProSA-Web. *J Viruses*. (2014) 2014:752656. doi: 10.1155/2014/752656

41. Dym O, Eisenberg D, Yeates TO. Detection of errors in protein models. *International Tables for Crystallography*. (2012) 677–83. doi: 10.1107/9780955360206000881

42. Ponomarenko J, Bui H-H, Li W, Fusseder N, Bourne PE, Sette A, et al. ElliPro: a new structure-based tool for the prediction of antibody epitopes. *BMC Bioinf*. (2008) 9:1–8. doi: 10.1186/1471-2105-9-514

43. Szklarczyk D, Gable AL, Lyon D, Junge A, Wyder S, Huerta-Cepas J, et al. STRING v11: protein–protein association networks with increased coverage, supporting functional discovery in genome-wide experimental datasets. *Nucleic Acids Res*. (2019) 47:D607–D13. doi: 10.1093/nar/gky1131

44. Kushwaha SK, Shakya M. Protein interaction network analysis—approach for potential drug target identification in Mycobacterium tuberculosis. *J Theor Biol*. (2010) 262:284–94. doi: 10.1016/j.jtbi.2009.09.029

45. Srivastava S, Kamthania M, Singh S, Saxena AK, Sharma N. Structural basis of development of multi-epitope vaccine against Middle East respiratory syndrome using in silico approach. *Infection Drug resistance*. (2018) 11:2377–91. doi: 10.2147/IDR.S175114

46. Dar HA, Waheed Y, Najmi MH, Ismail S, Hetta HF, Ali A, et al. Multiepitope subunit vaccine design against COVID-19 based on the spike protein of SARS-CoV-2: an in silico analysis. *J Immunol Res*. (2020) 2020:8893483. doi: 10.1155/2020/8893483

47. Sabourin M, Tuzon CT, Fisher TS, Zakian VA. A flexible protein linker improves the function of epitope-tagged proteins in Saccharomyces cerevisiae. *Yeast*. (2007) 24:39–45. doi: 10.1002/yea.v24:1

48. Yan Y, Tao H, He J, Huang S-Y. The HDOCK server for integrated protein–protein docking. *Nat Protoc*. (2020) 15:1829–52. doi: 10.1038/s41596-020-0312-x

49. Laskowski RA. PDBsum: summaries and analyses of PDB structures. *Nucleic Acids Res*. (2001) 29:221–2. doi: 10.1093/nar/29.1.221

50. Hebditch M, Carballo-Amador MA, Charonis S, Curtis R, Warwicker J. ProteinSol: a web tool for predicting protein solubility from sequence. *Bioinformatics*. (2017) 33:3098–100. doi: 10.1093/bioinformatics/btx345

51. Wilkins MR, Gasteiger E, Bairoch A, Sanchez JC, Williams KL, Appel RD, et al. Protein identification and analysis tools in the ExPASy server. *Methods Mol Biol*. (1999) 112:531–52. doi: 10.1385/1-59259-584-7:531

52. Gould N, Hendy O, Papamichail D. Computational tools and algorithms for designing customized synthetic genes. *Front bioengineering Biotechnol*. (2014) 2:41. doi: 10.3389/fbioe.2014.00041

53. Rapin N, Lund O, Bernaschi M, Castiglione F. Computational immunology meets bioinformatics: the use of prediction tools for molecular binding in the simulation of the immune system. *PLoS One*. (2010) 5:e9862. doi: 10.1371/journal.pone.0009862

54. Albekairi TH, Alshammari A, Alharbi M, Alshammary AF, Tahir Ul Qamar M, Anwar T, et al. Design of a Multi-Epitope Vaccine against Tropheryma whipplei Using Immunoinformatics and Molecular Dynamics Simulation Techniques. *Vaccines*. (2022) 10. doi: 10.3390/vaccines10050691

55. Brandon MC, Ruiz-Pesini E, Mishmar D, Procaccio V, Lott MT, Nguyen KC, et al. MITOMASTER: a bioinformatics tool for the analysis of mitochondrial DNA sequences. *Hum Mutat*. (2009) 30:1–6. doi: 10.1002/humu.20801

56. Damte D, Suh J-W, Lee S-J, Yohannes SB, Hossain MA, Park S-C. Putative drug and vaccine target protein identification using comparative genomic analysis of KEGG annotated metabolic pathways of Mycoplasma hyopneumoniae. *Genomics*. (2013) 102:47–56. doi: 10.1016/j.ygeno.2013.04.011

57. Kanehisa M, Goto S. KEGG: kyoto encyclopedia of genes and genomes. *Nucleic Acids Res*. (2000) 28:27–30. doi: 10.1093/nar/28.1.27

58. Wishart DS, Feunang YD, Guo AC, Lo EJ, Marcu A, Grant JR, et al. DrugBank 5.0: a major update to the DrugBank database for 2018. *Nucleic Acids Res*. (2018) 46:D1074–D82.

59. Turnbaugh PJ, Ley RE, Hamady M, Fraser-Liggett CM, Knight R, Gordon JI. The human microbiome project. *Nature*. (2007) 449:804–10. doi: 10.1038/nature06244

60. Zhang R, Ou HY, Zhang CT. DEG: a database of essential genes. *Nucleic Acids Res*. (2004) 32:D271–D2. doi: 10.1093/nar/gkh024

61. Judson N, Mekalanos JJ. TnAraOut, a transposon-based approach to identify and characterize essential bacterial genes. *Nat Biotechnol*. (2000) 18:740–5. doi: 10.1038/77305

62. Conlan JW, Shen H, Webb A, Perry MB. Mice vaccinated with the O-antigen of Francisella tularensis LVS lipopolysaccharide conjugated to bovine serum albumin develop varying degrees of protective immunity against systemic or aerosol challenge with virulent type A and type B strains of the pathogen. *Vaccine*. (2002) 20:3465–71. doi: 10.1016/S0264-410X(02)00345-6

63. Apicella MA, Post DM, Fowler AC, Jones BD, Rasmussen JA, Hunt JR, et al. Identification, characterization and immunogenicity of an O-antigen capsular polysaccharide of Francisella tularensis. *PloS One*. (2010) 5:e11060. doi: 10.1371/journal.pone.0011060

64. Hickey AJ, Hazlett KR, Kirimanjeswara GS, Metzger DW. Identification of Francisella tularensis outer membrane protein A (FopA) as a protective antigen for tularemia. *Vaccine*. (2011) 29:6941–7. doi: 10.1016/j.vaccine.2011.07.075

65. Kaur R, Chen S, Arévalo MT, Xu Q, Chen Y, Zeng M. Protective immunity against tularemia provided by an adenovirus-vectored vaccine expressing Tul4 of Francisella tularensis. *Clin Vaccine Immunol*. (2012) 19:359–64. doi: 10.1128/CVI.05384-11

66. Huntley JF, Conley PG, Rasko DA, Hagman KE, Apicella MA, Norgard MV. Native outer membrane proteins protect mice against pulmonary challenge with virulent type A Francisella tularensis. *Infect Immun*. (2008) 76:3664–71. doi: 10.1128/IAI.00374-08

67. Ashtekar AR, Katz J, Xu Q, Michalek SM. A mucosal subunit vaccine protects against lethal respiratory infection with Francisella tularensis LVS. *PLoS One*. (2012) 7: e50460. doi: 10.1371/journal.pone.0050460

68. Richard K, Mann BJ, Stocker L, Barry EM, Qin A, Cole LE, et al. Novel catanionic surfactant vesicle vaccines protect against Francisella tularensis LVS and confer significant partial protection against F. tularensis Schu S4 strain. *Clin Vaccine Immunol*. (2014) 21:212–26. doi: 10.1128/CVI.00738-13

69. Banik S, Mansour AA, Suresh RV, Wykoff-Clary S, Malik M, McCormick AA, et al. Development of a multivalent subunit vaccine against tularemia using tobacco mosaic virus (TMV) based delivery system. *PLoS One*. (2015) 10:e0130858. doi: 10.1371/journal.pone.0130858

70. Grandi G. Bacterial surface proteins and vaccines. *F1000 Biol Rep*. (2010) 2. doi: 10.3410/B2-36

71. Sutherland MD, Goodyear AW, Troyer RM, Chandler JC, Dow SW, Belisle JT. Post-exposure immunization against Francisella tularensis membrane proteins augments protective efficacy of gentamicin in a mouse model of pneumonic tularemia. *Vaccine*. (2012) 30:4977–82. doi: 10.1016/j.vaccine.2012.05.037

72. Ireland R, Olivares-Zavaleta N, Warawa JM, Gherardini FC, Jarrett C, Hinnebusch BJ, et al. Effective, broad spectrum control of virulent bacterial infections using cationic DNA liposome complexes combined with bacterial antigens. *PLoS Pathog*. (2010) 6:e1000921. doi: 10.1371/journal.ppat.1000921

73. Chandler JC, Sutherland MD, Harton MR, Molins CR, Anderson RV, Heaslip DG, et al. Francisella tularensis LVS surface and membrane proteins as targets of effective post-exposure immunization for tularemia. *J Proteome Res*. (2015) 14:664–75. doi: 10.1021/pr500628k

74. Sette A, Rappuoli R. Reverse vaccinology: developing vaccines in the era of genomics. *Immunity*. (2010) 33:530–41. doi: 10.1016/j.immuni.2010.09.017

75. Bahadori Z, Shafaghi M, Madanchi H, Ranjbar MM, Shabani AA, Mousavi SF. In silico designing of a novel epitope-based candidate vaccine against Streptococcus pneumoniae with introduction of a new domain of PepO as adjuvant. *J Transl Med*. (2022) 20:389. doi: 10.1186/s12967-022-03590-6

76. Medini D, Stella M, Wassil J. MATS: Global coverage estimates for 4CMenB, a novel multicomponent meningococcal B vaccine. *Vaccine*. (2015) 33:2629–36. doi: 10.1016/j.vaccine.2015.04.015

77. Serruto D, Bottomley MJ, Ram S, Giuliani MM, Rappuoli R. The new multicomponent vaccine against meningococcal serogroup B, 4CMenB: immunological, functional and structural characterization of the antigens. *Vaccine*. (2012) 30 Suppl 2:B87–97. doi: 10.1016/j.vaccine.2012.01.033

78. Goumari MM, Farhani I, Nezafat N, Mahmoodi S. Multi-epitope vaccines (MEVs), as a novel strategy against infectious diseases. *Curr Proteomics*. (2020) 17:354–64. doi: 10.2174/1570164617666190919120140

79. Dey J, Mahapatra SR, Lata S, Patro S, Misra N, Suar M. Exploring Klebsiella pneumoniae capsule polysaccharide proteins to design multiepitope subunit vaccine to fight against pneumonia. *Expert Rev Vaccines*. (2022) 21:569–87. doi: 10.1080/14760584.2022.2021882

80. Cole LE, Laird MH, Seekatz A, Santiago A, Jiang Z, Barry E, et al. Phagosomal retention of Francisella tularensis results in TIRAP/Mal-independent TLR2 signaling. *J Leukoc Biol*. (2010) 87:275–81. doi: 10.1189/jlb.0909619

81. Metzger DW, Salmon SL, Kirimanjeswara G. Differing effects of interleukin-10 on cutaneous and pulmonary Francisella tularensis live vaccine strain infection. *Infect Immun*. (2013) 81:2022–7. doi: 10.1128/IAI.00024-13

82. Stenmark S, Sunnemark D, Bucht A, Sjöstedt A. Rapid local expression of interleukin-12, tumor necrosis factor alpha, and gamma interferon after cutaneous Francisella tularensis infection in tularemia-immune mice. *Infect Immun*. (1999) 67:1789–97. doi: 10.1128/IAI.67.4.1789-1797.1999

83. Lindgren H, Eneslätt K, Golovliov I, Gelhaus C, Sjöstedt A. Analyses of human immune responses to Francisella tularensis identify correlates of protection. *Front Immunol*. (2023) 14:1238391. doi: 10.3389/fimmu.2023.1238391

84. Kubelkova K, Macela A. Francisella and antibodies. *Microorganisms*. (2021) 9. doi: 10.3390/microorganisms9102136

85. Sansom DM, Manzotti CN, Zheng Y. What's the difference between CD80 and CD86? *Trends Immunol*. (2003) 24:314–9.

86. Swain SK, Panda S, Sahu BP, Mahapatra SR, Dey J, Sarangi R, et al. Inferring B-cell derived T-cell receptor induced multi-epitope-based vaccine candidate against enterovirus 71: a reverse vaccinology approach. *Clin Exp Vaccine Res*. (2024) 13:132–45. doi: 10.7774/cevr.2024.13.2.132

87. Khan A, Ali SS, Khan A, Zahid MA, Alshabrmi FM, Waheed Y, et al. Structural proteomics guided annotation of vaccine targets and designing of multi-epitopes vaccine to instigate adaptive immune response against Francisella tularensis. *Microb Pathog*. (2024), 106777. doi: 10.1016/j.micpath.2024.106777

88. Moradkasani S, Maurin M, Farrokhi AS, Esmaeili S. Development, strategies, and challenges for Tularemia vaccine. *Curr Microbiol*. (2024) 81:126. doi: 10.1007/s00284-024-03658-0

89. McLendon MK, Apicella MA, Allen LA. Francisella tularensis: taxonomy, genetics, and Immunopathogenesis of a potential agent of biowarfare. *Annu Rev Microbiol*. (2006) 60:167–85. doi: 10.1146/annurev.micro.60.080805.142126

90. Hua YH, Wu CY, Sargsyan K, Lim C. Sequence-motif detection of NAD(P)-binding proteins: discovery of a unique antibacterial drug target. *Sci Rep*. (2014) 4:6471. doi: 10.1038/srep06471

91. Oberto J, Bonnefoy E, Mouray E, Pellegrini O, Wikström PM, Rouvière-Yaniv J. The Escherichia coli ribosomal protein S16 is an endonuclease. *Mol Microbiol*. (1996) 19:1319–30. doi: 10.1111/j.1365-2958.1996.tb02476.x

92. Zhang L, He J, Bai L, Ruan S, Yang T, Luo Y. Ribosome-targeting antibacterial agents: Advances, challenges, and opportunities. *Medicinal Res Rev*. (2021) 41:1855–89. doi: 10.1002/med.21780

93. Giuliodori AM, Spurio R, Milón P, Fabbretti A. Antibiotics targeting the 30S ribosomal subunit: a lesson from nature to find and develop new drugs. *Curr Topics Medicinal Chem*. (2018) 18:2080–96. doi: 10.2174/1568026618666181025092546

94. Aktas M, Gleichenhagen J, Stoll R, Narberhaus F. S-adenosylmethionine-binding properties of a bacterial phospholipid N-methyltransferase. *J Bacteriol*. (2011) 193:3473–81. doi: 10.1128/JB.01539-10

95. Allen KN, Dunaway-Mariano D. Markers of fitness in a successful enzyme superfamily. *Curr Opin Struct Biol*. (2009) 19:658–65. doi: 10.1016/j.sbi.2009.09.008

96. Bernardo-Seisdedos G, Gil D, Blouin J-M, Richard E, Millet O. Chapter 18 - Natural and pharmacological chaperones against accelerated protein degradation: uroporphyrinogen III synthase and congenital erythropoietic porphyria. In: Pey AL, editor. *Protein Homeostasis Diseases*. Academic Press (2020). p. 389–413.

frontiers | Frontiers in Cellular and Infection Microbiology

TYPE Original Research
PUBLISHED 08 May 2025
DOI 10.3389/fcimb.2025.1531880

OPEN ACCESS

EDITED BY
Omid Teymournejad,
University of Illinois Chicago, United States

REVIEWED BY
Eugenia M Bastos,
Independent researcher, Sommerville, MA, United States
Cheng Zhang,
Hebei Agricultural University, China

*CORRESPONDENCE
Baoju Wang
bjwang73@163.com
Zhihang Peng
zhihangpeng@njmu.edu.cn

†These authors have contributed equally to this work and share first authorship

‡These authors have contributed equally to this work and share senior authorship

RECEIVED 21 November 2024
ACCEPTED 16 April 2025
PUBLISHED 08 May 2025

CITATION
Zhong F, Zhang S, Zheng C, Zhayier D, Liu S, You Q, Huang H, Zhu B, Tian J, Hu Z, Zheng X, Wang B and Peng Z (2025) Fatal risk factors and the efficacy of glucocorticoid therapy in severe fever with thrombocytopenia syndrome: a multicenter retrospective cohort study. *Front. Cell. Infect. Microbiol.* 15:1531880. doi: 10.3389/fcimb.2025.1531880

Fatal risk factors and the efficacy of glucocorticoid therapy in severe fever with thrombocytopenia syndrome: a multicenter retrospective cohort study

Fang Zhong[1†], Shiyu Zhang[2†], Chengxi Zheng[1†], Dilihumaer Zhayier[2], Shuting Liu[2], Qinyu You[1], Hongming Huang[2], Bin Zhu[2], Jin Tian[2], Zhiliang Hu[3,4,5], Xin Zheng[2], Baoju Wang[2*‡] and Zhihang Peng[1,6,7*‡]

[1]School of Public Health, Nanjing Medical University, Nanjing, China, [2]Department of Infectious Disease, Union Hospital, Tongji Medical College, Huazhong University of Science and Technology, Wuhan, China, [3]Department of Infectious Disease, the Second Hospital of Nanjing, School of Public Health, Nanjing Medical University, Nanjing, China, [4]Nanjing Hospital, Nanjing University of Chinese Medicine, Nanjing, China, [5]Center for Global Health, School of Public Health, Nanjing Medical University, Nanjing, China, [6]National Key Laboratory of Intelligent Tracking and Forecasting for Infectious Diseases, Chinese Center for Disease Control and Prevention, Beijing, China, [7]Chinese Center for Disease Control and Prevention, Beijing, China

Background: Severe fever with thrombocytopenia syndrome (SFTS) is an emerging tick-borne infectious disease characterized by rapid progression and high mortality. Glucocorticoids (GCs) can be used as anti-inflammatory agents for SFTS, but no standardized protocols have been proposed.

Methods: A total of 901 patients with SFTS diagnosed at two hospitals between July 2017 and October 2023 were included in this retrospective cohort study. Univariate and multivariate logistic regression were performed along with LASSO regression to identify independent risk factors of fatal outcomes and further develop mortality prediction model. A nomogram was used to visualize the predictive model. ROC curves, calibration curves, and DCA curves were conducted to assess model accuracy and clinical applicability. The efficacy of GC was assessed using survival analyses, and further subgroup analyses of the effects of different GC regimens on fatal outcomes and hospital-acquired infections (HAI) were performed. Propensity score matching (PSM) analyses were conducted to control confounding factors.

Results: Older age (age > 69 years), consciousness disturbance, decreased monocyte counts, prolonged activated partial thromboplastin time (APTT), and high viral load were identified as strong predictors of fatal outcomes in patients with SFTS. Patients were classified into mild and severe groups according to risk scores calculated by the nomogram (cut-off value = 121.43). Survival analyses showed that GCs treatment may reduce the mortality in severe patients (p = 0.004). Further subgroup analyses indicated that relatively high doses and early treatment with GCs may increase mortality in SFTS patients [OR = 2.292 (1.071,

5.066); OR = 3.693 (1.710, 8.345) respectively]. GCs treatment was associated with an elevated risk of HAI in patients both with mild and severe SFTS (p = 0.024; p = 0.015, respectively). Initiation of GCs therapy at a low level of aspartate aminotransferase (AST < 189.75 U/L) reduced the mortality before and after PSM (p<0.001; p = 0.004, respectively).

Conclusions: A new nomogram based on five independent risk factors effectively predicts the prognosis of SFTS. Severe patients and those with low AST levels might benefit from GCs therapy while early and relatively high doses of GCs therapy should be used with caution.

KEYWORDS

nomogram, prediction model, severe fever with thrombocytopenia syndrome, case fatality rate, glucocorticoids

1 Introduction

Severe fever with thrombocytopenia syndrome (SFTS) is an emerging tick-borne infectious disease caused by *Dabie bandavirus* (formerly known as SFTS virus [SFTSV]) (Kim and Park, 2023). The first case of SFTS in China was confirmed in 2009 (Yu et al., 2011), followed by a total of 7,721 laboratory-confirmed SFTS cases during 2010-2018, with an overall case fatality rate (CFR) of 10.5%. Despite this high CFR, no specific antiviral therapy has been established.

Previous studies and meta-analyses have shown that among clinical symptoms and laboratory markers of SFTS, age, emesis, neurologic symptoms, disseminated Intravascular Coagulation (DIC), multiorgan dysfunction, and shock were significantly associated with death, whereas its risk also increases significantly in those with abnormalities in viral load, prothrombin time (TT), activated partial thromboplastin time (APTT), percentage of mononuclear cells, percentage of lymphocytes, and coagulation and liver function (Wang et al., 2022a; Wang et al., 2022b; Wang et al., 2024). Thus, early risk stratification is critical to improve patients' prognosis. Models based on a joint of indices have been developed to predict mortality in patients with SFTS, but most of them are single-centered and size-limited, which in turn restricts their clinical applications (Jia et al., 2017; Katsurada et al., 2017; Wei X. et al., 2022). In a recent multicenter study, 377 patients with SFTS were divided into double-positive, single-positive, and double-negative groups based on their neurological symptoms; a model incorporating age, gastrointestinal bleeding, and SFTS viral load (AUC=0.859) was generated for assessing the effectiveness of ribavirin, antibiotics, and gamma globulin (Xia et al., 2023). Nevertheless, the sample size of this study was still limited, and the efficacy of GCs, a common anti-inflammatory agent in the treatment of SFTS, was not evaluated.

The poor prognosis of SFTS may be attributed to high viral load, cytokine storm, and immune dysfunction (Chinese Society of Infectious Diseases and Chinese Medical Association, 2022). Consequently, therapeutic strategies can only be efficacious when bearing antiviral, anti-inflammatory, and immunostimulatory properties. Systemic GCs combat inflammation by inhibiting pro-inflammatory genes and inflammatory cytokines, making them potentially effective against diseases correlated with cytokine release (FakhriRavari et al., 2021). However, GCs-induced immunosuppression may also delay viral clearance and increase the risk of secondary infection (Shang et al., 2020). Guideline issued by the National Health and Wellness Commission of China recommend systemic application of glucocorticoids as adjunctive therapy for patients with severe SFTS, but it not contain criteria for identifying patients suitable for SFTS treatment and specific treatment regimens with optimal clinical efficacy (Chen et al., 2022). This may lead to inappropriate use of GCs in the treatment of SFTS, resulting in adverse outcomes for patients.

Therefore, this study aimed to establish a new model to early identify patients at high risk of death and predict the effect of GCs therapy.

2 Materials and methods

2.1 Study design and patient enrollment

This retrospective cohort study included patients with SFTS admitted at the Union Hospital of Tongji Medical College, Huazhong University of Science and Technology (Wuhan, China) from May 2020 to October 2023, and the Second Hospital of Nanjing (Nanjing, China) from January 2017 to June 2023. SFTS was laboratory-confirmed according to criteria released by the National Health Commission of China (2010 version) (Ministry of Health, PRC, 2011): (1) an exposure history of previous field activities in SFTS-endemic areas or tick bites within two weeks before febrile symptom onset, acute fever with thrombocytopenia

and/or leukopenia); (2) detection of SFTSV RNA by reverse-transcriptase PCR (RT-PCR). Exclusion criteria included: (1) age under 18 years; (2) length of hospitalization less than 48 hours; (3) missing important laboratory results; (4) presence of autoimmune disease, acquired immunodeficiency syndrome (AIDS), and malignant tumor (see Supplementary Figure 1).

This study was approved by the Ethics Committee of Union Hospital of Tongji Medical College, Huazhong University of Science and Technology (Ethics No. (2021) 1047-01) and the Ethics Committee of Nanjing Medical University, China (Ethics No. (2020) 211) according to the Declaration of Helsinki. This study was restricted to secondary data analysis, so the requirement for informed consent from participants was waived.

2.2 Data collection and study definitions

This retrospective analysis was based on patients' demographic and epidemiological data, clinical manifestations, initial laboratory results following admission, and treatment-related information. SFTS onset was marked as the first occurrence of fever or thrombocytopenia. Endpoint was set as discharge or a fatal outcome, the primary outcome as 28-day mortality, and the secondary outcome as hospital-acquired infection (HAI). HAI was determined if the infection was neither present nor incubating at admission, but occurred within ≥48 h after admission for SFTS (Ge et al., 2022). Systemic GCs therapy was defined as at least one dose of GCs administered via intravenous routes. Considering that dexamethasone is the most commonly prescribed, other types of GCs were converted to dexamethasone equivalents. According to a previous study, the doses of methylprednisolone, dexamethasone, and hydrocortisone were comparable, with a conversion ratio of 1:5.3 for dexamethasone to methylprednisolone and 5:1 for hydrocortisone to methylprednisolone (Wang et al., 2023). The timing (classified as early (≤ 6 days) and late (>6 days from onset to GCs use)), duration (classified as long-term (> 3 days) and short-term (≤ 3 days)), and dose of GCS treatment (classified as high (> 5 mg/day) and low (≤ 5 mg/day dexamethasone or its equivalents)) were defined based on median number of patients in the multicenter cohort.

2.3 Statistical analysis

As many eligible cases as possible were included due to the exploratory nature of the study. Variables with more than 20% missing data were removed and other missing cases were resolved by multiple interpolation. Data normality was assessed using the Kolmogorov-Smirnov test. Continuous variables were expressed as medians (interquartile range [IQR]), and categorical variables were expressed as frequencies (percentages). For continuous data, differences between groups were measured using the independent samples t-test or Mann-Whitney U-test, as appropriate. Categorical data were analyzed using the Pearson chi-square test or Fisher's exact test.

This study involved a large number of variables, and to screen for potential predictors, least absolute shrinkage and selection operator (LASSO) regression and univariate logistic regression were used. The screened variables were subsequently incorporated into multivariate logistic regression using stepwise regression to identify independent predictors of death in patients with SFTS. A prediction model was developed with all patients' data (avoiding data segmentation), and internal validation of model discrimination and calibration was performed using bootstrapping with 1000 resamples (Riley et al., 2020). Receiver operating characteristics (ROC) curves and calibration curves were used to determine the accuracy and consistency of the model. The overall benefit of the model was demonstrated by Decision Curve Analysis (DCA). Kaplan-Meier curves and log-rank tests were used to compare the survival rate and survival time. To reduce the effects of selection bias and potential confounders, we also performed propensity score matching (PSM) in a 1:1 ratio to divide the patients into two risk groups based on the logit of the propensity score (PS) using nearest-neighbor matching with a caliper width of 0.1. After PSM, subgroup analyses were performed based on patient characteristics and treatment regimens. Data processing and statistical analysis were performed in R software (version 4.3.2). All tests were two-tailed, with p-values less than 0.05 considered significant.

3 Results

3.1 Demographic and clinical data of SFTS patients

Of the 901 patients with SFTS, 105 patients (50 males and 55 females) died, with an overall mortality rate of 11.65%. The median age of the patients was 64.00 (56.00-70.00) years, and the median time from symptom onset to hospital admission was 6.0 (4.0-7.0) days. Fever, diarrhea, vomiting, muscle pain, and cough were the most common symptoms. Basic clinical indicators, such as gender, age, white blood cell (WBC) count, platelets, and log-transformed viral load (lg viral load), were compared between the survival and fatal groups. Compared with the survival group, the fatal group had an older age, a shorter time from onset to admission, and higher incidences of consciousness disturbance, hypertension, myalgia, and hemorrhagic tendencies (see Supplementary Table 1).

3.2 Risk factors for fatal outcomes

A total of 53 variables were measured at hospital admission (see Supplementary Figure 3). After LASSO regression (see Supplementary Figure 2), 12 variables remained significant between survival and fatal groups, including older age, consciousness disturbance, WBC, decreased monocyte counts,

SCr, BUN, LDH, INR, prolonged APTT, PCT, bleeding, and lg viral load. Subsequently, the univariate regression analysis showed that older age (>69 years), time from onset to admission, consciousness disturbance, diarrhea, muscle pain, white blood cell (WBC) count, lymphocyte count, decreased monocyte count ($<0.12\times10^9$/L), platelet count (PLT), aspartate aminotransferase (AST), GLOB, serum creatinine (SCr), blood urea nitrogen (BUN), lactate dehydrogenase (LDH), creatine phosphokinase (CK), calcium (Ca), D-dimer, international normalized ratio (INR), prolonged APTT (>53 s), fibrinogen (FIB), bleeding and lg viral load were screened out as independent predictors (all $p < 0.05$) (Table 1).

3.3 Predictive value of the nomogram

Based on the results of the multivariable analysis, five variables were incorporated into the nomogram, including older age, consciousness disturbance, decreased monocyte counts, prolonged APTT, and lg viral load. In this nomogram, the risk score was calculated using the regression equation formula:

$$\begin{aligned}\text{Nomogram score} &= 1.050 * \text{old age} + 2.564 * \text{consiousness disturbance} \\ &+ 1.249 * \text{decreased monocyte counts} \\ &+ 0.935 * \text{prolonged APTT} + 0.331 * \lg(\textit{viral load})\end{aligned}$$

After logistic regression analysis (Table 1), the five significant and independent variables were incorporated into the nomogram ($R^2 = 0.483$, C-index = 0.908) (Figure 1A). Its predictive accuracy was evaluated with ROC curves and calibration plots. The ROC curve produced an AUC of 0.908 (95% CI: 0.879-0.936) (Figure 1B). The calibration curve was close to the standard diagonal (Figure 1C). The DCA showed excellent net benefits of the nomogram (Figure 1D), indicating its high concordance and reliability.

TABLE 1 Univariate and multivariate logistic regression analyses of risk factors for fatal outcomes in patients with SFTS.

Variables	AUC	Univariate logistic regression		Multivariate logistic regression	
		OR (95%CI)	p-Value	aOR (95%CI)	p-Value
Old age	0.640	3.314 (2.191, 5.034)	<0.001	2.857 (1.694, 4.820)	<0.001
Time from onset to admission	0.584	0.895 (0.817, 0.973)	<0.05		
Consciousness disturbance	0.805	20.303 (12.697, 33.266)	<0.001	12.994 (7.625, 22.142)	<0.001
Diarrhea	0.553	1.532 (1.018, 2.307)	<0.05		
Muscle pain	0.571	0.418 (0.228, 0.716)	<0.05		
WBC	0.599	0.894 (0.818, 0.966)	<0.05		
Lymphocytes	0.677	0.355 (0.202, 0.583)	<0.001		
Decreased monocyte counts	0.664	3.916 (2.545, 6.150)	<0.001	3.486 (2.022, 6.008)	<0.001
PLT	0.659	0.976 (0.966, 0.986)	<0.001		
AST	0.688	1.001 (1.001, 1.001)	<0.001		
GLOB	0.582	1.043 (1.011, 1.075)	<0.05		
SCr	0.693	1.01 (1.006, 1.014)	<0.001		
BUN	0.692	1.091 (1.045, 1.139)	<0.001		
LDH	0.672	1.001 (1.001, 1.001)	<0.001		
CK	0.650	1.000 (1.000, 1.000)	<0.05		
Ca	0.653	0.059 (0.017, 0.195)	<0.001		
D-dimer	0.646	1.040 (1.021, 1.063)	<0.001		
INR	0.704	33.454 (8.652, 142.429)	<0.001		
Prolonged APTT	0.631	3.089 (2.042, 4.685)	<0.001	2.547 (1.503, 4.316)	<0.001
FIB	0.689	0.349 (0.234, 0.507)	<0.001		
Bleeding	0.594	3.504 (2.157, 5.603)	<0.001		
Lg viral load	0.745	1.597 (1.433, 1.791)	<0.001	1.393 (1.218, 1.594)	<0.001

AUC, area under the curve; OR, odds ratio; aOR, adjusted odds ratio; CI, confidence interval; PLT, platelet count; AST, aspartate aminotransferase; GLOB, globulin; SCr, serum creatinine; BUN, blood urea nitrogen; LDH, lactate dehydrogenase; CK, creatine phosphokinase; Ca, calcium; INR, international normalized ratio; APTT, activated partial thromboplastin time; FIB, fibrinogen; Lg viral load, log-transformed viral load.

3.4 Effect of GCs on mild and severe SFTS patients

The risk score was calculated for each patient, with a higher score indicating a higher risk of a fatal outcome. According to a cut-off value of 121.434, all patients were categorized into mild and severe groups. The Kaplan-Meier curve showed a significant difference in the survival rate between the mild and severe groups ($p < 0.001$) (Figure 2). In the comparative analysis of patients treated with and without GCs, the mortality and co-infection rates were significantly different between the two groups (see Supplementary Table 2). The impacts of GCs were further analyzed in patients with mild and severe SFTS. Before and after PSM, the total CFRs were 2.5% (17/679) and 2.3% (11/474) in patients with mild SFTS, and 39.6% (88/222) and 33.3% (44/132) in patients with severe SFTS, respectively. After PSM, 474 patients with mild SFTS and 132 patients with severe SFTS were analyzed, and the baseline characteristics in the GC group were comparable to those in the non-GC group (see Supplementary Table 3). Survival analyses showed no significant difference in CFR between the GC and non-GC groups before and after PSM in mild patients ($p = 0.089$, $p = 0.360$, Figures 3A, C). In contrast, in patients with severe SFTS, CFR was significantly higher in the non-GC group than in the GC group before PSM ($p = 0.004$, Figure 3B), however, significance disappeared after PSM ($p = 0.560$, Figure 3D).

Further subgroup analyses were conducted according to age, sex, and time from onset to admission after PSM. The administration of GCs demonstrated no notable correlation with CFR in any subgroup (see Supplementary Figures 3A, B). However, the administration of GCs was associated with an elevated risk of HAI in patients both with mild and severe SFTS ($p = 0.024$, $p = 0.015$, see Supplementary Figures 3C, D).

3.5 Effect of GCs regimens on patients with SFTS

GCs therapy appeared to reduce mortality in severe patients, but this effect became insignificant after PSM. Therefore, we further investigated the effect of GCs regimen on the CFR and HAI in patients with SFTS, including the timing, duration and dose of GCs treatment. The use of high-dose GCs was associated with an increased CFR ($p = 0.001$, OR = 3.693, 95% CI: 1.710-8.345); especially in mild patients ($p = 0.018$, OR = 13.167, 95% CI: 2.195-251.087). Early use of GCs was also associated with increased CFR ($p = 0.035$, OR = 2.292, 95% CI: 1.071-5.066); especially in severe patients ($p = 0.050$, OR = 2.868, 95% CI: 1.021-8.546) (Table 2). The timing, duration, and dose of GCs therapy did not have a significant effect on HAI (see Supplementary Table 4).

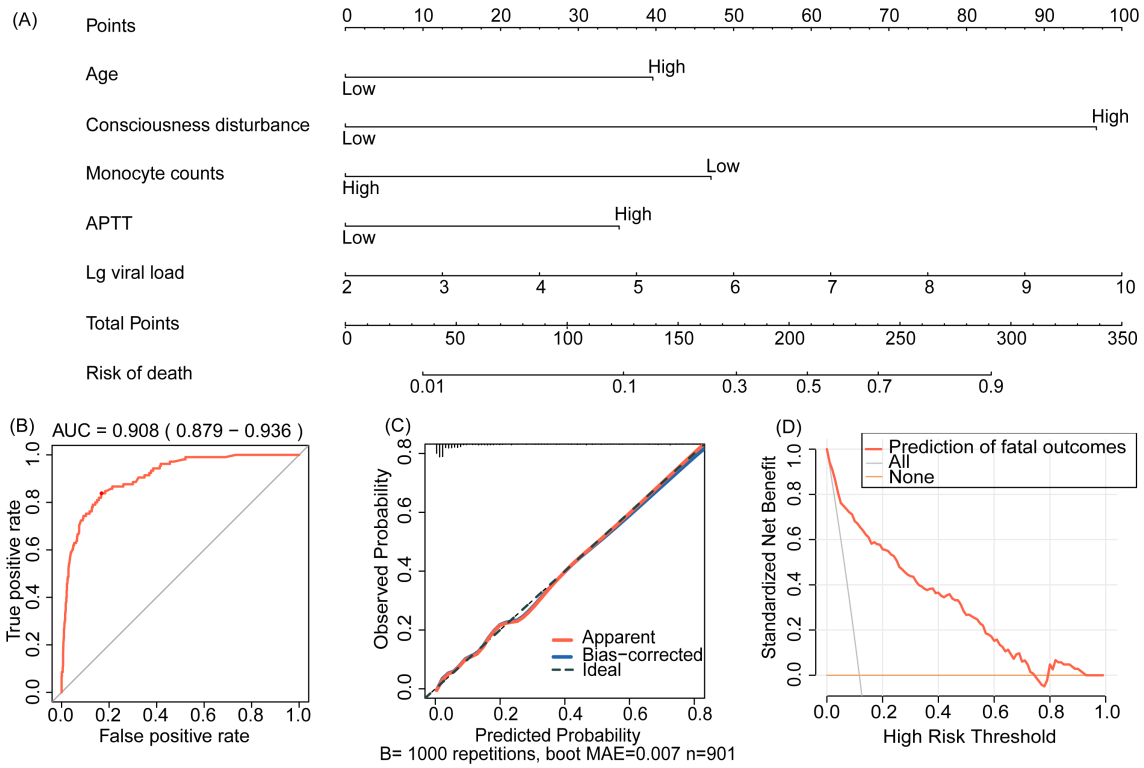

FIGURE 1
(A) The nomogram for predicting fatal outcomes in patients with SFTS. **(B)** Receiver operating characteristics (ROC) curve, **(C)** calibration curves, and **(D)** decision curve analysis (DCA) for the prediction model. Lg viral load, log-transformed viral load; APTT, activated partial thromboplastin time.

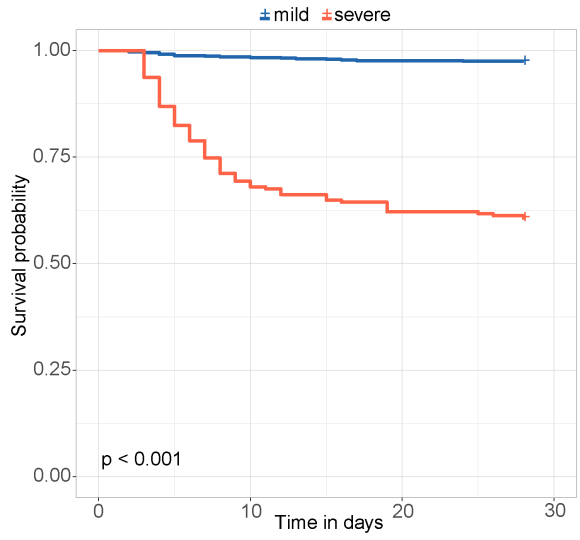

FIGURE 2
Kaplan-Meier survival curves in mild and severe groups.

ROCs were depicted to evaluate the predictive capabilities of PCT, CAR, CRP, NLR, PLR as biomarkers of inflammation and AST, LDH, CK as organ injury biomarkers (Figure 4). CRP, NLR, and PLR showed poor predictive performances (p values of 0.125, 0.193, and 0.401, respectively). The AUCs for AST, LDH, PCT, CK and CAR were 0.688 (95% CI: 0.634-0.742, $p < 0.001$), 0.672 (95% CI: 0.614-0.730, $p < 0.001$), 0.660 (95% CI: 0.605-0.715, $p = 0.001$), 0.650 (95% CI: 0.595-0.705, $p = 0.001$), and 0.608 (95% CI: 0.557-0.659, $p = 0.032$), respectively. The maximum Youden index identified 189.75 U/L as the optimal critical value of AST, at which its sensitivity and specificity reached 0.733 and 0.606, respectively. Then, the patients were divided into low and high AST groups based on this value. GCs therapy reduced the mortality in both the low and high AST groups ($p < 0.001$) (Figures 5A, B). After PSM, this effect remained only in the low AST group ($p = 0.004$, Figure 5C).

4 Discussion

In this multicenter retrospective analysis, we identified older age, consciousness disturbance, decreased monocyte counts, prolonged APTT, and high viral load as significant risk factors for fatal outcomes in SFTS patients. Based on these factors, the new nomogram showed a good prognostic performance, with an AUC of 0.908 (95% CI: 0.879-0.936), a sensitivity of 83.2%, and a specificity of 76.7%.

Older age has been recognized as a risk factor for serious and fatal outcomes of SFTS in previous studies (Li et al., 2018; Zhong et al., 2024). Neurologic symptoms have long been associated with the severity of SFTS outcomes, as evidenced by the mortality exceeds 40% in patients with SFTS-related encephalopathy (Xu et al., 2021). In our study, the results of multivariate analysis showed that consciousness disturbance was a strong predictor of death ($p<0.001$, aOR 12.994, 95% CI: 7.625-22.142). Neurologic symptoms have been a major component of prognostic models developed by Wang et al. and Xia et al (Wang et al., 2021; Xia et al., 2023). Therefore, the consciousness of SFTS patients should be fully evaluated for predicting their prognoses. SFTSV attacks the central nervous system through such mechanisms as direct invasion, cytokine storms, and immune dysregulation (Shan et al., 2024). It has been proposed that peripheral monocytes may be a key cell type affected by SFTS, and the results of this study suggest that acute SFTSV infection leads to significant loss of monocyte subsets and impaired monocyte function, and that the involvement of monocytes in the pathogenesis of SFTS is through the mechanism of disturbed innate immune response (Peng et al., 2016). Significant elevation in viral load can induce excessive release of pro-inflammatory cytokines that arouse a storm to cause severe inflammatory responses and widespread tissue and organ damage (He et al., 2021). Coagulation dysfunction is a common event in patients with SFTS, as shown by a significant prolongation of APTT observed in fatal patients compared to survivors. SFTSV infection results in substantial endothelial damage, which ends up with DIC and hemorrhage in vital tissues and organs (Wang et al., 2022a). In the present study, the predictive nomogram incorporated clinical, virological, and laboratory variables, thereby achieving an accuracy higher than its precedents.

Cytokine storm has been demonstrated to correlate with the severity of SFTS. Consequently, we proceeded to evaluate the efficacy of GCs as an anti-inflammatory intervention. It has been reported that the addition of GCs may be beneficial for treating acute encephalopathy and myocardial dysfunction after SFTSV infection (Nakamura et al., 2018). However, several retrospective studies from China, Korea, and Japan have shown that GCs use may increase the risk of mortality and secondary infections in SFTS patients (Jung et al., 2021; Kawaguchi et al., 2021; Xiong et al., 2022). A recent study shows that patients with severe SFTS may benefit from low to moderate doses of GCs, whereas in patients with mild SFTS, GCs treatment is significantly associated with increased CFR (Wang et al., 2023). Therefore, the efficacy of GCs on SFTS remains controversial, due to methodological limitations in previous studies.

In the present study, we observed that GCs therapy reduced mortality in severe patients but not in mild patients. However, significance disappeared after matching patients' baseline information. We also verified that early and high-dose GCs use was associated with an elevated risk of mortality. One explanation may be that the host immune response is not sufficient enough to inhibit viral replication during the initial stage, while early utilization of GCs may impede viral clearance (Liu WD. et al., 2024). GCs can inhibit the protective function of T cells and prevent B cells from producing antibodies, thus increasing plasma viral load and impairing host immune function (He et al., 2018). The results of the present study showed that in mild patients, the increased CFR was mainly attributed to high-dose GCs, a finding that is consistent with that of Wang et al (Wang et al., 2023). Previous studies also suggested that GCs therapy was associated with other adverse events, especially secondary bacterial/fungal infections (Jung et al.,

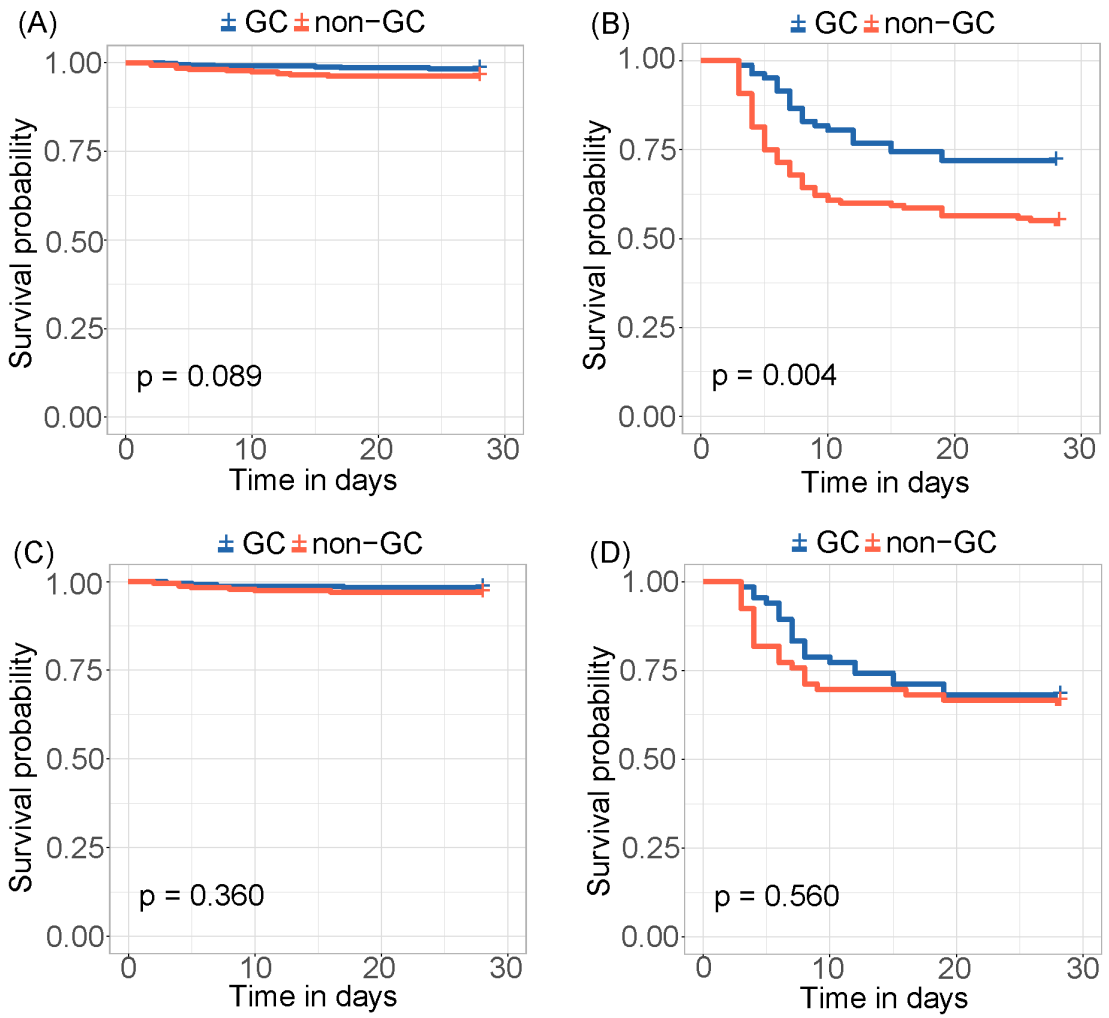

FIGURE 3
Kaplan-Meier survival curves stratified by GCs treatment for **(A)** mild patients and **(B)** severe patients. Kaplan-Meier survival curves stratified by GCs treatment for **(C)** mild patients and **(D)** severe patients after PSM.

TABLE 2 Effect of GC regime on CFR in patients with SFTS after propensity score matching.

Severity of SFTS	Variables	Levels	CFR (%)	p-Value	OR (95%CI)
All patients (n =303)	Initiation of GC therapy	> 6 days	12 (6.78%)	0.035	–
		≤ 6 days	18 (14.29%)		2.292 (1.071, 5.066)
	Duration of GC therapy	> 3 days	14 (10.69%)	0.690	1.167 (0.541, 2.489)
		≤ 3 days	16 (9.3%)		–
	Dose of GC therapy	high	19 (17.92%)	0.001	3.693 (1.710, 8.345)
		low	11 (5.58%)		–
Mild patients (n=237)	Initiation of GC therapy	> 6 days	4 (2.8%)	0.861	–
		≤ 6 days	3 (3.19%)		1.146 (0.221, 5.312)
	Duration of GC therapy	> 3 days	5 (5.26%)	0.109	3.889 (0.819, 27.559)
		≤ 3 days	2 (1.41%)		–

(Continued)

TABLE 2 Continued

Severity of SFTS	Variables	Levels	CFR (%)	p-Value	OR (95%CI)
	Dose of GC therapy	high	6 (7.69%)	0.018	13.167 (2.195, 251.087)
		low	1 (0.63%)		–
Severe patients (n=66)	Initiation of GC therapy	> 6 days	8 (23.53%)	0.050	–
		≤ 6 days	15 (46.88%)		2.868 (1.021, 8.546)
	Duration of GC therapy	> 3 days	9 (25%)	0.069	–
		≤ 3 days	14 (46.67%)		2.625 (0.941, 7.661)
	Dose of GC therapy	high	13 (46.43%)	0.093	2.427 (0.870, 7.002)
		low	10 (26.32%)		–

GC doses were calculated as dexamethasone equivalence, with > 5 mg/d defined as high dose and ≤ 5 mg/d defined as moderate dose.
GC, glucocorticoid; CFR, case fatality rate; OR, odds ratio; CI, confidence interval.

2021; Kawaguchi et al., 2021) and hyperglycemia (Cai et al., 2021). Besides, these findings indicated that secondary infections were increased in both severe and mild patients treated with glucocorticoids, and the use of high-dose GCs compared with low-dose therapy was associated with more severe adverse effects, thus further worsening the prognosis, most likely through hyperglycemia and secondary infections. Consequently, early and high-dose use of GCs is ineffective or even harmful in patients with SFTS, especially in mild patients. Also, monitoring is needed for adverse events especially secondary infections that may occur during and after treatment.

The therapeutic efficacy of GCs owes primarily to their anti-inflammatory properties, whereas excessive activation of inflammatory responses represents a significant contributor to multi-organ injury. Therefore, we plotted ROC curves with the most commonly used markers of inflammation and organ injury, including AST, LDH, CK, PCT, CRP, CAR, NLR, and PLR (Wei Y. et al., 2022; Liu Z. et al., 2024). Among them, AST generated the largest AUC. Moreover, AST-stratified analysis indicated that administration of GCs was associated with a reduction in mortality after PSM (p=0.004) in patients with low-level AST (<189.75 U/L). Consistent with the results of the large single-

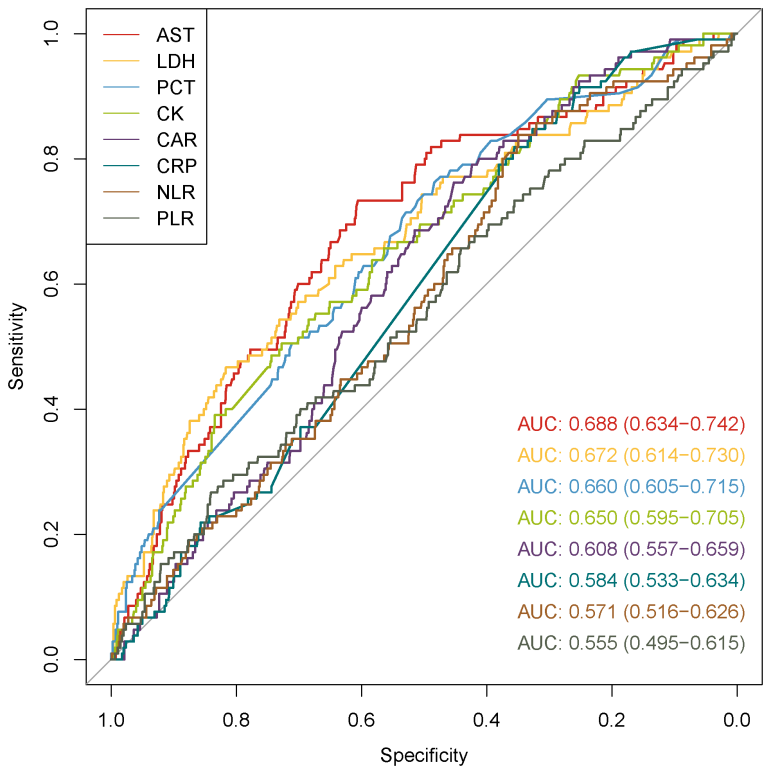

FIGURE 4
ROC curves of inflammatory and organ injury biomarkers for predicting fatal outcomes in patients with SFTS.

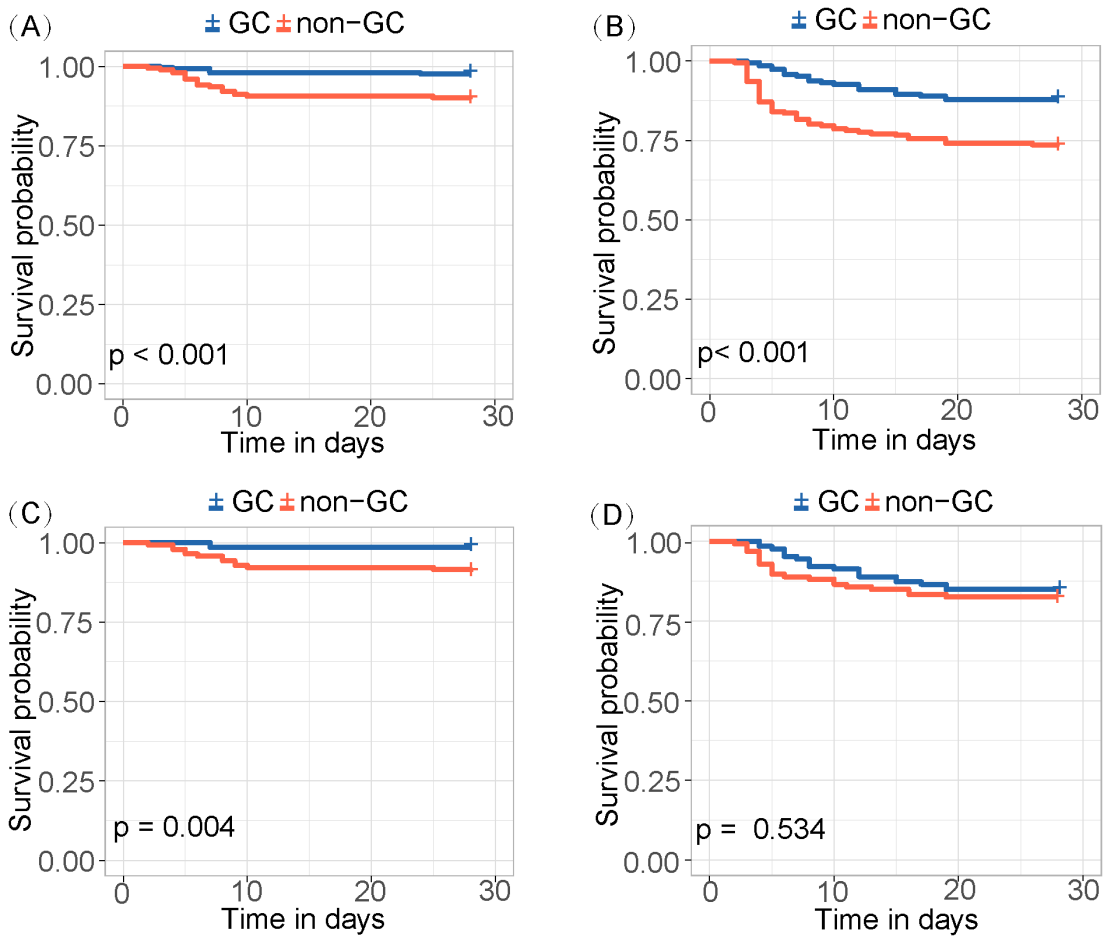

FIGURE 5
Kaplan-Meier survival curves for **(A)** low-level AST and **(B)** high-level AST groups before PSM. Kaplan-Meier survival curves for **(C)** low-level AST and **(D)** high-level AST groups after PSM.

center study by Li et al., elevated AST indicates the presence of acute inflammation and multiorgan damage in the early stage of SFTS (Li et al., 2018). Therefore, the use of GCs before the onset of excessive inflammatory response and multiorgan injury may reduce the mortality of SFTS patients, and AST may be a reliable indicator for predicting the progression of SFTS and determining the start of GCs therapy. In addition, during the use of GCs in patients with SFTS, HAI should be monitored, especially in females and those with an onset-to-admission time of less than 6 days.

However, our study does have certain limitations. First, as a retrospective study, it is inevitably subject to bias. There are currently no standardized protocols for GCs therapy. Usually relying on their clinical experience, physicians often hold confusion about indications and tend to use GCs in severe SFTS cases. Second, due to the absence of cytokines and ferritin-related data, we could not fully explore the anti-inflammatory mechanism of GCs. Third, consciousness disturbance was based on subjective criteria, rather than the Glasgow Coma Scale for quantitative measurement. Last, there are inherent limitations in the prognostic model, as patient mortality rates differ between the two hospitals. Nevertheless, our findings should be validated in an external cohort.

5 Conclusions

A new nomogram based on five independent risk factors has demonstrated a strong ability to predict prognosis in SFTS. GCs therapy may reduce mortality in patients with severe SFTS, whereas early use of GCs may increase mortality in patients with severe SFTS and high dose of GCs may increase mortality in patients with mild SFTS. Initiation of GCs therapy in patients with low AST may reduce mortality. In addition, the risk of hospital-acquired infections after treatment with GCs should be monitored in all patients with SFTS.

Data availability statement

The data analyzed in this study is subject to the following licenses/restrictions: The raw data supporting the conclusions of this article will be made available by the authors, without undue reservation. Requests to access these datasets should be directed to ZP, zhihangpeng@njmu.edu.cn.

Ethics statement

The studies involving humans were approved by the Ethics Committee of Union Hospital of Tongji Medical College, Huazhong University of Science and Technology and the Ethics Committee of Nanjing Medical University, China. The studies were conducted in accordance with the local legislation and institutional requirements. Written informed consent for participation was not required from the participants or the participants' legal guardians/next of kin in accordance with the national legislation and institutional requirements.

Author contributions

FZ: Data curation, Methodology, Writing – original draft, Writing – review & editing, Formal Analysis. SZ: Data curation, Formal Analysis, Writing – original draft, Writing – review & editing. CZ: Data curation, Formal Analysis, Writing – original draft, Writing – review & editing. DZ: Data curation, Writing – review & editing. SL: Data curation, Writing – review & editing. QY: Data curation, Writing – review & editing. HH: Data curation, Writing – review & editing. BZ: Data curation, Writing – review & editing. JT: Data curation, Writing – review & editing. ZH: Data curation, Writing – review & editing. XZ: Data curation, Writing – review & editing. BW: Conceptualization, Methodology, Writing – review & editing, Funding acquisition. ZP: Conceptualization, Methodology, Writing – review & editing, Funding acquisition.

Funding

The author(s) declare that financial support was received for the research, authorship, and/or publication of this article. This work was supported by the National Key Research and Development Program of China (grant numbers 2024YFC2311500 and 2022YFC2304004 to ZP grant numbers 2021YFC2301803 and 2022YFC2305101 to BW), the National Natural Science Foundation of China (grant number 82320108018 to ZP), and the Foundation for Innovative Research Groups of Hubei Province (grant number 2022CFA010 to BW).

Acknowledgments

All authors thank the institutions for their collaboration in collecting patient information.

Conflict of interest

The authors declare that the research was conducted in the absence of any commercial or financial relationships that could be construed as a potential conflict of interest.

The author(s) declared that they were an editorial board member of Frontiers, at the time of submission. This had no impact on the peer review process and the final decision.

Generative AI statement

The author(s) declare that no Generative AI was used in the creation of this manuscript.

Publisher's note

Supplementary material

The Supplementary Material for this article can be found online at: https://www.frontiersin.org/articles/10.3389/fcimb.2025.1531880/full#supplementary-material

References

Cai, J., Li, H., Zhang, C., Chen, Z., Liu, H., Lei, F., et al. (2021). The neutrophil-to-lymphocyte ratio determines clinical efficacy of corticosteroid therapy in patients with COVID-19. *Cell Metab.* 33, 258–269.e3. doi: 10.1016/j.cmet.2021.01.002

Chen, G., Chen, T., Shu, S. N., Ma, K., Wang, X. J., and Wu, D. (2022). Expert consensus on diagnosis and treatment of severe fever with thrombocytopenia syndrome. *Chin. J. Clin. Infect. Diseases* 15, 253–263. doi: 10.3760/cma.j.issn.1674-2397.2022.04.003

Chinese Society of Infectious Diseases and Chinese Medical Association (2022). Consensus on the diagnosis and treatment of severe fever with thrombocytopenia syndrome. *Chin. J. Infect. Dis.* 40, 711–721. doi: 10.3760/cma.j.cn311365-20221017-00425

FakhriRavari, A., Jin, S., Kachouei, F. H., Le, D., and Lopez, M. (2021). Systemic corticosteroids for management of COVID-19: Saving lives or causing harm? *Int. J. Immunopathol. Pharmacol.* 35, 20587384211063976. doi: 10.1177/20587384211063976

Ge, H. H., Wang, G., Guo, P. J., Zhao, J., Zhang, S., Xu, Y. L., et al. (2022). Coinfections in hospitalized patients with severe fever with thrombocytopenia syndrome: A retrospective study. *J. Med. Virol.* 94, 5933–5942. doi: 10.1002/jmv.v94.12

He, Q., Song, X., Huang, Y., Huang, W., Ye, B., Luo, H., et al. (2018). Dexamethasone stimulates hepatitis B virus (HBV) replication through autophagy. *Med. Sci. Monit.* 24, 4617–4624. doi: 10.12659/MSM.906250

He, Z., Wang, B., Li, Y., Hu, K., Yi, Z., Ma, H., et al. (2021). Changes in peripheral blood cytokines in patients with severe fever with thrombocytopenia syndrome. *J. Med. Virol.* 93, 4704–4713. doi: 10.1002/jmv.26877

Jia, B., Yan, X., Chen, Y., Wang, G., Liu, Y., Xu, B., et al. (2017). A scoring model for predicting prognosis of patients with severe fever with thrombocytopenia syndrome. *PloS Neglected Trop. Diseases* 11, e0005909. doi: 10.1371/journal.pntd.0005909

Jung, S. I., Kim, Y. E., Yun, N. R., Kim, C. M., Kim, D. M., Han, M. A., et al. (2021). Effects of steroid therapy in patients with severe fever with Thrombocytopenia syndrome: A multicenter clinical cohort study. *PloS Negl. Trop. Dis.* 15, e0009128. doi: 10.1371/journal.pntd.0009128

Katsurada, N., Suzuki, M., Aoshima, M., Yaegashi, M., Ishifuji, T., Asoh, N., et al. (2017). The impact of virus infections on pneumonia mortality is complex in adults: a prospective multicentre observational study. *BMC Infect. Dis.* 17, 755. doi: 10.1186/s12879-017-2858-y

Kawaguchi, T., Umekita, K., Yamanaka, A., Hara, S., Yamaguchi, T., Inoue, E., et al. (2021). Corticosteroids may have negative effects on the management of patients with severe fever with thrombocytopenia syndrome: A case–control study. *Viruses* 13, 785. doi: 10.3390/v13050785

Kim, E. H., and Park, S. J. (2023). Emerging tick-borne dabie bandavirus: virology, epidemiology, and prevention. *Microorganisms* 11, 2309. doi: 10.3390/microorganisms11092309

Li, H., Lu, Q. B., Xing, B., Zhang, S. F., Liu, K., Du, J., et al. (2018). Epidemiological and clinical features of laboratory-diagnosed severe fever with thrombocytopenia syndrome in China, 2011-17: a prospective observational study. *Lancet Infect. Dis.* 18, 1127–1137. doi: 10.1016/S1473-3099(18)30293-7

Liu, Z., Ge, Z., Pan, W., Zhang, R., Jiang, Z., Zhao, C., et al. (2024). Development and validation of the PLNA score to predict cytokine storm in acute-phase SFTS patients: A single-center cohort study. *Int. Immunopharmacol.* 136, 112288. doi: 10.1016/j.intimp.2024.112288

Liu, W. D., Wang, J. T., Shih, M. C., Chen, K. H., Huang, S. T., Huang, C. F., et al. (2024). Effect of early dexamethasone on outcomes of COVID-19: A quasi-experimental study using propensity score matching. *J. Microbiol. Immunol. Infect.* 57, 414–425. doi: 10.1016/j.jmii.2024.02.002

Ministry of Health, PRC (2011). Guideline for prevention and treatment of severe fever with thrombocytopenia syndrome (2010 version). *Chin. J. Clin. Infect. Dis.* 04, 193–194. doi: 10.3760/cma.j.issn.1674-2397.2011.04.001

Nakamura, S., Azuma, M., Maruhashi, T., Sogabe, K., Sumitani, R., Uemura, M., et al. (2018). Steroid pulse therapy in patients with encephalopathy associated with severe fever with thrombocytopenia syndrome. *J. Infect. Chemother.* 24, 389–392. doi: 10.1016/j.jiac.2017.11.004

Peng, C., Wang, H., Zhang, W., Zheng, X., Tong, Q., Jie, S., et al. (2016). Decreased monocyte subsets and TLR4-mediated functions in patients with acute severe fever with thrombocytopenia syndrome (SFTS). *Int. J. Infect. Diseases* 43, 37–42. doi: 10.1016/j.ijid.2015.12.009

Riley, R. D., Ensor, J., Snell, K. I. E., Harrell, F. E., Martin, G. P., Reitsma, J. B., et al. (2020). Calculating the sample size required for developing a clinical prediction model. *BMJ* 368, m441. doi: 10.1136/bmj.m441

Shan, D., Chen, W., Liu, G., Zhang, H., Chai, S., and Zhang, Y. (2024). Severe fever with thrombocytopenia syndrome with central nervous system symptom onset: a case report and literature review. *BMC Neurol.* 24, 158. doi: 10.1186/s12883-024-03664-6

Shang, L., Zhao, J., Hu, Y., Du, R., and Cao, B. (2020). On the use of corticosteroids for 2019-nCoV pneumonia. *Lancet* 395, 683–684. doi: 10.1016/S0140-6736(20)30361-5

Wang, B., He, Z., Yi, Z., Yuan, C., Suo, W., Pei, S., et al. (2021). Application of a decision tree model in the early identification of severe patients with severe fever with thrombocytopenia syndrome. *PloS One* 16, e0255033. doi: 10.1371/journal.pone.0255033

Wang, Y., Song, Z., Wei, X., Yuan, H., Xu, X., Liang, H., et al. (2022a). Clinical laboratory parameters and fatality of Severe fever with thrombocytopenia syndrome patients: A systematic review and meta-analysis. *PloS Negl. Trop. Dis.* 16, e0010489. doi: 10.1371/journal.pntd.0010489

Wang, Y., Song, Z., Xu, X., Wei, X., Yuan, H., Liang, H., et al. (2022b). Clinical symptoms associated with fatality of severe fever with thrombocytopenia syndrome: A systematic review and meta-analysis. *Acta Trop.* 232, 106481. doi: 10.1016/j.actatropica.2022.106481

Wang, W., Wang, Z., Chen, Z., Liang, M., Zhang, A., Sheng, H., et al. (2024). Construction of an early differentiation diagnosis model for patients with severe fever with thrombocytopenia syndrome and hemorrhagic fever with renal syndrome. *J. Med. Virol.* 96, e29626. doi: 10.1002/jmv.29626

Wang, G., Xu, Y. L., Zhu, Y., Yue, M., Zhao, J., Ge, H. H., et al. (2023). Clinical efficacy of low-dose glucocorticoid therapy for critically ill patients with severe fever with thrombocytopenia syndrome: A retrospective cohort study. *Int. J. Infect. Dis.* 130, 153–160. doi: 10.1016/j.ijid.2023.03.015

Wei, X., Tu, L., Qiu, L., Chen, M., Wang, Y., Du, M., et al. (2022). Scoring model for predicting the occurrence of severe illness in hospitalized patients with severe fever with thrombocytopenia syndrome. *Jpn. J. Infect. Dis.* 75, 382–387. doi: 10.7883/yoken.JJID.2021.716

Wei, Y., Wang, Z., Kang, L., He, L., Sheng, N., Qin, J., et al. (2022). NLR, A convenient early-warning biomarker of fatal outcome in patients with severe fever with thrombocytopenia syndrome. *Front. Microbiol.* 13, 907888. doi: 10.3389/fmicb.2022.907888

Xia, G., Sun, S., Zhou, S., Li, L., Li, X., Zou, G., et al. (2023). A new model for predicting the outcome and effectiveness of drug therapy in patients with severe fever with thrombocytopenia syndrome: A multicenter Chinese study. *PloS Neglected Trop. Diseases* 17, e0011158. doi: 10.1371/journal.pntd.0011158

Xiong, L., Xu, L., Lv, X., and Zheng, X. (2022). Effects of corticosteroid treatment in patients with severe fever with thrombocytopenia syndrome: A single-center retrospective cohort study. *Int. J. Infect. Dis.* 122, 1026–1033. doi: 10.1016/j.ijid.2022.07.001

Xu, Y., Shao, M., Liu, N., Dong, D., Tang, J., and Gu, Q. (2021). Clinical feature of severe fever with thrombocytopenia syndrome (SFTS)-associated encephalitis/encephalopathy: a retrospective study. *BMC Infect. Dis.* 21, 904. doi: 10.1186/s12879-021-06627-1

Yu, X. J., Liang, M. F., Zhang, S. Y., Liu, Y., Li, J. D., Sun, Y. L., et al. (2011). Fever with thrombocytopenia associated with a novel bunyavirus in China. *N. Engl. J. Med.* 364, 1523–1532. doi: 10.1056/NEJMoa1010095

Zhong, F., Lin, X., Zheng, C., Tang, S., Yin, Y., Wang, K., et al. (2024). Establishment and validation of a clinical risk scoring model to predict fatal risk in SFTS hospitalized patients. *BMC Infect. Diseases* 24, 975. doi: 10.1186/s12879-024-09898-6

Frontiers in
Cellular and Infection Microbiology

Investigates how microorganisms interact with their hosts

Explores bacteria, fungi, parasites, viruses, endosymbionts, prions and all microbial pathogens as well as the microbiota and its effect on health and disease in various hosts.

Discover the latest Research Topics

See more →

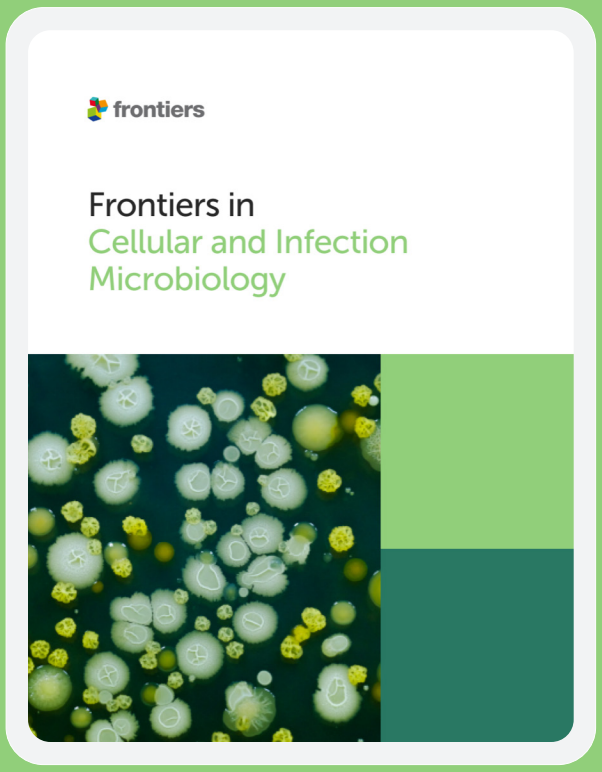

Frontiers

Avenue du Tribunal-Fédéral 34
1005 Lausanne, Switzerland
frontiersin.org

Contact us

+41 (0)21 510 17 00
frontiersin.org/about/contact